



THE UNIVERSITY  
*of* LIVERPOOL

**Development of Coal Mill and Aggregate Load Area Models  
in Power Systems using Genetic Algorithms**

Thesis submitted in accordance with the requirements of  
the University of Liverpool for the degree of Doctor of  
Philosophy

in

Electrical Engineering and Electronics

by

Jianlin Wei

B.Eng., M.Sc.

May 2007

*Dedicate to  
my mother Huiyan Ou,  
my father Shengji Wei,  
and  
my wife Lixin Ma*

# Acknowledgements

First and foremost, I would like to take this opportunity to express my deepest appreciation and acknowledgement to my supervisor, Dr Jihong Wang, for her supports and guidance throughout the duration of my PhD study. Her intellectual advices and encouragements were indispensable for this dissertation.

I would like to thank my co-supervisor Professor Qinghua Wu as well for many helpful discussions and much valuable advice.

I would also like to thank Dr. George Oluwande and Ms. Megan Boardman from RWEnPower Plc. for their innumerable discussions and supports.

Finally, I would like to thank all colleagues working in Intelligence Engineering Group for their kind assistant during my study.

# Abstract

Quality and reliability is one of the most important issues in power generation and distribution. With the recent advances in computer and network technology, the Operational Information Systems (OIS) have been installed in almost all power plants and substations. The data stored in databases covers long periods of time, which presents a challenge as how to extract the useful, task-oriented knowledge from the data to improve power system reliability and power quality. The thesis presents the research work in development of mathematical models for power systems by analysing the data available from on-site measurement using evolutionary computation techniques. The project contributes to aspects in power generation and distribution: coal mill modelling and electrical load area modelling.

Coal-fired power stations are now obliged to vary their outputs in response to changing electricity demand and are required to operate more flexibly with more varied coal specifications. The operations of a mill need to be controlled to respond effectively to changes in plant load and coal quality. Combustion optimization relies heavily on optimization of the mill output. Frequently start-ups and shut-downs of mills bring the impact on power plant to achieve both low NO<sub>x</sub> and CO<sub>2</sub> emissions. Operational safety and efficient combustion require better understanding to the milling process. The work described in the thesis has three new contributions: 1) Development of an improved normal grinding coal mill process model which provide more accurate prediction of mill states than the previous version; 2) Development of a new multi-segment coal mill model which covers the whole milling process from start-ups to shut-downs; 3) Development of a prototype software programme to implement the multi-segment mill model on-line. The software has been passed to RWEnPower



Plc. for further test.

Stable operation of a power system depends on the ability to continuously match the electrical output of generation units to the electrical load. So it is important to have a reliable mechanism to predict the power load on time. Model based approach is one of the options. With the sponsorship from the National Grid Transco Plc, a study of modelling electricity area load has been carried out through this project. A methodology using evolutionary computation techniques based on system measurements to construct power system area load models and achieve distribution network reduction is proposed in the thesis. Three aggregate load area model (ALAM) approaches entitled Voltage-Two-Step, Current-Two-Step and Direct-One-Step have been studied in the thesis. Simulations studies are carried out for these three approaches, and it found that the Direct-One-Step offers the best performance among the three ALAM approaches. Verification studies are performed through the project and some rules for constructing a good ALAM are obtained.

# Contents

<b>List of Figures .....</b>	<b>ix</b>
<b>List of Tables.....</b>	<b>xv</b>
<b>Chapter 1 Introduction.....</b>	<b>1</b>
1.1 Overview.....	1
1.2 Coal Mill Modelling .....	1
1.3 Electricity Area Load Modelling.....	3
1.4 Project Objective.....	5
1.5 Thesis Outline .....	6
1.6 Publications arising from the research work.....	8
<b>PART I: COAL MILL MODELLING.....</b>	<b>10</b>
<b>Chapter 2 Introduction to Coal Mills and Evolutionary     Computation Techniques.....</b>	<b>10</b>
2.1 Introduction.....	10
2.2 Description of Coal Mills .....	12
2.2.1 Coal-Fired Power Generation Process .....	12
2.2.2 Introduction to Low Speed Mills .....	16
2.2.3 Introduction to Medium Speed Mills.....	17
2.2.4 Introduction to High Speed Mills.....	19
2.3 Evolutionary Computation Techniques .....	20
2.3.1 Introduction.....	20
2.3.2 Genetic Algorithms (GAs) .....	21
2.3.3 Simulation Studies of the RSPGA .....	25
2.4 Summary and Discussion .....	29
<b>Chapter 3 Coal Mill Model for Normal Grinding Process .....</b>	<b>30</b>
3.1 Introduction.....	30
3.2 Development of the Coal Mill Model by Analysing the Normal Grinding Process.....	32
3.2.1 Identification of Input and Output Variables of the Process ..	32
3.2.2 Mass Flow Analysis .....	34
3.2.3 Mill Product Pressure .....	37
3.2.4 Power Consumption Analysis .....	38
3.2.5 Thermodynamic Process .....	39
3.2.6 Mathematical Model of the Milling Process .....	41
3.3 Model Parameter Identification.....	42
3.3.1 Description of On-Site Measurement Data.....	42

3.3.2	Identification of Model Coefficients Using RSPGA.....	43
3.3.3	Simulation Results .....	46
3.4	Summary and Discussions.....	51
<b>Chapter 4</b>	<b>Multi-Segment Coal Mill Model .....</b>	<b>52</b>
4.1	Overview of a Complete Milling Process .....	52
4.2	Multi-Segment Coal Mill Mathematical Model .....	55
4.2.1	Coal Mill Model - Segment I .....	55
4.2.2	Coal Mill Model - Segment II.....	57
4.2.3	Coal Mill Model - Segment III.....	58
4.2.4	Coal Mill Model - Segment IV .....	59
4.2.5	Coal Mill Model - Segment V.....	60
4.2.6	Coal Mill Model - Segment 0.....	62
4.2.7	Summary of the Multi-Segment Model .....	63
4.3	Model Parameter Identification and Model Validation.....	64
4.3.1	Overview of the Data Sets.....	64
4.3.2	Identification of Unknown Model Parameters .....	65
4.3.3	Mill Model Validations .....	71
4.4	Summary and Discussion .....	79
<b>Chapter 5</b>	<b>On-Line Implementation of the Coal Mill Model.....</b>	<b>81</b>
5.1	Introduction.....	81
5.2	Program I - Data Supplying.....	83
5.3	Program II - On-Line Implementation of the Mill Model.....	88
5.4	Summary and Discussion .....	99
<b>PART II: AGGREGATE LOAD AREA MODELLING .....</b>		<b>101</b>
<b>Chapter 6</b>	<b>Introduction to Power System Load Modelling.....</b>	<b>101</b>
6.1	Introduction.....	101
6.2	The Standard Load Models .....	103
6.3	Aggregate Load Area Modelling (ALAM).....	108
6.4	Newton-Raphson Method for Power Flow Calculation .....	110
6.5	Summary and Discussion .....	117
<b>Chapter 7</b>	<b>ALAM Parameter Identification – Three Approaches.....</b>	<b>118</b>
7.1	Introduction.....	118
7.2	ALAM Approach One: Voltage-Two-Step (VTS) Approach..	122
7.3	ALAM Approach Two: Current-Two-Step (CTS) Approach..	127
7.4	ALAM Approach Three: Direct-One-Step (DOS) Approach..	132
7.5	Summary and Discussion .....	135
<b>Chapter 8</b>	<b>Verification Studies on the ALAM .....</b>	<b>137</b>
8.1	Introduction.....	137



8.2	Verification Study of ALAM Based on the IEEE-39-Bus Power System	137
8.3	Verification Study of ALAM Based on the IEEE-57-Bus Power System	144
8.4	Verification Study of ALAM Based on the IEEE-118-Bus Power System	152
8.5	Summary and Discussion .....	161
<b>Chapter 9 Summary and Recommendations for Future Work .....</b>		<b>164</b>
9.1	Summary .....	164
9.2	Recommendations for Future Work.....	165
<b>References.....</b>		<b>167</b>
<b>Appendix I: Mill Operation Sequence Table.....</b>		<b>174</b>
<b>Appendix II: Validation results using Data Set C.....</b>		<b>178</b>

# List of Figures

Figure 2-1 Coal-fired power stations in UK (QAA 2006) .....	12
Figure 2-2 Coal fire power plant (RWE Innogy Plc 2002) .....	15
Figure 2-3 Low speed mill currently used in EDF Energy Plc (EDF Plc 1981) .....	16
Figure 2-4 E-type, medium speed mill (RWE Innogy Plc 2000) .....	18
Figure 2-5 The high-speed mill (CEGB 1963) .....	20
Figure 2-6 The structure of a traditional genetic algorithm .....	22
Figure 2-7 2-dimensional Rosenbrock function .....	26
Figure 2-8 RSPGA performance (Rosenbrock function) .....	27
Figure 2-9 2-dimensional Rastrigin's function .....	28
Figure 2-10 RSPGA performance (Rastrigrin function) .....	28
Figure 3-1 Demonstration of the coal mill modelling procedure .....	31
Figure 3-2 Coal mill control system .....	33
Figure 3-3 Dynamic process of coal flow .....	37
Figure 3-4 Coal mill heat balance illustration .....	39
Figure 3-5 The coal mill model coefficients identification procedure .....	45
Figure 3-6 The measured and simulated results using Data 2 .....	46
Figure 3-7 The measured and simulated results using Data 3 .....	47
Figure 3-8 The measured and simulated results using Data 4 .....	47
Figure 3-9 Partly enlarged figure of the measured and simulated results using Data 4 .....	48
Figure 3-10 The measured and simulated results using Data set 5 Mill F, 7 <sup>th</sup> Mar 2003 10:16:40 ~ 14:56:21 .....	48
Figure 3-11 Partly enlarged figure 2 of the measured and simulated results using Data 5 .....	49
Figure 3-12 Partly enlarged figure 3 of the measured and simulated results using Data 5 .....	49
Figure 3-13 Comparison of the average errors between the simulated output ( $T_{out}$ ) and the measured output .....	50
Figure 4-1 Coal mill start-up sequence .....	53
Figure 4-2 Coal mill shut-down sequence .....	54
Figure 4-3 Coal mill six-segment model .....	55
Figure 4-4 Structure of the coal mill multi-segments model .....	64
Figure 4-5 Simulation results for start-up process using the single grinding model .....	67
Figure 4-6 Simulation results for shut-down process using the single grinding model .....	68



Figure 4-7 Simulation results for overall process using the single grinding model.....	68
Figure 4-8 Simulation results for start-up process using the multi-segment model.....	69
Figure 4-9 Simulation results for shut-down process using the multi-segment model.....	70
Figure 4-10 Simulation results for overall process using the multi-segment model.....	70
Figure 4-11 Simulated and measured mill outlet temperature for all segments using Data Set B.....	72
Figure 4-12 Simulated and measured mill outlet temperature for Segments IV&V (zoom in) using Data Set B.....	72
Figure 4-13 Simulated and measured mill outlet temperature for segments I&II (zoom in) using Data Set B.....	72
Figure 4-14 Simulated and measured mill current for all segments using Data Set B.....	73
Figure 4-15 Simulated and measured mill current for segments IV&V (zoom in) using Data Set B.....	73
Figure 4-16 Simulated and measured mill current for segments I&II (zoom in) using Data Set B.....	73
Figure 4-17 Simulated and measured mill differential pressure for all segments using Data Set B.....	74
Figure 4-18 Simulated and measured mill differential pressure for segments IV&V (zoom in) using Data Set B.....	74
Figure 4-19 Simulated and measured mill differential pressure for segments I&II (zoom in) using Data Set B.....	74
Figure 4-20 Simulated coal mass in mill for all segments using Data Set B.....	75
Figure 4-21 Simulated coal mass in mill for segment IV & V (zoom in ) using Data Set B.....	75
Figure 4-22 Simulated coal mass in mill for segment I & II (zoom in) using Data Set B.....	75
Figure 4-23 Simulated pulverized mass of coal in mill for all segments using Data Set B.....	76
Figure 4-24 Simulated pulverized mass of coal in mill for segment IV & V (zoom in ) using Data Set B.....	76
Figure 4-25 Simulated pulverized mass of coal in mill for segment I & II (zoom in) using Data Set B.....	76
Figure 4-26 Coal mass flow rate into mill for all segments using Data Set B.....	77
Figure 4-27 Coal mass flow rate into mill for segment IV & V	

(zoom in) using Data Set B.....	77
Figure 4-28 Coal mass flow rate into mill for segment I & II (zoom in) using Data Set B.....	77
Figure 4-29 Simulated pulverized mass flow rate out of mill for all segments using Data Set B .....	78
Figure 4-30 Simulated pulverized mass flow rate for segment IV & V (zoom in ) using Data Set B.....	78
Figure 4-31 Simulated pulverized mass flow rate for segment I & II (zoom in ) using Data Set B.....	78
Figure 5-1 Schematic structure of the software for on-line implementation .....	82
Figure 5-2 On-line modelling software based on the shared memory idea .....	83
Figure 5-3 User interface structure of the Program I .....	84
Figure 5-4 Data loading from data files.....	85
Figure 5-5 Main window displaying the data loaded.....	86
Figure 5-6 Dynamically displaying of the shared memory buffer.....	87
Figure 5-7 Stop loading data into shared memory buffer .....	88
Figure 5-8 Structure of Program II .....	89
Figure 5-9 Update the model parameters - demo 1.....	90
Figure 5-10 Update the coal mill model parameters - demo 2.....	90
Figure 5-11 Update the coal mill model parameters - demo 3.....	91
Figure 5-12 Starting the on-line coal mill model .....	92
Figure 5-13 Flow chart for share memory idea .....	92
Figure 5-14 Starting the coal mill modelling 2.....	93
Figure 5-15 Pausing or Stopping the coal mill modelling .....	94
Figure 5-16 Coal mill modelling information display.....	95
Figure 5-17 Coal mill model variables display .....	96
Figure 5-18 Coal mill model simulated outputs and measured outputs.....	97
Figure 5-19 Result saving - demo 1 .....	98
Figure 5-20 Result saving - demo 2.....	99
Figure 6-1 “Bus Load”, including feeders, transformers, and shunt capacitors, as well as load devices .....	104
Figure 6-2 A load area composed of seven load buses .....	109
Figure 6-3 The fictitious load bus and its connected transmission lines .....	109
Figure 6-4 IEEE 14-bus power system (Zimmerman <i>et al.</i> 2004).....	111



Figure 6-5	The Newton-Raphson method's convergence performance for the bus 4 in the IEEE 14-bus power system .....	115
Figure 6-6	The Newton-Raphson method's convergence performance for the bus 40 in the IEEE 57-bus power system .....	116
Figure 6-7	IEEE 57-bus power system.....	116
Figure 7-1	The IEEE-14-Bus power system .....	120
Figure 7-2	The equivalent power system from IEEE 14-bus power system .....	121
Figure 7-3	Nominal $\pi$ circuit for the fictitious transmission line.....	123
Figure 7-4	Maximum errors of the bus voltages of the equivalent power system approached by CTS in verification Test1.....	126
Figure 7-5	Maximum errors of the bus voltages of the equivalent power system approached by CTS in verification Test2.....	127
Figure 7-6	Maximum errors of the bus voltages of the equivalent power system approached by CTS in verification Test3.....	127
Figure 7-7	Maximum errors of the bus voltages of the equivalent power system approached by CTS in verification Test1.....	131
Figure 7-8	Maximum errors of the bus voltages of the equivalent power system approached by CTS in verification Test2.....	131
Figure 7-9	Maximum errors of the bus voltages of the equivalent power system approached by CTS in verification Test3.....	131
Figure 7-10	The identification process of the DOS approach .....	132
Figure 7-11	Max errors of the bus voltages of the equivalent power system approached by DOS in verification Test1 .....	134
Figure 7-12	Maximum errors of the bus voltages of the equivalent power system approached by DOS in verification Test2 .....	134
Figure 7-13	Maximum errors of the bus voltages of the equivalent power system approached by DOS in verification Test3 .....	135
Figure 8-1	IEEE-39 bus power system.....	138
Figure 8-2	Equivalent IEEE-39 bus power system for ALAM of Load Area 1 .....	139
Figure 8-3	Maximum errors of the bus voltages in each operation state while changing the active power output of bus 37 from -10% to 10% .....	140
Figure 8-4	Maximum errors of the bus voltages in each operation state while changing tap ratio between bus 12 and bus 13 from 10% below to 10% above its normal operation value .....	141

Figure 8-5 Maximum errors of the bus voltages in each operation state while changing the voltage outputs in bus 32 from 10% below to 10% above its normal output.....	141
Figure 8-6 Equivalent IEEE-39-Bus power system for ALAM of Load Area 2 .....	142
Figure 8-7 Maximum errors of the bus voltages in each operation state while changing the active power output of bus 37 from 10% below to 10% above its normal operation value.....	143
Figure 8-8 Maximum errors of the bus voltages in each operation state while changing tap ratio between bus 12 and bus 13 from 10% below to 10% above its normal operation value.....	143
Figure 8-9 Maximum errors of the bus voltages in each operation state while changing the voltage outputs in bus 32 from 10% below to 10% above its normal operation value .....	144
Figure 8-10 The original IEEE 57-bus power system.....	145
Figure 8-11 Equivalent IEEE-57-Bus power system for aggregating load area 1 .....	146
Figure 8-12 Maximum errors of the bus voltages in each operation state while changing the active power output of bus 1 from -10% to 10% .....	148
Figure 8-13 Maximum errors of the bus voltages in each operation state while changing tap ratio between bus 20 and bus 21 from 10% below to 10% above its normal operation value.....	148
Figure 8-14 Maximum errors of the bus voltages in each operation state while changing the voltage outputs in bus 3 from 10% below to 10% above its normal output.....	149
Figure 8-15 Equivalent IEEE-57-Bus power system for aggregating load area 2.....	150
Figure 8-16 Maximum errors of the bus voltages in each operation state while changing the active power output of bus 1 from 10% below to 10% above its normal operation value.....	151
Figure 8-17 Maximum errors of the bus voltages in each operation state while changing tap ratio between bus 20 and bus 21 from 10% below to 10% above its normal operation value.....	151
Figure 8-18 Maximum errors of the bus voltages in each operation state while changing the voltage outputs in bus 3 from 10% below to 10% above its normal operation value .....	152



Figure 8-19 The IEEE 118-bus power system with the two load areas, Load Area A and Load Area B .....	154
Figure 8-20 Partially enlarged equivalent IEEE-118-Bus power system for aggregating Load Area A .....	155
Figure 8-21 Maximum errors of the bus voltages in each operation state while changing the active power output of bus 69 from -10% to 10% .....	156
Figure 8-22 Maximum errors of the bus voltages in each operation state while changing tap ratio between bus 65 and bus 66 from 10% below to 10% above its normal output value .....	157
Figure 8-23 Maximum errors of the bus voltages in each operation state while changing the voltage outputs in Bus 1 from 10% below to 10% above its normal output value .....	157
Figure 8-24 Partially enlarged equivalent IEEE-118-Bus power system for aggregating Load Area B .....	158
Figure 8-25 Maximum errors of the bus voltages in each operation state while changing the active power output of bus 69 from 10% below to 10% above its normal output value .....	159
Figure 8-26 Maximum errors of the bus voltages in each operation state while changing tap ratio between Bus 65 and Bus 66 from 10% below to 10% above its normal output value .....	160
Figure 8-27 Maximum errors of the bus voltages in each operation state while changing the voltage outputs in bus 1 from 10% below to 10% above its normal output value .....	160



# List of Tables

Table 2-1 Genetic algorithm toolboxes .....	24
Table 2-2 The property settings for real-value RSPGA.....	25
Table 3-1 List of coal mill model variables.....	35
Table 3-2 Five on-site measurement data sets.....	42
Table 3-3 Identified system parameters.....	45
Table 4-1 Identified parameters for the model segments I, II and III.....	66
Table 4-2 Identified parameters for the model segments IV, V and 0.....	67
Table 4-3 Average errors of the simulated results.....	79
Table 6-1 Common values for exponential indices $np$ and $nq$ .....	106
Table 6-2 The admittance values in $Y$ .....	112
Table 7-1 The twelve identified parameters of the equivalent IEEE-14-Bus power system .....	126
Table 7-2 The twelve identified parameters of the equivalent IEEE-14-Bus power system .....	130
Table 7-3 The twelve identified parameters of the equivalent IEEE-14-Bus power system .....	133
Table 8-1 The identified parameters for modelling load area 1 in the IEEE-39-Bus power system .....	139
Table 8-2 The identified parameters for modelling load area 2 in the IEEE-39 bus power system .....	143
Table 8-3 The identified parameters for modelling Load Area I in the IEEE-57-Bus power system .....	147
Table 8-4 The identified parameters for modelling load area 2 in the IEEE-57-Bus power system .....	150
Table 8-5 The identified parameters for modelling load area 1 in the IEEE-118-Bus power system .....	155
Table 8-6 The identified parameters for modelling load area 2 in the IEEE-118-Bus power system .....	159

# Chapter 1

## Introduction

### 1.1 Overview

Power generation industry has always been a dynamic industrial sector and there have been many major changes occurring over its history, such as, the introduction of automatic control, the movement to large efficient generating units and introduction of computers into the control process and the control room (Rees 1998). Over last 50 years, remarkable changes in information technology have been envisaged. With the advances in modern distributed control systems, the Operational Information Systems (OIS) have been installed in almost all power plants (Rees *et al.* 2002). The data of measured signals can be stored in databases which cover long periods of time. The availability of such a large volume of data presents a challenge as how to extract the useful, task-oriented knowledge from the data. Therefore, the research project is proposed to develop mathematical models of power systems by analysing the data available from on-line measurement using evolutionary computation techniques. The project particularly focuses on coal mill modelling in power generation and electrical load area modelling in power distribution.

### 1.2 Coal Mill Modelling

Coal-fired power stations are now obliged to vary their outputs in response to the changes in electricity demands (load following operation) and are required to operate more flexibly with more varied coal specifications. All plants must be capable of operating at partial load, frequently changing



load and even starting up and shutting down daily (Rees *et al.* 2002). Coal mill controls need to respond effectively to the changes in plant load and coal quality as the coal mills are the hearts of the pulverised coal preparation system in coal-fired power stations (Zhang *et al.* 2002). The response of coal delivery to the burners is one of the major factors affecting the performance of the power plant during large load changes (Peet *et al.* 1994). However, the coal mill has received much less attention from modelling and control specialists (Rees *et al.* 2003). At the present, many practical mill-control problems, like the accurate measurement of mill PF (pulverized fuel) flow, fuel CV (calorific value), the detection of mill choking and coal caking on the grinding table, and the determination of the degree of mill roller wear, are difficult to measure and therefore to control effectively (Fan *et al.* 1997; Rees *et al.* 2003). Operational safety and efficient combustion require better understanding to the milling process.

A wide range search of literature shows that there are very few reports about coal mill modelling and controls using evolutionary techniques. A mathematical model of coal milling process has been investigated by L. Blach (Blach *et al.* 1978), which built up a linearised coal mill model based on the process physical and thermo-dynamical relations. Numerical studies of coal mill models using frequency response testing have been carried out by Neal *et al.* in 1980 (Neal *et al.* 1980). Similar research has been reported by K.E. Bollinger in 1983 & 1986 (Bollinger *et al.* 1983, 1986), where the coal mill model was developed to be represented by a set of transfer functions. Detailed studies about the crashing and grinding process was reported in 1981 (Prasher 1981). Simplified mass breakage phenomena in coal mills was studied in 1984, where linearised dynamic analysis has been carried out (Corti *et al.* 1984). An approximated linear time varying mill model was reported by G.Q. Fan, *et al.* in 1994, 1997 & 2003, where a

more simplified grinding model based on the size mass balance model is developed (Fan *et al.* 1994, 1997; Rees *et al.* 2003). A polynomial matrix model was recently report by Hamiane, *et al* in 2000, where system identification method was adopted (Hamiane 2000). However almost all the reported work describes the milling process by approximated linear mathematical models, which cannot reflect the nonlinear features of coal mill processes in general. The milling process may look like a simple mechanical process but it is complex in nature as the process involves complicated interactions between coal quality and mill conditions, which leads to immense difficulties for obtaining physics based nonlinear models of milling processes.

With the sponsorship from RWEnPower Plc., modelling studies of the coal mill systems have been on-going at the University of Liverpool since 1999. A number of papers were published to report the achievements from Liverpool (Zhang 1999a, 1999b; Zhang *et al.* 2002). After the work conducted by Zhang, a modified version has been studied later by Wan and Thomarkos in 1999 and 2000 (Wan 1999; Thomakos 2000). As a research student, I started working on the project from 2002 which can be partly considered as a continuation of the previous work.

### **1.3 Electricity Area Load Modelling**

Recently, several collapses of power systems happened around the world (for example, 14<sup>th</sup> Aug. 2003, Unite State and Canada; 28<sup>th</sup> Aug. 2003, London, UK; 28<sup>th</sup> Sept. 2003, Italy; 12<sup>th</sup> July 2004, Greece; 14<sup>th</sup> Mar. 2005, Australia; 25<sup>th</sup> May 2005, Moscow) so it is urged to strengthen the robustness of power system operations. To obtain the accurate power system models will help to predict the potential power system failures and to reduce power system operational uncertainty (Horowitz *et al.* 2003). Reasonably accurate models for generators, lines and transformers are



available nowadays, whereas load models are usually simplified (Anon 1993; Price *et al.* 1995; Srinivasan *et al.* 1995). Stable operation of a power system depends on the ability to continuously match the electrical output of generating units to the electrical load demand on the system (Lee *et al.* 1985; Horowitz *et al.* 2003). It has been shown in a number of reports that power system load characters can have a significant impact on the power system stability analysis (Kundur *et al.* 1994; Machowski *et al.* 1998; Horowitz *et al.* 2003). Unfortunately deriving an accurate model of electricity load is a difficult task, due to several factors, such as, a large number of diverse load components; ownerships and locations of load devices in customer facilities that are not directly accessible to the electric utility; changing load composition with time of hours, days and weeks, seasons and weather; lack of precise information on the composition of load; uncertainties regarding the characteristics of many load components; difficulties in on-line measurement for wider range of voltage and frequency variations (Anon 1993; Wen *et al.* 2003a). Most of the existing load modelling methods can only deal with “bus load”, where “load” refers to the representation of the aggregate effect of many individual end-user devices connected to the bus (Price *et al.* 1995). In modern power systems, almost all distribution systems and load areas (load centres) are supplied by more than one power source to improve the security and reliability of the whole system (Wang *et al.* 1997). As a number of source buses are distributed and connected to the load area rather than single unified bus, the bus load model is reluctant to represent the load area.

With the sponsorship from the National Grid Company Plc, study of modelling electricity area load has been carried out at the University of Liverpool. A methodology using evolutionary computation techniques based on system measurements to construct power system area load models and achieve distribution network reduction is proposed. The area



load model was tested both in a 5-bus (Wen *et al.* 2003a), where three load buses were aggregated into one fictitious load, and also in the IEEE 30-bus power system (Wu *et al.* 2003; Wen *et al.* 2003b), where eleven load buses were aggregated into one fictitious load. Good results have been obtained, but more studies need to be carried out, for example, the verification studies about the area load model, which is to show whether area load model works in the same degree of accuracy for different combinations of the load buses in a power system.

## **1.4 Project Objective**

The main objective of the project is to develop mathematical models for power systems by analysing the data available from on-line measurement using evolutionary computation techniques. Two particular aspects are concerned in the project: coal mill modelling in power generation and the electrical area load modelling in power distribution.

The coal mill mathematical dynamic model is required to reflect the dynamics of mill temperatures, differential pressure, mass flow rate of pulverised coal and air flow, which includes the start-up and shut-down process. The coal mill model developed in the project will help engineers to have a better understanding to mill processes, to achieve a more efficient control and operations of milling plants.

In the second part of the project, further study on power system area load models will be carried out and the methodology will approximate the relationships between the power consumptions (active power, reactive power) and the bus voltages (magnitudes and frequency). Verification studies are proposed to see whether different combinations of the load area buses can achieve the same degree of accuracy in the area load modelling. The power system area load model developed in the project will be a very

practical technique with a great potential for exploitation in power system load modelling.

## **1.5 Thesis Outline**

The thesis is organised into nine chapters and the first chapter is to give the background and motivation of the research project. The rest of chapters are briefly described as follows.

**Chapter 2** gives a background introduction to the coal mills and evolutionary computation techniques. Brief discussions about the working principle and also mechanical structure of coal mills are given in the beginning of the chapter. In the second part of the chapter, introduction to Genetic Algorithms are presented. Simulation studies of the RSPGA (Real-Value Single-Population Genetic Algorithm) based on two well known benchmark functions (Rosenbrock function and the Rastrigin function) are carried out to illustrate the optimization performance of the RSPGA .

**Chapter 3** presents the coal mill modelling process. By analysing the coal flow process, mill product pressure, power consumption, and the thermodynamic process, the coal mill model for normal grinding milling process is developed, which composes of eight equations and sixteen unknown parameters. The RSPGA is adopted for model coefficient identification. Simulation studies based on five sets of on-site collected data are carried out, where validation results show that the coal mill model offers a more accurate result compared to the model developed previously in 2002.

**Chapter 4** proposes a multi-segment coal mill model which covers the whole coal milling process including start-up and shut-down process. According to the operation sequence, the whole process is partitioned into six segments, where six sets of model equations are developed to represent



the coal mill in the respective states. Simulations and validation studies of the coal mill model are carried out using on-site collected data.

**Chapter 5** presents a prototype of software that developed for the coal mill model on-line implementation. The software is divided into two parts, which are namely Program I - Data Supplying and Program II - Model On-line Implementation. The shared memory technique is employed in the programming development.

**Chapter 6** gives a background introduction to the power system load modelling and the power flow calculations. In the first part of the chapter, the six commonly used load models are reviewed. A novel Aggregate Load Area Model (ALAM) is introduced afterward, which models the aggregate load effects to a load area rather than a load bus. In the second part of the chapter, the power flow calculations are reviewed, where Newton-Raphson method are discussed. Simulation studies based on an IEEE-14 bus power system and IEEE-57 bus power system are carried out to demonstrate the method's performance .

**Chapter 7** dedicates to an introduction of three different approaches for the ALAM. The first one is the Voltage-Two-Step approach, which was first proposed in 2003. The second and third ones are the Current-Two-Step approach and the Direct-One-Step approach, which are a newly development through this research project. Simulation studies have been carried out to compare the performances of the three different approaches.

**Chapter 8** This chapter presents the verification studies of the ALAM. Three IEEE standard power systems are applied for the studies, which are IEEE-39 power system, IEEE-57 power system and the IEEE-118 power system. In each power system, two load areas are selected for the ALAM, and simulation results are compared. Rules for constructing accurate

ALAM are summarized accordingly.

Finally, the main contributions of the thesis and work summary are given in Chapter 9. Also, some suggested future research directions are proposed in the chapter. One particular research in Tube-Ball mill modelling is on-going within the research group.

## **1.6 Publications arising from the research work**

### **Journal Papers:**

1. **J Wei, J Wang, and Q H Wu, Development of a Multi-Segment Coal Mill Model Using an Evolutionary Computation Technique, accepted by *IEEE transaction on Energy Conversion*, 2006.**
2. **J Wei, J Wang, Q H Wu, J Chen, and N Jia, Multi-Segment Pulverised Coal Mill Model and On-Line Implementation for Condition Monitoring, accepted by *International Journal of Modelling, Identification and Control*, Vol. 1, No. 3, pp. 206 -214, 2006.**
3. **J Wei, J Wang, Q.H. Wu, and N Lu, Power System Aggregate Load Area Modelling by Particle Swarm Optimization, *International Journal of Automation and Computing*, Vol. II, pp.171-178, 2005.**
4. **J Wei, J Wang, N Jia, and Q H Wu, Coal Mill On-Line Modelling, *Chinese Journal of Shan Dong Da Xue Xue Bao*, Vol. 35, pp.75-87, 2005.**

### **Conference papers:**

1. **J Wei, J Wang, Q H Wu, and N Lu, Power system aggregate load area modelling by particle swarm optimization, *Proc. of the 11<sup>th</sup> Chinese Automation & Computing Society Conference in the UK*, Sheffield, England, pp55-pp60, 2005. (Nominate to the best paper award, and invite to publish in the *International Journal of Automation and Computing*.)**
2. **J Wei, J Wang, L Yang and Q H Wu, Power System Aggregate Load Area Modelling, *Proc. of 2005 IEEE/PES Transmission and Distribution Conference and Exhibition: Asia and Pacific*, Dalian World Expo Plaza, Dalian, China, F0511, No. 1-6, August 14-18, 2005**

3. **J Wei, J Wang, and Q H Wu**, Coal mill modelling using evolutionary computation techniques and its on-line implementation, *IEE Control Conference*, Ref. 80, Bath UK, 2004.
4. **J Wei, J Wang, and Q H Wu**, Study of Fitness Function in Identifying Unknown Parameters of Dynamic Processes using Genetic Algorithms, *Proc. of Postgraduate Research Conference in Electronics, Photonics, Communications and Networks, and Computing Science*, p123 - p124, Hertfordshire UK, 2004.
5. **J Wei, J Wang, Q H Wu, G Oluwande and M Boardman**, Further study on coal mill modelling by machine learning based on onsite measurements, *International Conference on System Engineering*, Vol II, p736 – p741, Coventry UK, 2003.



# **PART I: COAL MILL**

## **MODELLING**

### **Chapter 2**

## **Introduction to Coal Mills and Evolutionary Computation Techniques**

### **2.1 Introduction**

Almost 40% of the world's electricity is produced by coal-fired power plants (Fernando 2006). In the UK, there are currently 19 coal-fired power stations, with generation capacities of between about 100 megawatt and 3800 megawatt. The power stations are distributed around the UK at the locations shown in Figure 2-1. Of the various systems available, by far the most widely used is pulverized coal (or pulverized fuel, PF) combustion, used in power station boilers to raise steam to drive steam turbines (DTI 2001). As coal mills are the heart of the pulverized coal preparation system in coal-fired stations, research into coal mill processes is of great significance to operation safety and efficiency. The mill-related factors that influence plant combustion performance include coal properties (mainly calorific value (CV), grindability, abrasiveness, moisture content), mill design type (low-speed mill, medium-speed mill, high-speed mill), pulverized coal distribution system (presence of bifurcations and trifurcations) and control strategy, *etc.* Different design configurations,

wear between overhauls, and instrumentation systems design will all results in diversity of mill characteristics. Operational safety and efficient combustion require better understanding to the milling process. This project is to develop a mathematical coal mill model for mill operation safety and combustion efficiency using evolutionary computation techniques.

Four well-know paradigms currently exist in Evolutionary Computation Techniques: Genetic Algorithms, Evolutionary Programming, Evolution Strategies, and Genetic Programming (Eberhart *et al.* 1998). The most widely used evolutionary computation technique is Genetic Algorithms (GAs). GAs are a class of stochastic search algorithms that start with a population of randomly generated candidates and evolve towards better solutions by applying genetic operators (reproduction, crossover, mutation, *etc.*). GAs have been successfully applied in many areas. For example, in aerospace applications, Krishnakumar and Glodberg (Krishnakumar *et al.* 1992) and Bramletter and Cusin (Bramlette *et al.* 1989) have demonstrated how genetic optimization methods can be used to derive superior controller structures in less time (in terms of evaluations) than that of traditional methods such as LQR and Powell's gain set design. In mineral process application, Karr *et al.* used genetic algorithms in designing air injected hydrocyclone and tuning the fuzzy logic controller in the mineral process system (Karr 1993; Karr *et al.* 1996). In power transmission applications, Rashtchi *et al.* have employed genetic algorithm to identify the transformer R-L-C-M Mode for studying transient phenomena in a transformer and detecting mechanical faults (Rashtchi *et al.* 2006). Loads of researches have been proved that GA is a robust optimization method for the parameter identification problems (Alonge *et al.* 2001; Chumsamutr *et al.* 2003; Nyarko *et al.* 2004; Wang *et al.* 2004; Shi *et al.* 2005).



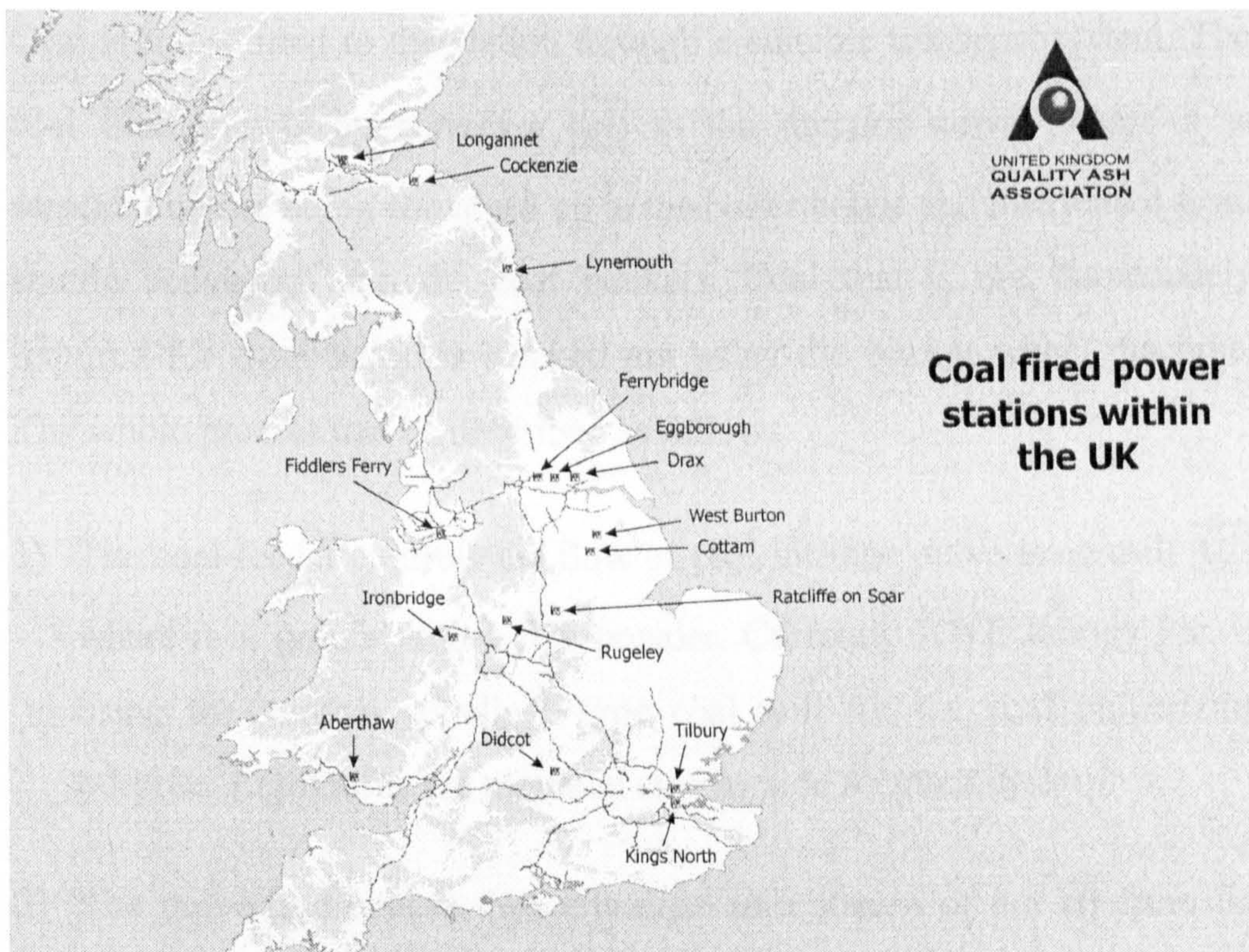


Figure 2-1 Coal-fired power stations in UK (QAA 2006)

At the beginning of this chapter, detailed descriptions to power plant coal mills are given. The second part of this chapter dedicates to the necessary knowledge of GAs. Simulation examples of using those algorithms are given to illustrate their optimisation capacity and performance.

## 2.2 Description of Coal Mills

### 2.2.1 Coal-Fired Power Generation Process

Coal, oil and nuclear power stations produce electricity in a similar process - fuel is used to generate heat to raise pressurised steam to turn a turbine to generate an electric current. Coal power station uses coal as fuel which may have a rather simple process. The coal-fired power generation process used by RWEnPower Plc. is illustrated in Figure 2-2 and a brief introduction to the process is given as follows.



Coal is transported to the station through a suitable transport system. The coal then travels by conveyor [01] to the junction tower where it is screened before being conveyed up to the boiler house and distributed from shuttle conveyors into the coal bunkers. Coal that is not immediately required for combustion is stocked out using the bucket wheel machine. The whole process can be described as follows:

- 1) The coal feeder controls the flow of coal into the pulverising mill [02] where it is ground into a fine powder. Currently RWE Innogy Plc. is using the vertical spindle E-type coal mill for the coal pulverizing purpose. Eight mills are mounted side by side for each boiler.
- 2) The pulverised coal is then entrained in a stream of hot air from the primary air fan and carried to the burners on the boiler front wall [03] where it burns like a gas jet to produce the heat for steam raising.
- 3) The products of burning pulverised coal in the furnace are ash and dust. The ash falls to the bottom of the boiler and is periodically sluiced away to the ash pits for sale. The dust is carried in the flue gases to the precipitators [09] where it is extracted by high voltage electrodes. The cleansed flue gases then pass via the induced fans to the main chimney.
- 4) The heat released by burning the pulverized coal is absorbed by the miles of tubing which form the boiler walls. Inside the tubes extremely pure water is converted by heat into steam at high pressure. The steam is then passed via control valves in the turbine [04] where it is discharged through nozzles into the turbine blades. The energy of the steam makes the turbine shaft rotate.
- 5) Coupled to the turbine shaft is the rotor [05] of the generator - a large



cylindrical electro-magnet. When the turbine rotates, the electrical rotor rotates with it. Electricity is produced in the stator copper conductor bars by the rotation of the magnetic fields created by the rotor electro-magnets.

- 6) The electricity produced, usually at 22.5kV is supplied to the generator transformer [06] which increases the voltage to 400kV a voltage suitable for transmission on the overhead power lines of the grid system.
- 7) Meanwhile, the steam which has exhausted its useful energy in rotating the turbine is turned back into water in the condenser [07] to be used again in the boiler. The heat which the water extracts from the steam in the condenser is removed by passing the water through the cooling towers [08] which act as chimneys to create a draught of cold air.



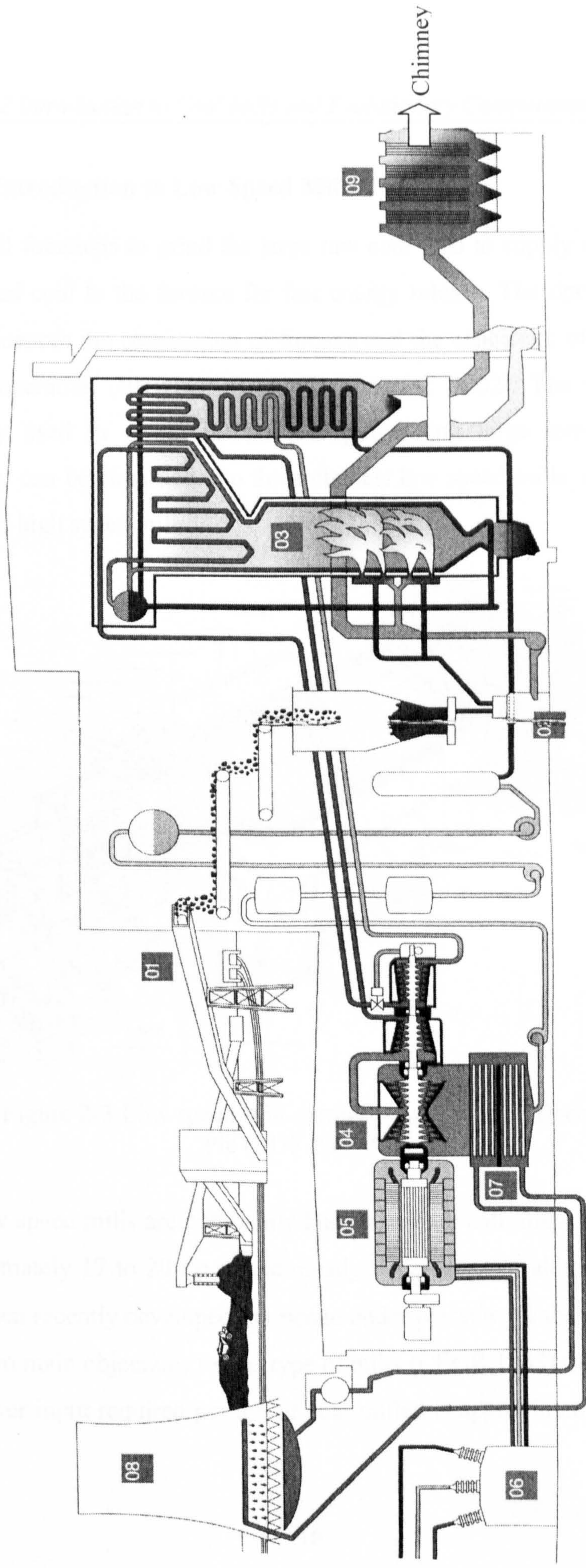


Figure 2-2 Coal fire power plant (RWE Innogy Plc 2002)







than for the commonly used medium speed mill. And secondly, the reliability of the mill has been in doubt principally because of bearing and gearbox failures. In recent year, however, improvements in design have almost eliminated failures of this kind and manufacturers' claims that the latest mills can operate from one annual overhaul to another with only the periodic addition of ball charge are gradually being realised.

Figure 2-3 shows the tube ball mill that is currently used in EDF Energy Plc (Cottam power station). The mill is basically a motor driven tumbling barrel charged with steel balls. The horizontal barrel, carried on a hollow trunnion at each end, is rotated by a girth ring attached to the discharge end trunnion. Coal is discharged from a feed box into the inlet end trunnion and fed into the mill by a scroll in the trunnion. The tumbling action of the balls crushes the coal to power which is extracted from the mill through the discharge end trunnion by air flow.

### **2.2.3 Introduction to Medium Speed Mills**

The medium speed mills are the most widely used in power generation industry nowadays, which are also known as vertical spindle mills. The ball-and-race and the roll-and-race mills are the type in common use. They operate on the principles of crushing and attrition, where the grinding action takes place between two surfaces, one rolling on top of the other. The rolling elements may be balls or ring-shaped rolls that roll between two races in the manner of a ball bearing.

Figure 2-4 shows the medium speed vertical spindle E-type mill that is equipped in the RWE Innogy Plc (DidcotA power station). The main structure of the mill is fabricated from mild steel in three circular sections: 1). A base



which supports the entire unit and encloses the mill drive gear box; 2). A centre housing that contains the rotary grinding elements; 3) An upper section comprising an outlet turret and classifier housing assembly, which also accommodates the hydro-pneumatic units of the ball mill loading gear. The grinding elements comprise 10 hollow cast steel balls which run between

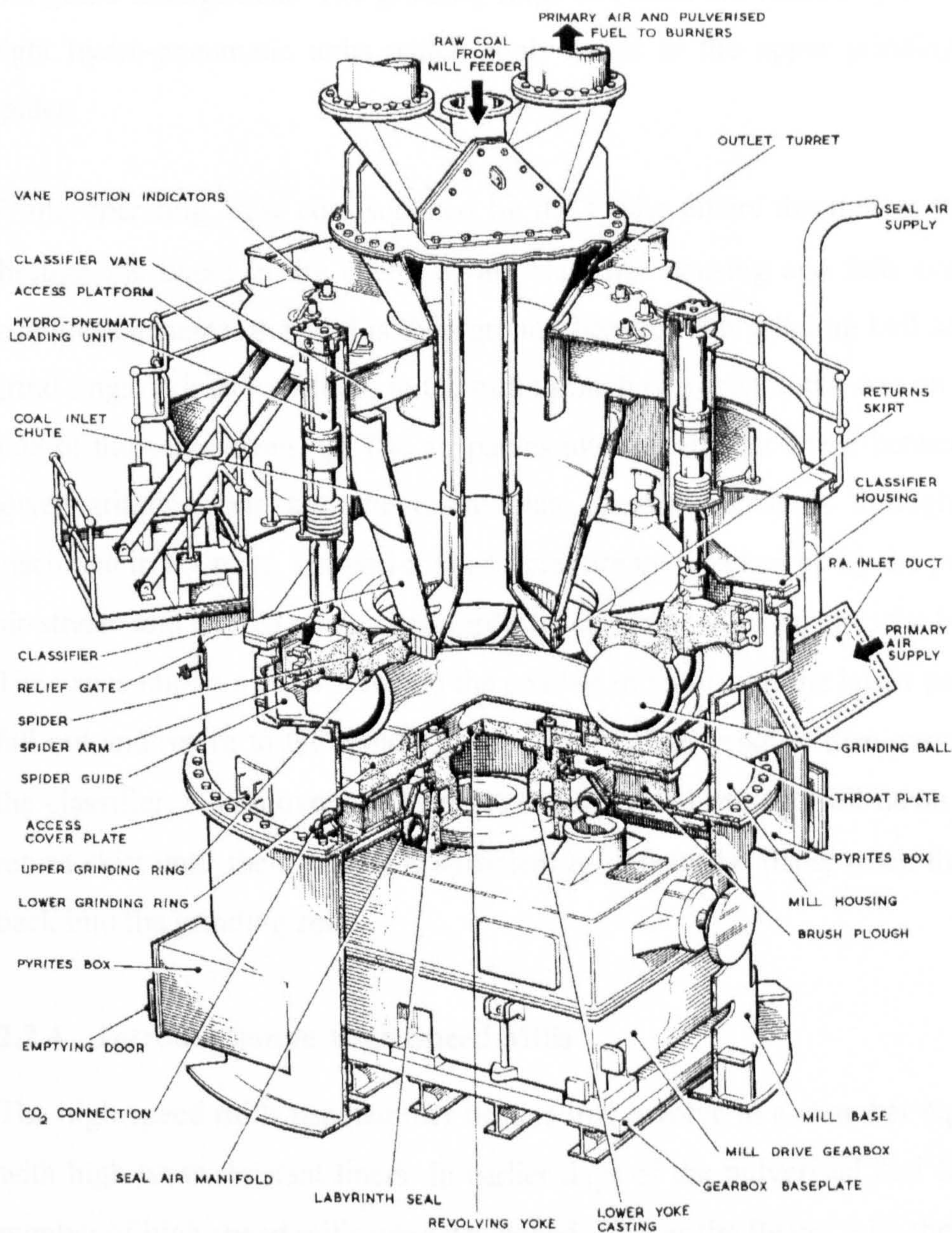


Figure 2-4 E-type, medium speed mill (RWE Innogy Plc 2000)



grooved 'Elverite' grinding rings. The lower grinding ring is keyed to a revolving yoke, which is bolted to the flanged output coupling of the gearbox. The upper grinding ring is keyed to a circular spider which carries four arms engaged and located by guides in the mill centre housing. The spider and upper ring are free to move vertically, but are fixed against rotation by the arm and guide arrangement. The grinding rings and balls are loaded by means of eight hydro-pneumatic units which apply thrust to the upper grinding ring spider.

While operating, raw coal supplied by the feeder enters the mill at the top through the chute in the centre of the classifier housing and falls onto the grinding elements, the coal is then ground between the grinding ball and the grind rings. Primary air feeds to the mill through two inlet ducts, one on either side of the centre housing. The air passes into the annular space between the lower grinding ring and the throat plate, flowing upwards through slots machined in the plate. Ground coal particles are then picked up by the primary air-stream and carried upwards towards the classifier and further to the burners. The vanes impart a swirl action to the coal/air mixture, and the larger particles fall out and return to the grinding zone. The coal/air mixture then passes into the classifier, where oversize particles are separated out and fall down to the return skirt until their weight is sufficient to deflect the flaps, when they fall back into the grinding zone.

#### **2.2.4 Introduction to High Speed Mills**

The high-speed mills use hammer beaters that revolve in a chamber equipped with high-wear-resistant liners. In earlier days of the pulverised fuel firing, a number of high speed mills were developed, such as the Beater mill, the Impax mill and the Attrition mill. However, due to the rapid wear of hammer tips and



the heavy maintenance required, the high-speed mills are not widely used for pulverized coal systems (CEGB 1963). Figure 2-5 shows a high-speed Attrition mill which is survived in some power stations as an auxiliary for lighting up and light load carrying. The mill was designed to be compact. The mill, classifier and the exhauster are all on the same driving shaft.

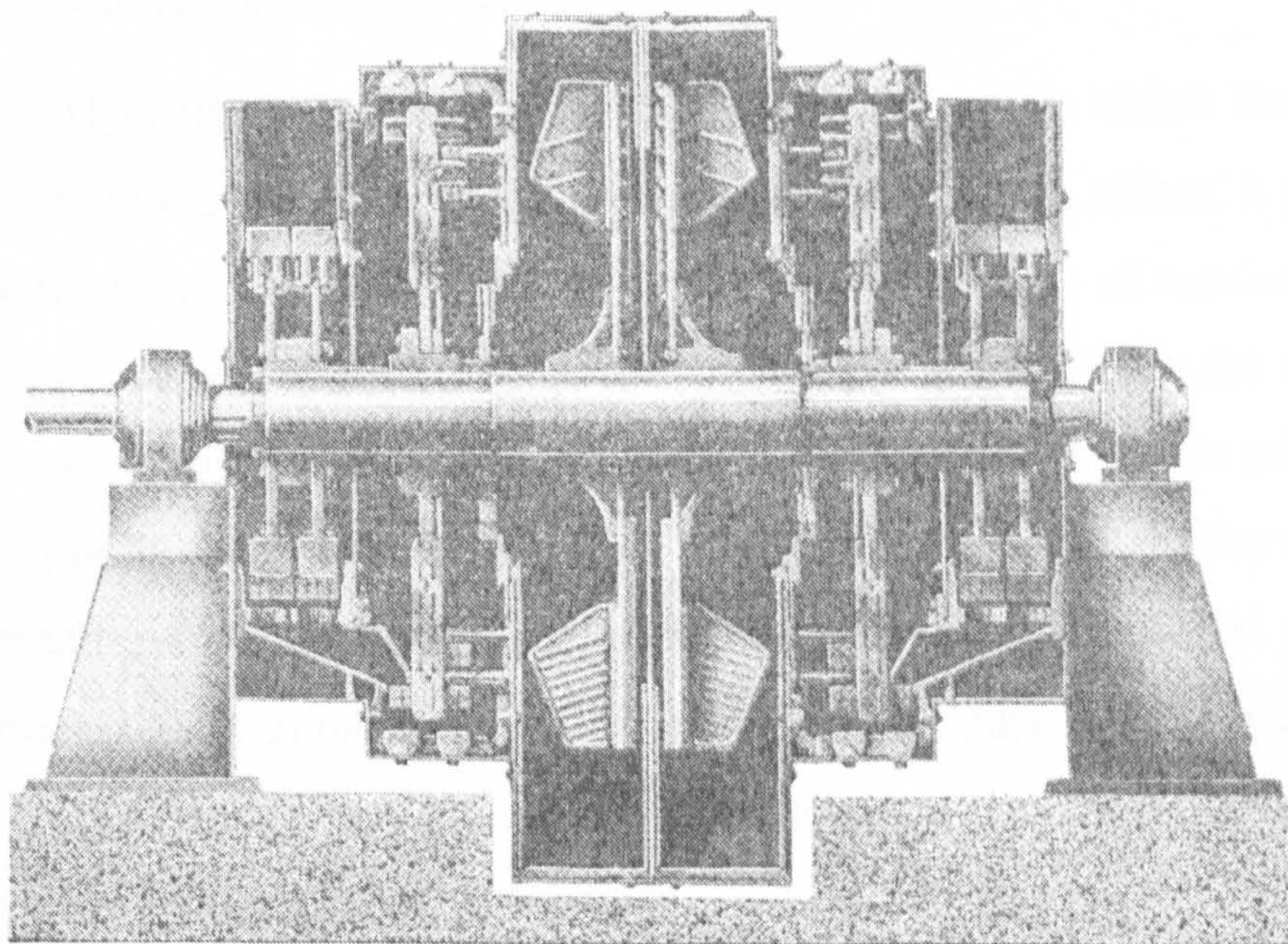


Figure 2-5 The high-speed mill (CEGB 1963)

## **2.3 Evolutionary Computation Techniques**

### **2.3.1 Introduction**

Genetic Algorithms (GAs) and Particle Swarm Optimization algorithm are introduced in this section. The evolutionary processes of the two algorithms are reviewed. Simulation studies of the two algorithms based on some bench



mark functions are carried out and compared at the end of the section. The best performance algorithm will be adopted for the project. The purpose of comparison is not to conclude which algorithm is better. The goal is to provide insights into how GAs and PSO work, and choose one for the research project for the task of coefficients identification.

### **2.3.2 Genetic Algorithms (GAs)**

Genetic Algorithm (GA) is a model of machine learning which derives its behaviour from a metaphor of the processes of evolution in nature. It operates on a population of potential solutions applying the principle of survival of the fittest to produce (hopefully) better and better approximations to the solution. At each generation, a new set of approximations is created by the process of selecting individuals according to their level of fitness in the problem domain and breeding them together using operators borrowed from natural genetics. This process leads to the evolution of populations of individuals that are better suited to their environment than the individuals that they were created from, just as in natural adaptation.

There are many 'ways' to implement a genetic algorithm. Regardless of the specific implementation, a GA is usually at least composed of three fundamental operators: Selection (Reproduction), Recombination (Crossover) and Mutation (Davis 1987). A traditional genetic algorithm (GA) is summarized in Figure 2-6. Major components of the algorithms are explained below:

- 1) GA operates on a number of potential solutions, called a population. At the beginning of the computation, a number of individuals (the population) are randomly initialised. The number of potential solutions should be large



enough that there is a reasonable amount of genetic diversity in the population. And also it should be small enough for each generation to be computed in a ‘reasonable’ period of time using the computer resources available. Typically, a population is composed of between 20 and 100 individuals (Chipperfield *et al.* 1994B).

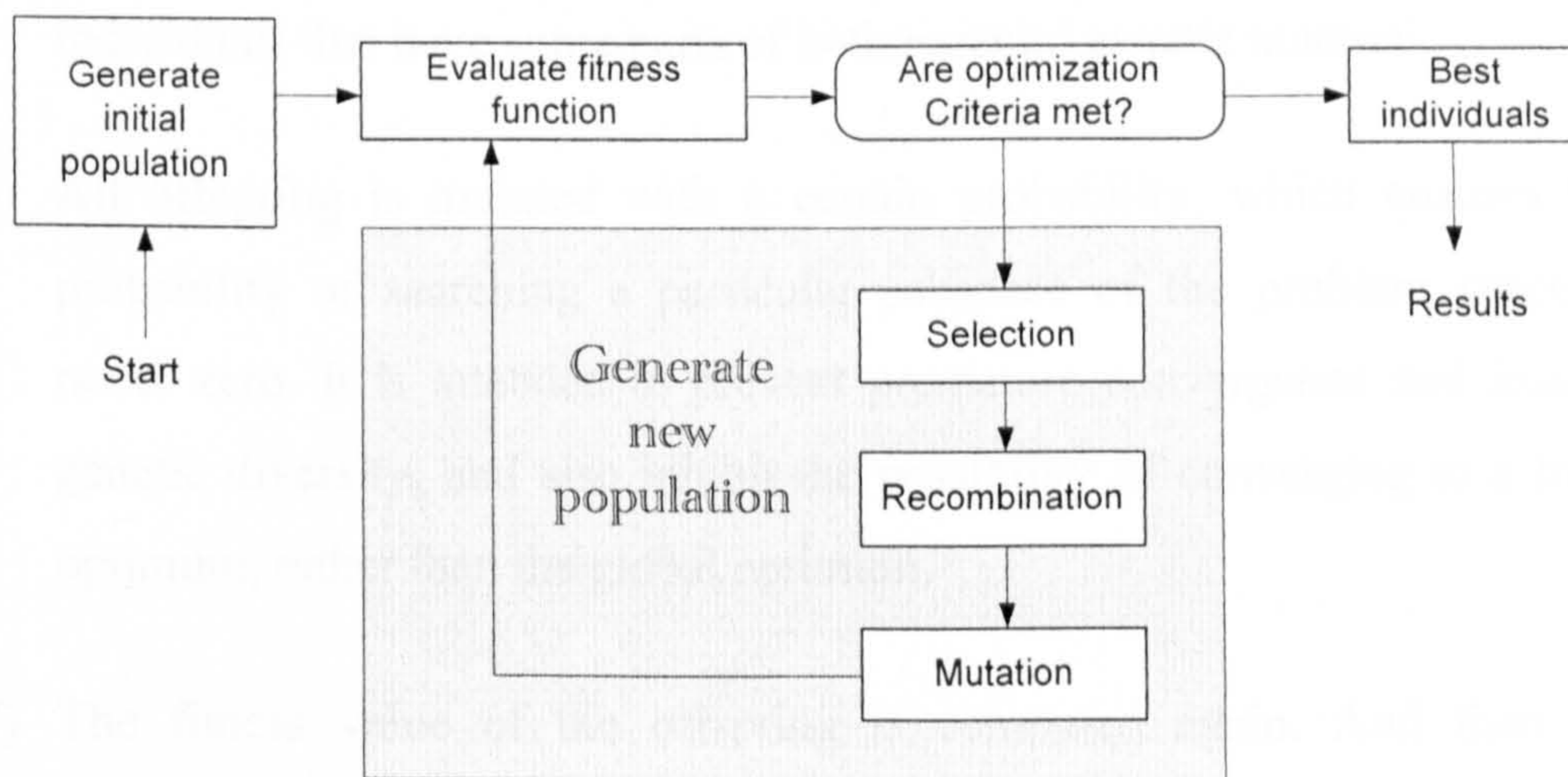


Figure 2-6 The structure of a traditional genetic algorithm

- 2) The fitness function is then evaluated for these individuals, which measures how well suited, or how close, the trial solution is to the desired result. In the case of a minimization problem, the most fitted individuals will have the lowest numerical value of the associated fitness function.
- 3) The first/initial generation is produced. If the optimization criteria are not met, the creation of a new generation starts.
- 4) Individuals are selected according to their fitness for the production of offspring. Selection determines which individuals are chosen for recombination (crossover) and how many offspring each selected individual produces. There are number of ways to select a new population,



e.g. roulette wheel selection (RWS), stochastic universal sampling (SUS). Comparing between RWS and SUS, SUS ensures a selection of offspring which is closer to what is deserved than RWS (Baker 1987).

- 5) After selection, individuals are recombined (crossover) to produce offspring. Like its counterpart in nature, recombination produces new individuals that have some parts of both parents' genetic material.
- 6) All offspring is mutated with a certain probability, which ensures the probability of searching a particular subspace of the problem space is never zero. It is intended to prevent premature convergence and loss of genetic diversity, and also inhibit the possibility of converging to a local optimum, rather than the global optimum.
- 7) The fitness value of the offspring is computed again. And then the offspring are inserted into the population replacing the parents according to their fitness value to produce a new generation.

This cycle is performed until the optimization criteria are reached.

In the current market, there are large amount well developed GA toolboxes existed for application purposes. Three major GA toolboxes are the Genetic Algorithms Toolbox V1.2 (Chipperfield *et al.* 1994A), the Genetic Algorithms Optimization Toolbox V1.1 (Houck *et al.* 1995), and the Genetic Algorithm Direct Search Toolbox V1.02 (MathWorks Inc. 2004). Brief comments and comparisons of the three toolboxes are shown in Table 2-1. Genetic Algorithm Toolbox V1.2 is adopted in the project for the identification and optimisation of coal mill models.



Table 2-1 Genetic algorithm toolboxes

Toolbox Name	Comments
Genetic Algorithms Toolbox V1.2	Good documentation, fitness function pursuits minimum, a bit difficult in programming, but fast convergence, excellent and powerful.
Genetic Algorithm Optimization Toolbox V1.1	Without very good documentation, fitness function pursuits maximum, easy programming, but not as powerful and well implement as prior.
Genetic Algorithm Direct Search Toolbox V1.02	Official toolbox in Matlab R14 Sp1 from Mathworks Inc, fitness function pursuits minimum, provides Graphic User Interface (GUI), easy programming, but feel like prototype, not well implement, e.g. no boundary restrictions to the variables to be identified, not as powerful as the first toolbox mentioned above.

Further to the traditional GA introduced above, GAs can be divided into two types - Binary and Real-value GAs while implementing, where the GA works with different representations of variables. And also, corresponding to the number of the subpopulations in each generation, the GA can be further divided into the Single-Population GA (SPGA) and the Multi-Population GA (MPGA). Detailed theoretical studies and simulation comparisons can be found in the author's MSc thesis (Wei 2002), which found that Real-value SPGA (RSPGA) offers a fast convergence, good performance and high efficient computation. For such algorithm, there are totally eleven properties to be chosen or set up and different settings will cause slightly different performances. Based on the typical setting in common use (Chipperfield *et al.* 1994A), the property settings of the RSPGA are given in Table 2-2.

Table 2-2 The property settings for real-value RSPGA

Name of the GA properties	Value of the GA properties
Number of generations	100
Number of individuals per subpopulations	20
Generation gap	0.9
Fitness Assignment	Rank-base fitness assignment
Selection	Stochastic universal sampling
Recombination	Discrete recombination
Crossover rate	0.7
Mutation	Real-value mutation
Mutation rate	0.0625
Reinsertion	Fitness-base reinsertion (global reinsertion)
Reinsertion rate	1.0

### 2.3.3 Simulation Studies of the RSPGA

In order to test and demonstrate the RSPGA introduced above, simulation studies have been carried out. Two benchmark functions that are commonly used in evaluating evolutionary computation algorithms are employed for the simulation studies. The two benchmark functions are:

#### 1. Rosenbrock function

Rosenbrock function is a classic optimization problem, also known as Banana function. The global optimum is inside a long, narrow, parabolic shaped flat valley (see Figure 2-7). To find the valley is trivial, however convergence to the global optimum is difficult and hence this problem has been repeatedly used in assessing the performance of optimisation algorithms. The function equation is shown in (2-1):

$$f(\bar{X}) = \sum_{i=1}^n \left( 100(x_{i+1} - x_i^2) + (x_i - 1)^2 \right) \quad (2-1)$$



where  $n$  is the dimension of the problem, and  $x_1 \sim x_n$  are the coefficients to be identified. The global minimum 0 is at the point that  $x_1 \sim x_n$  are all equal to 1. In order to demo the optimization ability of the RSPGA, a ten dimensional Rosenbrock function is adopted for the simulation studies.

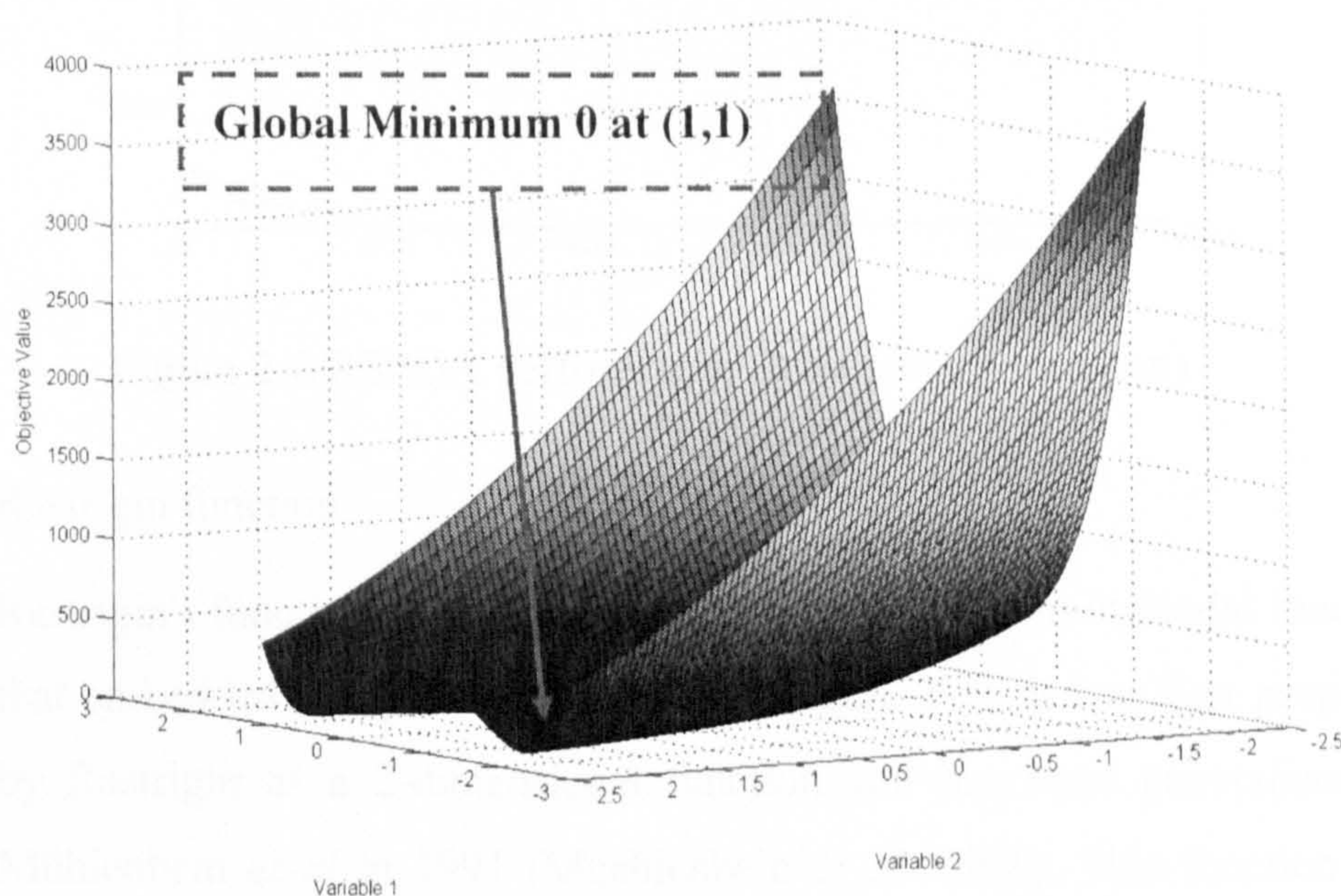


Figure 2-7 2-dimensional Rosenbrock function

The RSPGA optimization performance to the Rosenbrock function is shown in Figure 2-8. It can be seen that the optimization performance converges after 200 generations, and found the exact global optimal values of  $x_1 \sim x_n$ .



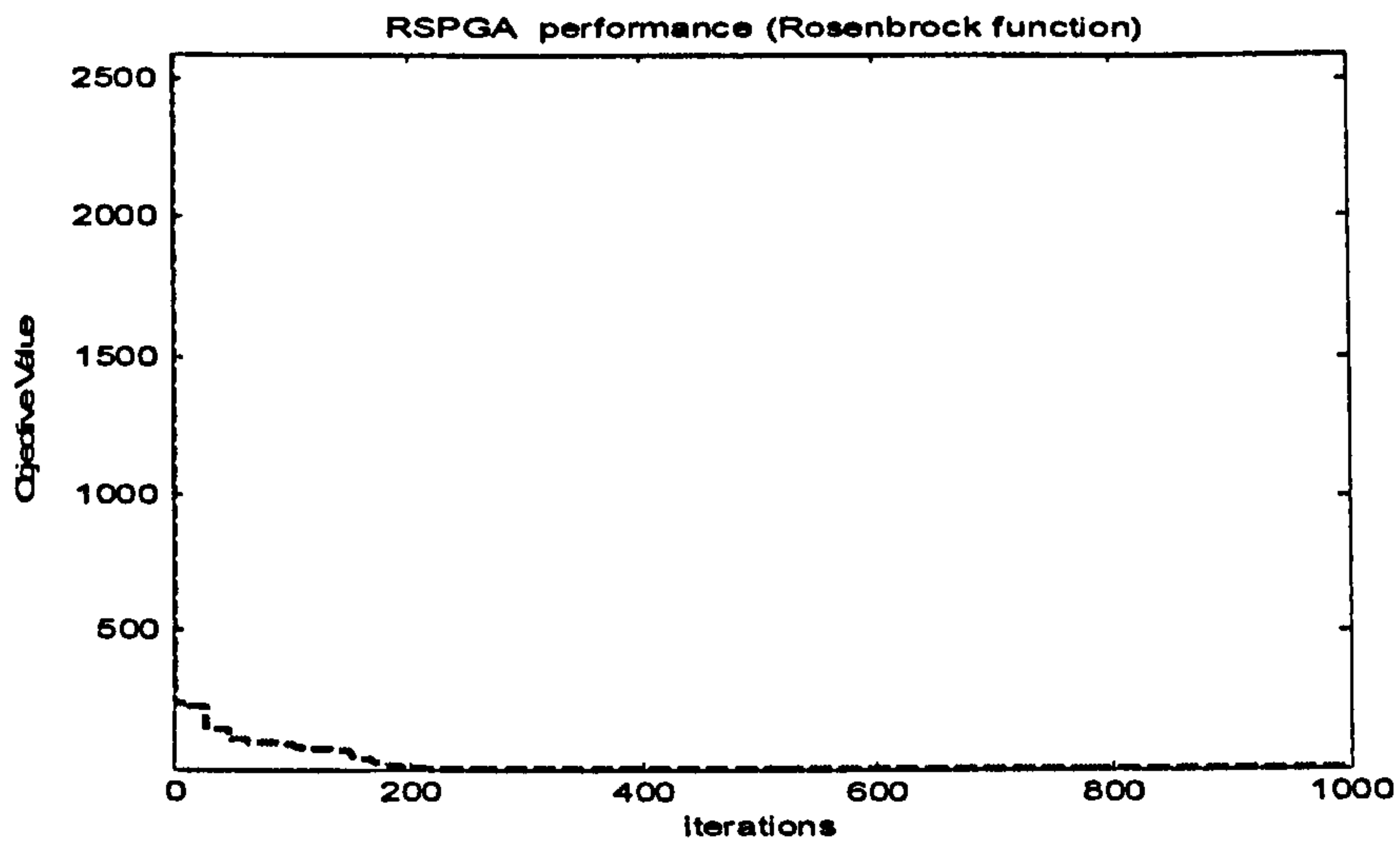


Figure 2-8 RSPGA performance (Rosenbrock function)

## 2. Rastrigin function

Rastrigin's function is a typical example of non-linear multimodal function that embedded many local minima (see Figure 2-9). It was first proposed by Rastrigin as a 2-dimensional function and has been generalized by Mühlenbein *et al* in 1991 (Muehlenbein *et al.* 1991). This function is a fairly difficult problem due to its large search space and its large number of local minima. The function equation is shown as follows:

$$f(\vec{X}) = 10 * n + \sum_{i=1}^n x_i^2 - 10 * \cos(2\pi * x_i) \quad (2-2)$$

where  $n$  is the dimension of the problem, and  $x_1 \sim x_n$  are the coefficients to be identified. The global minimum 0 is at the point that  $x_1 \sim x_n$  are all equal to 0. Similar to the Rosenbrock function, a ten dimensional Rastrigin's function is adopted for the simulation studies.



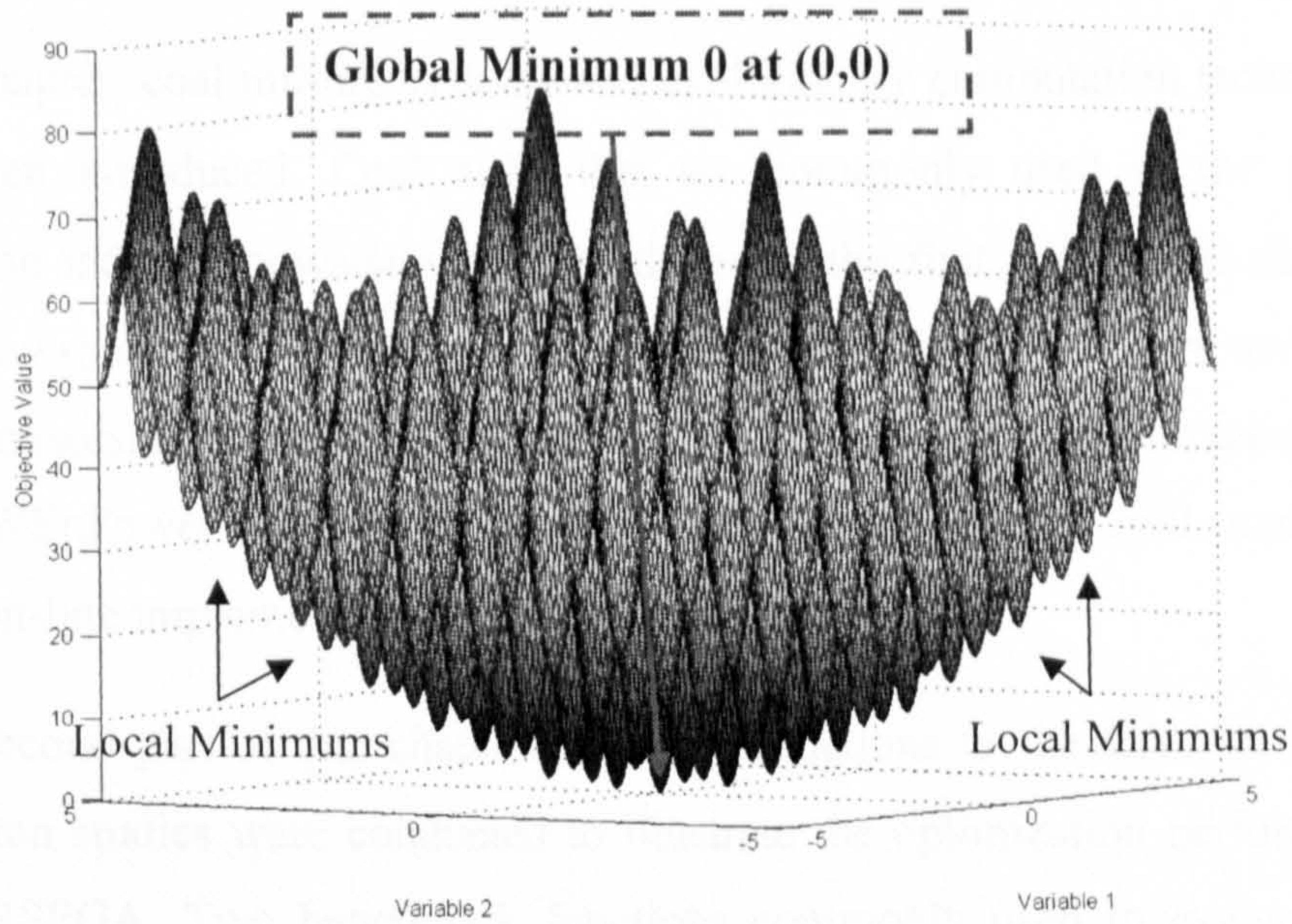


Figure 2-9 2-dimensional Rastrigin's function

The RSPGA optimization performance to the Rastrigin's function are shown in Figures 2-10. From the results, it can be seen that the RSPGA converges after 500 iterations, and obtain the exact global optimal values of  $x_1 \sim x_n$ .

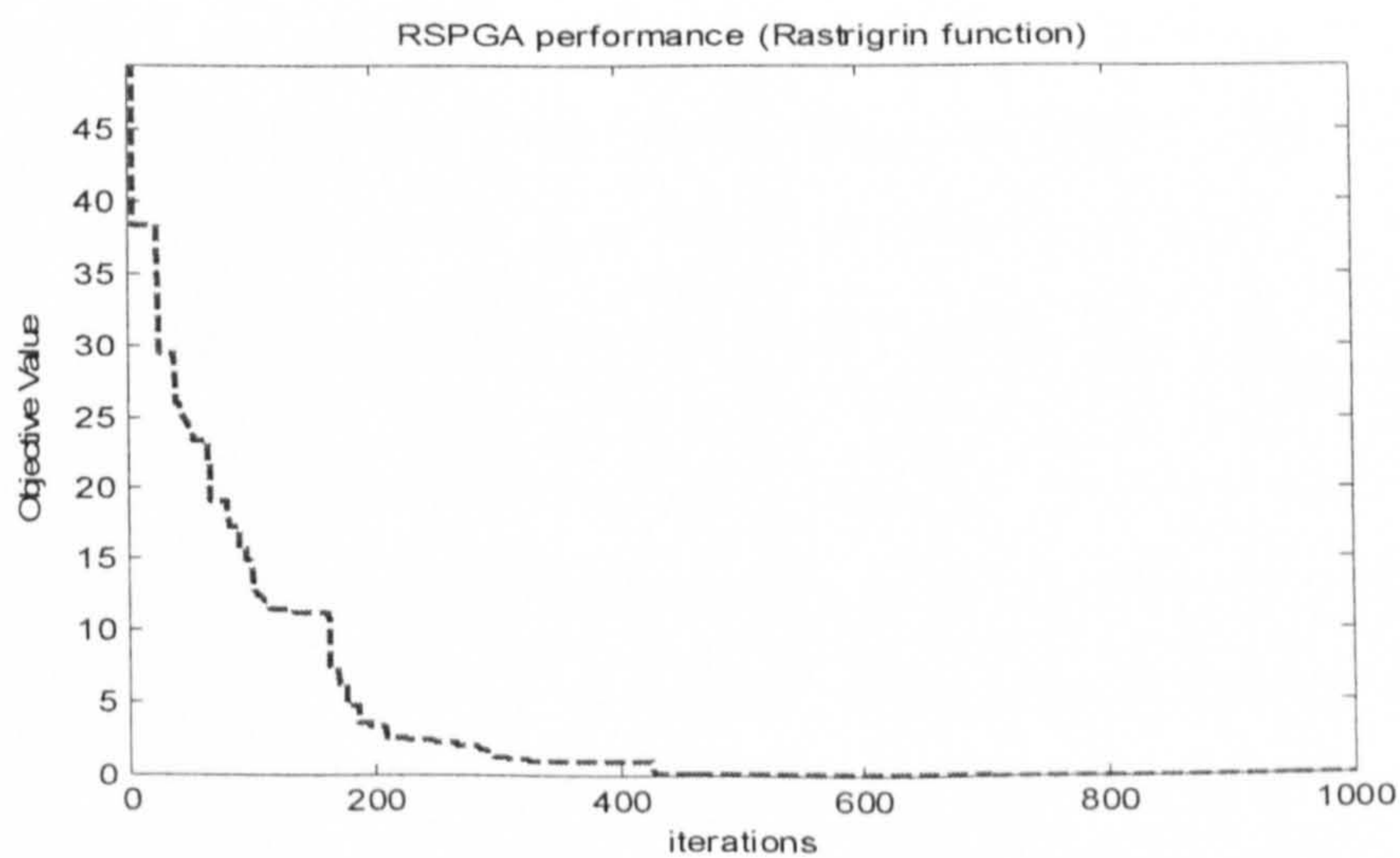


Figure 2-10 RSPGA performance (Rastrigin function)



## **2.4 Summary and Discussion**

In the chapter, coal milling systems and evolutionary computation techniques have been introduced. Coal mills that are commonly used in the power generation industry nowadays are introduced in the first part of this chapter, where low speed mills, medium speed mills and high speed mills are reviewed. With sponsorship from the RWEnPower Plc., the E-type medium speed mill from RWEnPower Plc. will be focused on in this project for mill modelling and its on-line implementation.

In the second part of this chapter, brief introductions to the GAs are given. Simulation studies were conducted to illustrate the optimization performance of the RSPGA. Two benchmark functions commonly used to evaluate the optimization performance of evolutionary computational technique are investigated for the studies. Simulation results showed that the RSPGA offer a good convergence rate and accurate final solutions.



## **Chapter 3**

# **Coal Mill Model for Normal Grinding Process**

### **3.1 Introduction**

The function of coal mills in power generation is to grind the large raw coal in order to supply dry and finely pulverised coal to the furnace for fast energy release. As mentioned earlier, a coal mill system has been received less attention from modelling and control specialists in power plants due to its high nonlinear multivariable features subject to uncertainties (Fan *et al.* 1994; Rees *et al.* 2003). At present, it is difficult to measure some variables related to many practical mill problems for improvement of its performance, for example, 1) there is lack of accurate measurement of mill PF flow thereby to control the air fuel ratio to maintain the efficiency of unit energy release and absorption and reducing environment emissions; 2) there is no accurate information for raw coal load in mill to prevent mill choking and coal caking during the grinding. Engineers in power plants will extremely welcome the ways for obtaining the information of those immeasurable variables.

A coal mill model for mill normal grinding process is developed and presented in this chapter. It provides a possible solution or an effective tool to obtain the information of those variables by a model based estimation method. It can predict the following immeasurable variables to a reasonably level of precision: the PF flow output, the amount of raw coal in mill, and all the states of the mill for better monitoring and controls in a power plant. The modelling procedure



used in the project is illustrated in Figure 3-1, which consists of the following steps:

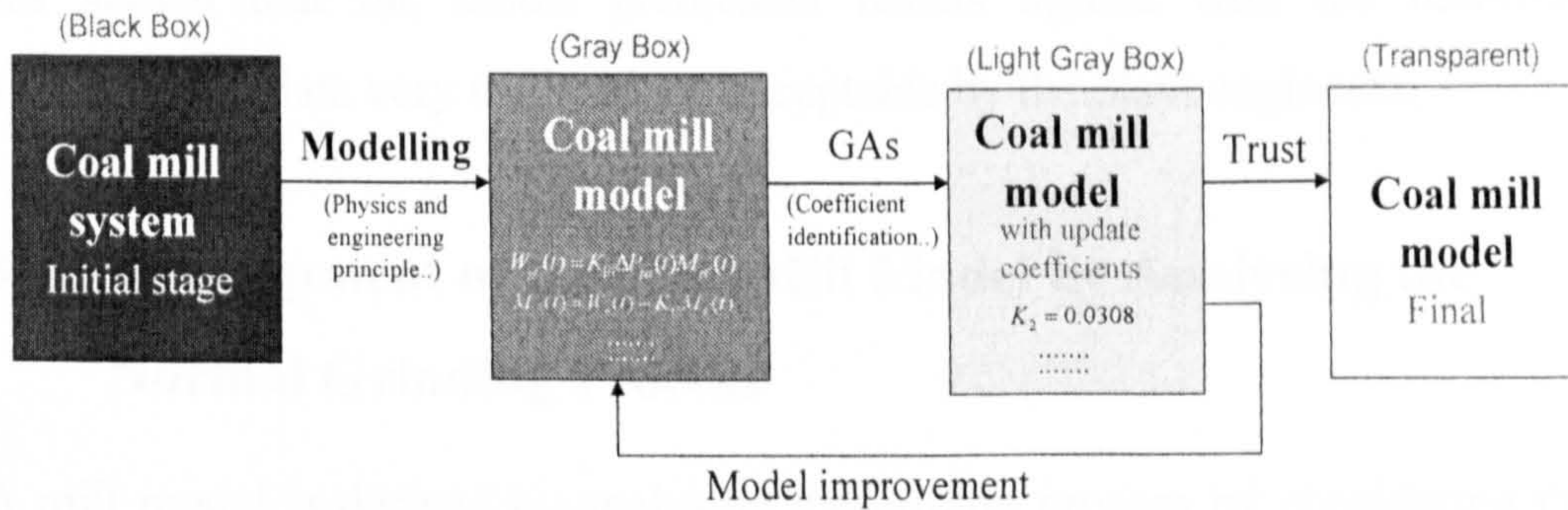


Figure 3-1 Demonstration of the coal mill modelling procedure

- 1) To derive the basic mill model dynamic equations through analysing the milling process, applying physics and engineering principles, and integrating the knowledge of experienced engineers;
- 2) To identify unknown parameters using evolutionary computation and system simulation techniques based on the on-site measurement data, where the range of the parameters are guided by the engineers' knowledge.
- 3) To analyse the simulation results and interpret the parameters identified through the discussions between the researchers and experienced engineers;
- 4) To improve the mill model equations and go back to Step 2 if any modification is required, or to conduct further simulation to validate the model and go back to Step 3.

The modelling work started from the initial version of the mill model developed at the University of Liverpool (Zhang 1999a, 1999b; Zhang *et al.* 2002). The early version of the mill model is then modified and improved by considering the thermal inertia term in the model. Over 10 sets of mill process



data has been collected for mill modelling and validation. The simulation results using the on-site measurement data are presented in the chapter, which has shown that the model predicated results agreed with the real-time measurement data very well and are acceptable by the plant engineers.

### **3.2 Development of the Coal Mill Model by Analysing the Normal Grinding Process**

A mill model is derived by analysing the milling process by considering the heat, load, and energy balance and applying the relevant engineering and physics principles. The procedure is described in this section in details.

#### **3.2.1 Identification of Input and Output Variables of the Process**

As introduced in the previous chapter, the E-type middle speed coal mill which equipped in RWEnPower Plc. (Didcot power station) is chosen as a prototype for model development in the project. A control system is employed by the RWEnPower Plc. as shown in Figure 3-2 in order to regulate the amount of pulverized fuel fed into the burners to meet the load requirements and to maintain optimum operation status of the mill. The system has three controllers, which are:

- 1) Control 1 regulates the coal feeder speed to maintain a predetermined relationship between the primary air differential pressure and the pressure drop across the mill. If too much or too little coal is delivered by the feeder, the mill will tend to increase or decrease the feeder's speed to fill it up with more or less coal. The resulting increase or decrease in the pressure drop across the mill will be corrected by the mill differential control (Control 2).



- 2) Control 2 is used to control the primary air fan. The demand of fuel is used to generate a desired-value signal for the primary air controller, which compares the demand with a signal derived from the differential pressure across a restriction in the primary air duct and the adjustments of the fan delivery accordingly.

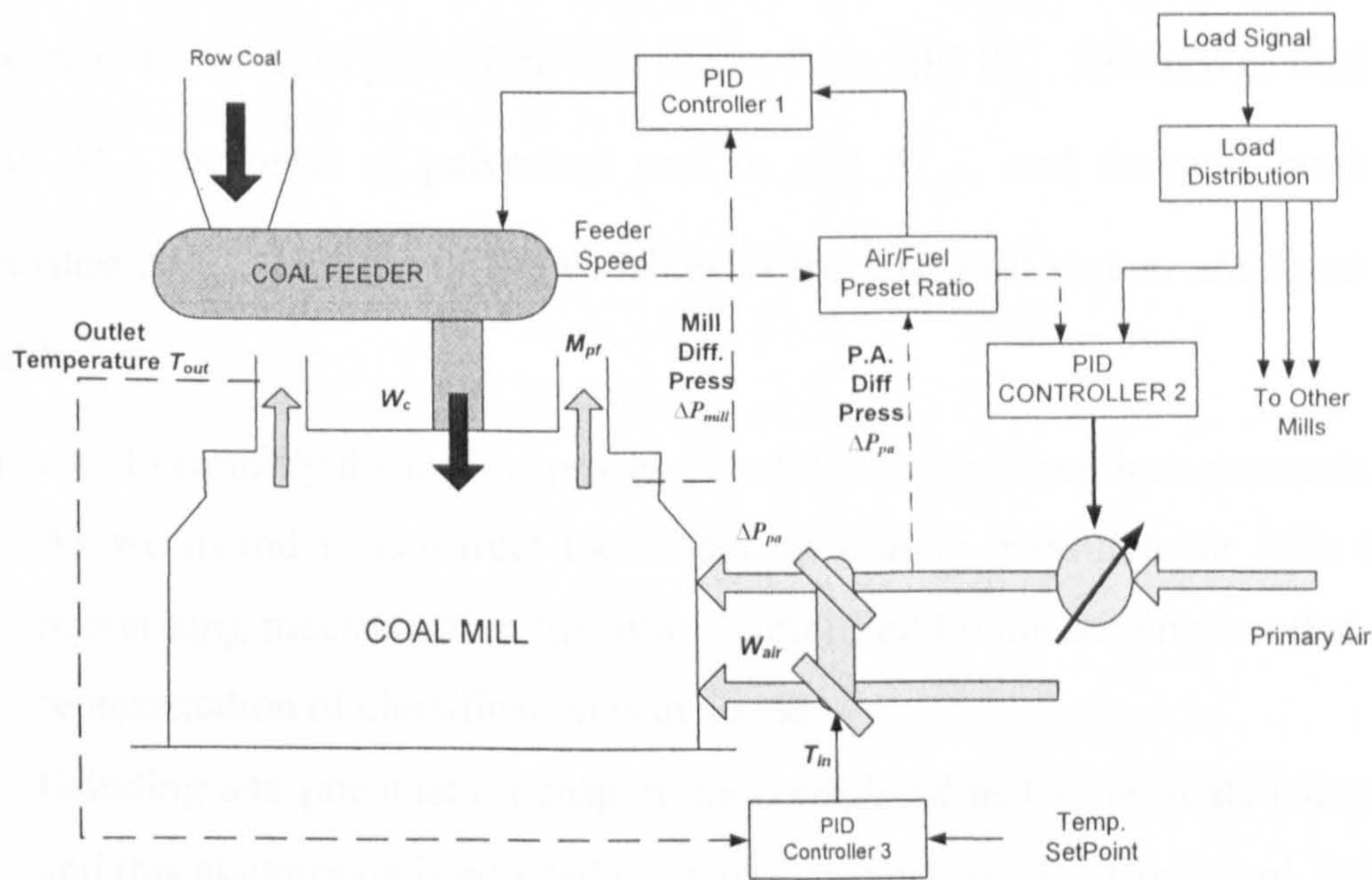


Figure 3-2 Coal mill control system

- 3) Control 3 is the temperature controller, which mixes cool tempering air with heated air to obtain the correct temperature. By controlling the air flow and the outlet temperature of the coal mill, it influences the burner's combustion efficiency, fly-ash quality etc.

For the purpose of mill modelling, the major measurable variables of the coal mill control system shown above are organized into system inputs and outputs. The input variables of this model are coal flow into the mill  $W_c$ , primary air pressure  $\Delta P_{pa}$ , and primary air inlet temperature  $T_{in}$ , which are used in practice as the control input to improve the coal mill performance; the output



variables are mill pressure  $\Delta P_{mill}$ , outlet temperature  $T_{out}$  and mill power consumed  $P$ , which are used as an indication to the control targets of mill operation. Some intermediated variables are introduced for modelling and those variables are not measurable from the power plants due to lack of suitable sensors or impossible for placement of sensors. Those variables are the mass flow rate of pulverized coal output from mill  $W_{pf}$ , the mass of coal in mill  $M_c$ , the mass of pulverised coal in mill  $M_{pf}$ , and the mill product pressure  $\Delta P_{mpd}$ . Full list of the variables of the coal mill system are listed in Table 3-1.

In order to simplify the milling process, the following assumptions are made:

- As we intend to construct the model on routine measurement data, the pulverizing mechanism in the mill is simplified by the assumption that no representation of classification is included.
- Grinding and pneumatic transport are considered as two separated stages, and this assumption is adopted in several research works (Corti *et al.* 1984; Zhang *et al.* 2002).
- To simplify the analysis, the size of coal in the mill is grouped into pulverised and un-pulverised two sets only.

### **3.2.2 Mass Flow Analysis**

As introduced in Chapter 2, the raw coal is fed into the coal mill for grinding by feeders. In Didcot Power Station, two different size feeders are in use, where the feeder speed  $F_s$  is measured in real time. Through experiment study in the power plant, the raw coal flow into the coal mill  $W_c$  is calculated by Equation (3-1).

$$W_c(t) = K_{fs} \cdot F_s(t) \quad (3-1)$$

where the value of  $K_{fs}$  is normally a constant for a certain period of mill operation but varies with respect to the size of different feeders. The values for  $K_{fs}$  provided by the engineers at the power plant are 0.16 kg/mm and 0.24 kg/mm respectively for the smaller feeder and the larger feeders that were equipped in the Didcot Power Station.

Table 3-1 List of coal mill model variables

Coal mill variables		
Input variables	Intermediate variables	Output variables
<ul style="list-style-type: none"> <li>- Coal flow into the mill <math>W_c</math></li> <li>- Primary air pressure into the mill <math>\Delta P_{pa}</math></li> <li>- Primary air temperature inlet the mill <math>T_{in}</math></li> </ul>	<ul style="list-style-type: none"> <li>- Mass of coal in mill <math>M_c</math></li> <li>- Mass of pulverised coal in mill <math>M_{pf}</math></li> <li>- Mill product pressure <math>\Delta P_{mpd}</math></li> <li>- Mass flow rate of pulverized coal out of mill <math>W_{pf}</math></li> </ul>	<ul style="list-style-type: none"> <li>- Mill pressure <math>\Delta P_{mill}</math></li> <li>- Mill outlet temperature <math>T_{out}</math></li> <li>- Mill power consumed <math>P</math></li> </ul>

The Primary Air (PA) fan is an important part of the coal mill system. It offers varied air flow in varied pressure from an electrically-driven fan. Right before the inlet duct into the coal mill, the primary air pressure  $\Delta P_{pa}(t)$  is measured on-site. From the fluid mechanism, the air wave inlet into the coal mil by the PA fan can be calculated by the following equation (Lu *et al.* 2002):

$$W_{air}(t) = K \cdot \sqrt{\Delta P_{pa}(t) \cdot \rho(t)} \quad (3-2)$$

where  $\rho(t)$  denotes the primary air density ( $kg/m^3$ ) and  $K$  is a constant. Combining with the ideal gas law,  $\rho(t)$  at the temperature  $T_{in}(t)$  can be



represented by  $\frac{273}{273+T_{in}(t)} \cdot \frac{28.8}{22.4}$ . The hot air flow into the coal mill delivered by the Primary Air (PA) fan therefore can be calculated by Equation (3-3), where the PA flow rate is related to the PA differential pressure and the density of air at the mill inlet temperature  $T_{in}$ .

$$W_{air}(t) = 10 \cdot \sqrt{\Delta P_{pa}(t) \cdot \frac{273}{273+T_{in}(t)} \cdot \frac{28.8}{22.4}} \quad (3-3)$$

As the assumptions made at the beginning of this chapter, the coal in mill is classified as pulverised and un-pulverised two categories only, and also the grinding and the transport are considered as two separate status, the dynamic process of coal mass flow during the mill operation can, therefore, be schematically illustrated by Figure 3-3. The raw coal is fed into the mill by a feeder for grinding at a mass flow rate of  $W_c$ . Due to the gravity, the raw coal  $M_c$  normally stays in the bottom of the coal mill, and then is ground through a grinding mechanism of the mill. When the raw coal is pulverized to the pulverised coal  $M_{pf}$ , it floats in the air due to high pressure circulating hot primary air injected. The pulverized coal will be blow out the mill from the outlet port to the furnace at a flow rate of  $W_{pf}$ . From the mass balance point of view, the total mass of the pulverised coal output from the mill at a flow rate  $W_{pf}$  should be equal to the total mass of the raw coal mill flowing into the mill at a flow rate  $W_c$  eventually.



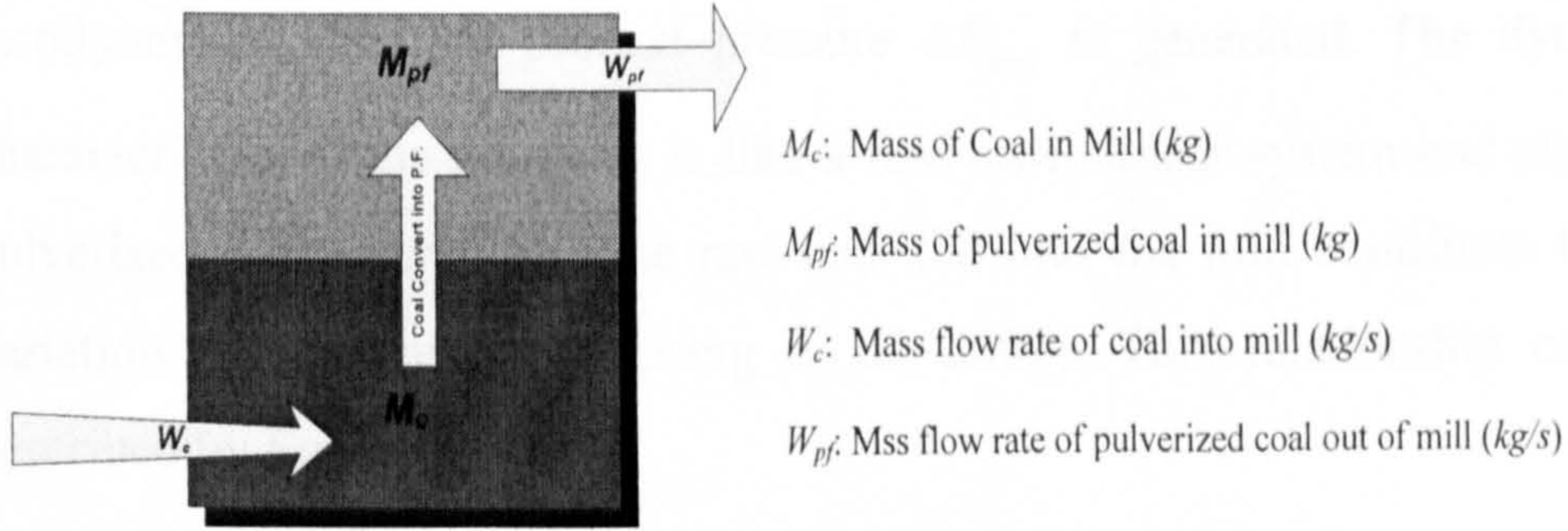


Figure 3-3 Dynamic process of coal flow

Based on the principle of mass balance, Equations (3-4) ~ (3-6) are derived.

$$W_{pf}(t) = K_{16} \Delta P_{pa}(t) M_{pf}(t) \quad (3-4)$$

$$\dot{M}_c(t) = W_c(t) - K_{15} M_c(t) \quad (3-5)$$

$$\dot{M}_{pf}(t) = K_{15} M_c(t) - W_{pf}(t) \quad (3-6)$$

Equation (3-4) represents that the flow rate of PF (pulverized fuel) out of mill  $W_{pf}(t)$  by the primary air flow is proportional to the mass of pulverized coal in mill  $M_{pf}(t)$  and the differential pressure produced by the primary air fan  $\Delta P_{pa}(t)$ . Equation (3-5) represents that the changes of mass of coal in the mill  $\dot{M}_c(t)$  is proportional to the difference between the coal flow into mill  $W_c(t)$  and a fraction of the coal pulverized  $K_{15} M_c(t)$ . Equation (3-6) describes that the changes of mass of pulverized fuel in mill  $\dot{M}_{pf}(t)$  is proportional to the difference between the fraction of pulverized coal  $K_{15} M_c(t)$  and the pulverized coal flow out from the mill  $W_{pf}(t)$ .

### 3.2.3 Mill Product Pressure

While the coal mill operates at the grinding status, the grinding mechanism rotates at a high speed (around 130 rpm). Due to the influence of



aerodynamics, the mill product pressure  $\Delta P_{mpd}$  is generated. The dynamic characteristics of the pressures is like a first order linear system and also the pulverised coal in mill and the raw coal fed into the mill contribute to the variation of the pressures (Zhang *et al.* 2002). This relationship can be described by Equation (3-7).

$$\Delta \dot{P}_{mpd}(t) = K_{11}M_{pf}(t) + K_{12}M_c(t) - K_{13}\Delta P_{mpd}(t) \quad (3-7)$$

where  $K_{11}$ ,  $K_{12}$  and  $K_{13}$  are unknown coefficients to be identified.

As introduced earlier in the chapter, the primary air with a pressure  $\Delta P_{pa}$  is injected from the bottom of the coal mill for circulating the pulverised coal in order to be transported to the outlet of the mill. By combining the mill product pressure  $\Delta P_{mpd}$  with the inlet primary air pressure  $\Delta P_{pa}$ , we can derive the mill pressure. The pressure is proportional to the primary air pressure  $\Delta P_{pa}$  and the mill product pressure  $\Delta P_{mpd}$ , which can be represented by the following equation:

$$\Delta P_{mill}(t) = K_9\Delta P_{pa}(t) + \Delta P_{mpd}(t) \quad (3-8)$$

where  $K_9$  is an unknown coefficient to be identified.

### **3.2.4 Power Consumption Analysis**

The power consumed by the coal mill is normally considered as an indicator to the amount of load (raw coal and pulverized coal) of the coal mill, which is measured by the mill current for rotating and grinding. It consists of three terms, which are: a) mill current required to rotate in the pulverised air; b) mill current to pulverise coal; and c) mill current to run empty mill (using the term of  $K_8$ ). Equation (3-9) describes the relationship.



$$P(t) = K_6 M_{pf}(t) + K_7 M_c(t) + K_8 \quad (3-9)$$

where  $K_6$  and  $K_7$  are the unknown coefficients to be identified and the empty mill current  $K_8$  needs to be identified as well.

### 3.2.5 Thermodynamic Process

Distinguishing from the mineral pulverisers, the coal mills in power plants are involved with thermodynamics. The hot primary air is blown into the mill from the bottom location of the coal mill to heat and dry the raw coal for easier grinding and efficient combustion of PF in the furnace. If the coal mill thermodynamic process is treated as happening in an isolated environment as shown in Figure 3-4, the heat input into the coal mill and the heat output from the coal mill complies with the heat balance rule. The heat into the coal mill  $Q_m$  includes the heat from raw coal  $Q_{coal}$ , the heat from hot primary air  $Q_{air}$  and the heat generated by the power consumes in grinding and rotating  $Q_p$ . The heat out from the coal mill  $Q_{out}$  includes: the heat outlet in the pulverised coal  $Q_{PF}$  and the heat emitted from the mill body to the environment  $Q_e$ .

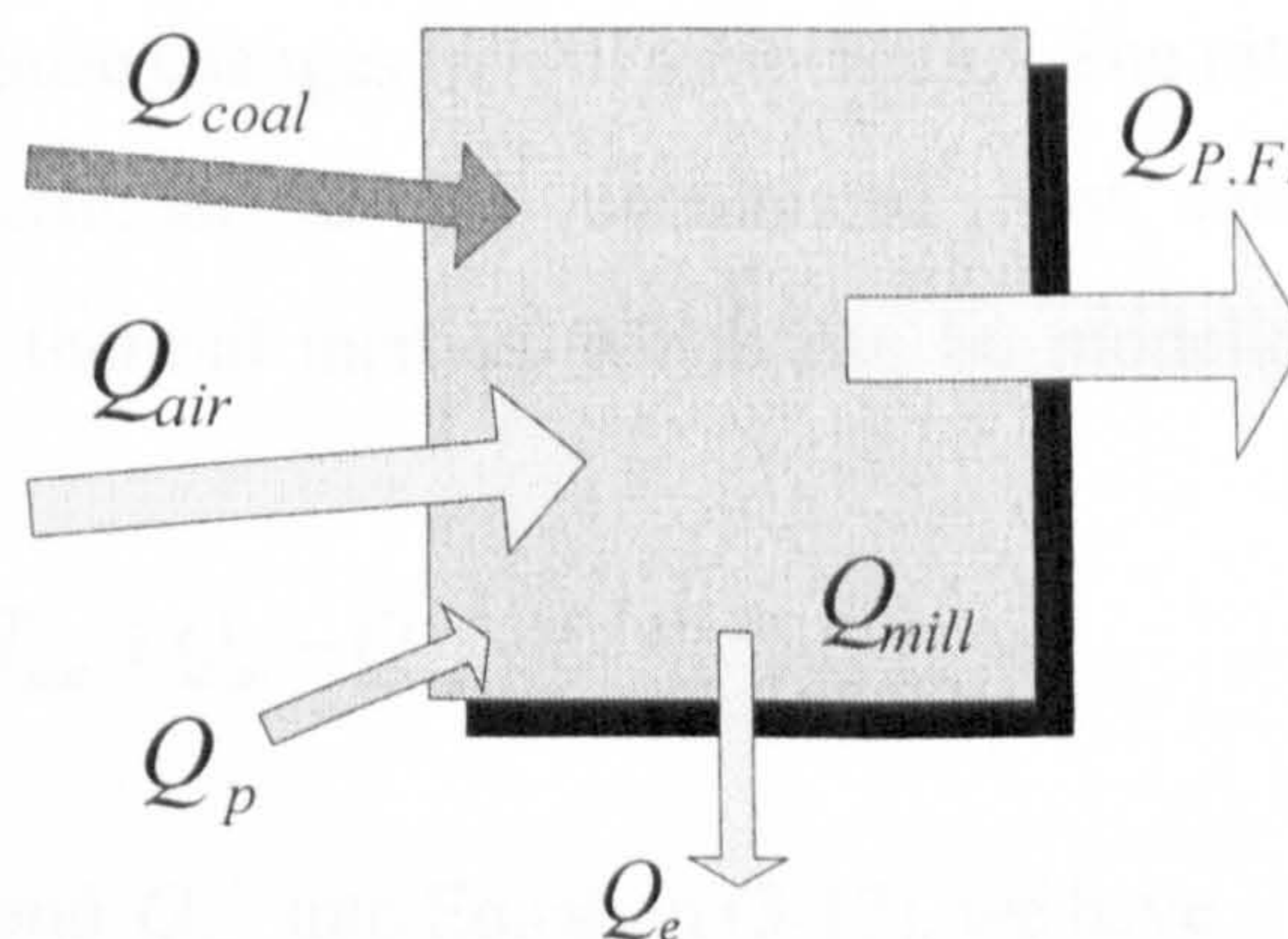


Figure 3-4 Coal mill heat balance illustration

The heat into the coal mill  $Q_m$  can be obtained through Equation (3-10),



where the heat of primary air into the mill  $Q_{air}$  is calculated by the terms  $K_1 T_{in} W_{air} + K_2 W_{air}$ ; the heat generated by the coal grinding process  $Q_p$  is represented by the term  $K_{14} P$ ; and the heat of raw coal bringing into the mill  $Q_{coal}$  is described by the term  $K_3 W_c$ .

$$\begin{aligned} Q_{in} &= Q_{air} + Q_p + Q_{coal} \\ &= [K_1 T_{in}(t) + K_2] W_{air}(t) + K_{14} P(t) + K_3 W_c(t) \end{aligned} \quad (3-10)$$

The heat output from the coal mill  $Q_{out}$  can be obtained by Equation (3-11), where the heat lost from the pulverised coal  $Q_{PF}$  is described by  $K_4 T_{out}(t) \cdot [W_{air}(t) + W_c(t)] + K_5 \cdot [W_{air}(t) + W_c(t)]$ , and the heat emitted from the mill body to the environment  $Q_e$  is ignored at the moment as it has little effects onto the heart balance comparing with the other terms.

$$\begin{aligned} Q_{out} &= Q_{P.F.} + Q_e \\ &= K_4 T_{out}(t) \cdot [W_{air}(t) + W_c(t)] + K_5 \cdot [W_{air}(t) + W_c(t)] \end{aligned} \quad (3-11)$$

From the knowledge of thermodynamics, the difference between the input and output heat will cause changes in mill temperature. The rate of the temperature change is proportional to the unbalanced heat and also shows the characteristics of thermal inertias, which can be modelled by the following equation:

$$\dot{T}_{out} \propto K_t T_{out} + Q_{in} - Q_{out} \quad (3-12)$$

Substituting  $Q_{in}$  and  $Q_{out}$  into Equation (3-12), we have

$$\begin{aligned} \dot{T}_{out} &= [K_1 T_{in}(t) + K_2] W_{air}(t) + K_{14} P(t) - K_3 W_c(t) - \\ &\quad [K_4 T_{out}(t) + K_5] \cdot [W_{air}(t) + W_c(t)] + K_t T_{out} \end{aligned} \quad (3-13)$$

where the notation of  $K_3$  has a negative sign to indicate that the input coal  $W_c$  absorbs the heat from the mill instead of radiating heat.

### 3.2.6 Mathematical Model of the Milling Process

Based on the mass balance, heat balance and some other engineering experience introduced in previous sections, the coal mill model for the complete milling process is derived as Equations (3-14) ~ (3-22).

$$W_{air}(t) = 10 \cdot \sqrt{\Delta P_{pa}(t) \cdot \frac{273}{273 + T_{in}(t)} \cdot \frac{28.8}{22.4}} \quad (3-14)$$

$$W_c(t) = K_{fs} \cdot F(t)_s \quad (3-15)$$

$$W_{pf}(t) = K_{16} \Delta P_{pa}(t) M_{pf}(t) \quad (3-16)$$

$$\dot{M}_c(t) = W_c(t) - K_{15} M_c(t) \quad (3-17)$$

$$\dot{M}_{pf}(t) = K_{15} M_c(t) - W_{pf}(t) \quad (3-18)$$

$$P(t) = K_6 M_{pf}(t) + K_7 M_c(t) + K_8 \quad (3-19)$$

$$\Delta P_{mill}(t) = K_9 \Delta P_{pa}(t) + \Delta P_{mpd}(t) \quad (3-20)$$

$$\Delta \dot{P}_{mpd}(t) = K_{11} M_{pf}(t) + K_{12} M_c(t) - K_{13} \Delta P_{mpd}(t) \quad (3-21)$$

$$\begin{aligned} \dot{T}_{out} = & [K_1 T_{in}(t) + K_2] W_{air}(t) + K_{14} P(t) - K_3 W_c(t) - \\ & [K_4 T_{out}(t) + K_5] \cdot [W_{air}(t) + W_c(t)] + K_1 T_{out} \end{aligned} \quad (3-22)$$

There are sixteen unknown parameters shown in the above equations which are required to be identified using on-site measurement data and intelligent algorithms. This model improved the early version of the mill model proposed by Zhang ((Zhang *et al.* 2002).



### **3.3 Model Parameter Identification**

In this section, the parameter identification procedure will be described and the simulation results will be presented. The data used for identification is provided by RWEnPower Plc. which covers mill processes working under different operational conditions and at different time periods. The RSPGA that discussed in previous chapter is applied for the coal mill model coefficients identification.

#### **3.3.1 Description of On-Site Measurement Data**

On-site measurement data in the thesis refers to the data obtained while the mill is in use and works at normal working conditions. That is, no any sets of data are obtained at a designed operation manner. Five sets of on-site measurement data from five different mills listed in Table 3-2 which are used in this section.

Table 3-2 Five on-site measurement data sets

<b>Data Sets</b>	<b>Descriptions</b>
Data 1	Mill A 13 <sup>th</sup> Nov 2002 12:49:10 ~ 13:34:10
Data 2	Mill B 13 <sup>th</sup> Nov 2002 15:20:18 ~ 15:44:23
Data 3	Mill C 13 <sup>th</sup> Nov 2002 15:50:22 ~ 16:54:57
Data 4	Mill G 13 <sup>th</sup> Nov 2002 11:08:04 ~ 15:43:49
Data 5	Mill F 13 <sup>th</sup> Nov 2002 10:16:40 ~ 14:56:21

All these five data sets were collected at the normal grinding processes of the coal mills at Didcot Power Station (RWEnPower Plc.), which do not include

the data for start-up and shut-down. Data set 1 is used for identification of model parameters and Data sets 2 ~ 5 are adopted for the verifications of the identified parameters.

### **3.3.2 Identification of Model Coefficients Using RSPGA**

As an optimisation method, GA has the advantage that it is able to reach an optimal solution without requiring explicit knowledge about the problem area. It has been verified that GA is a robust optimization method for the parameter identification problems (Karr 1993; Wang *et al.* 2004; Rashtchi *et al.* 2006). The only existing criterion to evaluate the quality of an individual is the fitness value associated with this individual (Mitchell 1996). Hence, the fitness function should provide the required information for GA to make decision. Fitness functions with different mathematical structures are used in GAs which is subject to the minimal requirement that the function can map the population into a partially ordered set. As stated, the fitness function is independent to the GA but greatly dependent on the problem itself. Traditionally, the statistical expectation of Mean Squared Errors (MSE) is widely used to construct fitness functions, which is reasonably effective for static optimisation cases. However, this fitness function may not give a convergent solution while used in the cases of the dynamic processes. Further investigation is, therefore, motivated to improve the convergence of the algorithm. After a number of different fitness functions were studied, it was found that one particular fitness function gives the algorithm a good convergence and leads to more accurate solutions, which is the sum of absolute values of errors between the measured and simulated data (Wei *et al.* 2004a).



Define

$$e_1(t) = {}^n T_{out}(t) - {}^n \hat{T}_{out}(t) = \frac{T_{out}(t)}{TopR_{T_{out}}} - \frac{\hat{T}_{out}(t)}{TopR_{T_{out}}} \quad (3-23)$$

$$e_2(t) = {}^n P(t) - {}^n \hat{P}(t) = \frac{P(t)}{TopR_P} - \frac{\hat{P}(t)}{TopR_P} \quad (3-24)$$

$$e_3(t) = {}^n \Delta P_{mill}(t) - {}^n \Delta \hat{P}_{mill}(t) = \frac{\Delta P_{mill}(t)}{TopR_{\Delta P_{mill}}} - \frac{\Delta \hat{P}_{mill}(t)}{TopR_{\Delta P_{mill}}} \quad (3-25)$$

Then the fitness function is defined as follows:

$$fitness = \frac{1}{N} \sum_{t=0}^N \{ W_1 \times |e_1(t)| + W_2 \times |e_2(t)| + W_3 \times |e_3(t)| \} \quad (3-26)$$

where the symbols used in the above fitness functions are explained below:

${}^n \hat{T}_{out}(t), {}^n \hat{P}(t), {}^n \Delta \hat{P}_{mill}(t)$	Normalized simulated outputs of the mill model at time t.
${}^n T_{out}(t), {}^n P(t), {}^n \Delta P_{mill}(t)$	Normalized measured outputs of the mill model at time t.
$T_{out}(t), P(t), \Delta P_{mill}(t)$	Measured outputs of the mill model at time t.
$\hat{T}_{out}(t), \hat{P}(t), \Delta \hat{P}_{mill}(t)$	Simulated outputs of the mill at mill model at time t.
$TopR_{T_{out}}, TopR_P, TopR_{\Delta P_{mill}}$	Top ranges of the variables.
$W_1, W_2, W_3$	Weighting coefficients.
$N$	Number of measured data points.

Following the identification procedure shown in Figure 3-5, Data set 1 in Table 3-2 is employed as measured inputs and outputs, and the real-value SPGA described in Table 3-4 is adopted for the coefficient identification of the coal mill model. The sixteen unknown parameters are identified and listed in Table 3-5.



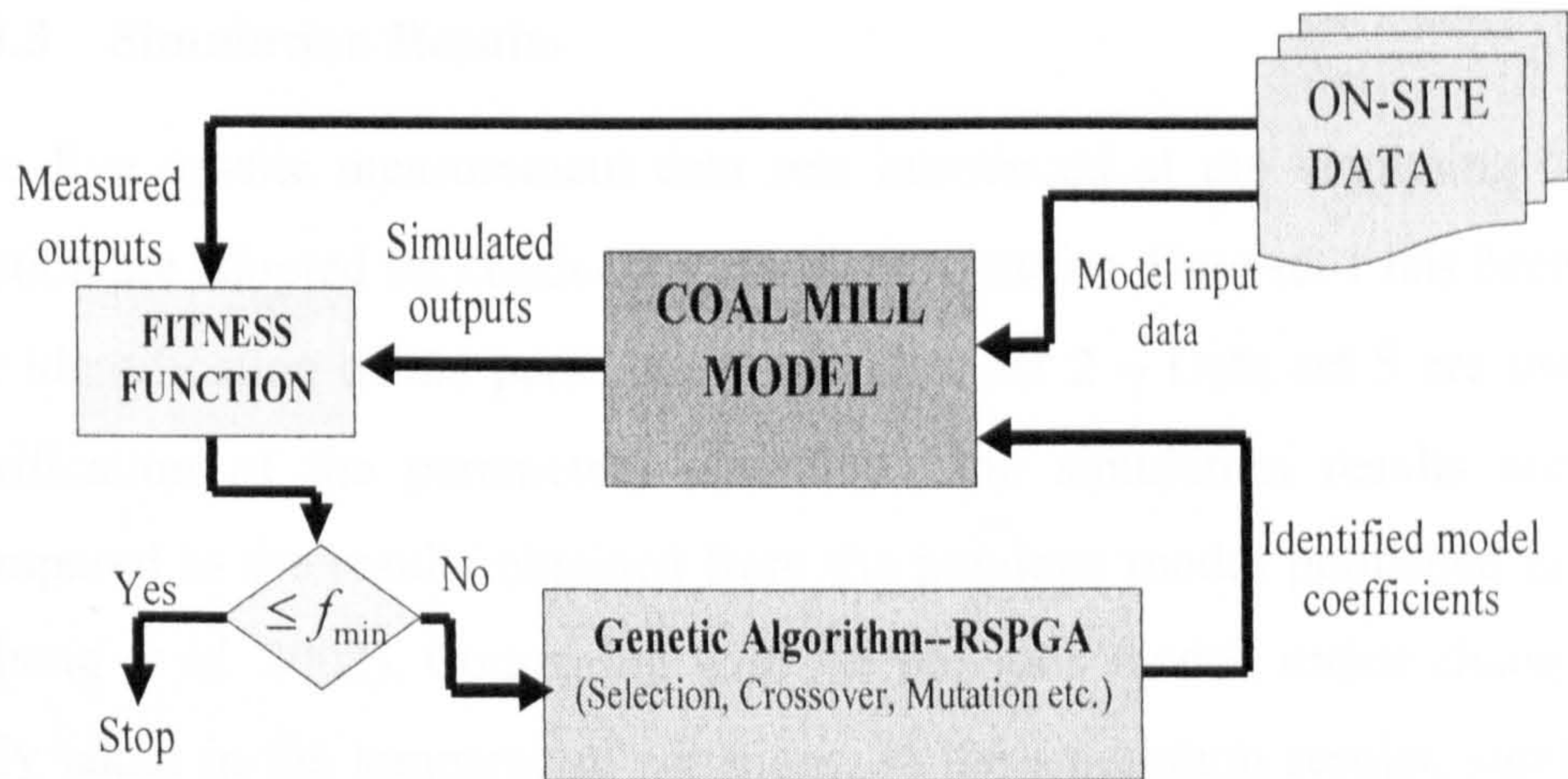


Figure 3-5 The coal mill model coefficients identification procedure

Table 3-3 Identified system parameters

System parameter using the modified mill model	
$K_1 = 0.000294$	$K_2 = 0.030822$
$K_3 = 0.002060$	$K_4 = 0.001677$
$K_5 = -0.043197$	$K_6 = 0.016553$
$K_7 = 0.017409$	$K_8 = 27.128681$
$K_9 = 2.619964$	$K_{11} = 0.004065$
$K_{12} = 0.000680$	$K_{13} = 0.058879$
$K_{14} = 0.01474969$	$K_{15} = 0.007422$
$K_{16} = 0.006284$	$K_l = -0.023677$
System parameter using the original mill model (Zhang <i>et al.</i> 2002)	
$K_1 = 0.000613$	$K_4 = 0.035083$
$K_3 = 0.036576$	$K_4 = 0.001305$
$K_6 = 0.054367$	$K_7 = 0.005450$
$K_8 = 27.758520$	$K_9 = 7.410860$
$K_{11} = 0.001948$	$K_{12} = 0.000430$
$K_{13} = 0.075413$	$K_{14} = 0.001669$
$K_{15} = 0.010552$	$K_{16} = 0.005452$



### 3.3.3 Simulation Results

The five on-site measurement data sets introduced at the beginning of this section are adopted for conducting simulation studies. Data set 1 has been used for identification of the parameters, and Data set 2 ~ Data set 5 are used for verification of the parameters identified. The simulation results are then compared to the results obtained from the previous model published in 2002 (Zhang *et al.* 2002). Comparing with the previous model, major changes are only taken in the temperature equations. In the simulation results, significant improvements are happened in approaching the model simulated  $T_{out}$  to its measured values. For the other two model output variables ( $P, \Delta P_{mill}$ ), only slightly improvement are gained accordingly. Figure 3-6 ~ Figure 3-12 show the validation results of the model  $T_{out}$  from using Data 2 ~ Data 5.

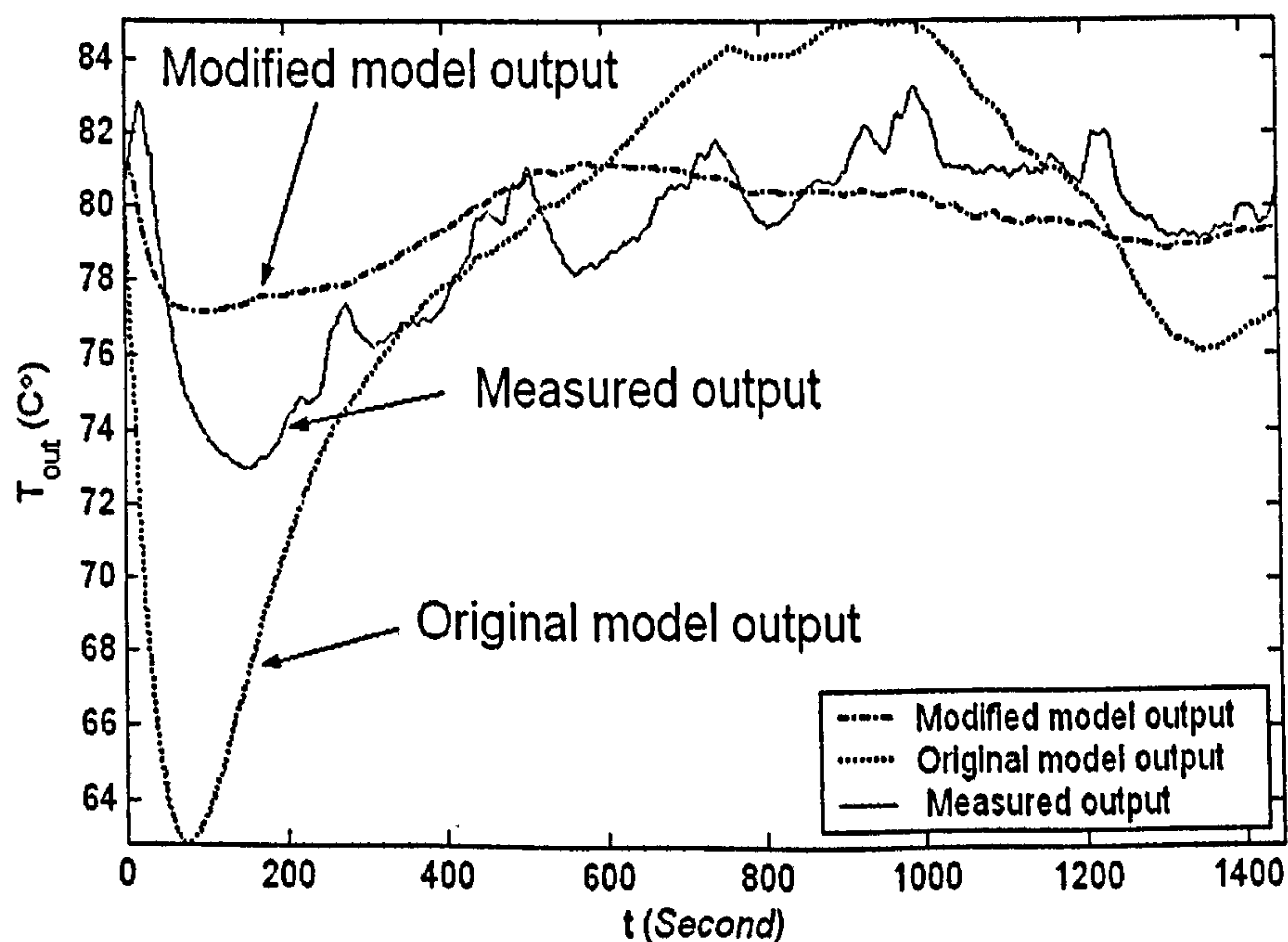


Figure 3-6 The measured and simulated results using Data 2

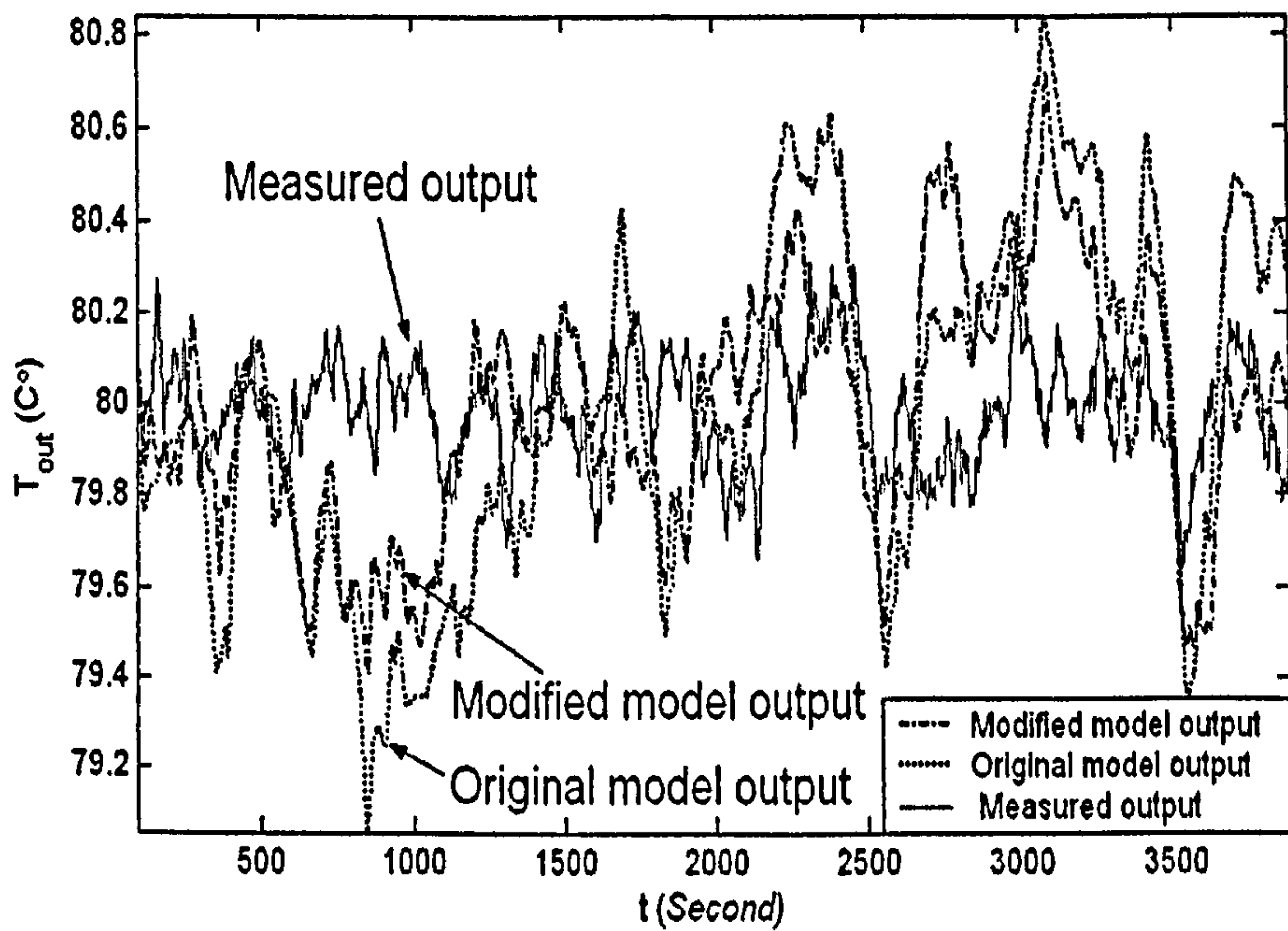


Figure 3-7 The measured and simulated results using Data 3

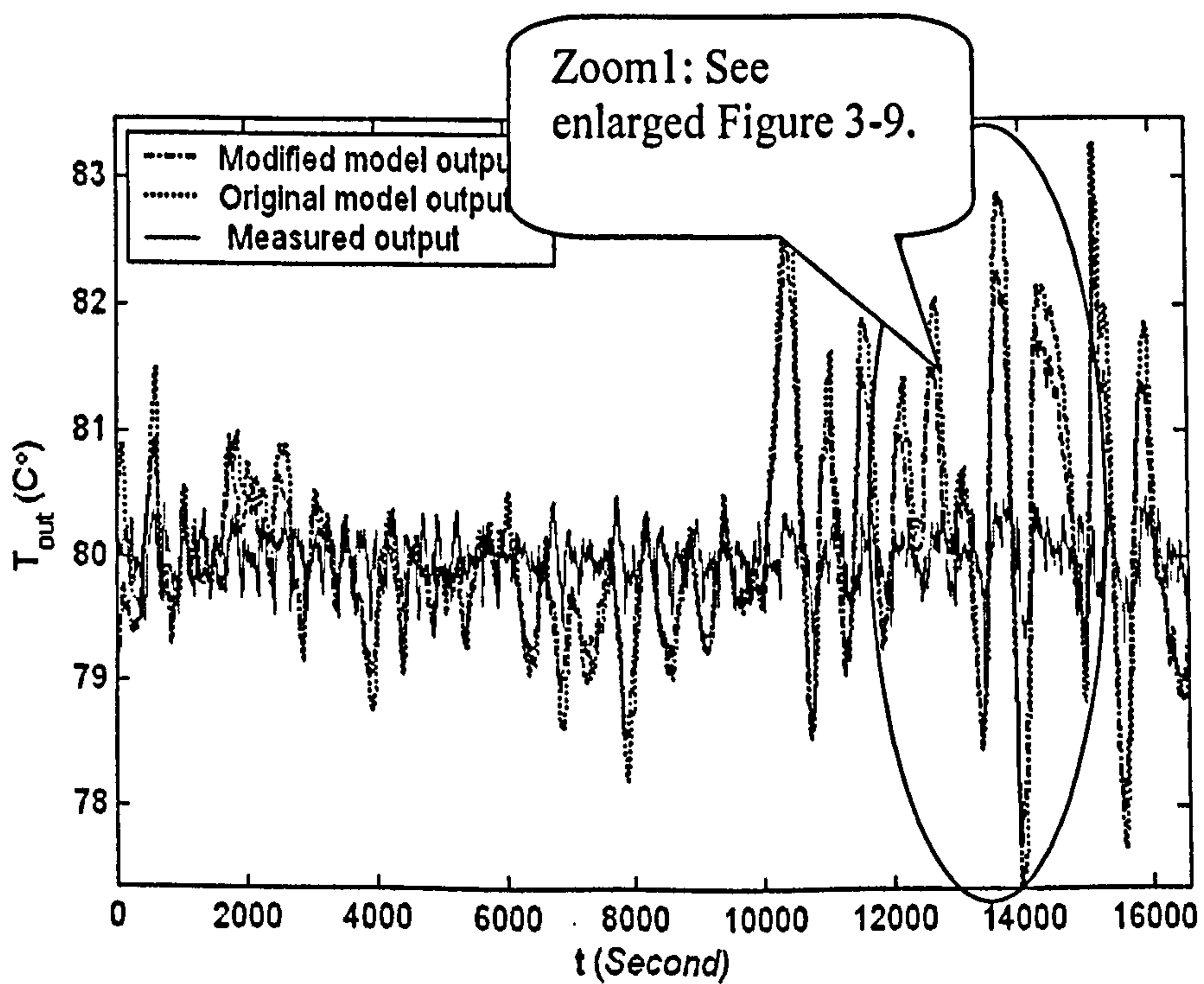


Figure 3-8 The measured and simulated results using Data 4



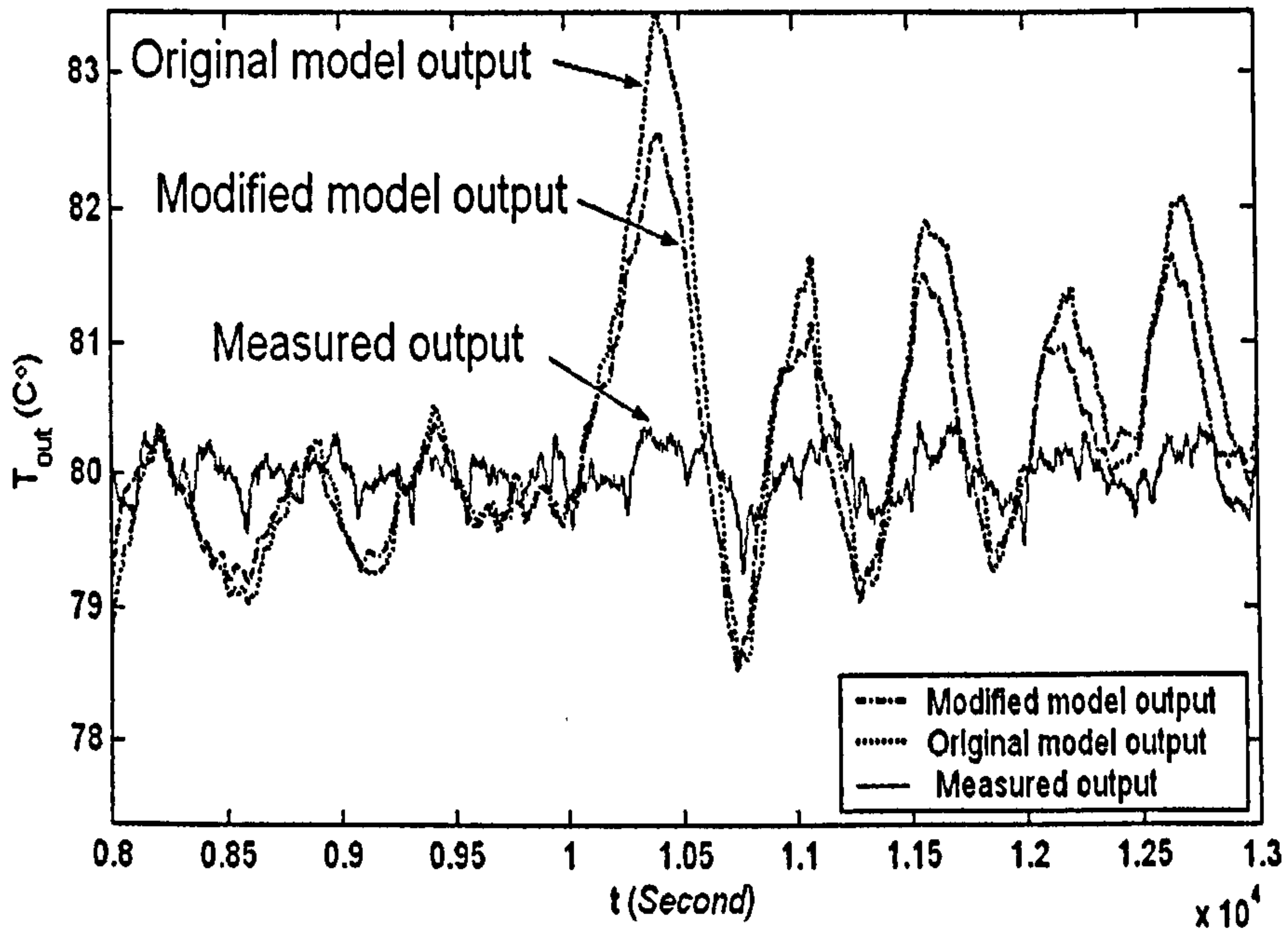


Figure 3-9 Partly enlarged figure of the measured and simulated results using Data 4

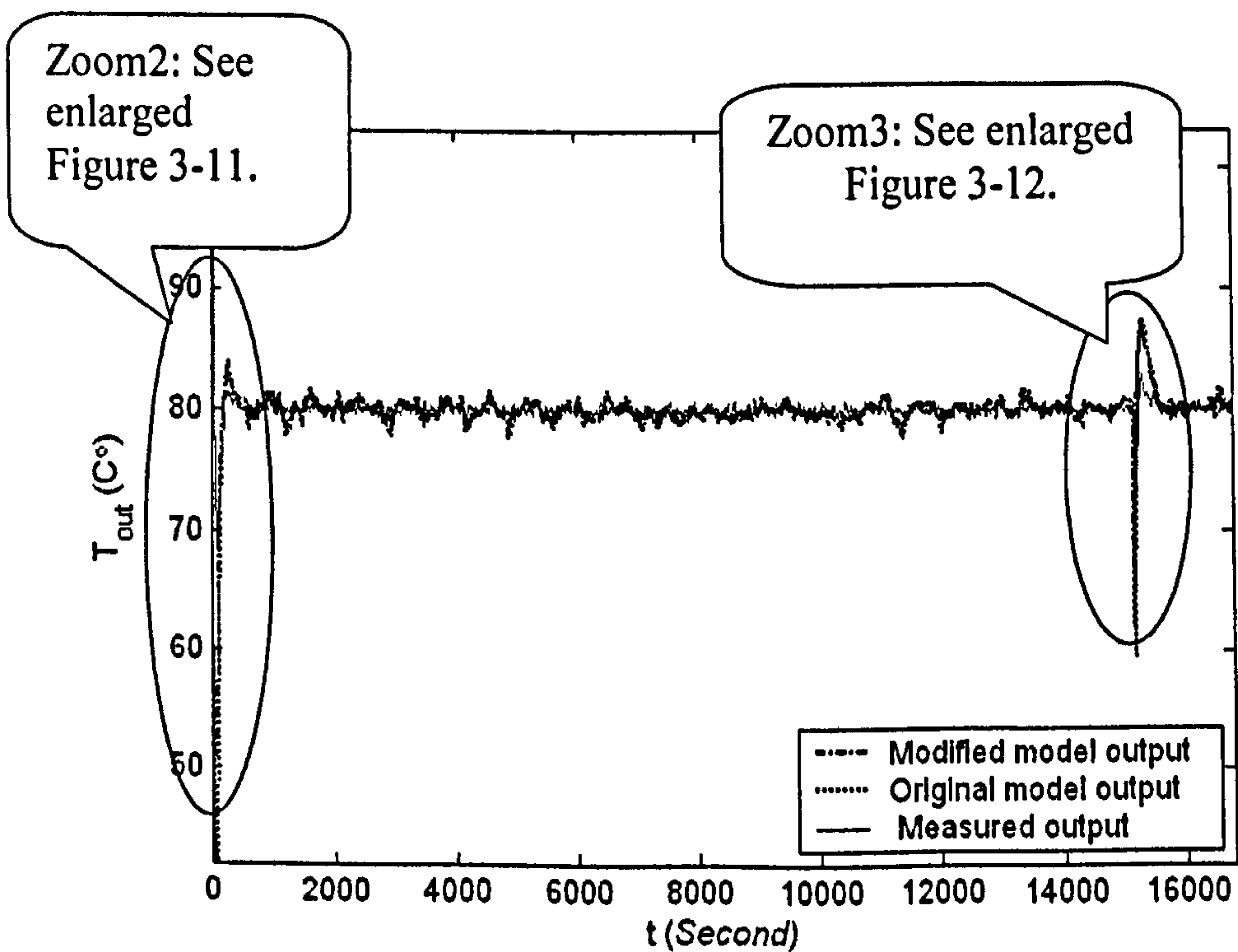


Figure 3-10 The measured and simulated results using Data set 5  
Mill F, 7<sup>th</sup> Mar 2003 10:16:40 ~ 14:56:21

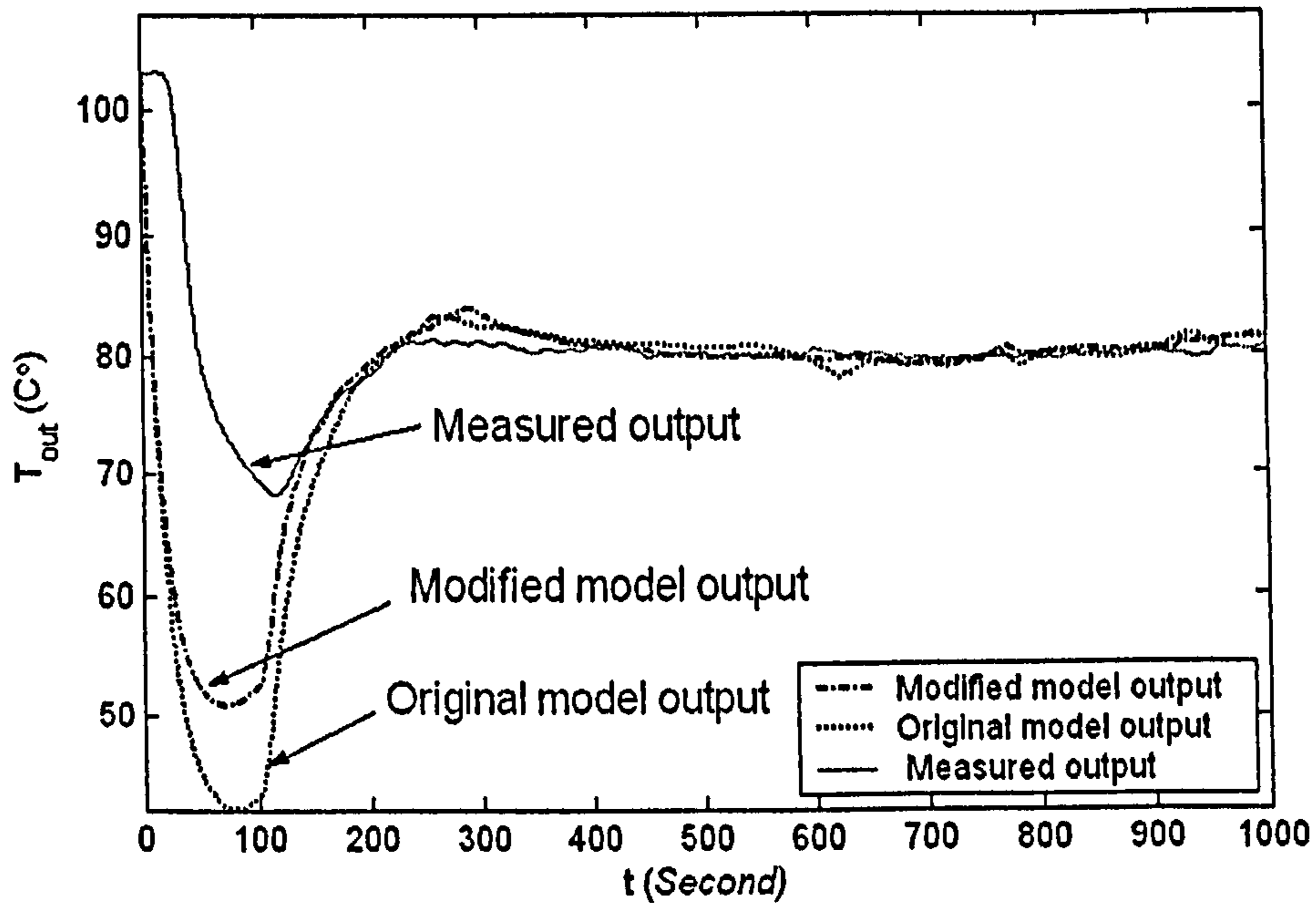


Figure 3-11 Partly enlarged figure 2 of the measured and simulated results using Data 5

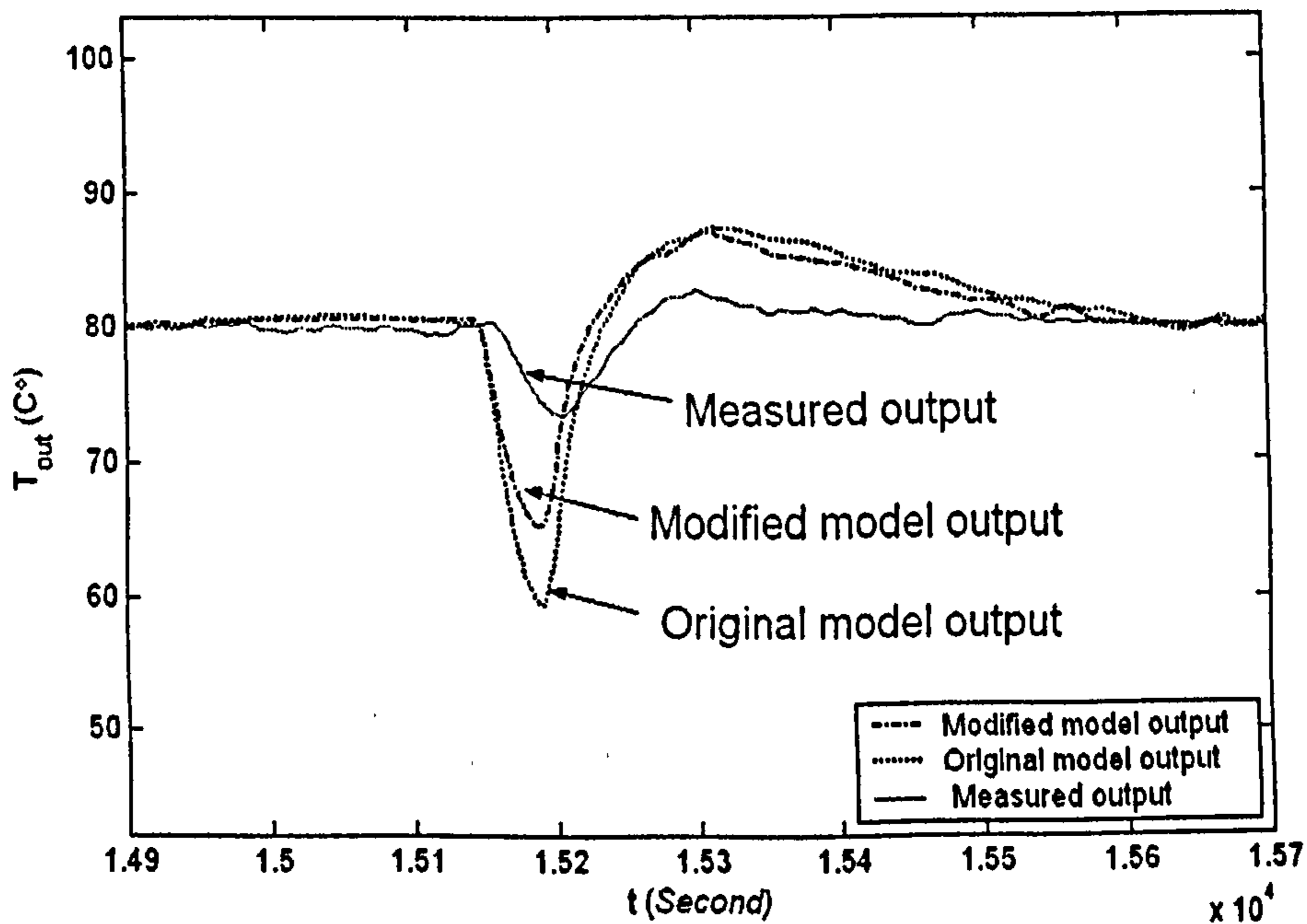


Figure 3-12 Partly enlarged figure 3 of the measured and simulated results using Data 5

From Figures 3-6 ~ 3-12, it can be seen that the responses of the simulated



outputs of the coal mill model can follow the measured output more closely than the results using the previously derived coal mill model (Zhang *et al.* 2002). The average errors between the simulated outputs and measured outputs are summarized in Figure 3-13 and Table 3-7 in which  $E_{T_{out}}$  is

$$\text{calculated by } \frac{1}{N} \sum_{i=1}^N |T_{out}(i) - \hat{T}_{out}(i)| .$$

Table 3-4 Average errors between the simulated output ( $T_{out}$ ) and the measured output

Data sets	Average error ( $E_{T_{out}}$ ) with the previous model	Average error ( $E_{T_{out}}$ ) with the modified model	Percentage of errors reduced
Data 2	3.07 °C	1.48 °C	51.79 %
Data 3	0.29 °C	0.23 °C	20.69 %
Data 4	0.66 °C	0.53 °C	19.70 %
Data 5	0.85 °C	0.69 °C	18.82 %

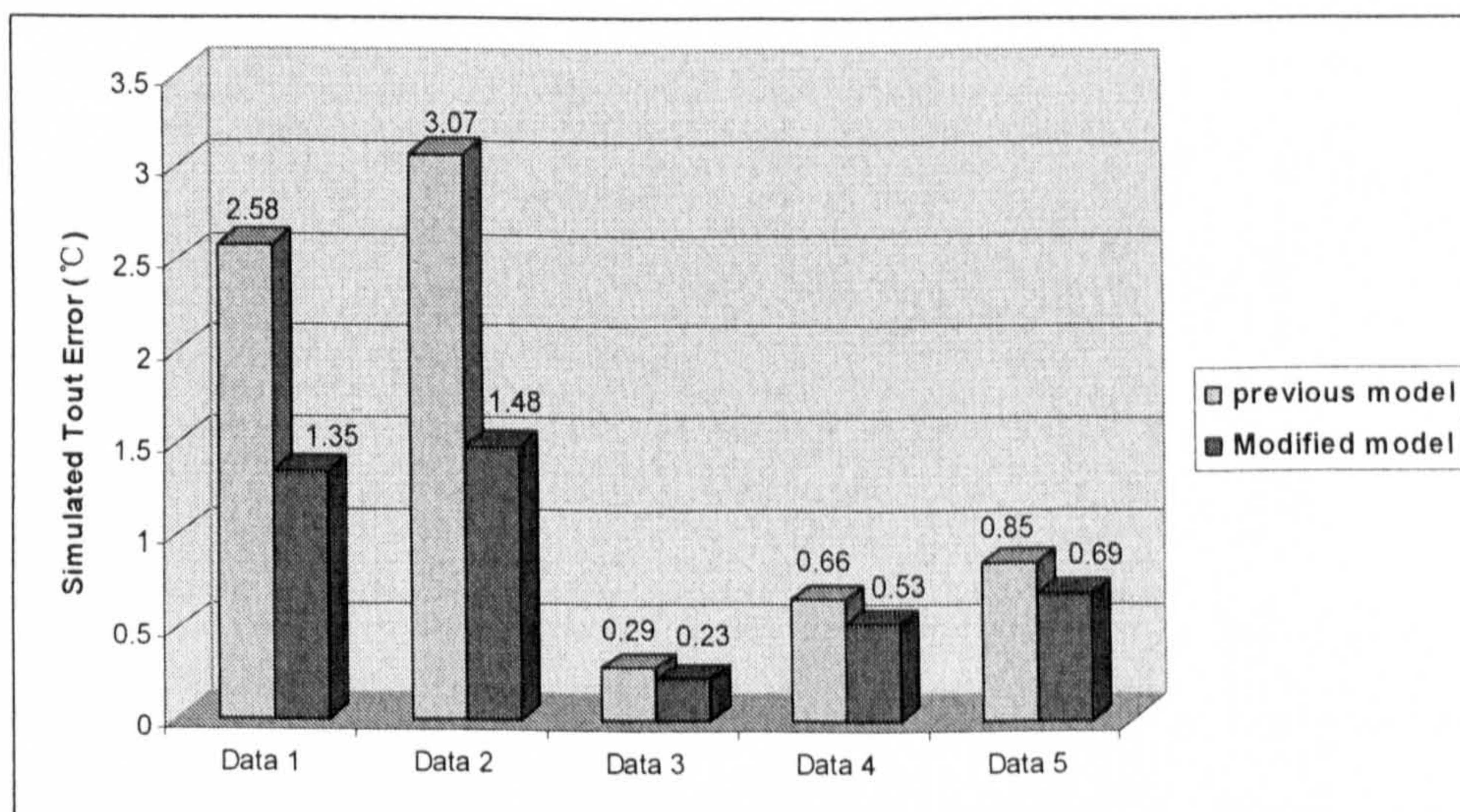


Figure 3-13 Comparison of the average errors between the simulated output ( $T_{out}$ ) and the measured output

The results shown above indicated that the model is improved in accuracy and can represent the real system better for both dynamic behaviour and the performance covering a long-term period of time.



### **3.4 Summary and Discussions**

In this chapter, the coal mill mathematical model for the normal grinding processes is developed by applying the physics and engineering principles and by integrating the knowledge of the experienced plant engineers. The RSPGA is adopted to identify the unknown coefficients of the model. Five on-site collected data sets are provided by RWEnPower Plc. and were used for the simulation studies. Simulation results revealed that the current model provides more agreeable system outputs comparing with that obtained using the previous version of coal mill model. This model covers only the normal grinding process, and does not cover the mill start-up and shut-down stages. Further investigations will be carried out in next chapter to develop a mill model covering the whole milling process.



# Chapter 4

## Multi-Segment Coal Mill Model

### 4.1 Overview of a Complete Milling Process

In power plants, there is a standard procedure for a complete milling process from mill start-up to shut-down to satisfy the quality and safety assurance regulations. Different functions in a mill system will start up and shut down in a sequence rather than simultaneously. For example, the grinding motor starts about 1~2 minutes before the coal feeder inputs any coal into the mill to prevent chokes; the grinding motor is shut-down in delays after the coal feeder is shut-down completely and the primary air (PA fan) is kept on blowing until the coal mill system is cool enough to prevent fire accidents. Brief description of the complete milling process as a sequence of events from start-up to shut-down is given in this section.

#### 1) Start-up Sequence

During the start-up sequence, all the components of the mill system (e.g. the primary fan, the lube oil pump, the feeder, and the grinding motor *etc*) are started in a pre-defined sequence, as shown in Figure 4-1. The tempering air is firstly switched on together with the procedure for checking the lube oil pump pressure and mill temperature, which warms up the coal mill before it starts. The coal mill grinding motor is then started to pre-grind the raw coal remained in the mill body from the previous session, which takes around 1~2 minutes. Finally the coal mill feeder is



started and the coal mill system goes into the normal grinding situation (Detail operational code of start-up sequence can be found in Appendix I.).

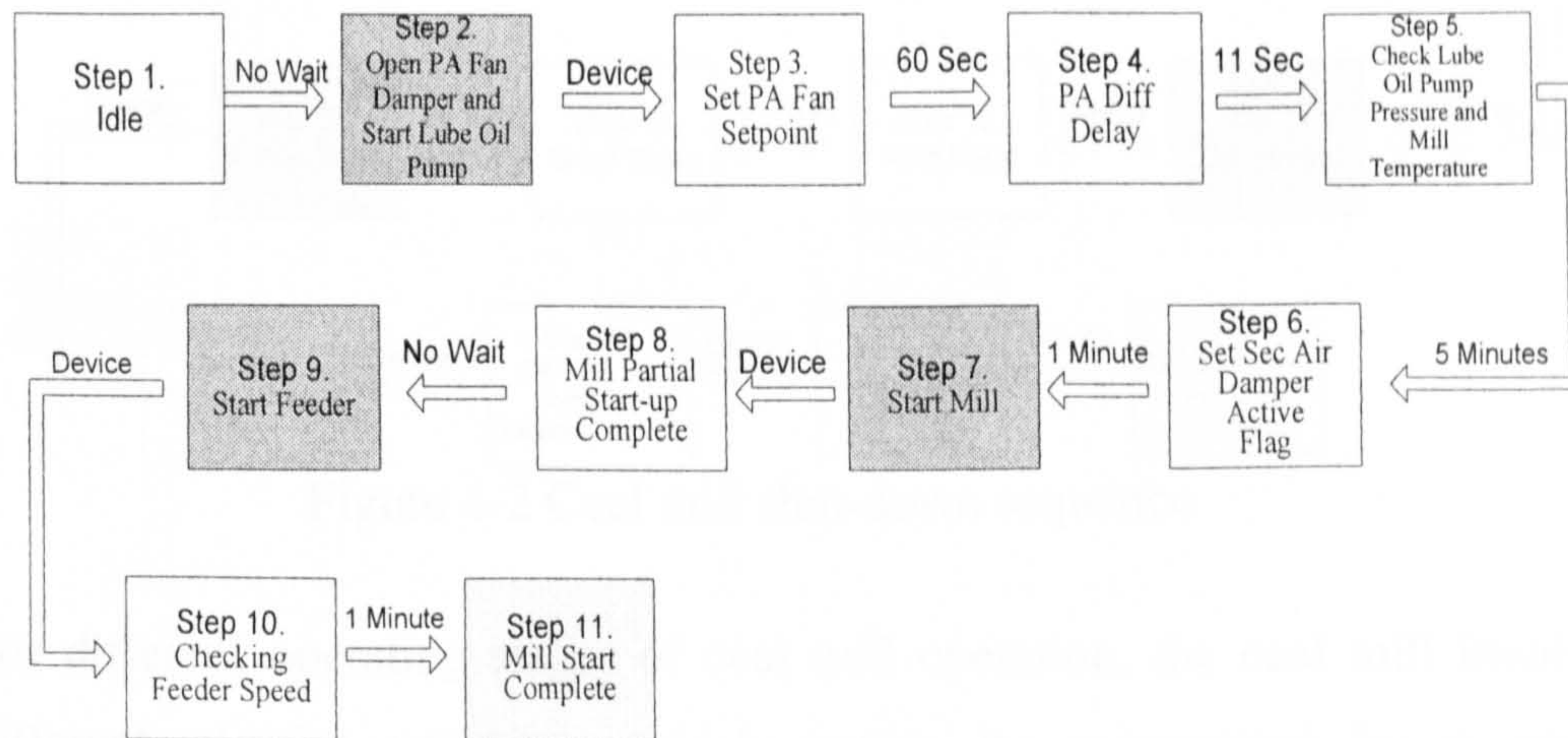


Figure 4-1 Coal mill start-up sequence

## 2) Shut-down Sequence

During the shut-down sequence, all the components of the mill system (e.g. the feeder, the grinding motor and the primary fan etc) are shut down in turn. Figure 4-2 shows the shut-down sequence. In the sequence, the tempering air is firstly set to be fully cool, and the coal feeder speed is reduced to be minimum at the beginning of the shut-down procedure, which takes about 5 ~ 6 minutes. Afterward, the feeder is tripped off, and then a grinding delay is held for 1 ~ 2 minutes, which grinds the raw coal remained in the mill. Finally the mill grinding motor is switched off, and the PA fan shuts down in sequence. The PA fan is kept on blowing to cool down the mill body for around two minutes (Detail operational code of start-up sequence please refer to Appendix I.).



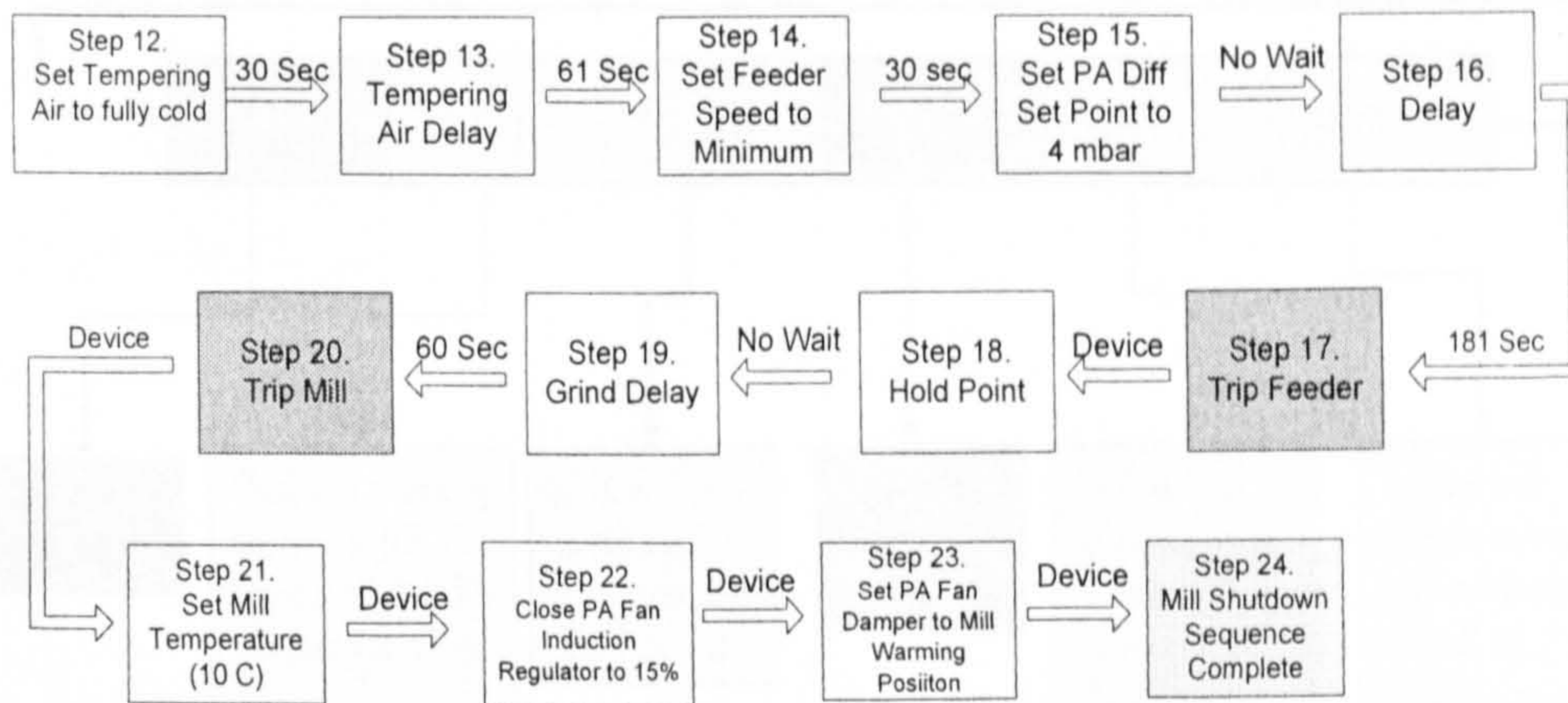


Figure 4-2 Coal mill shut-down sequence

For different operating stages of coal mill operation, the coal mill involves different physics variations which cannot be represented by a single mathematical model. A multi-segment mathematic mill model is developed in this chapter, which is composed of six different segments. A brief description of the six-segment of mill operation is illustrated in Figure 4-3, which covers the whole milling process. The segments are numbered from Segment 0 to Segment 5. As an example, the coal mill idle situation is modelled by the segment 0 in the multi-segment model, where all the components of the coal mill (e.g. feeder, grinding motor) are completely off.

All these segments are connected by a number of operation triggers. All the triggers of the model segments are determined by the mill operation procedures which is specified by the operating procedure of power plants, details are shown in the following sections.



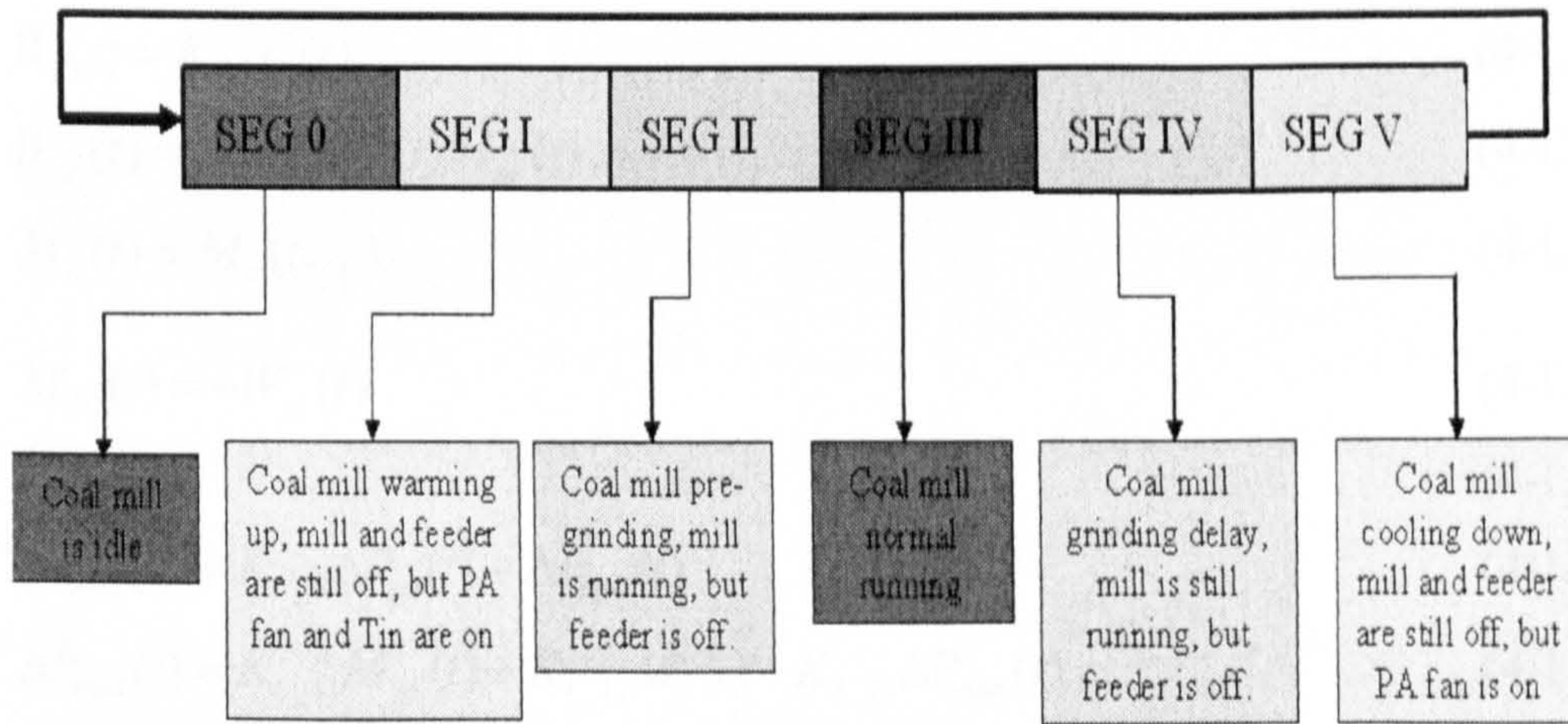


Figure 4-3 Coal mill six-segment model

## 4.2 Multi-Segment Coal Mill Mathematical Model

This section describes all the segment models for a complete milling process. Although the description starts from Segment I, it can start from any segment actually as the six segments form a cycle.

### 4.2.1 Coal Mill Model - Segment I

The coal mill model for Segment I represents the ‘warm-up’ process in the mill start-up procedure. During this period, the mill temperature is set to the point of the warming-up value, the PA Fan Damper is opened to the warming-up position, PA different pressure is set to a point to be higher than 4 mbar, and the mill lube oil pump starts running. The switch trigger for initiating this segment is set to be the moment that the Primary Air Damper and the Temperature Damper are just open, which could be represented modularly by the beginning of the Step 3 as shown in Figure 4-1. The coal mill model for Segment I is described by Equation (4-I.1) ~ Equation (4-I.9).

$$W_{air}(t) = 10 \cdot \sqrt{\Delta P_{pa}(t) \cdot \frac{273}{273 + T_m(t)} \times \frac{28.8}{22.4}} \quad (4-I.1)$$



$$W_c(t) = K_{fs} \cdot F_s(t) \quad (4-I.2)$$

$$W_{pf}(t) = K_{I\_16} \Delta P_{pa}(t) M_{pf}(t) \quad (4-I.3)$$

$$M_c(t) = M_c(t_{1\_0}) \quad (4-I.4)$$

$$\dot{M}_{pf}(t) = -W_{pf}(t) \quad (4-I.5)$$

$$P(t) = 0 \quad (4-I.6)$$

$$\Delta P_{mill}(t) = K_{I\_9} \Delta P_{pa}(t) + \Delta P_{mpd}(t) \quad (4-I.7)$$

$$\Delta \dot{P}_{mpd}(t) = K_{I\_11} M_{pf}(t) + K_{I\_12} M_c(t) - K_{I\_13} \Delta P_{mpd}(t) \quad (4-I.8)$$

$$\dot{T}_{out}(t) = [K_{I\_1} T_{in}(t) + K_{I\_2}] W_{air}(t) - [K_{I\_4} T_{out}(t) + K_{I\_5}] \cdot W_{air}(t) + K_{I\_17} T_{out} \quad (4-I.9)$$

where:

$M_c(t_{1\_0})$ : The initial value of mass of coal in mill at the beginning of segment 1 (kg)

$K_{I\_i}$ : Model coefficients to be identified respect to model segment I

The other notations are same as explained in Chapter 3.

Comparing with the grinding process mill model shown in Section 3.2, there are several significant modifications made, which are: i). The raw coal in mill  $M_c$  is set to be constant value  $M_c(t_{1\_0})$  through this segment (see Equation (4-I.4)) since no grinding happens during this segment; ii). The changing rate of the pulverized coal in mill  $\dot{M}_{pf}$  is reducing in a rate of being proportional to the mass flow rate of pulverized coal out from mill  $W_{pf}$  (see Equation (4-I.5)) since there is not any  $M_{pf}$  to be generated by grinding during this segment; iii). The coal mill current  $P$  is set to be zero since the coal mill motor is still off during this segment, where there is no power consumed to operate the mill motor; iv). The mill temperate is represented by Equation (4-I.9), which is similar to Equation (3-21) shown in Chapter 3.

### 4.2.2 Coal Mill Model - Segment II

The coal mill model for Segment II represents the ‘pre-grinding’ process in the mill start-up procedure. During this period, the coal mill grinding motor is started to pre-grind the coal left in the mill, while the coal feeder is still off. The switch trigger of Segment II is set to be the moment that the mill grinding motor is commanded to start which could be represented by the modular - beginning of Step 7 as shown in Figure 4-1. Segment II coal mill model can be described by Equation (4-II.1) ~ Equation (4-II.9)

$$W_{air}(t) = 10 \cdot \sqrt{\Delta P_{pa}(t) \cdot \frac{273}{273 + T_{in}(t)} \times \frac{28.8}{22.4}} \quad (4-II.1)$$

$$W_c(t) = K_{fs} \cdot F_s(t) \quad (4-II.2)$$

$$W_{pf}(t) = K_{II\_16} \Delta P_{pa}(t) M_{pf}(t) \quad (4-II.3)$$

$$\dot{M}_c(t) = -K_{II\_15} M_c(t) \quad (4-II.4)$$

$$\dot{M}_{pf}(t) = K_{II\_15} M_c(t) - W_{pf}(t) \quad (4-II.5)$$

$$P(t) = K_{II\_6} M_{pf}(t) + K_{II\_7} M_c(t) + K_{II\_8} \quad (4-II.6)$$

$$\Delta P_{mill}(t) = K_{II\_9} \Delta P_{pa}(t) + \Delta P_{mpd}(t) \quad (4-II.7)$$

$$\Delta \dot{P}_{mpd}(t) = K_{II\_11} M_{pf}(t) + K_{II\_12} M_c(t) - K_{II\_13} \Delta P_{mpd}(t) \quad (4-II.8)$$

$$\dot{T}_{out}(t) = [K_{II\_1} T_{in}(t) + K_{II\_2}] W_{air}(t) - [K_{II\_4} T_{out}(t) + K_{II\_5}] \cdot W_{air}(t) + K_{II\_14} P(t) + K_{II\_17} T_{out} \quad (4-II.9)$$

where:

$K_{II\_i}$ : Model coefficients to be identified respect to model segment II

The other notations have the same meanings as described in Chapter 3.

Comparing with the normal grinding mill model described in Section 3.2, there are some modifications in this segment, which are i). The raw coal in mill  $M_c$  is self-reducing due to the pre-grinding of the coal mill, which is represented by Equation (4-II.4); ii). The mill temperate is represented by



Equation (4-II.9), which is derived based on the heat balance principle of the coal mill system as described in Chapter 3.

### 4.2.3 Coal Mill Model - Segment III

The coal mill model for Segment III represents the steady state or normal grinding milling stage. During this period, the primary air fan, coal mill grinding motor and the coal feeder *etc.* have come into the steady state milling stage. The switch trigger for model Segment III is set to be the moment that the mill start-up sequence is completed, which could be represented by the modular at the beginning of Step 11 as shown in Figure 4-1. Segment III coal mill model is described by Equation (4-III.1) ~ Equation (4-III.9).

$$W_{air}(t) = 10 \cdot \sqrt{\Delta P_{pa}(t) \cdot \frac{273}{273 + T_{in}(t)} \times \frac{28.8}{22.4}} \quad (4-III.1)$$

$$W_c(t) = K_{fs} \cdot F_s(t) \quad (4-III.2)$$

$$W_{pf}(t) = K_{III\_16} \Delta P_{pa}(t) M_{pf}(t) \quad (4-III.3)$$

$$\dot{M}_c(t) = W_c(t) - K_{III\_15} M_c(t) \quad (4-III.4)$$

$$\dot{M}_{pf}(t) = K_{III\_15} M_c(t) - W_{pf}(t) \quad (4-III.5)$$

$$P(t) = K_{III\_6} M_{pf}(t) + K_{III\_7} M_c(t) + K_{III\_8} \quad (4-III.6)$$

$$\Delta P_{mill}(t) = K_{III\_9} \Delta P_{pa}(t) + \Delta P_{mpd}(t) \quad (4-III.7)$$

$$\Delta \dot{P}_{mpd}(t) = K_{III\_11} M_{pf}(t) + K_{III\_12} M_c(t) - K_{III\_13} \Delta P_{mpd}(t) \quad (4-III.8)$$

$$\begin{aligned} \dot{T}_{out}(t) = & [K_{III\_1} T_{in}(t) + K_{III\_2} W_{air}(t) - K_{III\_3} W_c(t) - [K_{III\_4} T_{out}(t) + K_{III\_5}] \cdot [W_{air}(t) + \\ & W_c(t)] + K_{III\_14} P(t) + K_{III\_17} T_{out} \end{aligned} \quad (4-III.9)$$

where:

$K_{III\_i}$ : Model coefficients to be identified respect to model segment III

The other notations have the same meanings as described in Chapter 3.

The equations are same as the normal grinding mill model shown in Section 3.2, which represents the same stage of the coal mill grinding process - coal milling steady state or normal grinding stage.

#### 4.2.4 Coal Mill Model - Segment IV

The coal mill model for Segment IV represents the ‘grinding-delay’ process in the mill shut-down procedure. During this period, the coal feeder is switched off but the grinding motor is still kept on grinding the remaining coal in the mill. The switch trigger for Segment IV is set to be the moment that the coal feeder is completely switched off, which could be represented by the modular at the beginning of Step 19 as shown in Figure 4.1.b. Segment IV coal mill model is described by Equation (4-IV.1) ~ Equation (4-IV.9).

$$W_{air}(t) = 10 \cdot \sqrt{\Delta P_{pa}(t) \cdot \frac{273}{273 + T_{in}(t)} \times \frac{28.8}{22.4}} \quad (4-IV.1)$$

$$W_c(t) = K_{fs} \cdot F_s(t) \quad (4-IV.2)$$

$$W_{pf}(t) = K_{IV\_16} \Delta P_{pa}(t) M_{pf}(t) \quad (4-IV.3)$$

$$\dot{M}_c(t) = -K_{IV\_15} M_c(t) \quad (4-IV.4)$$

$$\dot{M}_{pf}(t) = K_{IV\_15} M_c(t) - W_{pf}(t) \quad (4-IV.5)$$

$$P(t) = K_{IV\_6} M_{pf}(t) + K_{IV\_7} M_c(t) + K_{IV\_8} \quad (4-IV.6)$$

$$\Delta P_{mill}(t) = K_{IV\_9} \Delta P_{pa}(t) + \Delta P_{mpd}(t) \quad (4-IV.7)$$

$$\dot{\Delta P}_{mpd}(t) = K_{IV\_11} M_{pf}(t) + K_{IV\_12} M_c(t) - K_{IV\_13} \Delta P_{mpd}(t) \quad (4-IV.8)$$

$$\dot{T}_{out}(t) = [K_{IV\_1} T_{in}(t) + K_{IV\_2}] W_{air}(t) - [K_{IV\_4} T_{out}(t) + K_{IV\_5}] \cdot W_{air}(t) + K_{IV\_14} P(t) + K_{IV\_17} T_{out} \quad (4-IV.9)$$

where:

$K_{IV\_i}$ : Model coefficients to be identified respect to model segment IV.

The other notations have the same meanings as described in Chapter 3.



Comparing with the normal grinding mill model described in Section 3.2, there are several significant changes for this segment, which are: i). The raw coal in mill  $M_c$  is self-reducing due to the grinding-delay of the coal mill, which is modelled by Equation (4-IV.4); ii). The mill temperature is represented by Equation (4-IV.9), which is similarly modelled by the heat balance model of the coal mill system same as Equation (3-21) described in Chapter 3.

#### 4.2.5 Coal Mill Model - Segment V

The coal mill model for Segment V represents the 'cool-down' procedure in the mill start-up period. During this period, the mill temperature is set to the point of the cooling-down value, PA fan induction regulator is closed to 15%, opening and the PA fan damper is set to the mill warming position. The switch trigger for this segment is set to be the moment that the mill temperature reaches the point of the mill cool-down value, which is illustrated in the modular at the beginning of Step 21 in Figure 4-2. Segment V mill model is described by Equation (4-V.1) ~ Equation (4-V.10).

$$W_{air}(t) = 10 \cdot \sqrt{\Delta P_{pa}(t) \cdot \frac{273}{273 + T_{in}(t)} \times \frac{28.8}{22.4}} \quad (4-V.1)$$

$$W_c(t) = K_{fs} \cdot F_s(t) \quad (4-V.2)$$

$$W_{pf}(t) = K_{V\_16} \Delta P_{pa}(t) M_{pf}(t) \quad (4-V.3)$$

$$\dot{M}_{cDelay}(t) = -K_{V\_15} M_{cDelay}(t) \quad (4-V.4)$$

$$M_c(t) = M_c(t_{s\_0}) - [M_{cDelay}(t_{s\_0}) - M_{cDelay}(t)] \quad (4-V.5)$$

$$\dot{M}_{pf}(t) = K_{V\_15} M_{cDelay}(t) - W_{pf}(t) \quad (4-V.6)$$

$$P(t) = 0 \quad (4-V.7)$$

$$\Delta P_{mill}(t) = K_{V\_9} \Delta P_{pa}(t) + \Delta P_{mpd}(t) \quad (4-V.8)$$

$$\dot{\Delta P}_{mpd}(t) = K_{V\_11} M_{pf}(t) + K_{V\_12} M_c(t) - K_{V\_13} \Delta P_{mpd}(t) \quad (4-V.9)$$

$$\dot{T}_{out}(t) = \frac{[K_{V\_1}T_{in}(t) + K_{V\_2}]W_{air}(t) - [K_{V\_4}T_{out}(t) + K_{V\_5}]}{W_{air}(t) + K_{V\_17}T_{out}} \quad (4-V.10)$$

where

$M_c(t_{s\_0})$ : The initial value of mass of coal in mill at the beginning of segment V.

$M_{cDelay}$ : A term to indicate the grinding delay caused by the inertias of the grinding components

$K_{V\_i}$ : Model coefficients to be identified respect to model segment V

The other notations have the same meanings as described in Chapter 3.

Comparing with the normal grinding process coal mill model derived in Section 3.2, some modifications have been made in the model for Segment V, which are: i). At the beginning of the cool down process, the raw coal in mill  $M_c$  is self-reducing for a short period of time due to the grinding-delay caused by the grinding inertias. Afterward it stays at a constant value through the segment as the grinding process stops completely. Over the segment V, the raw coal in mill,  $M_c$ , is calculated by Equations (4-V.4) ~ (4-V.5), in which  $M_{cDelay}$  indicates the grinding delays caused by the inertias of the grinding components; ii). The changing rate of pulverized coal in mill,  $\dot{M}_{pf}$ , is reducing which is proportional to the mass flow rate of pulverized coal out from the mill,  $W_{pf}$ , and it is proportional to the pulverized coal generated by the grinding delays due to the inertias of the grinding motor  $M_{cDelay}$ , which is modelled by Equation (4-V.6); iii). The coal mill current  $P$  is set to be zero since the coal mill motor is switched off during this segment; iv). The mill temperature is modelled by Equation (4-V.10), which is derived based on the heat balance principle.



#### 4.2.6 Coal Mill Model - Segment 0

The coal mill model for Segment 0 represents the 'idle' stage of the milling process. During this period, the mill grinding motor, the coal feeder, the lube oil pump *etc.* are switched off. This segment model represents the natural cool down process of the coal mill system. The switch trigger for this segment is set to be the moment that the coal mill shut-down sequence completed, which is illustrated in Figure 4-1 (Step 1). This segment coal mill model is described by Equation (4-0.1) ~ Equation (4-0.8).

$$W_{air}(t) = 10 \cdot \sqrt{\Delta P_{pa}(t) \cdot \frac{273}{273 + T_m(t)} \times \frac{28.8}{22.4}} \quad (4-0.1)$$

$$W_c(t) = K_{fs} \cdot F_s(t) \quad (4-0.2)$$

$$W_{pf}(t) = 0 \quad (4-0.3)$$

$$M_c(t) = M_c(t_{0\_0}) \quad (4-0.4)$$

$$M_{pf}(t) = M_{pf}(t_{0\_0}) \quad (4-0.5)$$

$$P(t) = 0 \quad (4-0.6)$$

$$\Delta \dot{P}_{mill}(t) = K_{0\_9} \Delta P_{pa}(t) + K_{0\_19} \Delta P_{mill}(t) \quad (4-0.7)$$

$$\begin{aligned} \dot{T}_{out}(t) = & [K_{0\_1} T_m(t) + K_{0\_2}] W_{air}(t) - [K_{0\_4} T_{out}(t) + K_{0\_5}] \cdot W_{air}(t) - K_{0\_18} (T_{out} - \\ & T_e) + \frac{K_{0\_17}}{M_c(t) + M_{pf}(t)} T_{out} \end{aligned} \quad (4-0.8)$$

where

$M_c(t_{0\_0})$ : The initial value of mass of coal in mill at the beginning of segment 0 (kg)

$M_{pf}(t_{0\_0})$ : The initial value of pulverized mass of coal in mill at the beginning of segment 0 (kg)

$T_e$ : Temperature of the environment (°C)

$K_{0\_i}$ : Model coefficients to be identified respect to model segment 0

The other notations have the same meanings as described in Chapter 3.

In this segment, all the components of the coal mill system are off and there is

no grinding and blowing happening, so  $M_c$ ,  $M_{pf}$  etc. will stay at a constant level through this segment. Furthermore, the coal mill temperature and the pressure are gradually dropping as indicated in Equations (4-0.7) and (4-0.8).

Comparing with the standard coal milling model shown in Chapter 3, this segment model is different in the following aspects: i). In Segment 0, all the components of the coal mill system is idle, so  $M_c$ ,  $M_{pf}$ , and  $P$  are kept at a constant level or stay at zero, which are described by Equations (4-0.3) ~ (4-0.6); ii). PA fan damper and coal mill valves are closed solidly during the idle stage, so coal mill pressure is naturally dropping, which is indicated in Equation (4-0.7). iii). Equation (4-0.8) represents the naturally self-cooling process of the coal mill system through this segment. It is developed corresponding to the heat balance of the coal mill system as well, where the term  $K_{0_e}(T_{out} - T_e)$  represents the heat loss to the environment from the mill system via the mill body and valves etc.

#### **4.2.7 Summary of the Multi-Segment Model**

According to different working status of a coal mill, the coal mill model is developed to have six different segments. Segment model I and Segment model II represent the start-up process of coal mill; Segment III represents the steady state of the milling process; Segment IV and Segment V represent the shut-down process of the coal mill; Segment 0 represents the idle stage of the coal mill. All these model segments are connected by series switch triggers, and then it forms the continued coal milling process including the idle situation (see Figure 4-4).



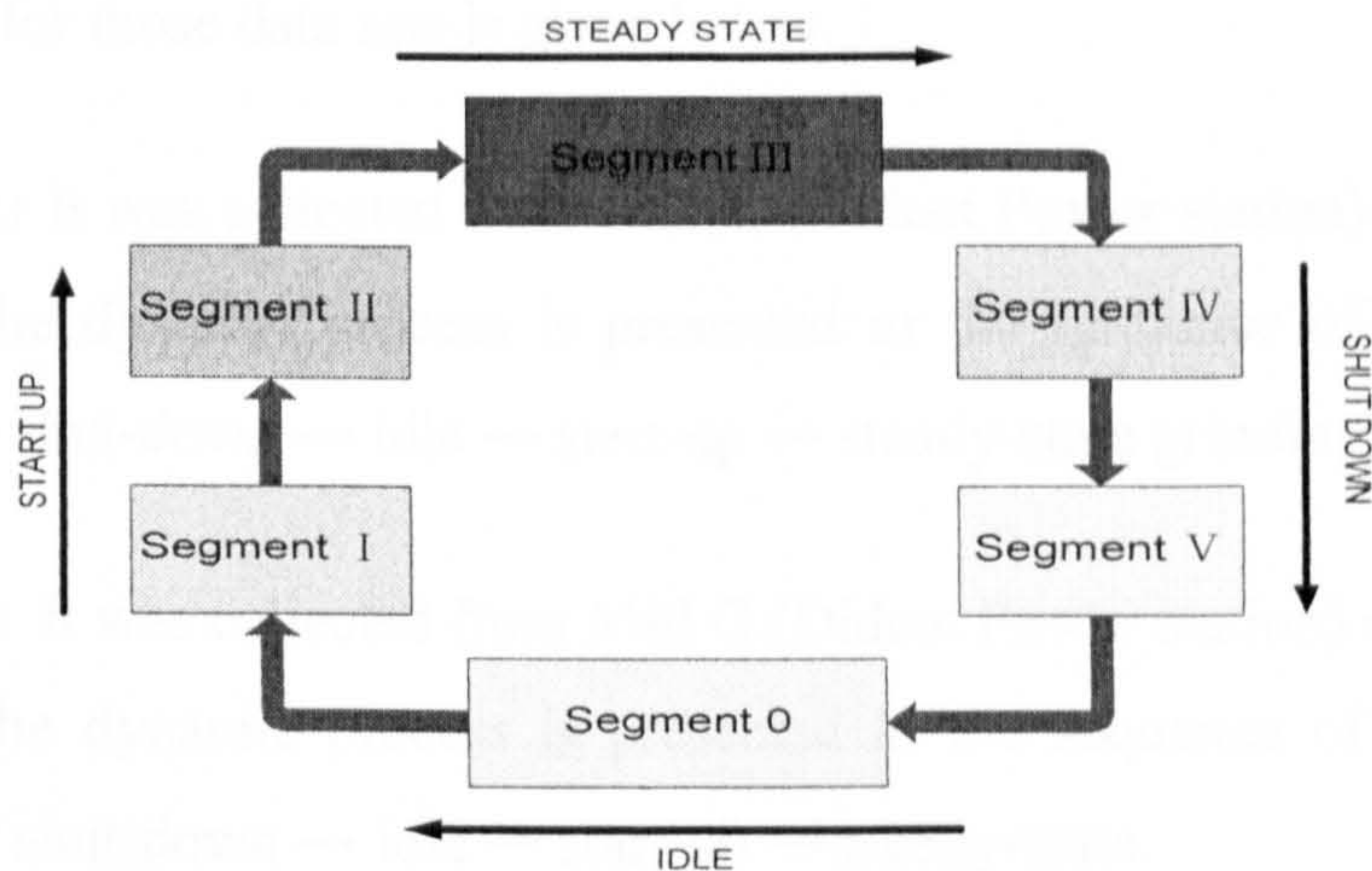


Figure 4-4 Structure of the coal mill multi-segments model

### 4.3 Model Parameter Identification and Model Validation

#### 4.3.1 Overview of the Data Sets

It is noticed that there are six sets of unknown model parameters for the multi-segment coal mill model so the next task is to find the values of those unknown parameters. Then the results will be compared with the single segment model that derived by Zhang in 2002 (Zhang *et al.* 2002). The validation of the new multi-segment model will be conducted as well. This section describes system parameter identification, simulation studies and model validation.

For the purpose of simulation studies to the multi-segment coal mill model, data covering a long period of time from start-up, grinding process to shut down process is required, where the operational sequence number as triggers is particularly logged for initiating different segments during the simulation. Three data sets with such features were provided by RWEnPower Plc. A brief



description for those data sets is given below.

**Data Set A:** It was collected from Mill C (Didcot Power station) on 6th May 2003 and the dynamic process is presented in the sequence of steady-state grinding → shut-down → idle → start-up → steady-state grinding.

**Data Set B:** It was collected from Mill G (Didcot Power station) on 24<sup>th</sup> April 2003 and the dynamic process is presented in the sequence of steady-state grinding → shut-down → idle → start-up → steady-state.

**Data Set C:** It was collected from Mill C (Didcot Power station) on 24<sup>th</sup> April 2003 and the dynamic process is presented in the sequence of steady-state → shut-down → Idle.

Comparing the three data sets, only Data Set A and Data Set B include the whole milling process, and Data Set A composes an average long period for grinding process and idle process. So Data Set A is adopted for the coal mill multi-segment model coefficients identifications, and then Data Set B and Data Set C are used for the validation studies of the multi-segment coal mill model.

### **4.3.2 Identification of Unknown Model Parameters**

Following the identification scheme introduced in last Chapter, coefficients of the multi-segment coal mill model are identified using Data Set A. The model parameters identified are summarized in Table 4-1 and Table 4-2. The results obtained have been compared with the previous single grinding model introduced by Zhang in 2002 (Zhang *et al.* 2002), especially, in the start-up, normal grinding operation, shut-down, and idle periods.



Table 4-1 Identified parameters for the model segments I, II and III

$i$	$K_{I,i}$ (Segment I)	$K_{II,i}$ (Segment II)	$K_{III,i}$ (Segment III)
1	0.000725	0.000806	0.000619
2	0.040103	0.030854	0.089614
3	N/A	N/A	0.003837
4	0.000572	0.000569	0.001553
5	-0.016754	-0.013897	-0.086348
6	N/A	0.006582	0.017125
7	N/A	0.00503	0.002937
8	N/A	29.464080	30.173294
9	5.604890	6.322785	5.549015
11	0.000124	0.000088	0.001701
12	0.000022	0.000361	0.000565
13	0.079430	0.020107	0.086773
14	N/A	0.090364	0.032505
15	N/A	0.000682	0.005133
16	0.000107	0.001448	0.002618
17	-0.013297	-0.056697	-0.057244
18	N/A	N/A	N/A
19	N/A	N/A	N/A

Figures 4-5, 4-6, and 4-7 show the simulation results using the single grinding model. The red solid line represents the measured outputs logged on-site from the power station, and the blue dotted line represents the simulated outputs from the model. Obviously it can be seen that the simulated data using the single segment normal grinding model cannot represent the start-up process (see Figure 4-5) and shut-down process (see Figure 4-6), and the idle process (see Figure 4-7) well as a large gap between the measured and simulated data appeared.

Table 4-2 Identified parameters for the model segments IV, V and 0

$i$	$K_{IV,i}$ (Segment IV)	$K_{V,i}$ (Segment V)	$K_{0,i}$ (Segment 0)
1	0.001071	0.000937	0.001532
2	0.038145	0.037150	0.053152
3	N/A	N/A	N/A
4	0.001102	0.001090	0.002390
5	-0.012738	-0.017498	-0.013517
6	0.005027	N/A	N/A
7	0.012719	N/A	N/A
8	26.193318	N/A	N/A
9	6.028041	5.976033	0.350150
11	0.000010	0.000007	N/A
12	0.000218	0.000013	N/A
13	0.005940	0.129483	N/A
14	0.060823	N/A	N/A
15	0.005010	0.150024	N/A
16	0.002844	0.000314	N/A
17	-0.049568	-0.008422	-0.097495
18	N/A	N/A	0.000277
19	N/A	N/A	-0.058633

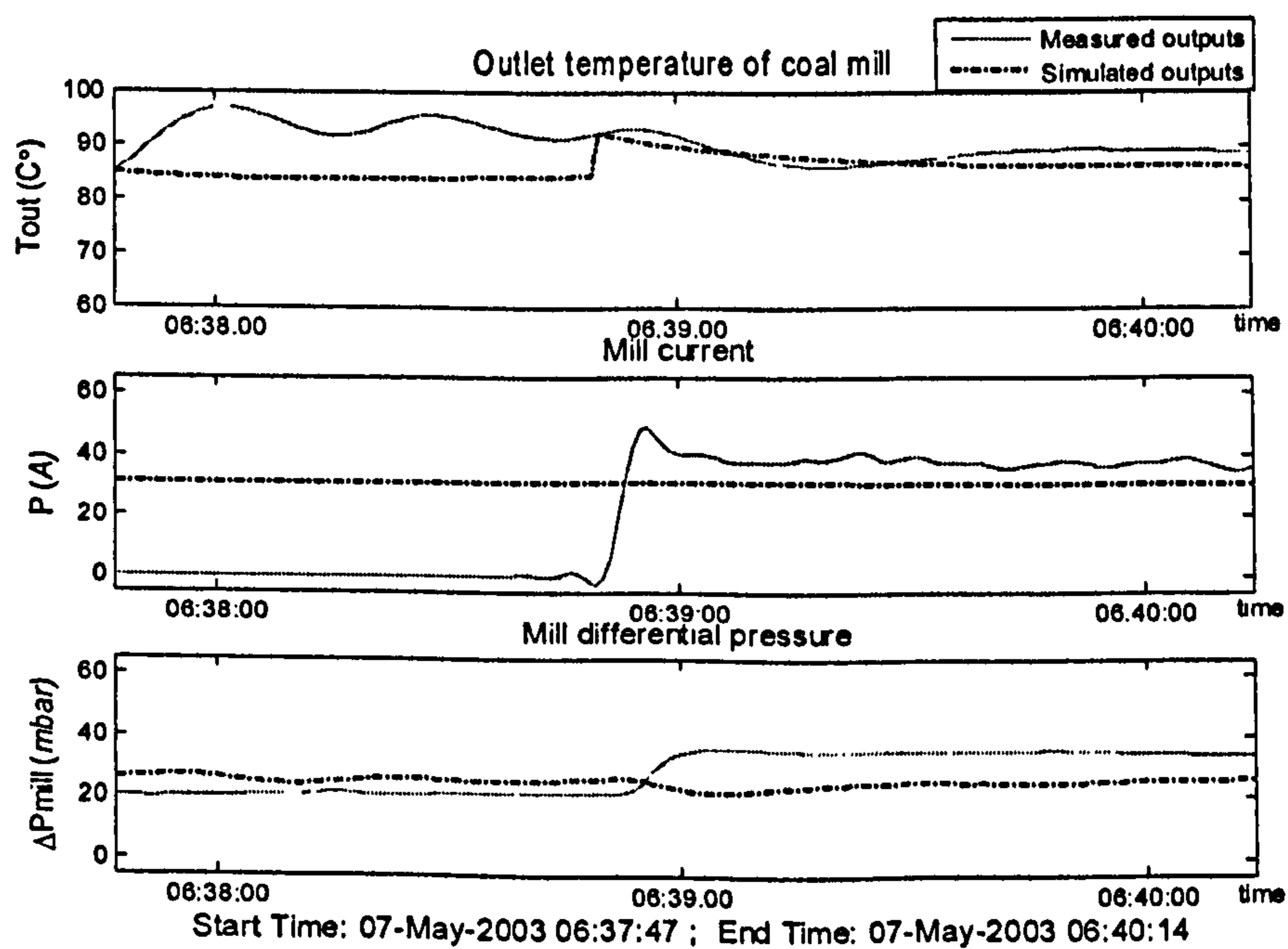


Figure 4-5 Simulation results for start-up process using the single grinding model



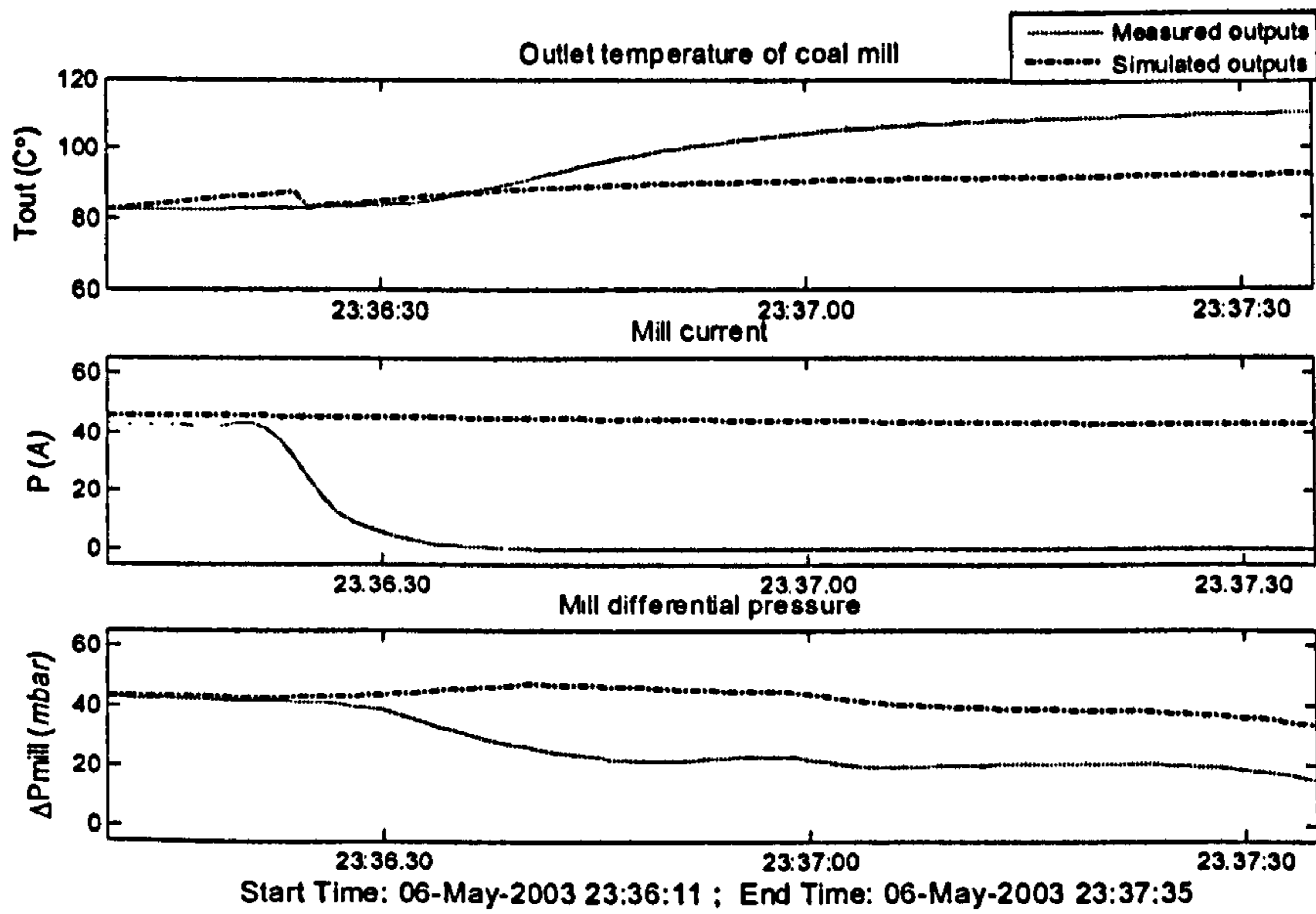


Figure 4-6 Simulation results for shut-down process using the single grinding model

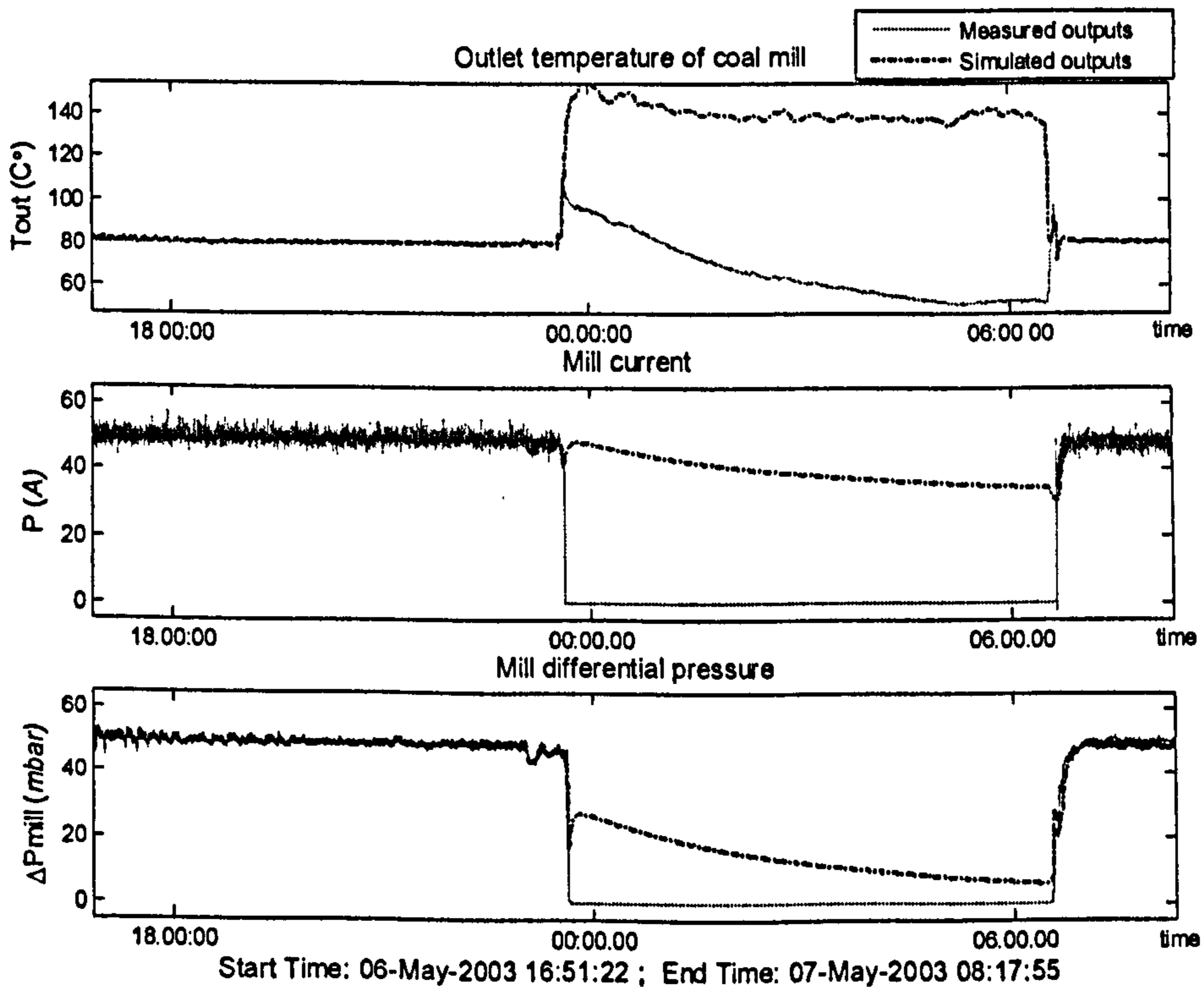


Figure 4-7 Simulation results for overall process using the single grinding model

Figures 4-8, 4-9, and 4-10 show the simulation results using the multi-segment model for the overall process from start-up to shut-down process. Comparing with the results obtained using the single segment normal grinding model, the simulated outputs approaches to the measured outputs much closer, especially in the start-up, shut-down and idle stages.

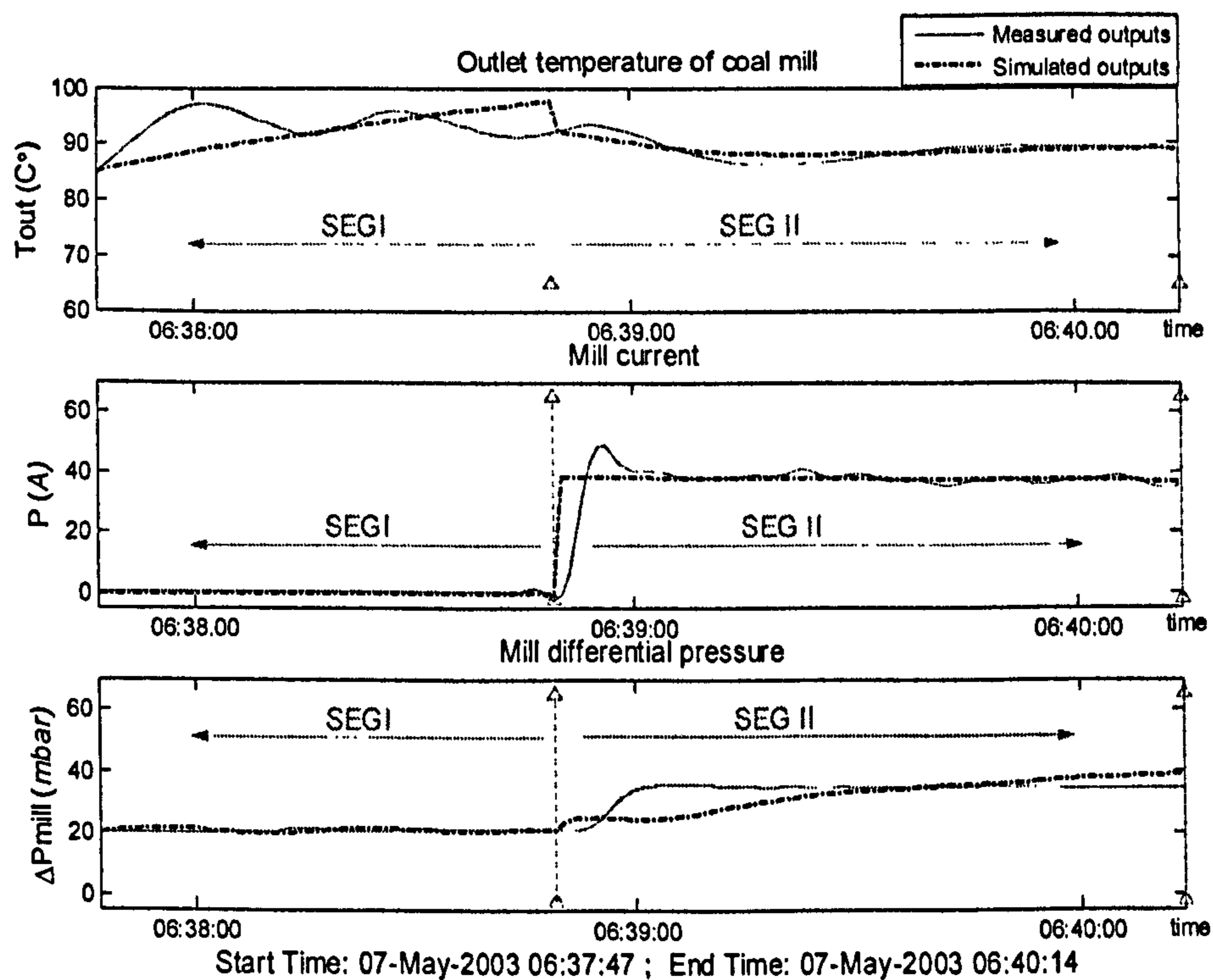


Figure 4-8 Simulation results for start-up process using the multi-segment model



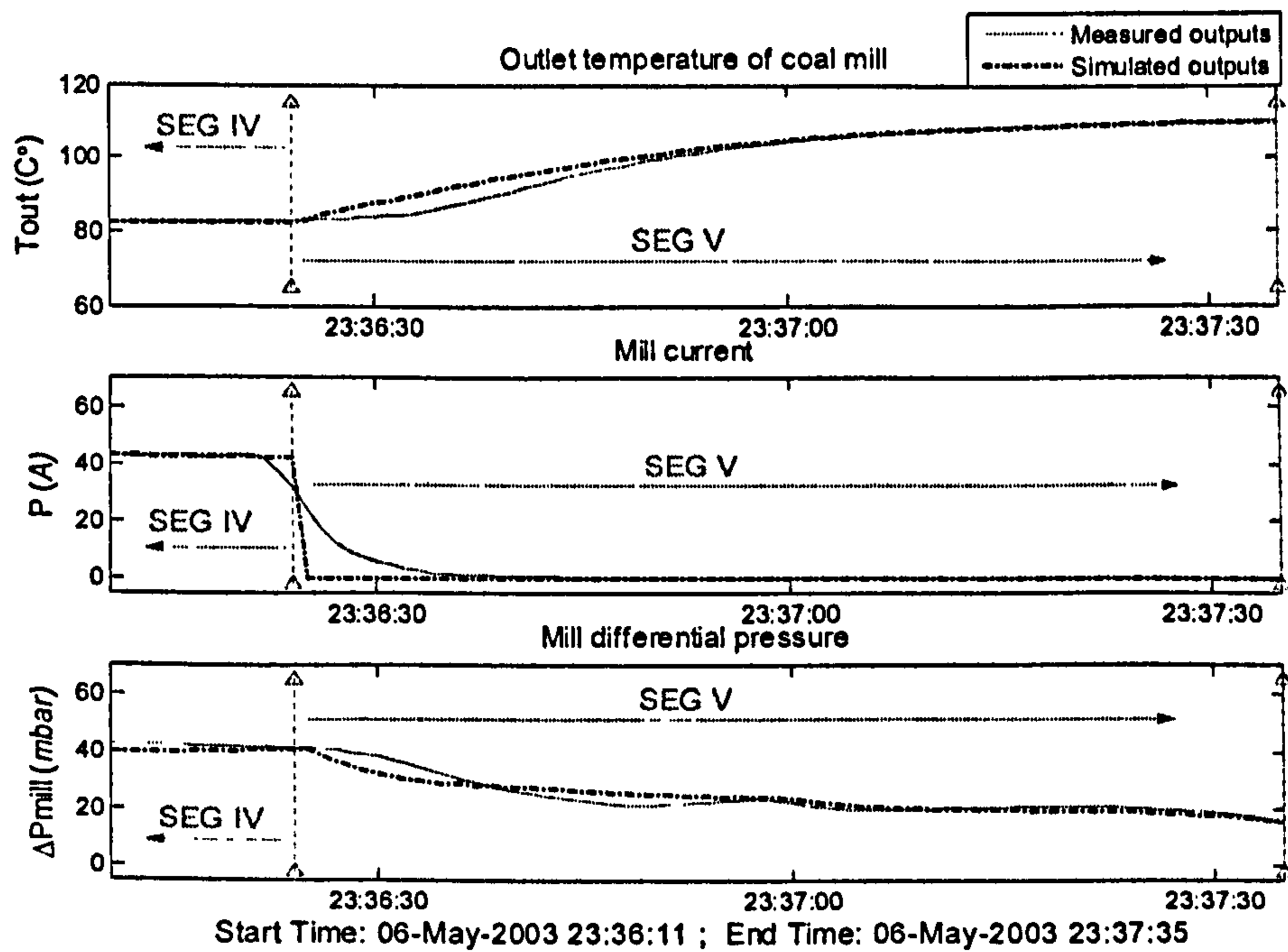


Figure 4-9 Simulation results for shut-down process using the multi-segment model

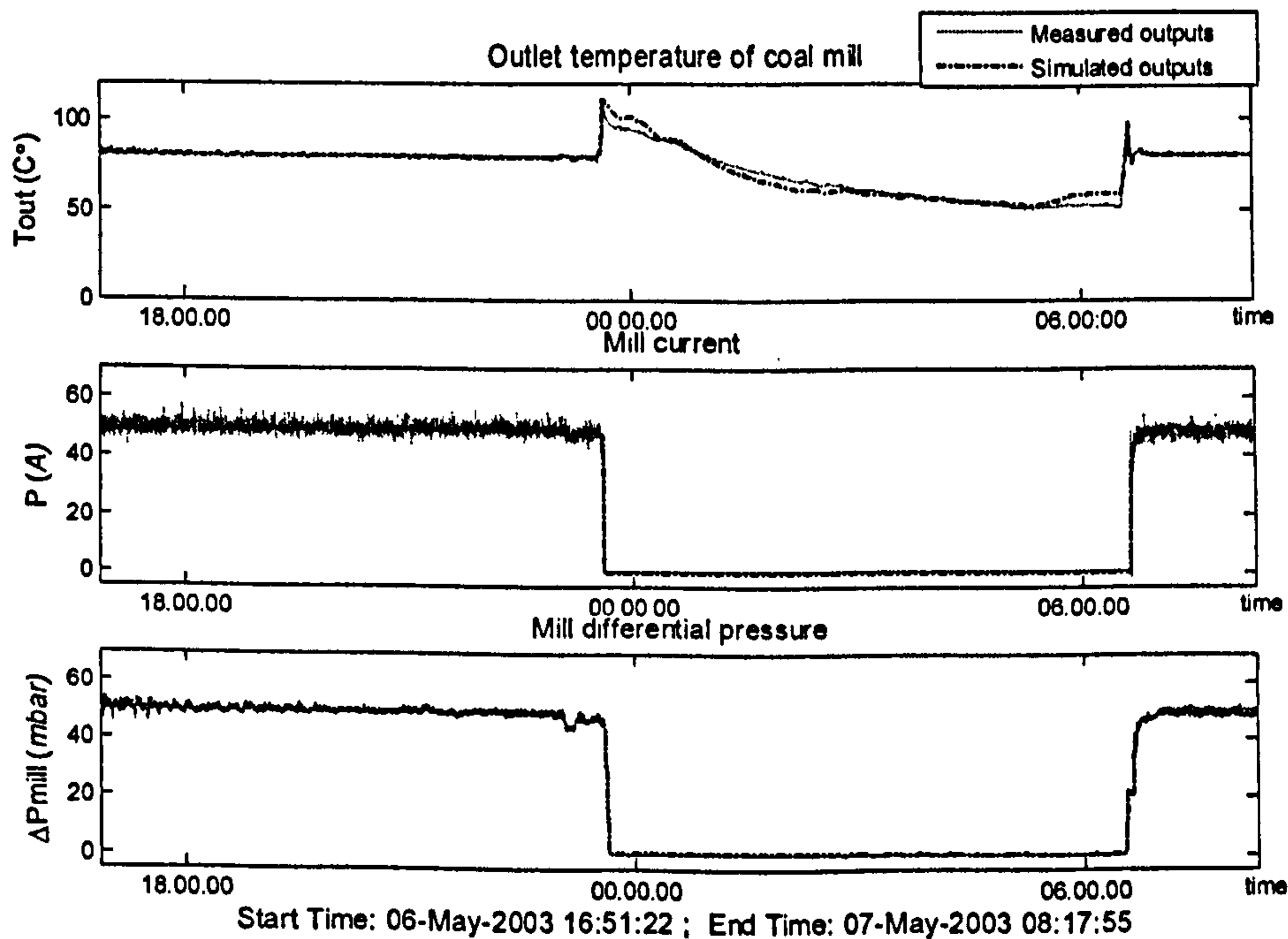


Figure 4-10 Simulation results for overall process using the multi-segment model

### **4.3.3 Mill Model Validations**

Data Sets B and C are adopted for validation of the multi-segment model. From the operational sequence logged in the data set, it is found that Data Set B operated in the sequence of steady-state grinding → shut-down → idle → start-up → steady-state grinding, which indicates all the six segments are included in Data Set B, that is, Segment III→ Segment IV→ Segment V→ Segment 0 → Segment I → Segment II→ Segment III. Data Set C operated in the sequence: steady-state grinding → shut-down → idle, which indicates only the three segments are included in Data Set C, that is, Segment III→ Segment IV→ Segment V→ Segment 0. In order to clearly display the validation results for the model segments, the simulation results respecting to the start-up, shut-down and the overall process are given separately in the figures of the validation results. The simulation results of the intermediate variables are given in the figures that the engineers in power plants are keen to know.

Model validation results using Data Set B are given in the Figures 4-11 ~ 4-31 and the validation results using Data Set C are given in Appendix II.



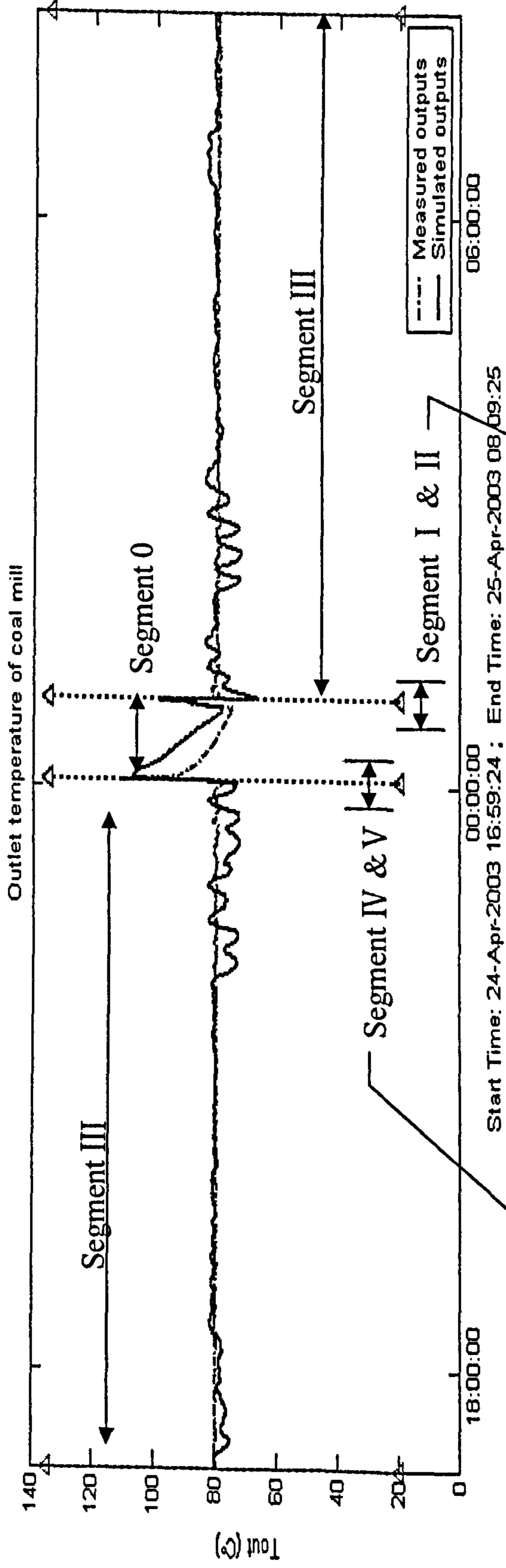


Figure 4-11 Simulated and measured mill outlet temperature for all segments using Data Set B

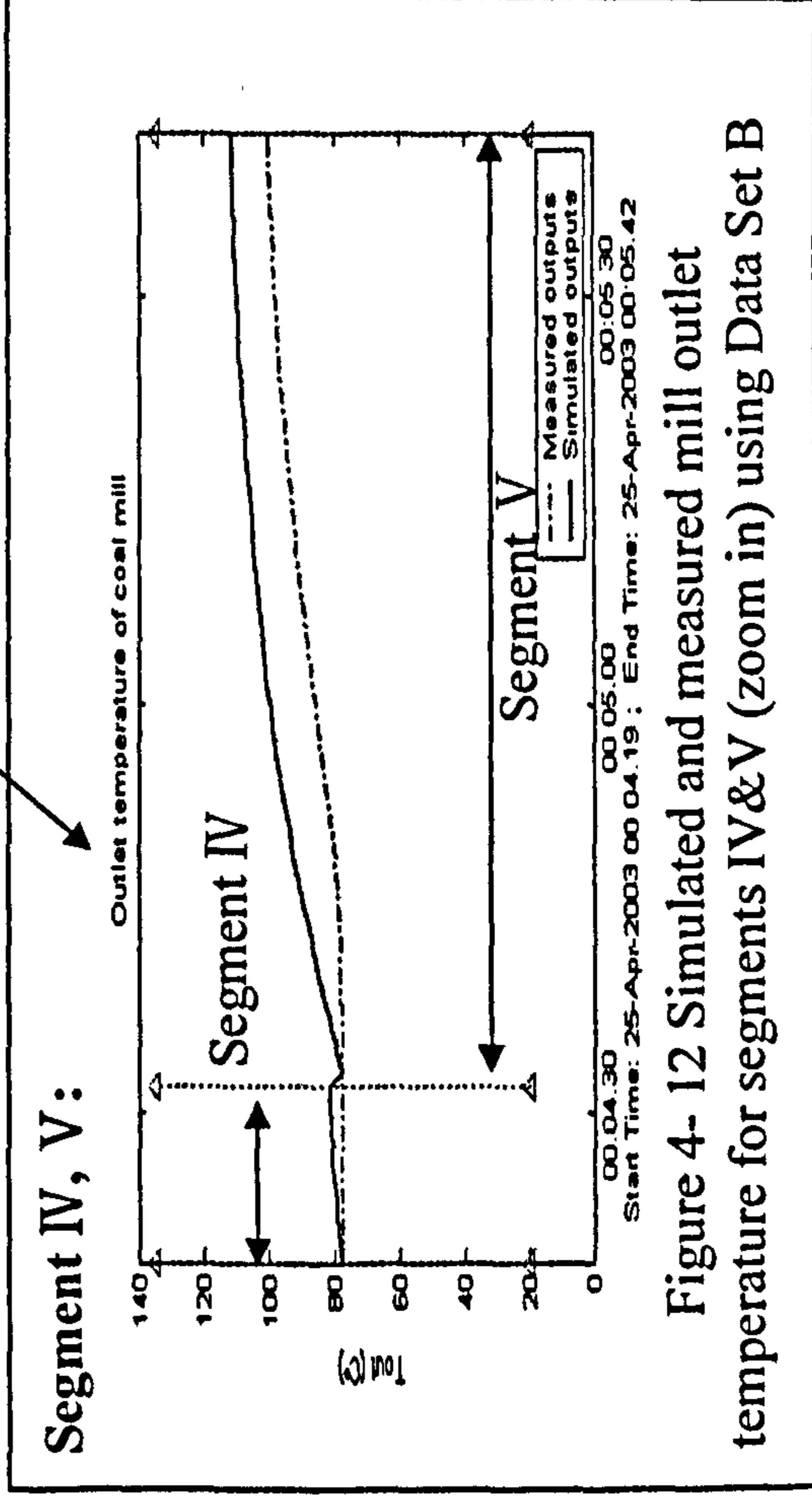


Figure 4-12 Simulated and measured mill outlet temperature for segments IV&V (zoom in) using Data Set B

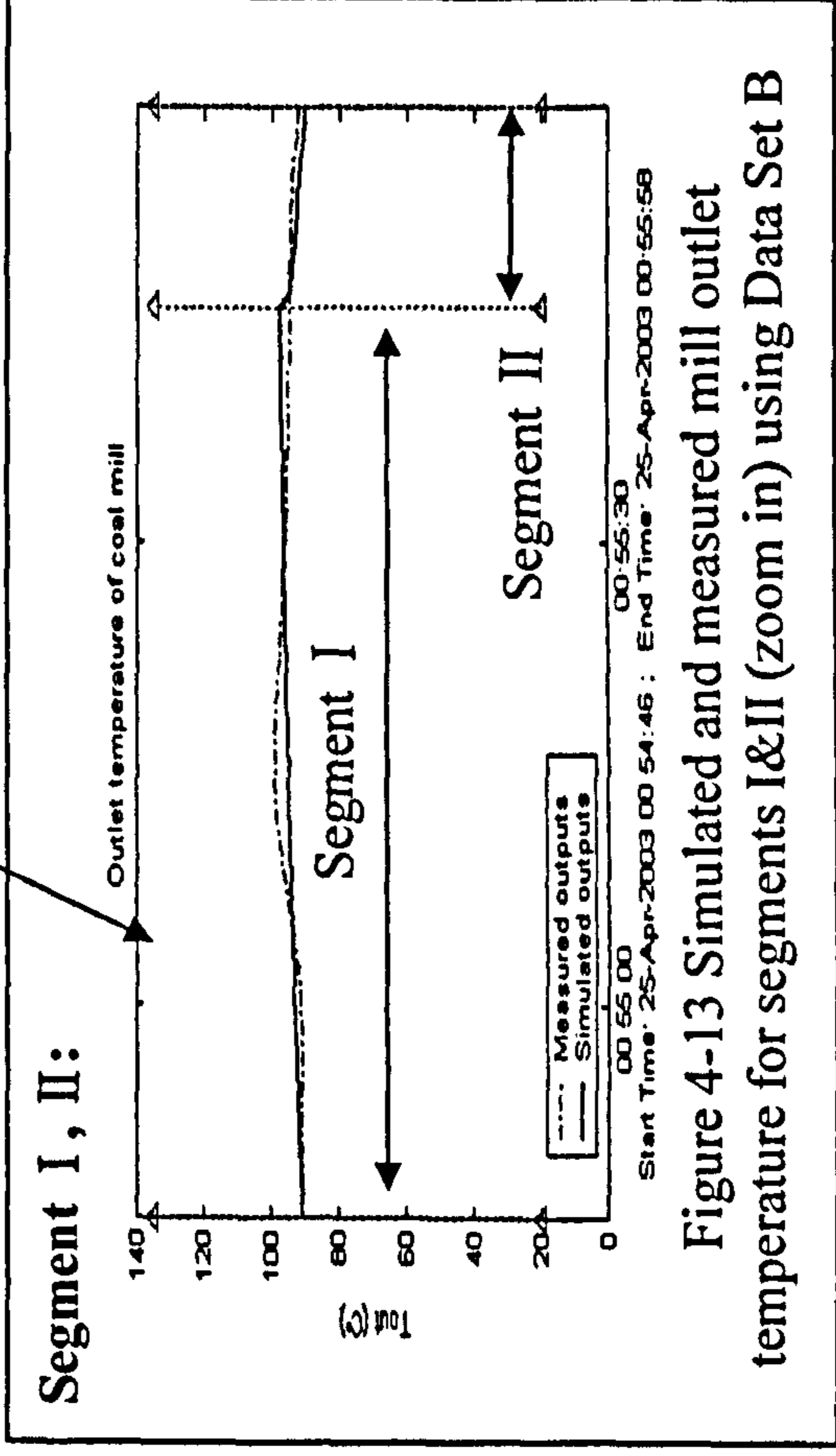


Figure 4-13 Simulated and measured mill outlet temperature for segments I&II (zoom in) using Data Set B

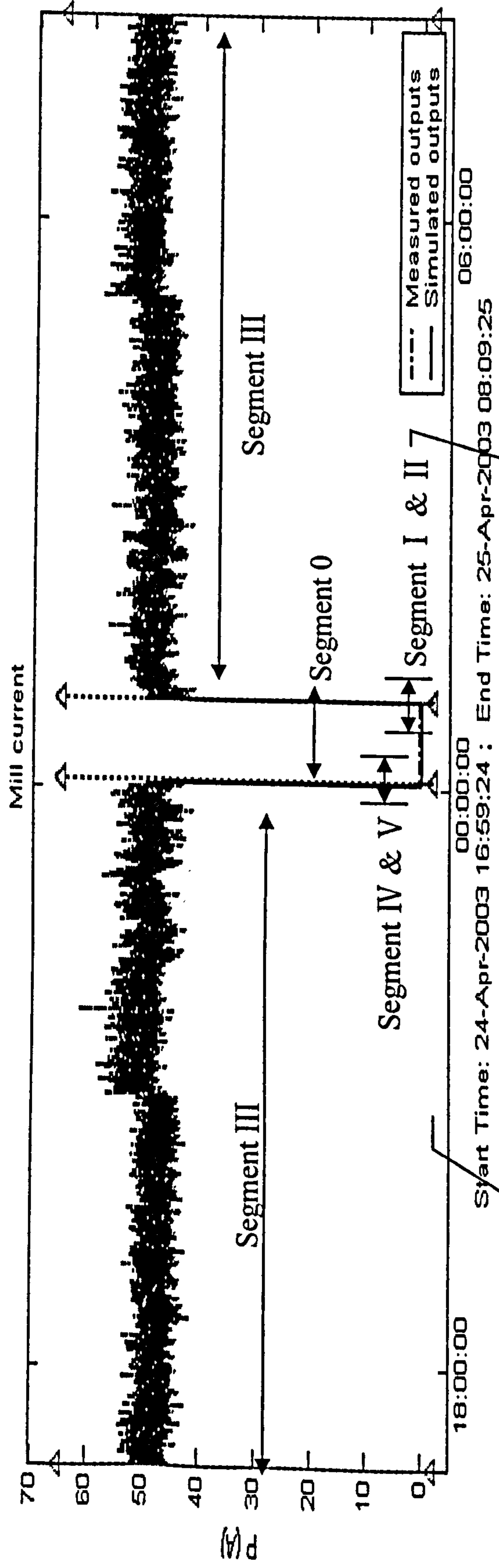


Figure 4-14 Simulated and measured mill current for all segments using Data Set B

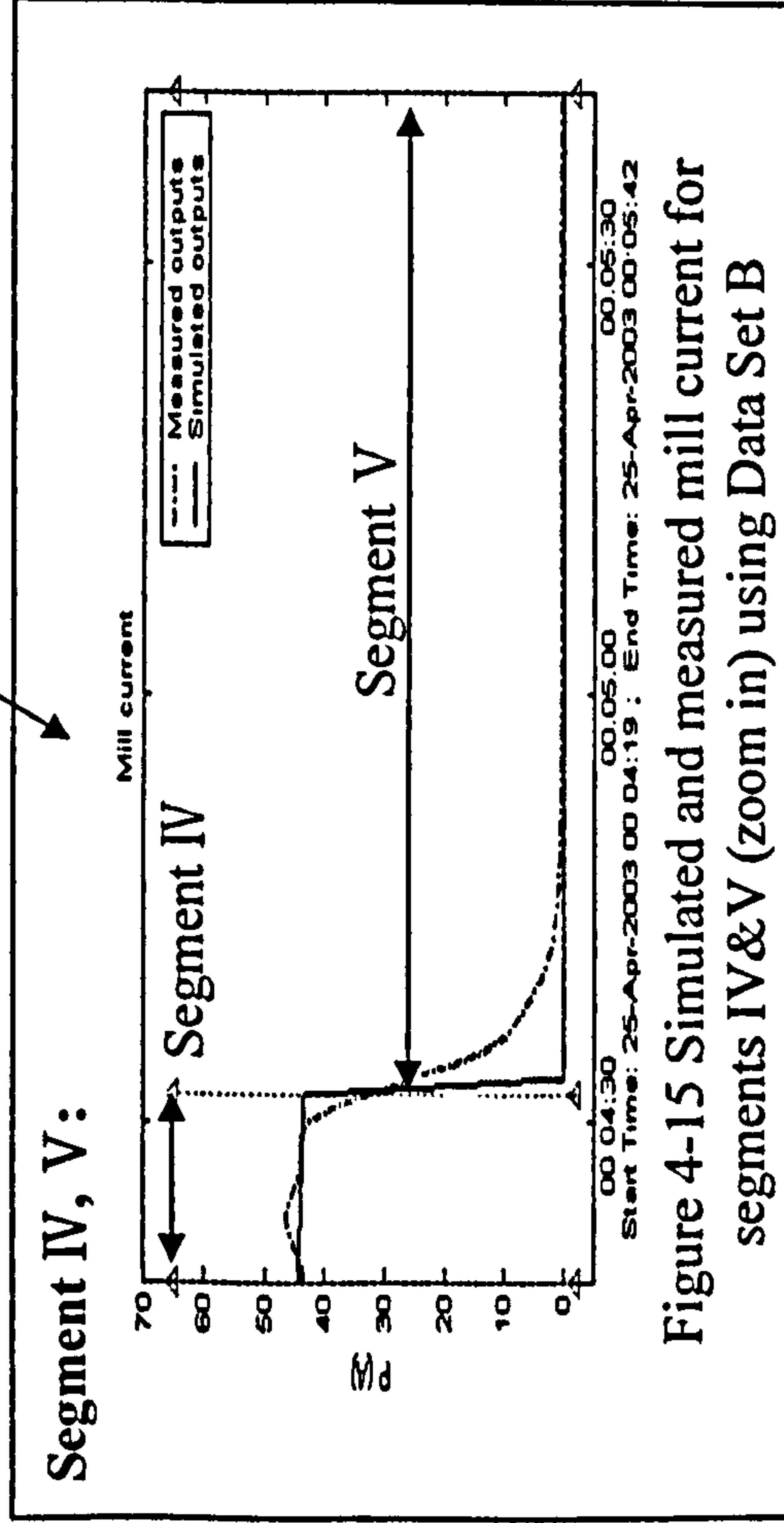


Figure 4-15 Simulated and measured mill current for segments IV&V (zoom in) using Data Set B

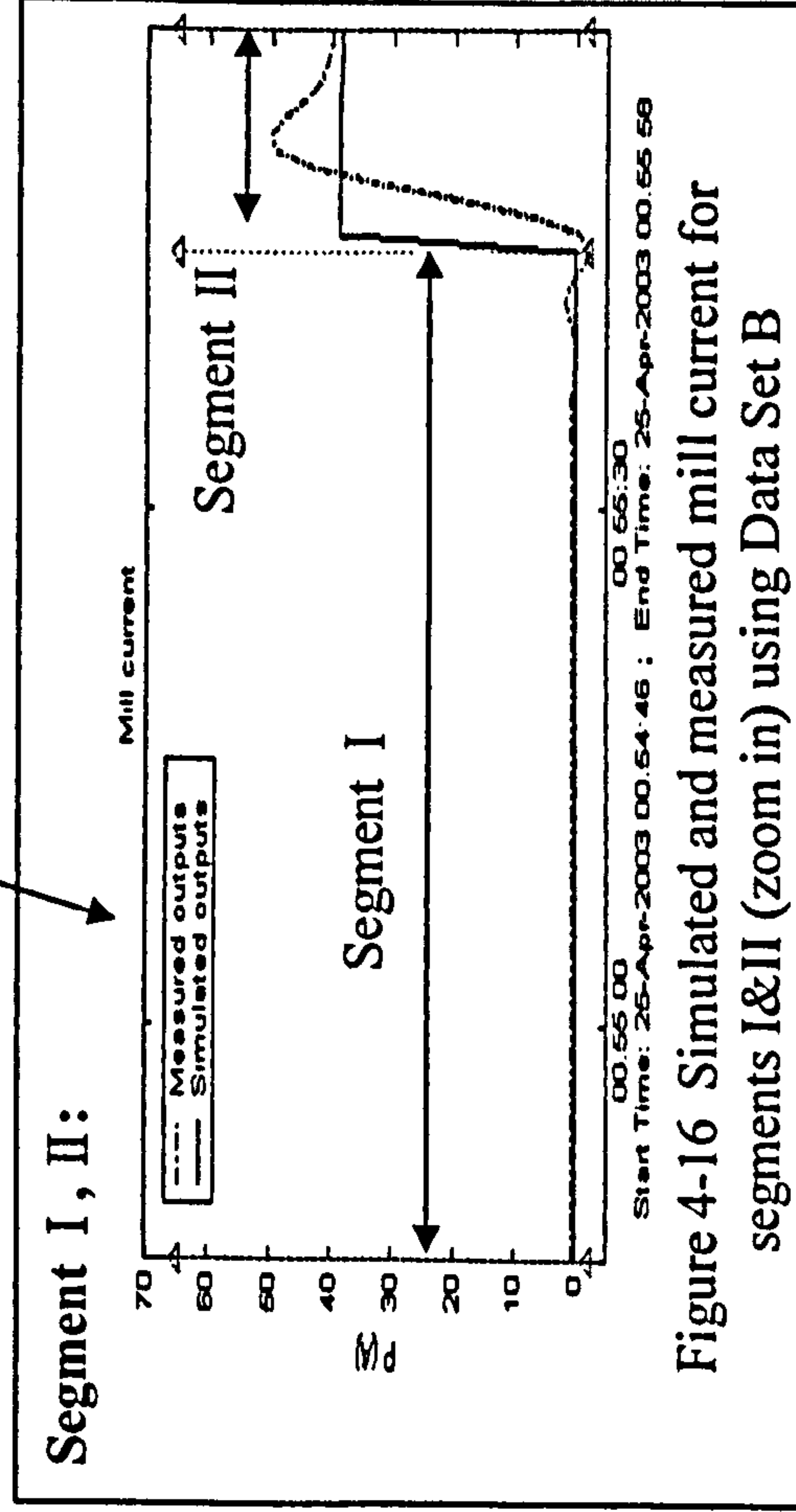


Figure 4-16 Simulated and measured mill current for segments I&II (zoom in) using Data Set B



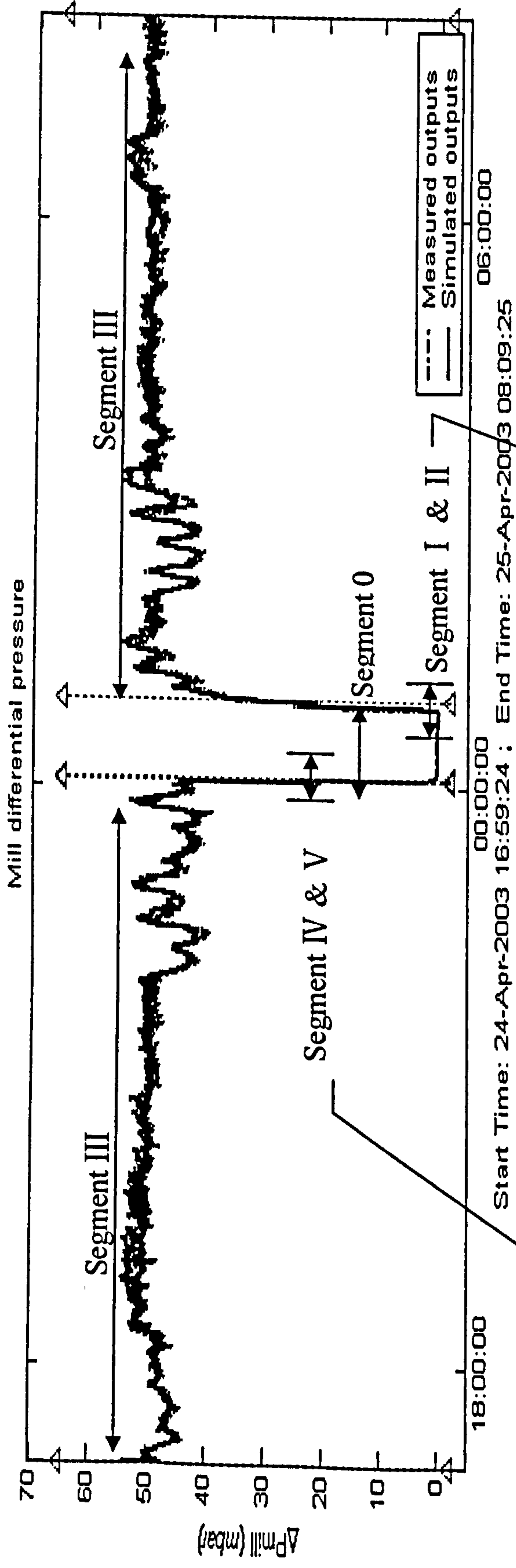


Figure 4-17 Simulated and measured mill differential pressure for all segments using Data Set B

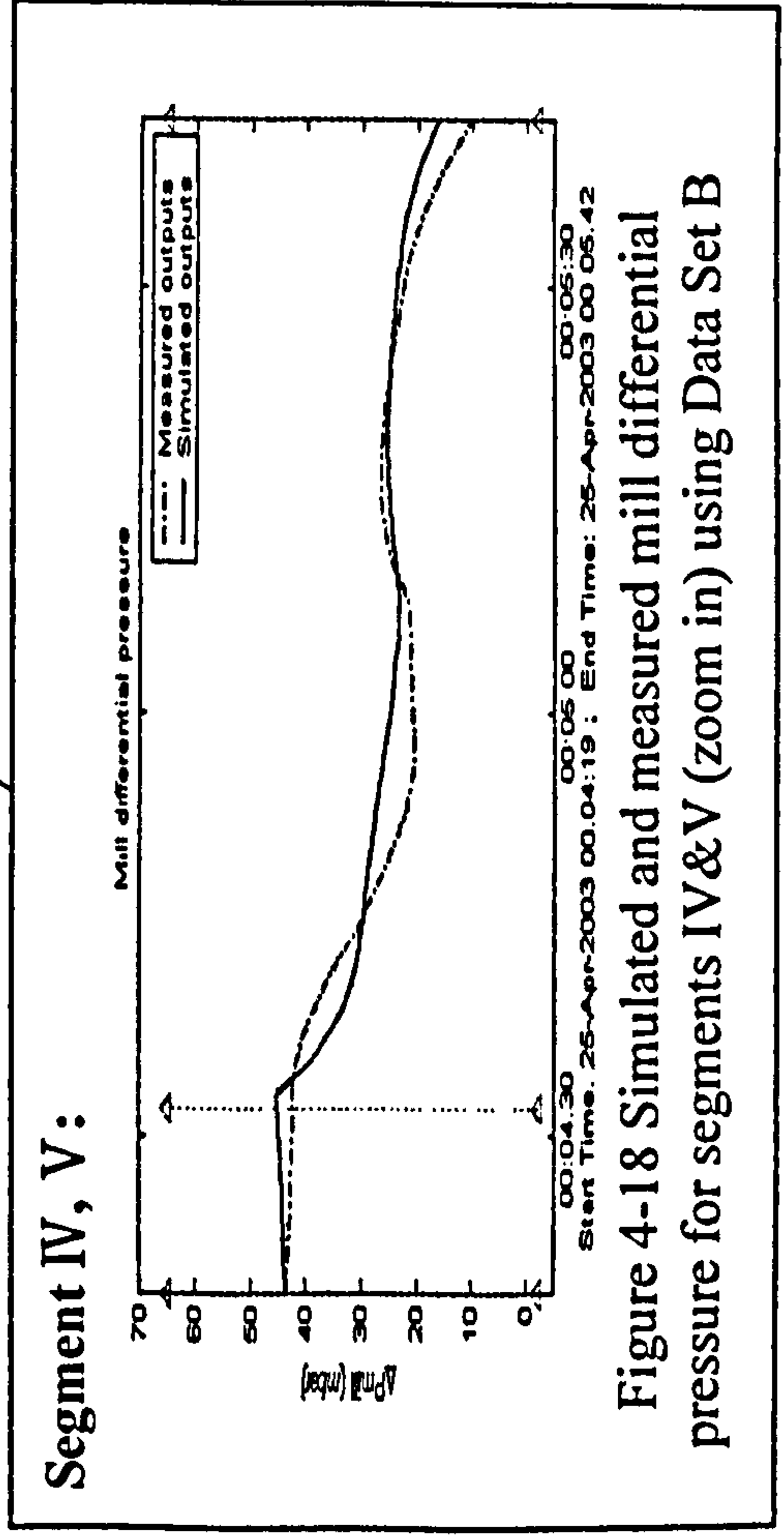


Figure 4-18 Simulated and measured mill differential pressure for segments IV&V (zoom in) using Data Set B

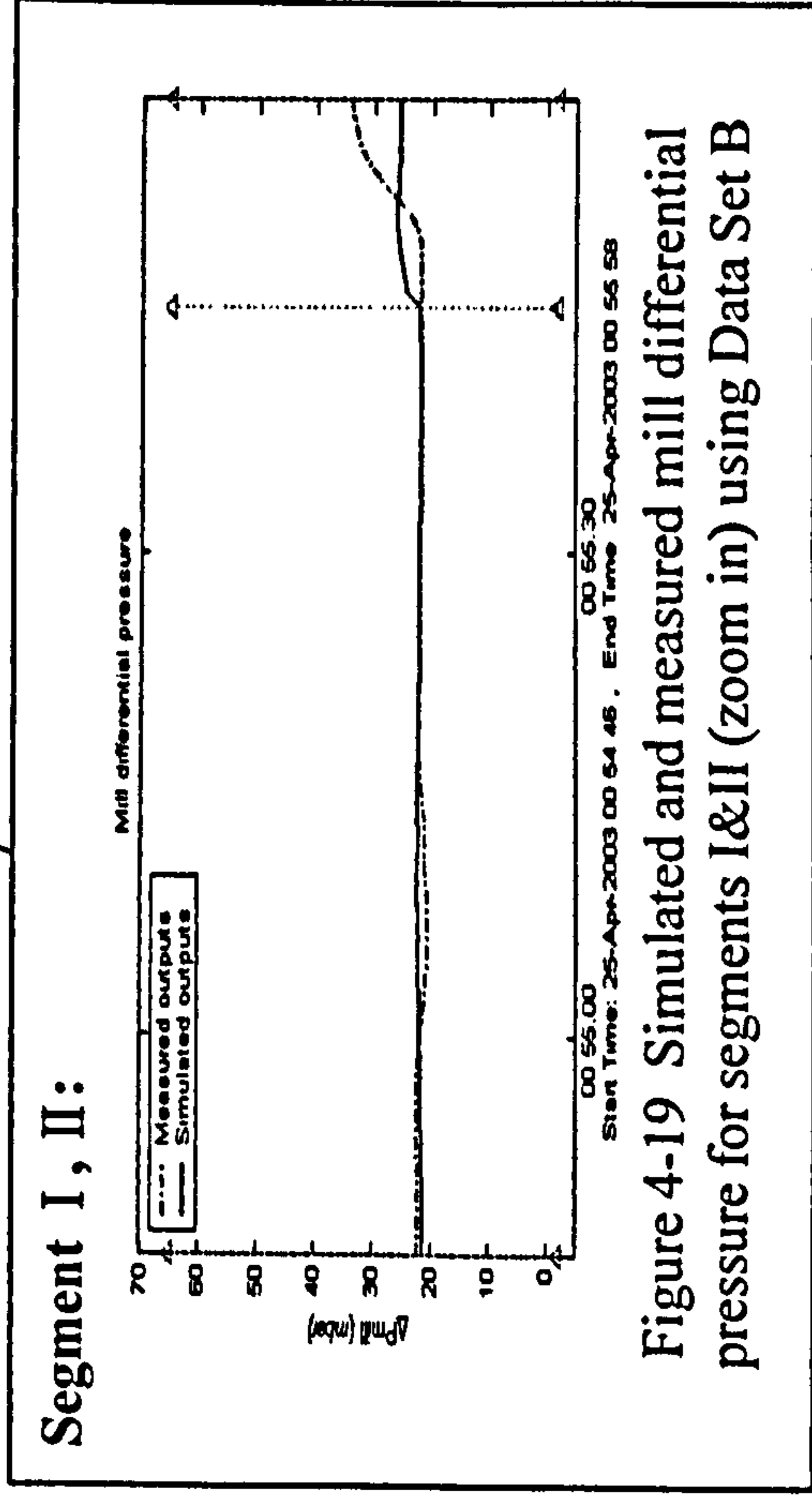


Figure 4-19 Simulated and measured mill differential pressure for segments I&II (zoom in) using Data Set B

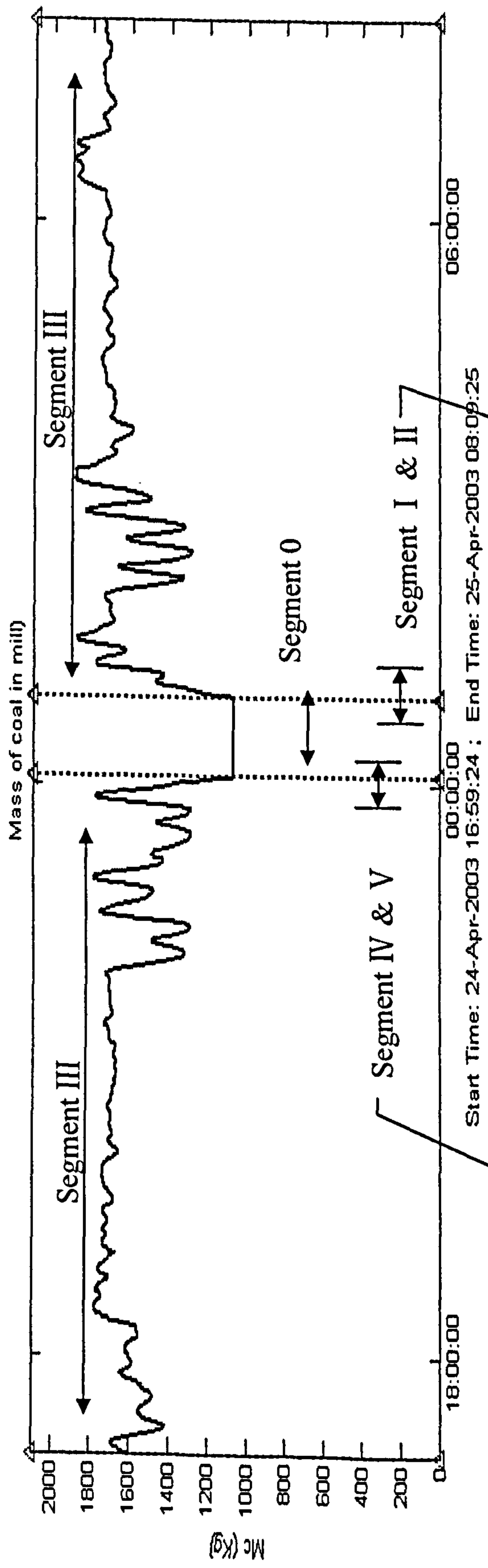


Figure 4-20 Simulated coal mass in mill for all segments using Data Set B

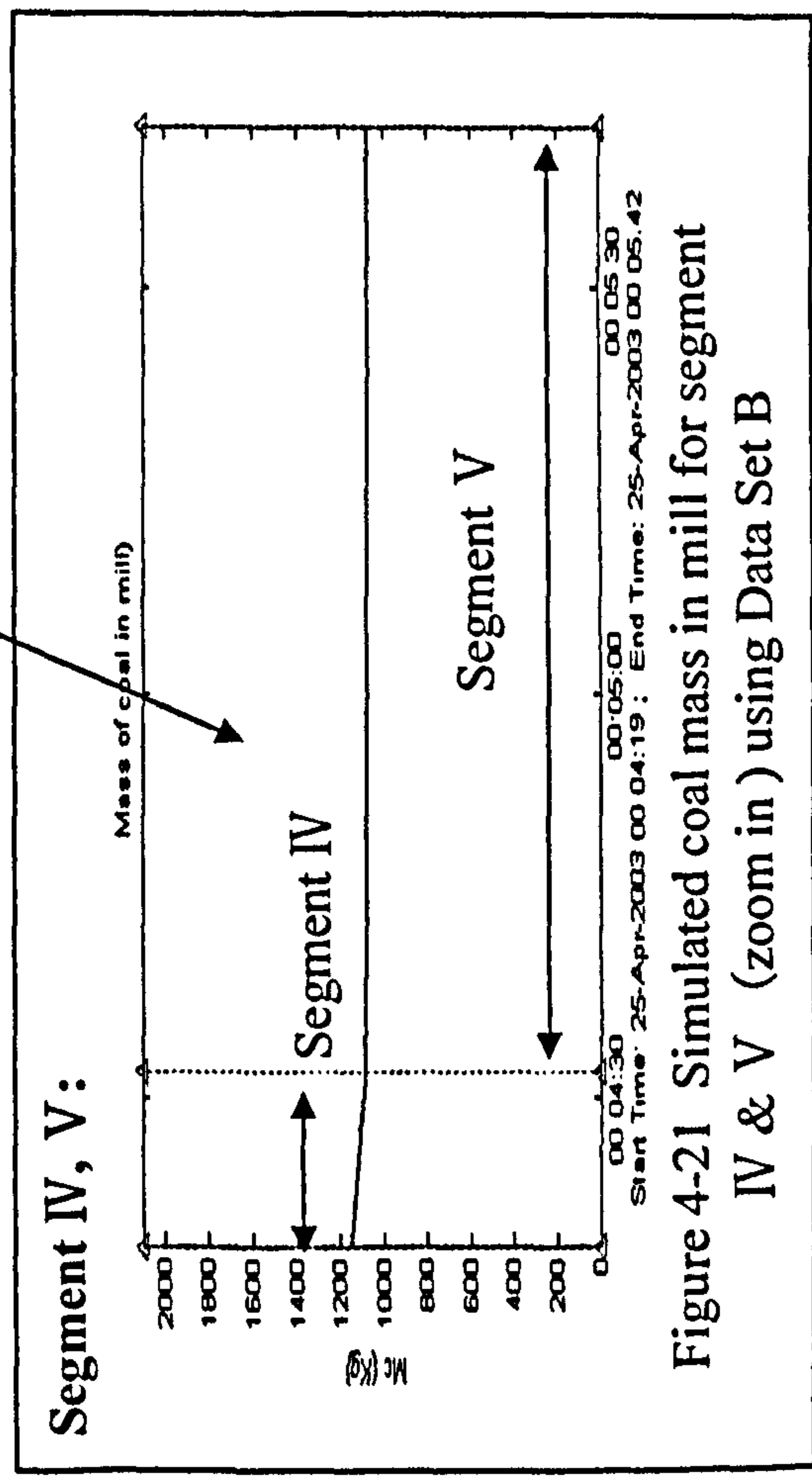


Figure 4-21 Simulated coal mass in mill for segment IV & V (zoom in) using Data Set B

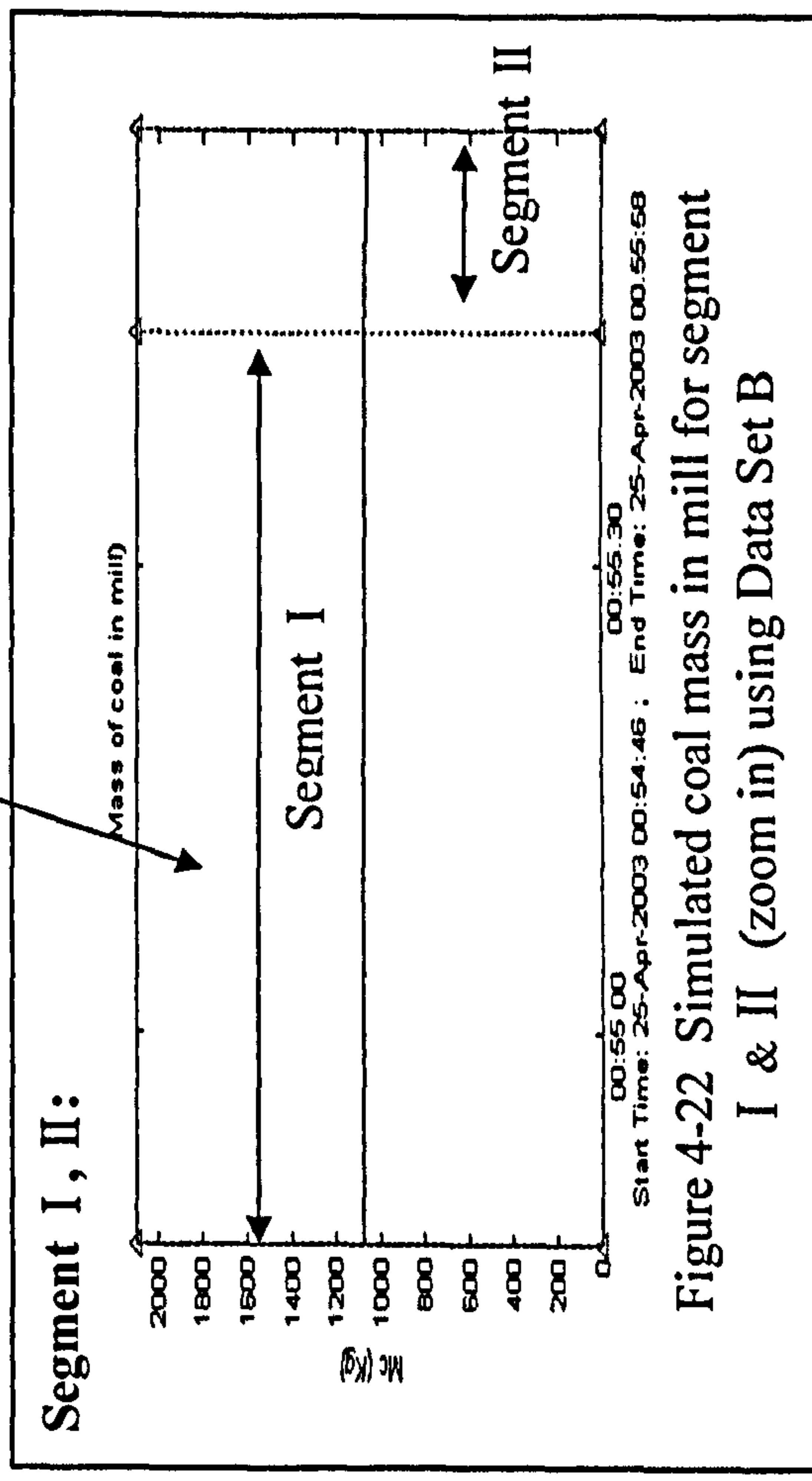


Figure 4-22 Simulated coal mass in mill for segment I & II (zoom in) using Data Set B



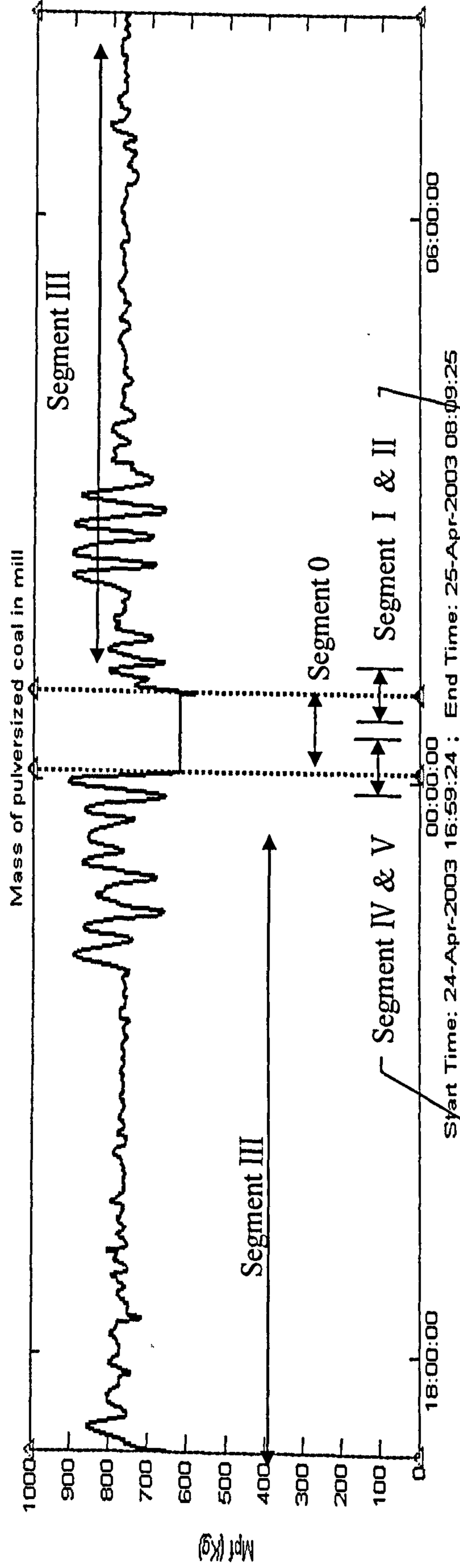


Figure 4-23 Simulated pulverized mass of coal in mill for all segments using Data Set B

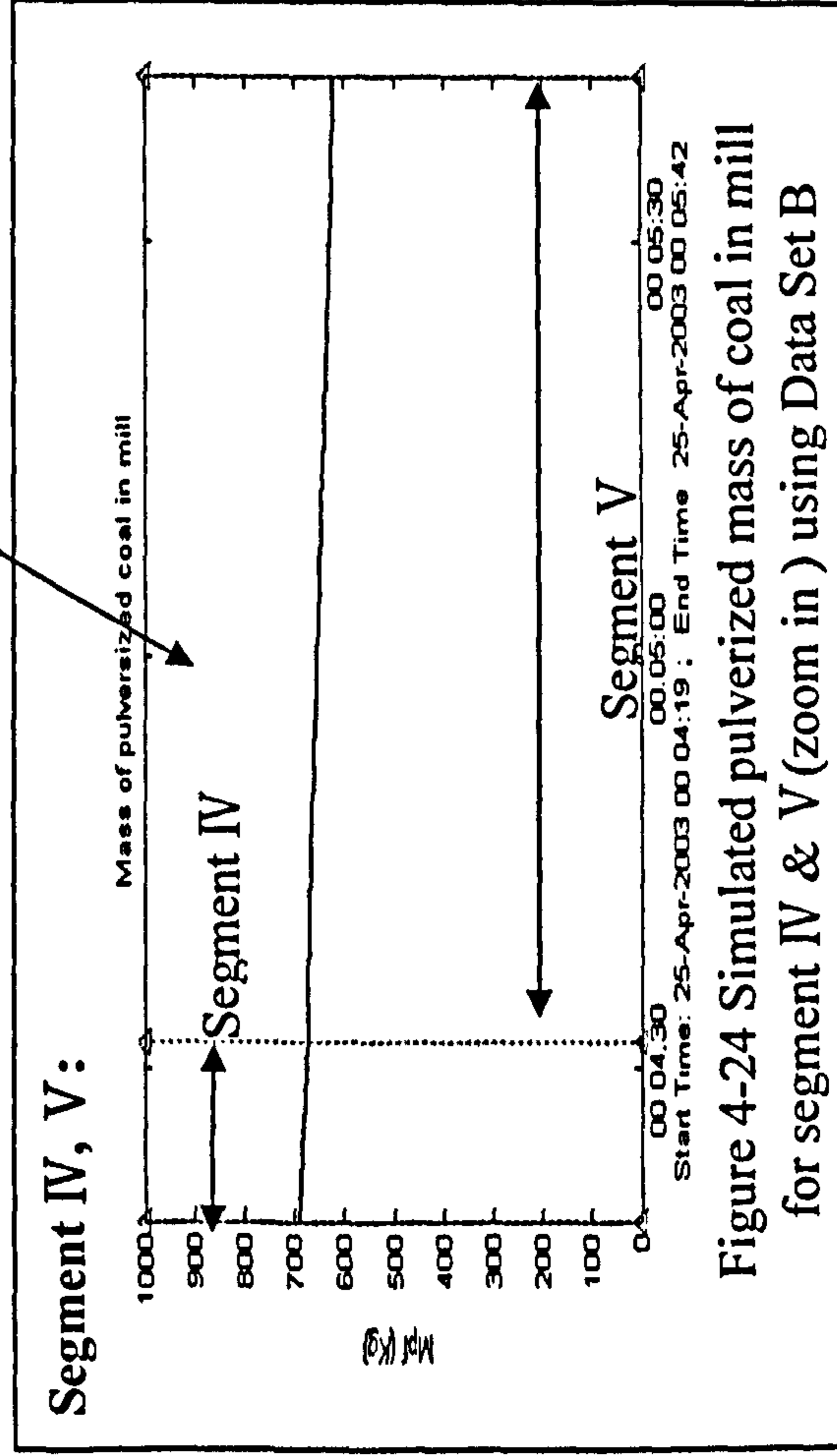


Figure 4-24 Simulated pulverized mass of coal in mill for segment IV & V (zoom in ) using Data Set B

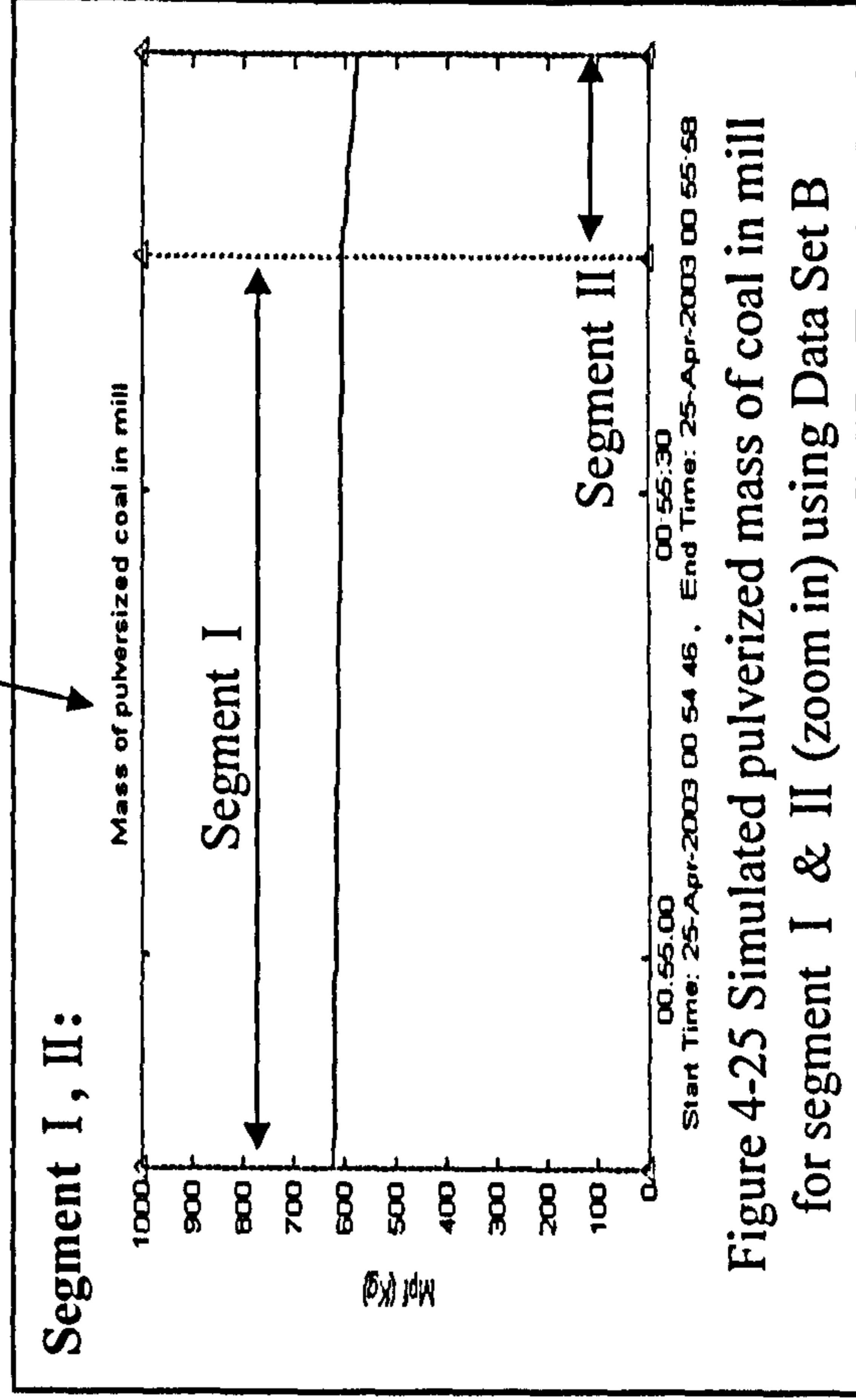


Figure 4-25 Simulated pulverized mass of coal in mill for segment I & II (zoom in) using Data Set B

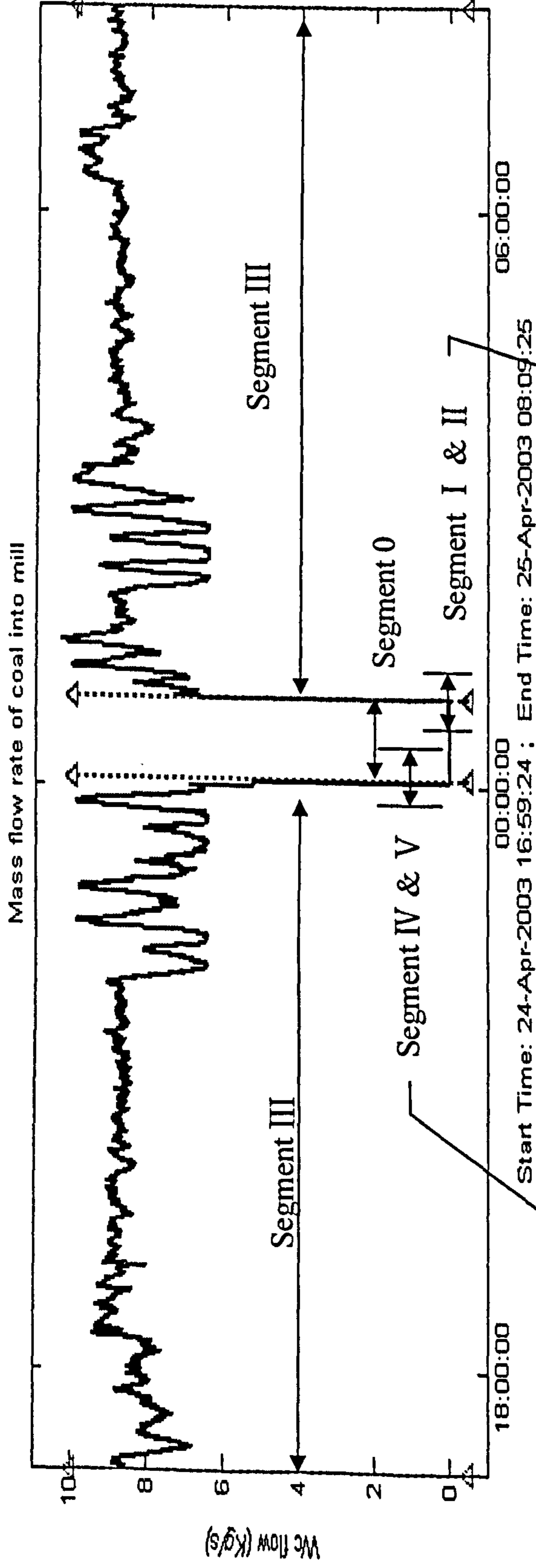


Figure 4-26 Coal mass flow rate into mill for all segments using Data Set B

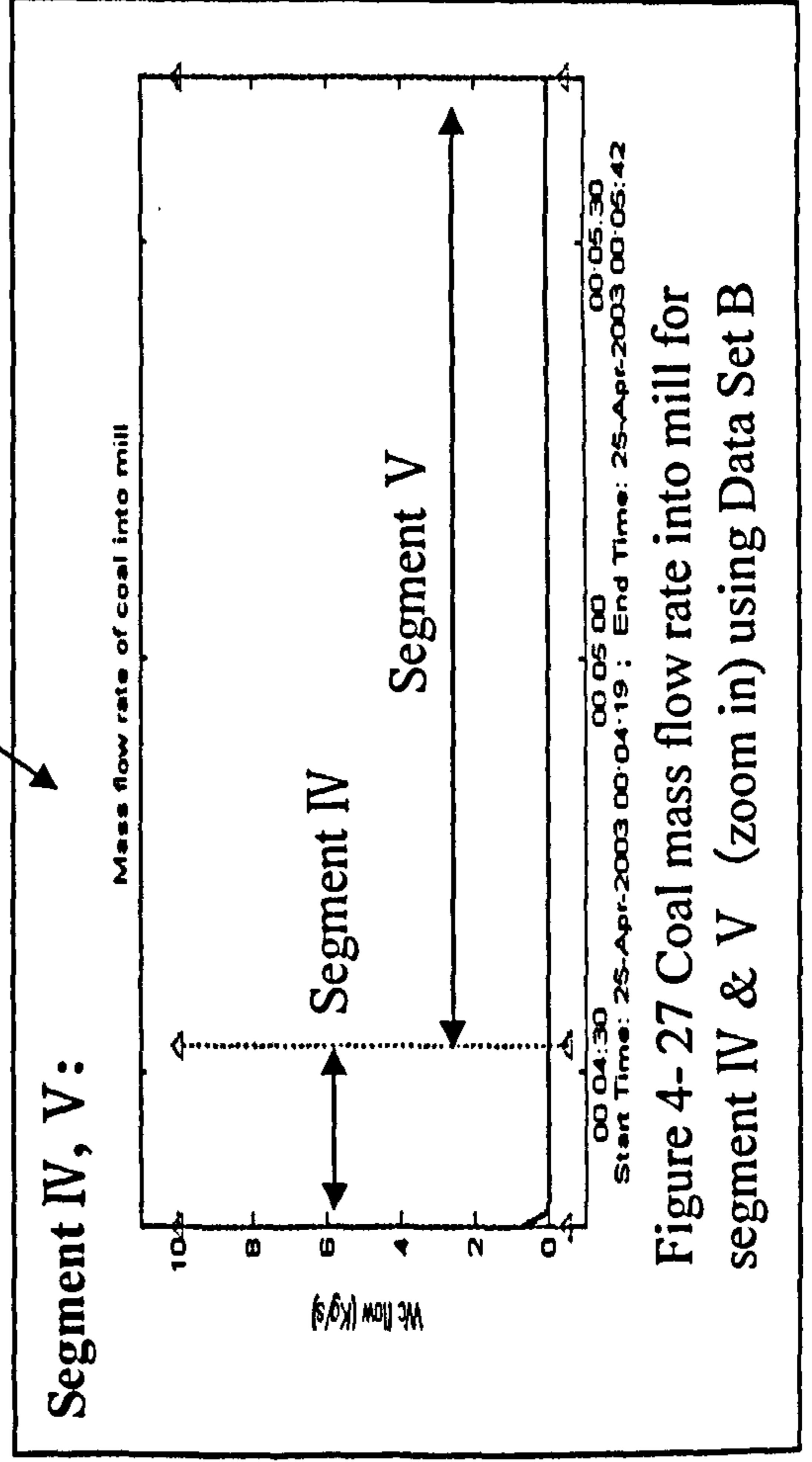


Figure 4-27 Coal mass flow rate into mill for segment IV & V (zoom in) using Data Set B

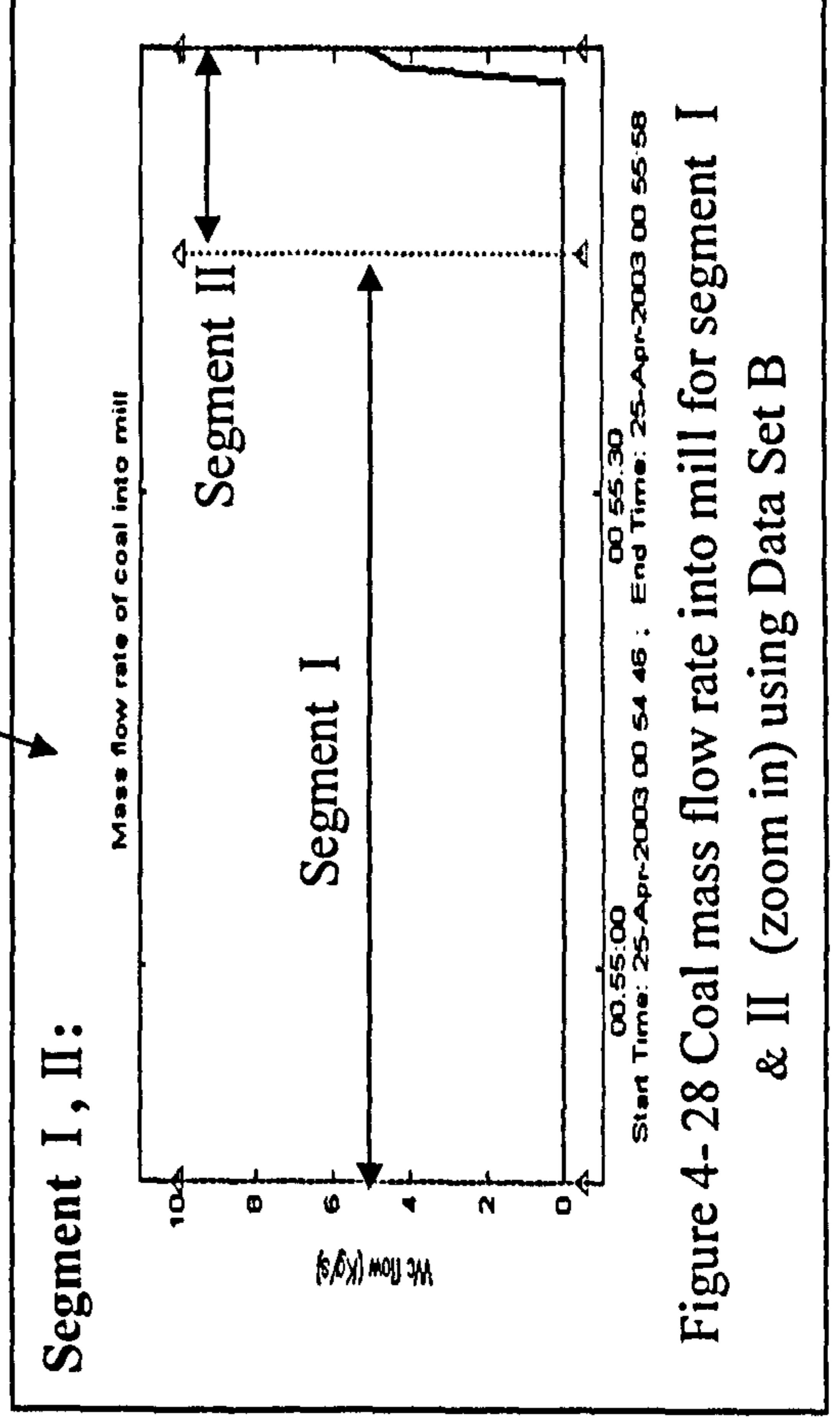


Figure 4-28 Coal mass flow rate into mill for segment I & II (zoom in) using Data Set B



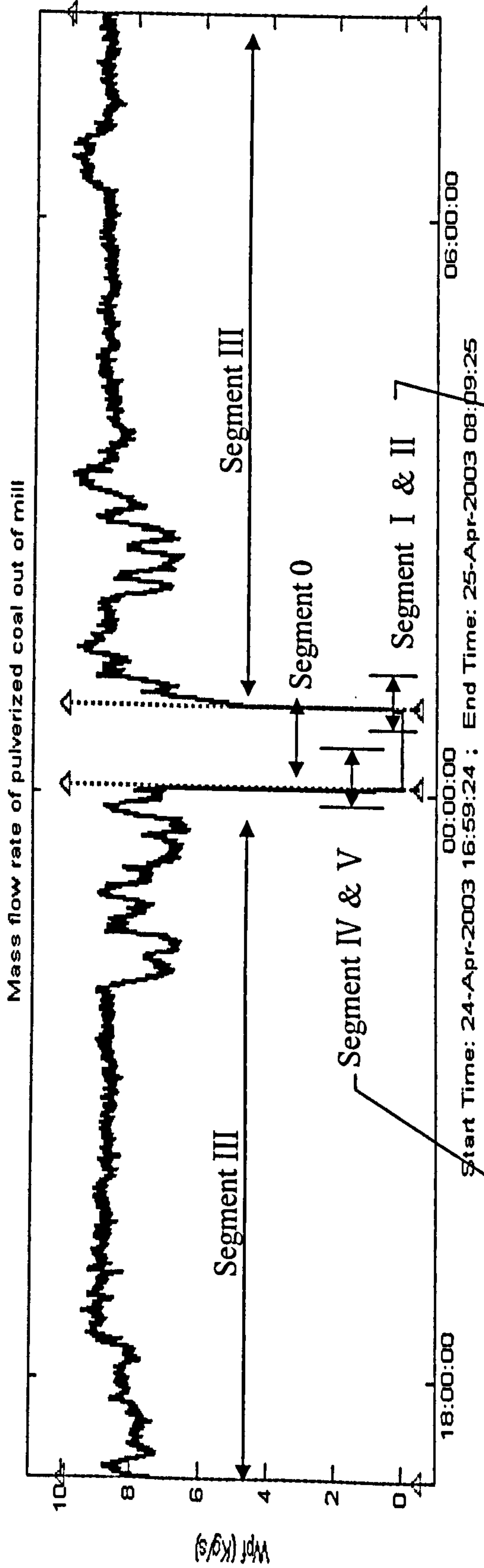


Figure 4-29 Simulated pulverized mass flow rate out of mill for all segments using Data Set B

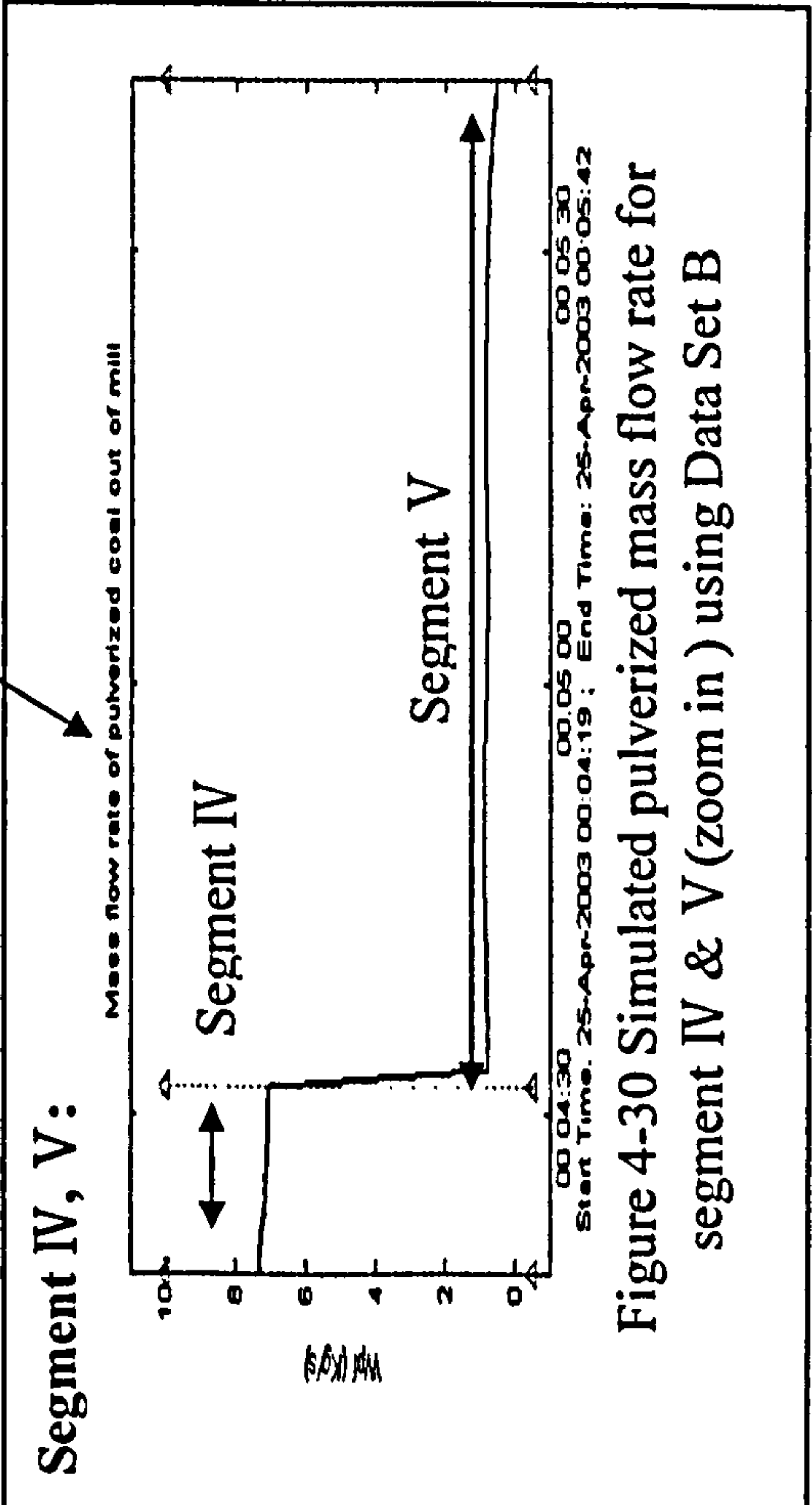


Figure 4-30 Simulated pulverized mass flow rate for segment IV & V (zoom in) using Data Set B

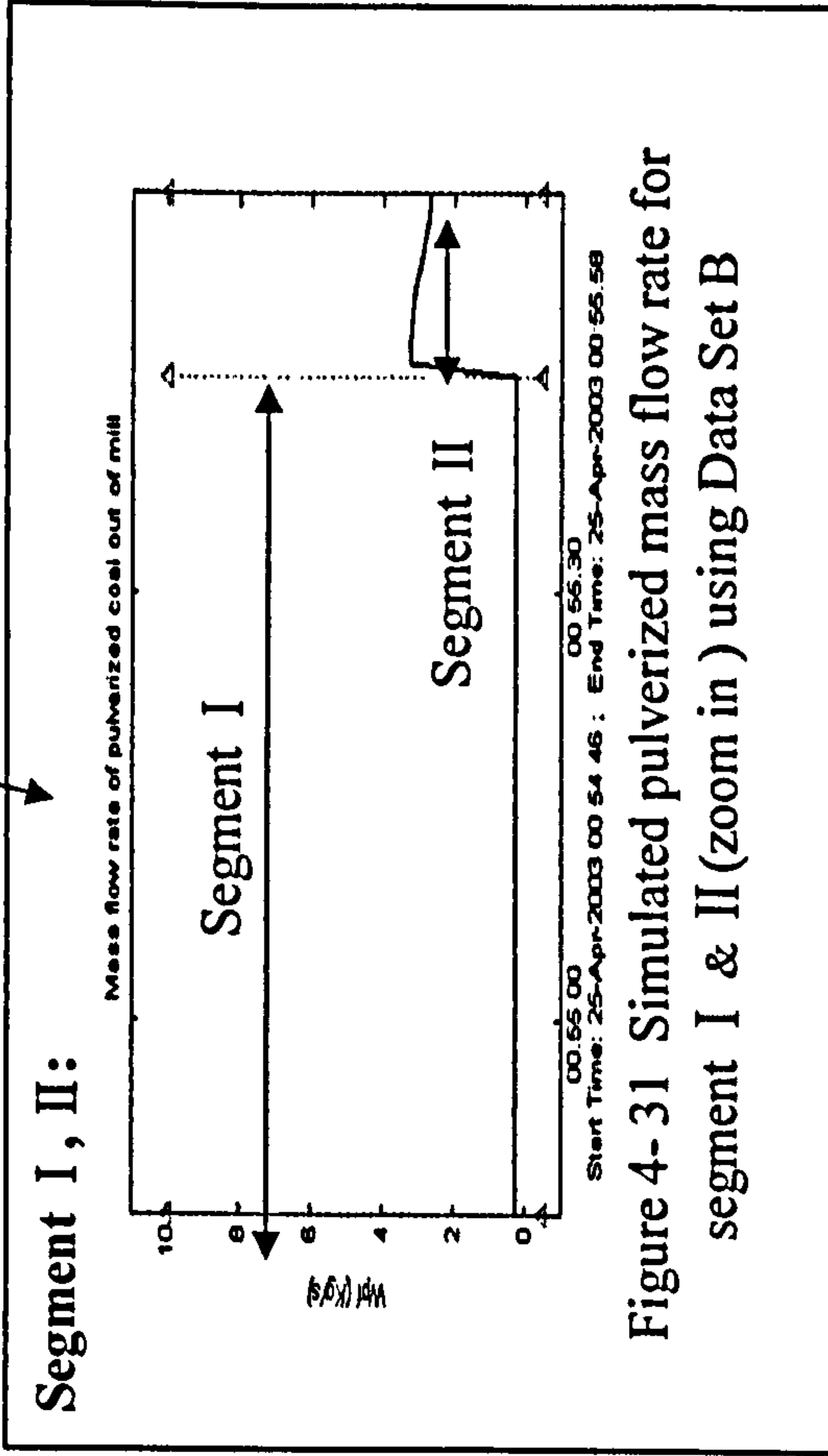


Figure 4-31 Simulated pulverized mass flow rate for segment I & II (zoom in) using Data Set B

The average errors between the simulated outputs and the measured outputs of all these simulation studies using the three different dynamic data sets are summarized in Table 4-3, in which the AbsError and RelError are calculated in the following formats. For example, AbsError of  $T_{out}$  is

calculated by  $\frac{1}{N} \sum_{i=1}^N |T_{out}(i) - \hat{T}_{out}(i)|$ , the RelError of  $T_{out}$  is calculated by

$$\frac{\frac{1}{N} \sum_{i=1}^N |T_{out}(i) - \hat{T}_{out}(i)|}{\max(T_{out})} \times 100\% .$$

Table 4-3 Average errors of the simulated results

Variables	Data Set A (Identification)		Data Set B (Validation 1)		Data Set C (Validation 2)	
	AbsError	RelError	AbsError	RelError	AbsError	RelError
$T_{out}$	2.02 °C	1.68%	2.19 °C	1.82%	2.99 °C	2.49%
$P$	0.83Amp	1.38%	1.73Amp	2.88%	1.84 Amp	3.07%
$\Delta P_{mill}$	0.50mbar	0.83%	1.00mbar	1.67%	1.81mbar	3.02%

From the results, it can be seen that the errors generated by using Data Set B and C for the validations are within the reasonable range comparing with the results obtained for parameter identification using Data Set A. Although some gaps exist between the measured and estimated outputs, the multi-segment coal mill model can represent the coal milling process well, especially, dynamical characteristics. Therefore, the model structure reported in this chapter can be applied to on-line estimation or prediction in milling processes. The results have been passed back to the engineers at RWEnPower Plc. and all agreed that the model is accurate enough to be accepted by the engineers for fault detection and condition monitoring.

#### 4.4 Summary and Discussion

In order to cover the start-up and shut-down process, a multi-segment coal



mill model is developed in this chapter. According the coal mill operation sequence, the whole milling process is partitioned into six segments, six sets of model equations are developed accordingly to represent the coal mill in the respective states. Simulation studies of the coal mill model are carried out based three data sets which cover the start-up, normal grinding process and shut-down process. Date Set A was employed for the model coefficients identification. Data Set B and Data Set C were applied for model validation. Simulation results show that the model can represent the coal milling process well, especially, dynamical characteristics.

# Chapter 5

## On-Line Implementation of the Coal Mill Model

### 5.1 Introduction

As described in Chapter 3, there is no accurate measurement for mill PF flow  $W_{pf}$  thereby to control the air fuel ratio to maintain the efficiency of unit energy release and absorption and reducing environment emissions and it is difficult to detect the coal load in mill  $M_c$  to prevent mill choking and coal caking on the grinding. The model developed in this project offers a hope to estimate those variables. To obtain the variable information, it is necessary to implement the model in real-time. A prototype of on-line implementation software is developed in the project and will be described in this chapter.

By analysing the information software system used by RWEnPower Plc., C++ computer language is chosen for real time implementation of the model, because C++ program can be compiled into executable code and the code does not depend on any commercial software package to run. Figure 5-1 illustrates the schematic structure of the on-line implementation of software program. The coal mill model runs in parallel with the real coal mill system and the estimated variables are compared with the real measurement in real time. Also the intermediate variables (*i.e.*  $W_{pf}$ ,  $M_c$ ) are estimated, reported, and displayed on computer screen so the engineers in the power plant will benefit from the extra information provided by the estimated variable values. The mill can be controlled in a better way then



the boiler would achieve higher combustion efficiency. At this stage of the software implementation, the coal mill parameters will be upgraded off-line as the updating is only required when the mill conditions are changed.

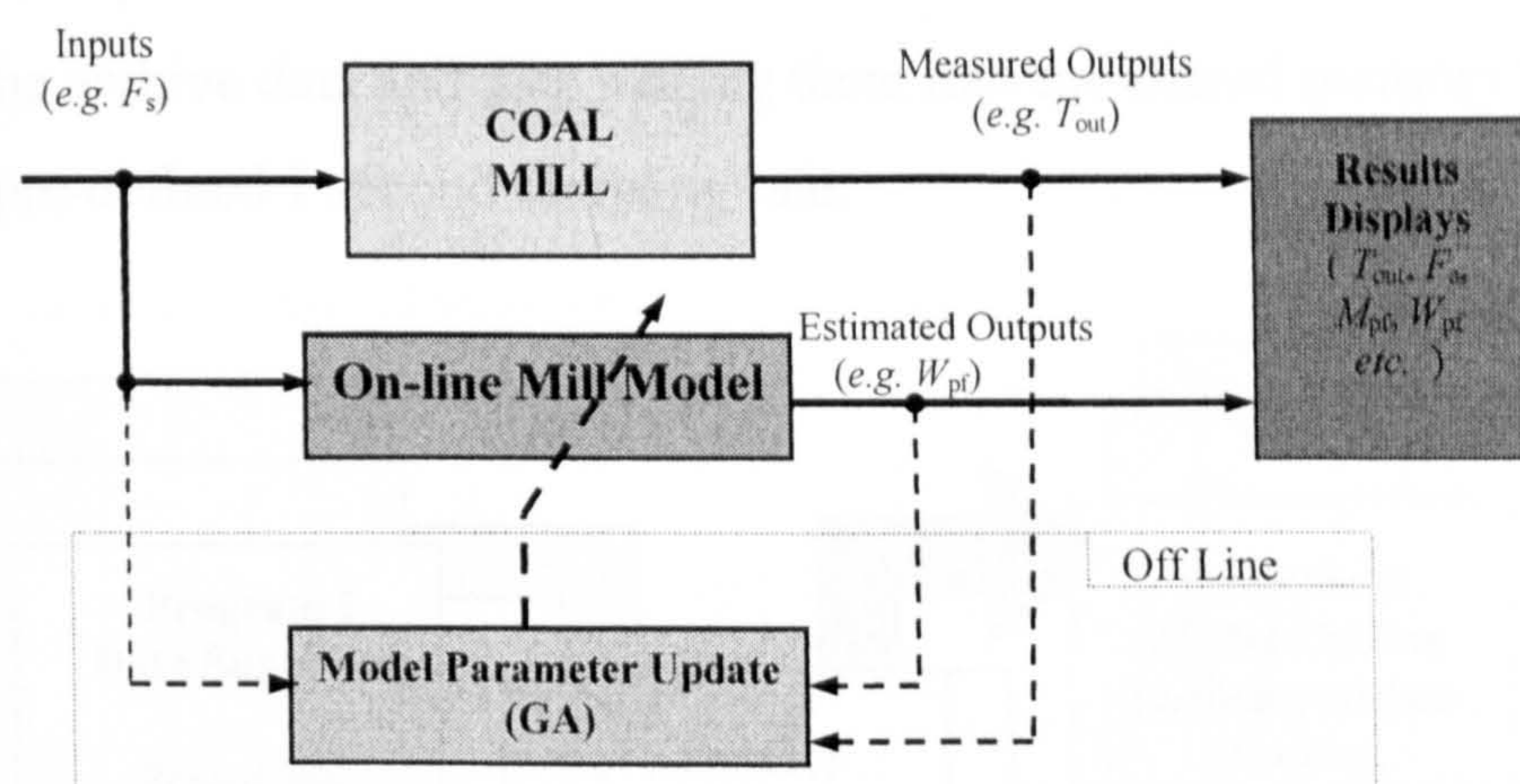


Figure 5-1 Schematic structure of the software for on-line implementation

In order to generate a generic structure of the software and to be used in any coal mills at power plants, the shared-memory software design technique is adopted, which is illustrated in Figure 5-2. The software requires mapping a set of memory with a known base address for accommodating the data logged from any data acquisition systems. The on-line model will be given the base address for the memory map. It will then take the data from the memory following the rule of FIFO (first in first out). The software is initially developed at the University of Liverpool and then passed onto RWE Power Plc. for test. The animation data acquisition system is formed first which will put the data into the memory in real-time with a pre-defined sampling rate. The software developed have the two parts - Data Supplying and On-line Modelling.

The software development is initially to match the software environment at Didcot Power Station. At the power plant, engineers use PI system for condition monitoring and collecting data on-line in real time. By adding a short software program in the PI system, engineers in power plants can



supply the on-site measured variables into the memory buffer in real time at a fixed 1 second updating rate. Data Supplying is a program that is particularly designed to simulate this on-site data supplying environment at the power plant. It reads the values of the coal mill measured variables from the archive data and then placing them into the shared memory buffer at the pre-defined 1 second sampling rate.

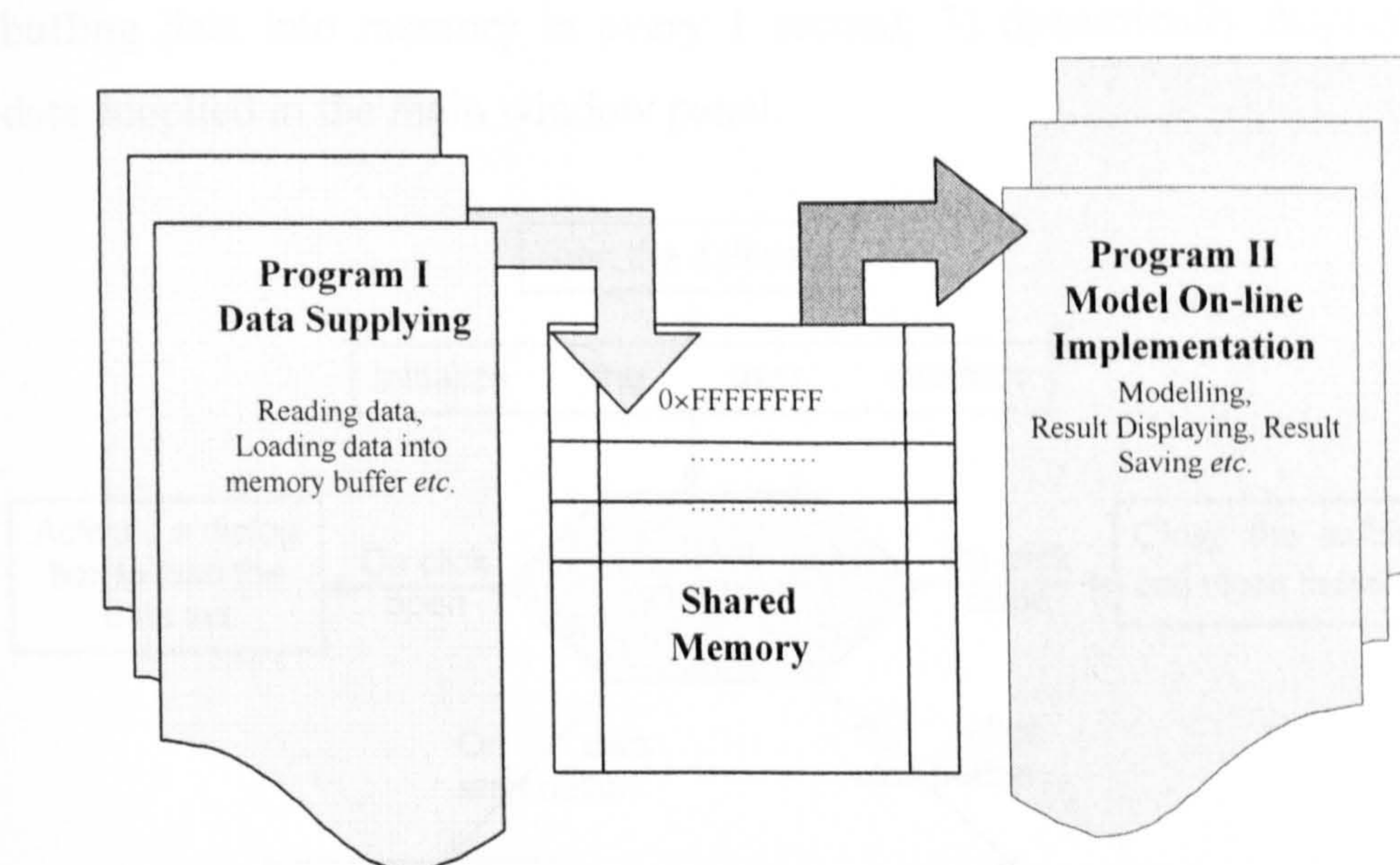


Figure 5-2 On-line modelling software based on the shared memory idea

On-line Modelling is a program of implementation of the coal mill model in real-time. It checks and reads the data from the shared memory buffer in every 1 second, and then estimates the mill variables on-line. The model updates its inputs and outputs once the data from shared memory buffer has been updated. The program provides many useful features, for example, calculating and displaying the errors between the estimated and measured values, and displaying all the variables of the coal mill model to users. The program can also save the estimated results into archive files for future use.

## 5.2 Program I - Data Supplying

Following the share memory idea introduced in the previous section, Data



Supplying Program is implemented particularly to simulate the data supplying environment in a power plant. It functions in reading data from archived data files and then loading data into the shared memory buffer in every 1 second for the coal mill modelling to be used in Program II. The user interface structure of this software is shown in Figure 5-3. It performs three basic functions: 1) data reading from data files and displaying; 2) buffering data into memory in every 1 second; 3) dynamically displaying data supplied in the main window panel.

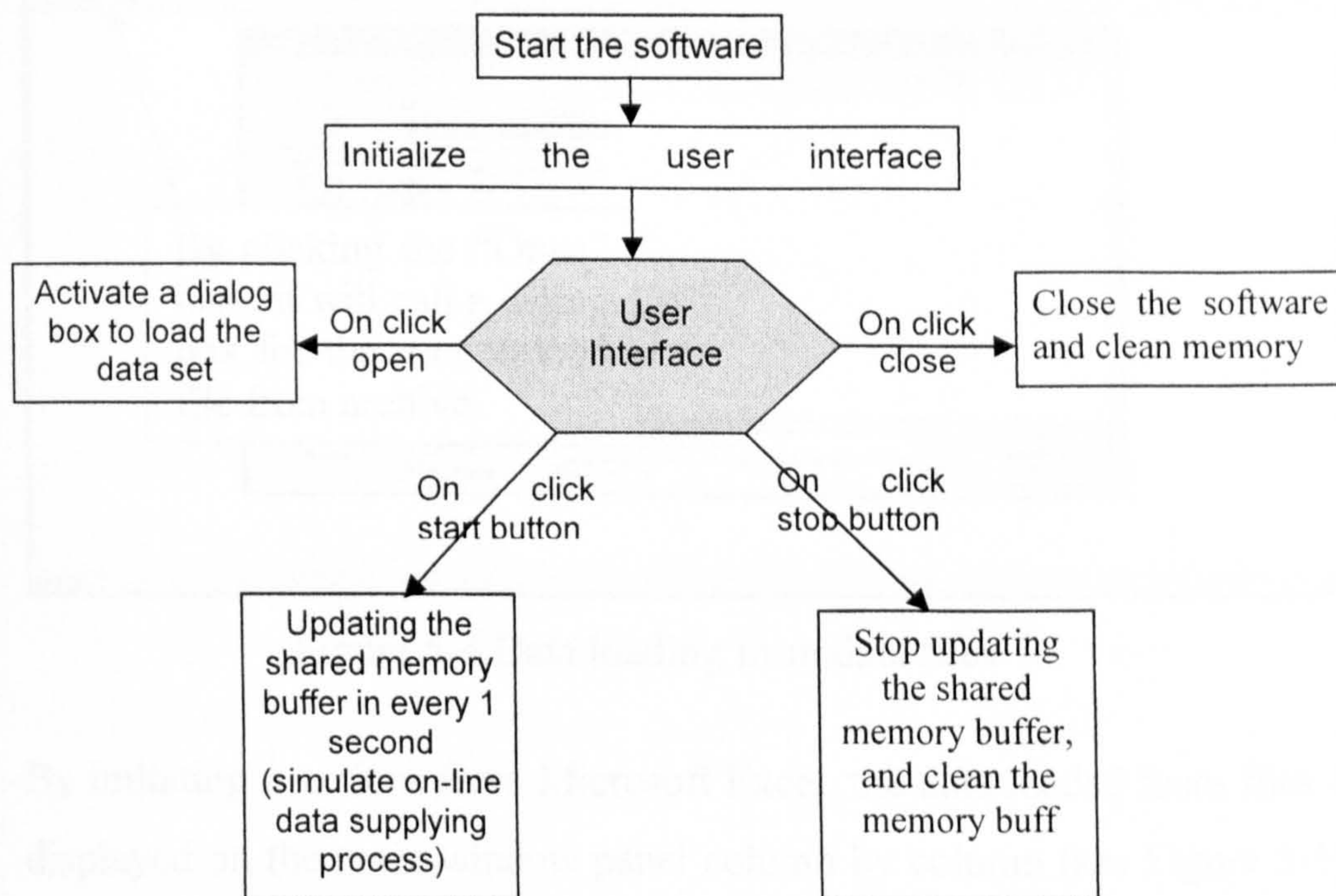


Figure 5-3 User interface structure of the Program I

With the simple and user friendly interface, Program I is very clear in functions and easy to understand for users. It is also ready to be linked to the database at power plants. Demos of the usage of the program are given below.

### 1) Loading the data from data files

The main page of Program I is shown in Figure 5-4. Since Data Supplying



is designed to simulate the data supplying environment in a power plant, it requires on-site collected data as a data source for the data supplying. Users can select the on-site collected data voluntarily as the source data. By clicking the program submenu 'Open' under the menu 'File' or clicking the 'Open' icon in the toolbar, it calls a dialog box for user to select the data file from archive to simulate the data supplying environment in power plant.

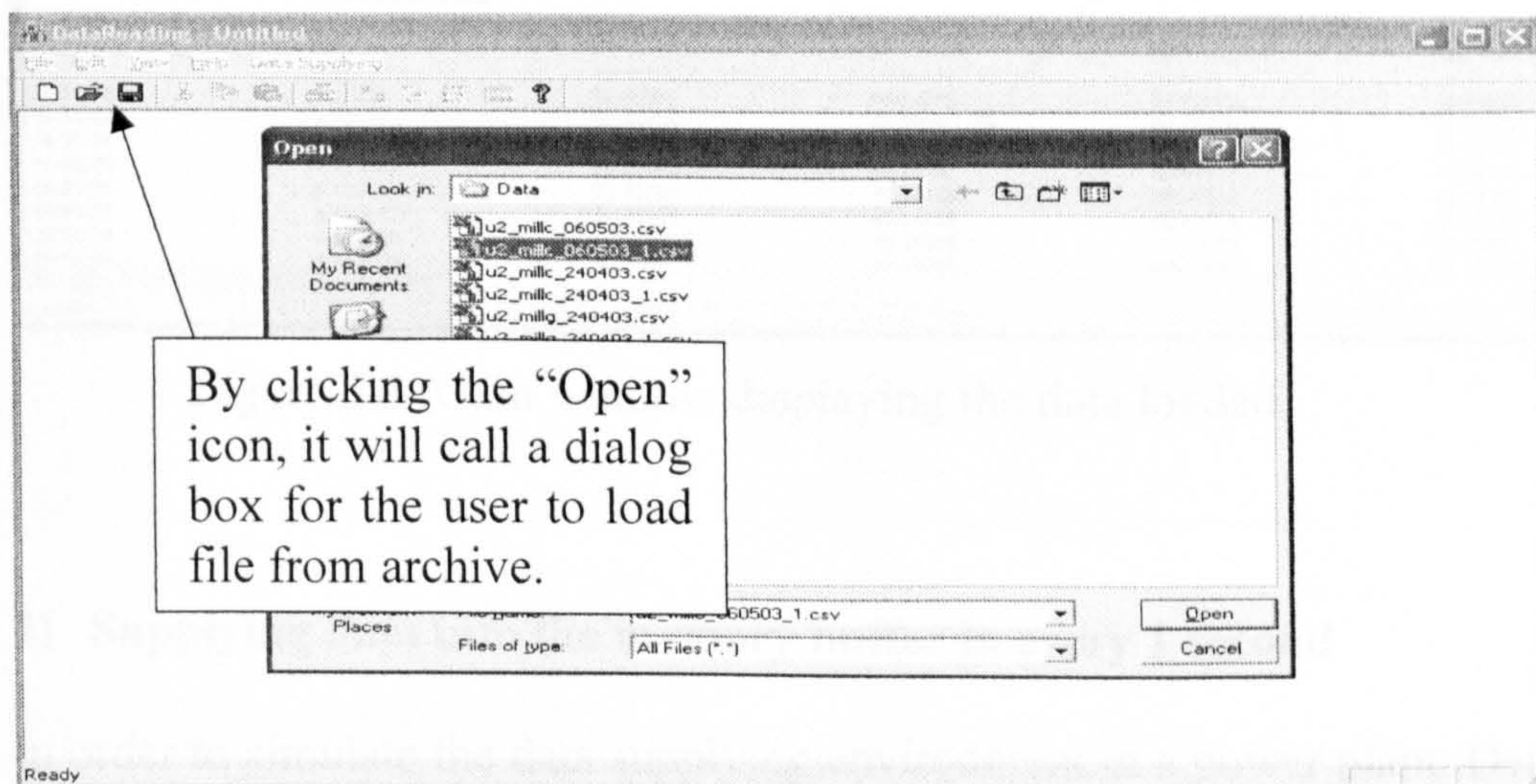


Figure 5-4 Data loading from data files

By imitating functions from Microsoft Excel, the data loaded from files is displayed on the main window panel column by column (see Figure 5-5). Users can read the detailed information of the content of the data before adopting it as the supplying data source.



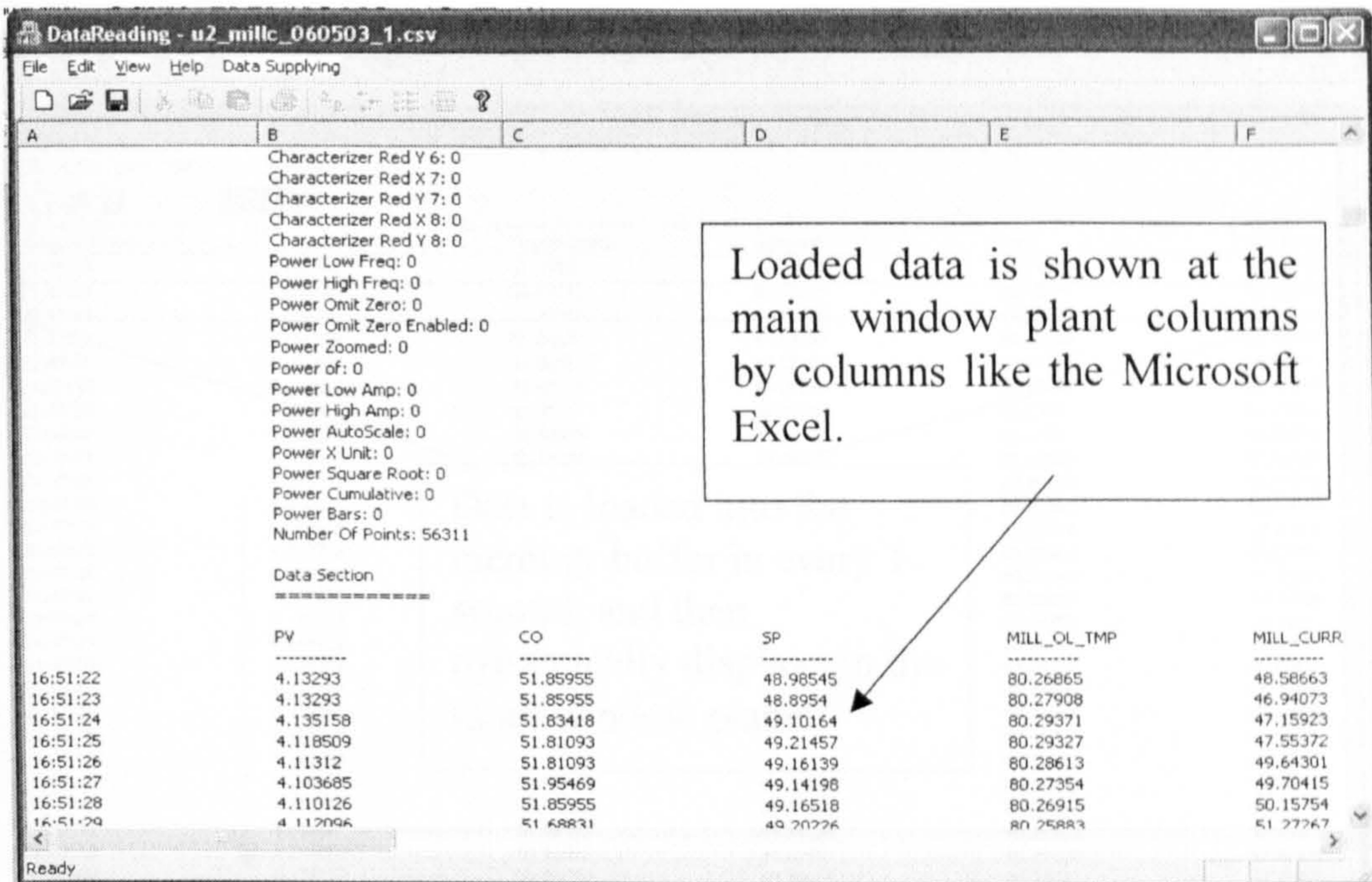


Figure 5-5 Main window displaying the data loaded

## 2) Supplying data into the memory buffer in every 1 second

In order to simulate the data supplying environment in a power plant, Data Supplying is programmed according to the purpose, where updated data is supplied into the shared memory buffer in every 1 second. Via the user interface shown in Figure 5-3, users can start and stop the data supplying into the memory buffer manually. A demo of this feature is shown in Figure 5-6. By clicking the submenu 'Start' under the main menu 'Data Supplying', the program will start loading the data into the shared memory buffer in every 1 second, and also the data supplied into the memory buffer will be dynamically displayed in the main window panel as well, where the values of the coal mill system variables are displayed column by column. In order to save the memory consumed, only the current system variables are saved into the memory buffer, and it consists of seven elements, which are: 1) current system time; 2) current primary air differential pressure  $\Delta P_{pa}$ ; 3) current feeder speed  $F_s$ ; 4) mill differential pressure  $\Delta P_{mill}$ ; 5)



outlet temperature  $T_{out}$  and 6) mill power consumed  $P$ .

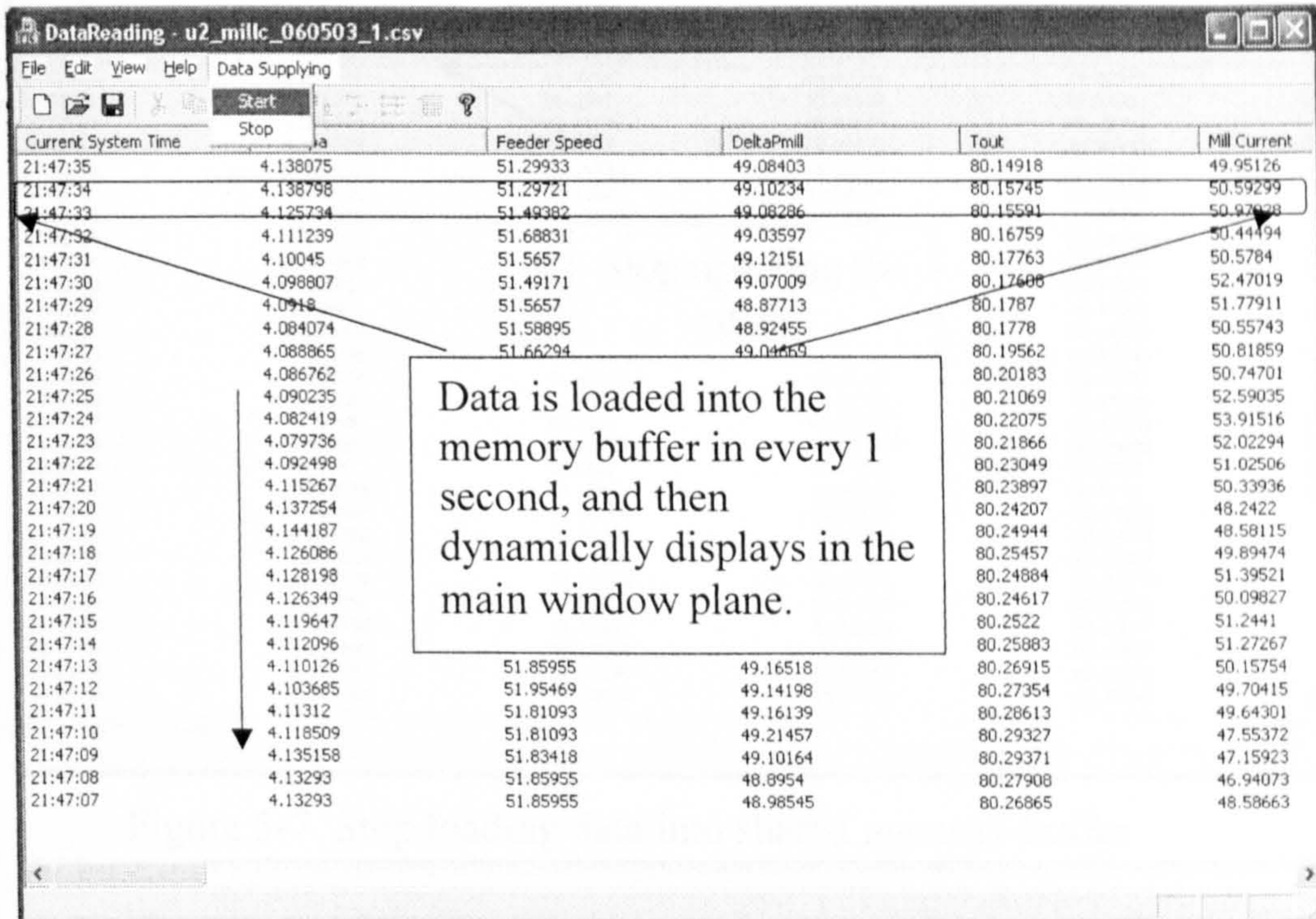


Figure 5-6 Dynamically displaying of the shared memory buffer

Similarly, by clicking the program menu 'Data Supplying' and then 'Stop', the program will stop updating the memory buffer and the data used before will be kept on displaying in the main window panel until the next 'Start' command is given (see Figure 5-7).



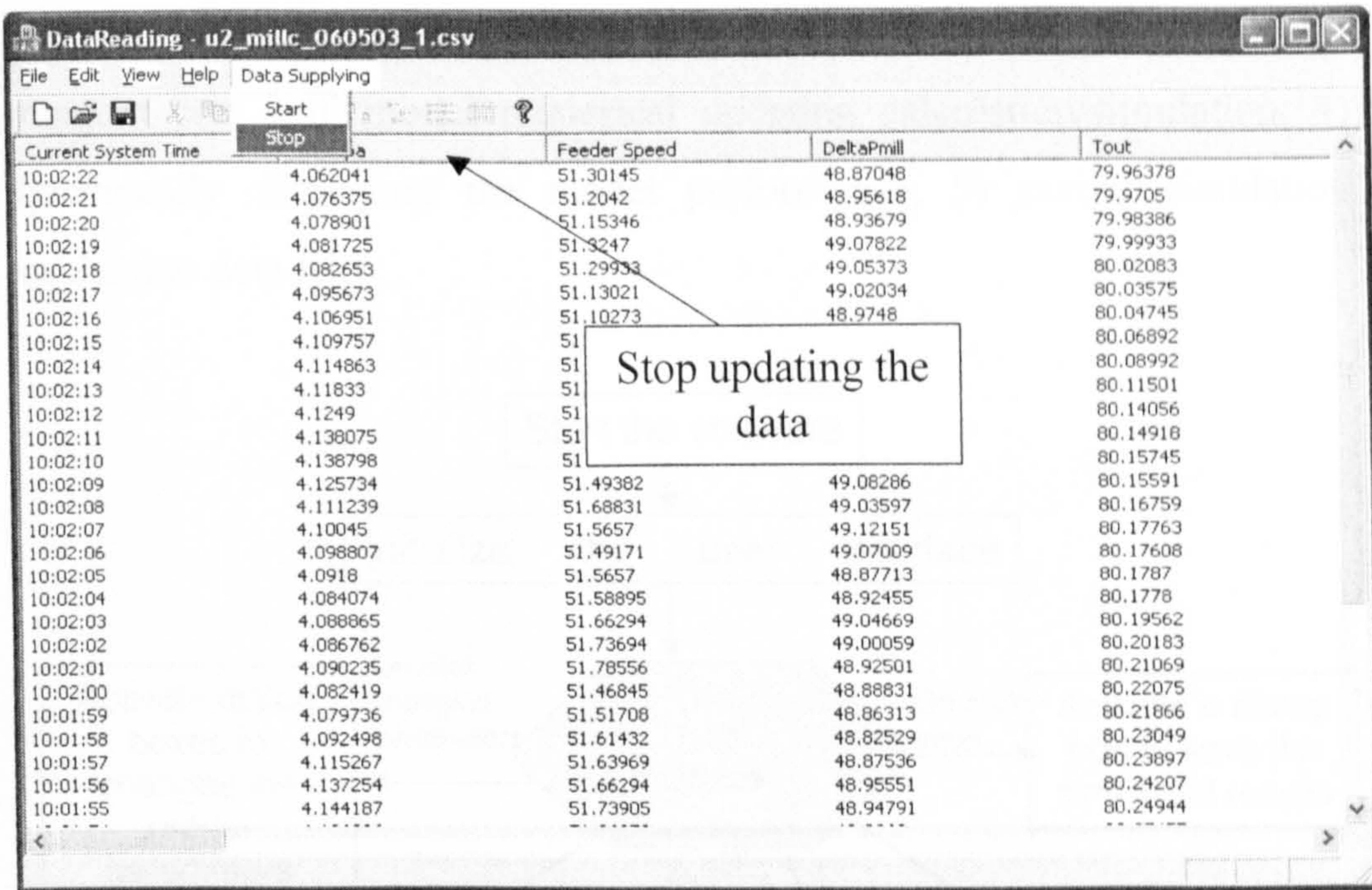


Figure 5-7 Stop loading data into shared memory buffer

Because Program I is particular designed to simulate the data supplying environment in a power plant, the program with clear objective has been developed. With the data ready on-line, the mill model can be implemented.

### 5.3 Program II - On-Line Implementation of the Mill Model

The major purpose for development of Program II is to implement the mill model in real-time and offer the calculated or predicated mill variable information to engineers in a power plant. The program checks the data buffer from the shared memory buffer in every 0.1 second and then updates the inputs and outputs of the mill model once the data buffer has been updated by Program I. The model inputs, outputs, simulated results and the errors between the measured and estimated outputs can be displayed in the chosen sub-windows. The structure of Program II is shown in Figure 5-8. It has five main functions: 1) data reading from shared



memory buffer; 2) loading model coefficients from data files; 3) multi-segment coal mill model numerical updating calculation/simulation; 4) dynamically displaying the model performance; 5) saving simulation results into data files.

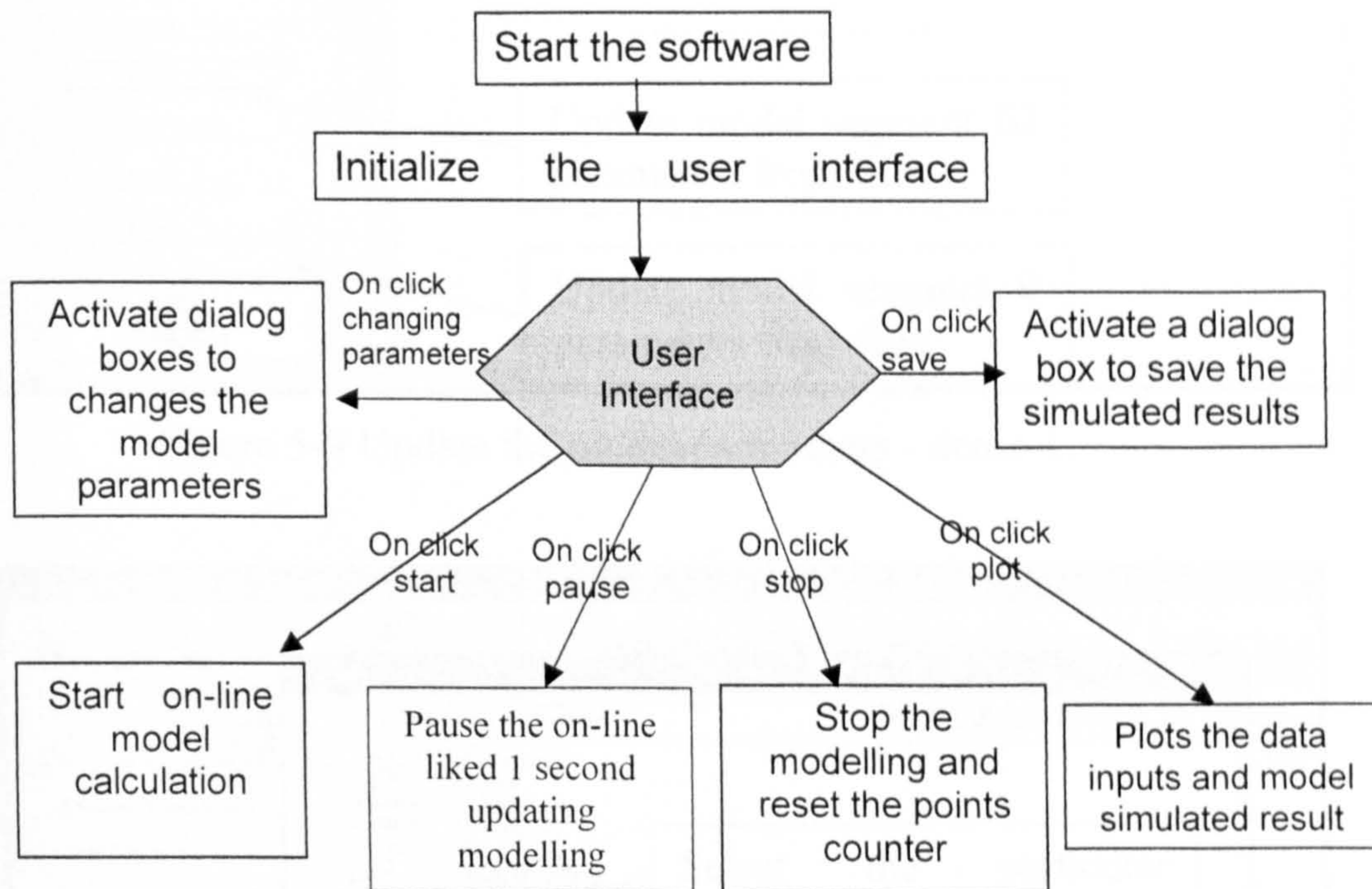


Figure 5-8 Structure of Program II

A user friendly interface has been developed for the program and the feature of the interface can be demonstrated by the following examples.

### 1) Update the coal mill model parameters from data files

Following the scheme shown in Figure 5-1, the model parameter identification is performed off-line. The identified parameters can be updated into Program II by reading the parameter files. In the user interface, by clicking the modelling parameter setting buttons in the left panel, *e.g.* ‘SEGI >>’, it will appear a dialog for you to select the parameter file to update the model parameters, *e.g.* SEGIII.pa. Demos are shown in the Figures 5-9, 5-10.



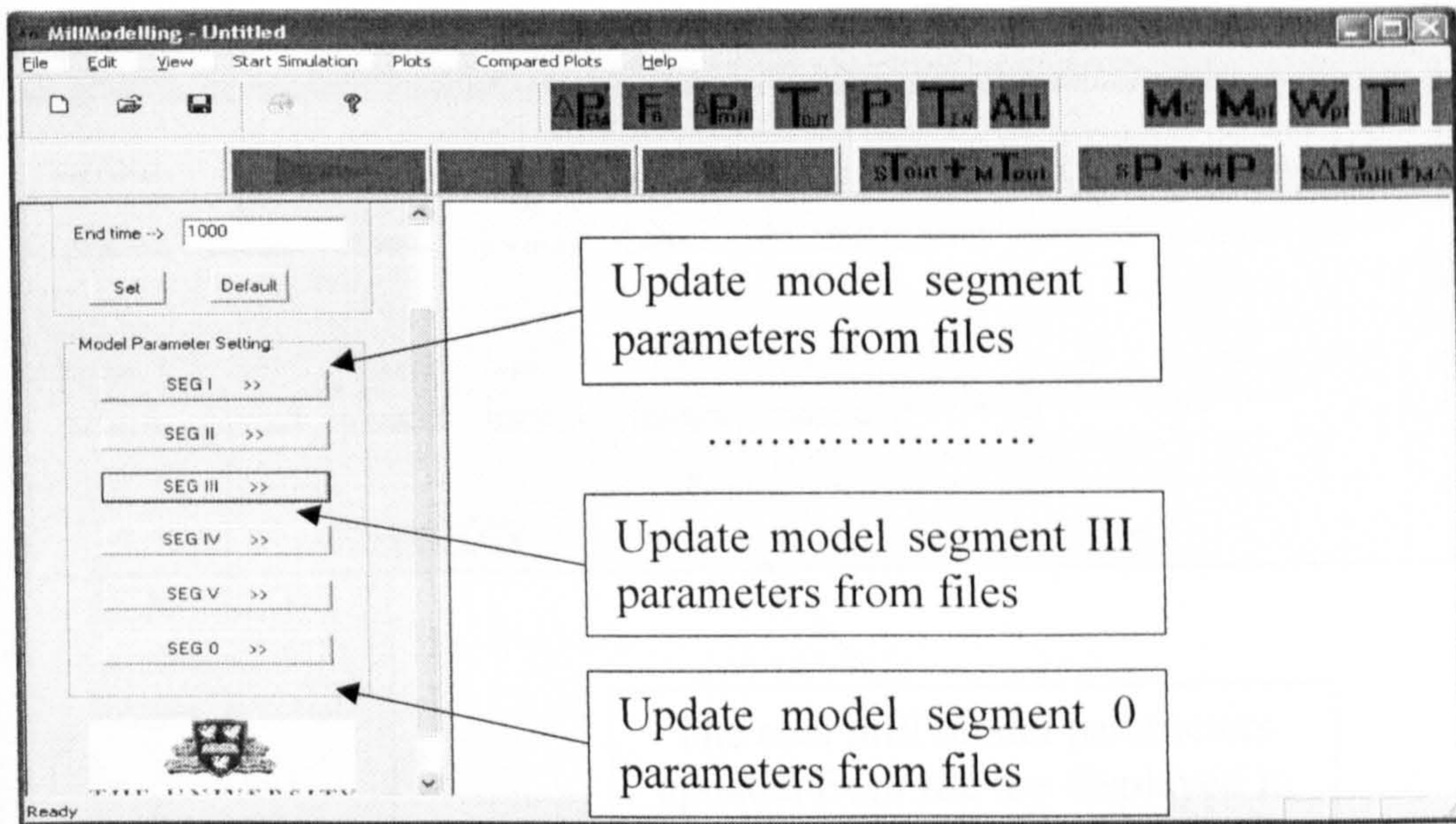


Figure 5-9 Update the model parameters - demo 1.

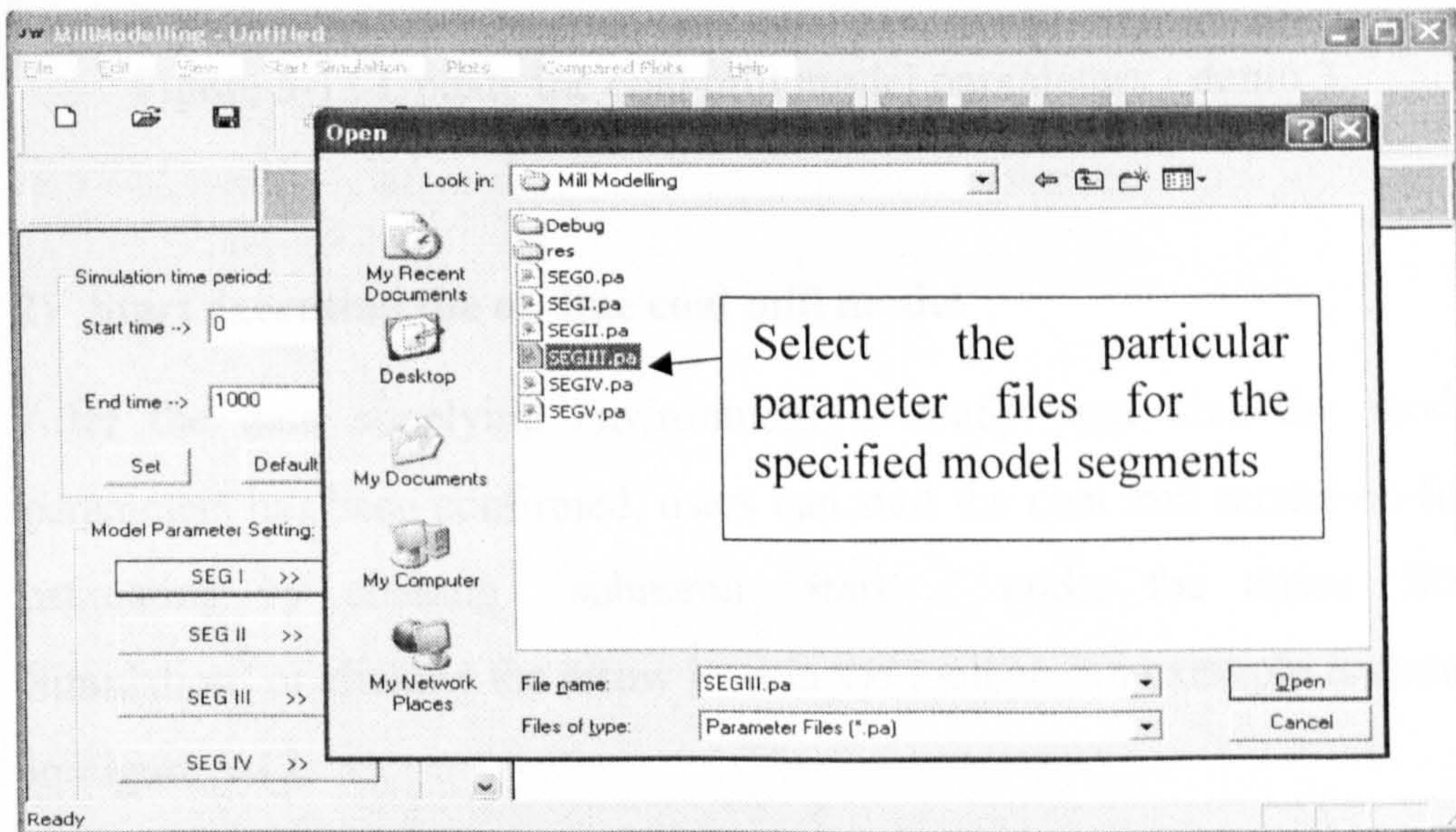


Figure 5-10 Update the coal mill model parameters - demo 2.

After updating the parameters from the files accommodating model parameters, the coal mill parameters will be displayed in the dialog box for users to view (see Figure 5-11).



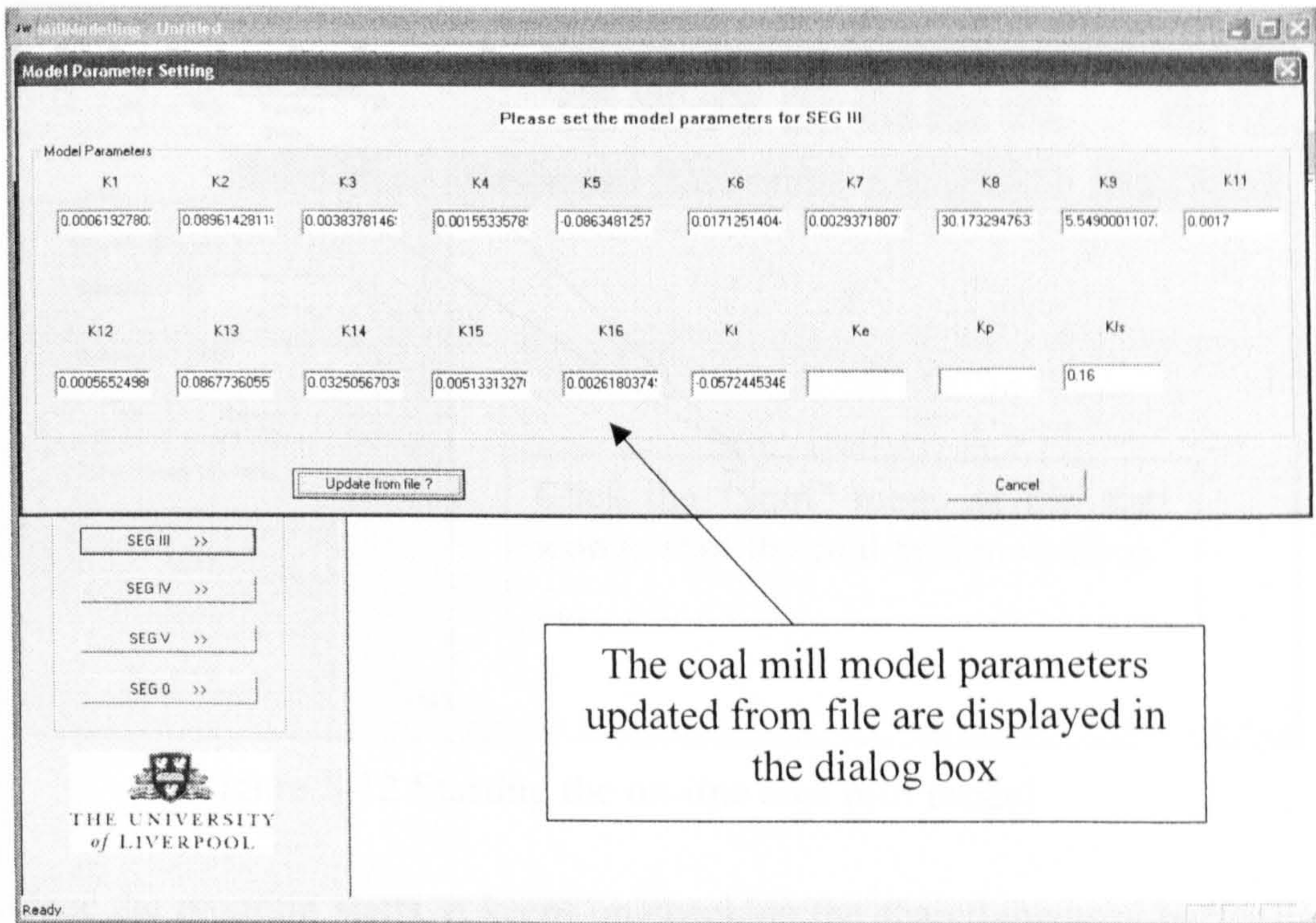


Figure 5-11 Update the coal mill model parameters - demo 3.

## 2) Start executing the on-line coal mill model

After the data supplying environment is ready, and also the model parameters has been confirmed, users can start the coal mill model on-line estimating by clicking submenu 'Start ..' under the menu 'Start Simulation' or clicking the arrow icon in the toolbar. An example is shown in Figure 5-12.



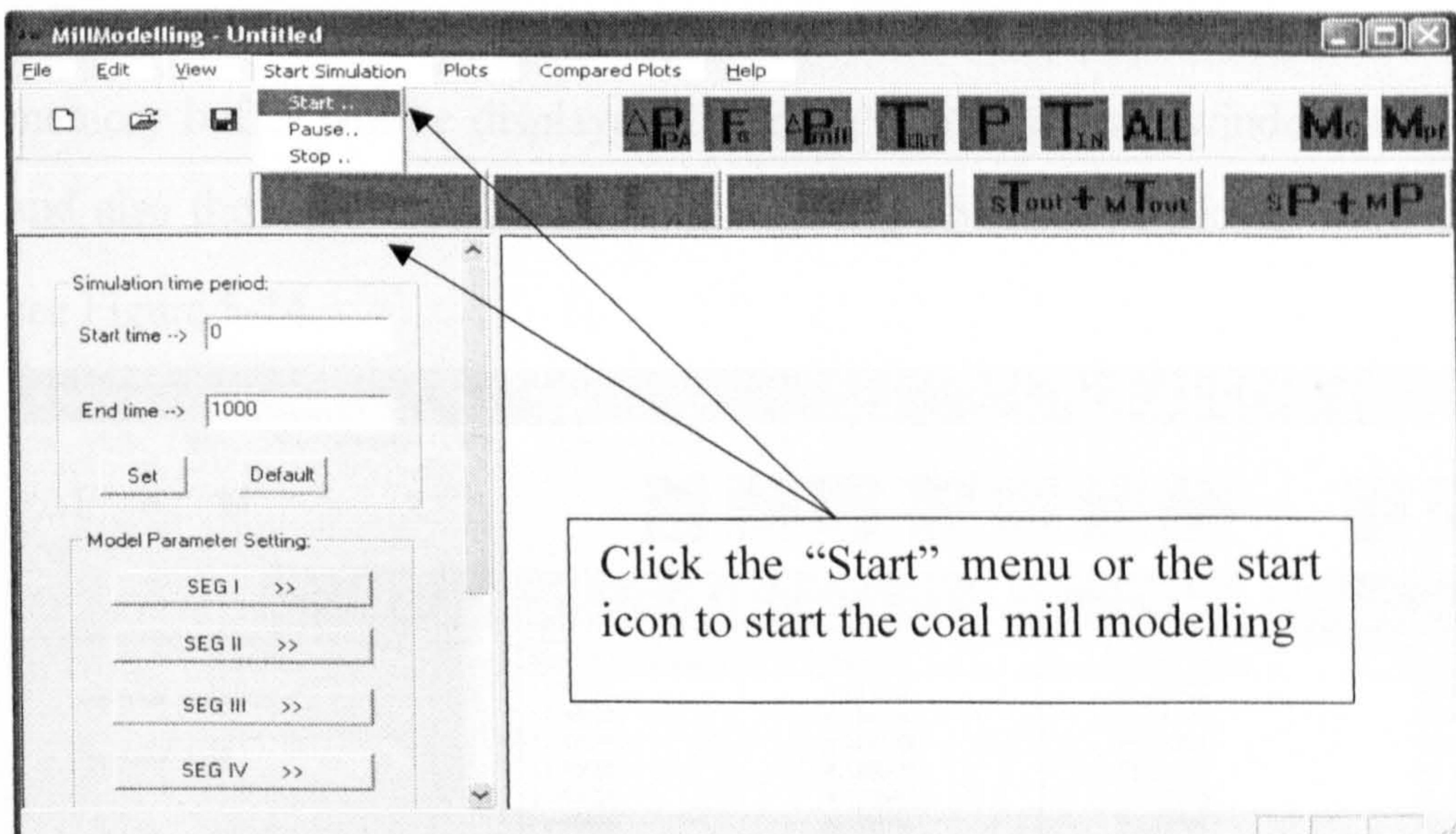


Figure 5-12 Starting the on-line coal mill model

Once the program starts, it keeps on checking the shared memory buffer in every 0.1 second to see if the data there has been updated or not. Once the data buffer has been updated, the on-line coal mill model will update its inputs and continue updating the prediction from the mill model, if not, it will keep on pending until the data buffer in the shared memory is updated by Program I. The flow chart of the program is shown in Figure 5-13.

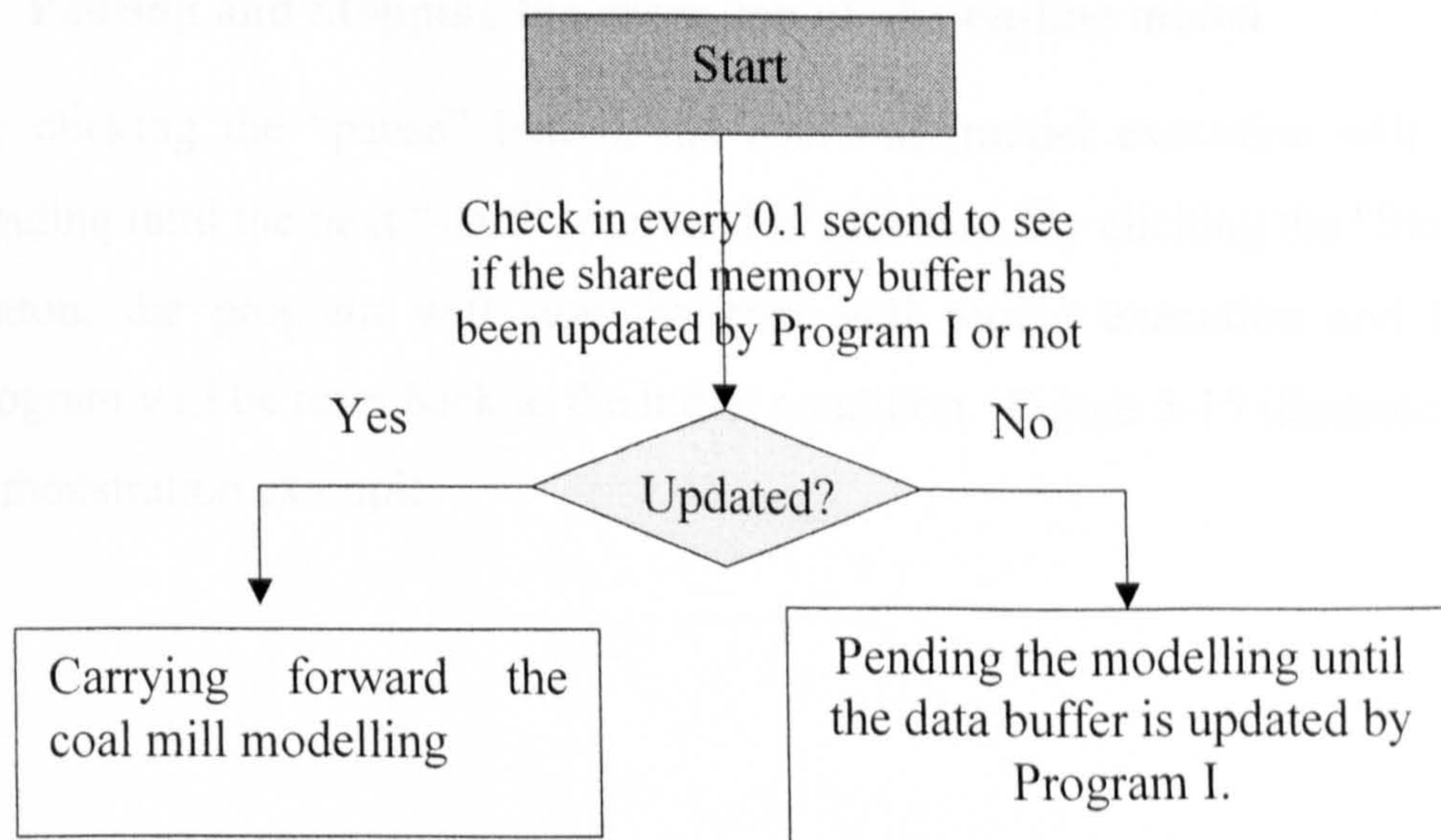


Figure 5-13 Flow chart for share memory idea



When the coal mill model is in operation, the data loaded from the shared memory buffer will be displayed dynamically on the main window panel, and also the simulation results (e.g.  $M_c, M_{pf}$ ) will be displayed as well, see Figure 5-14.

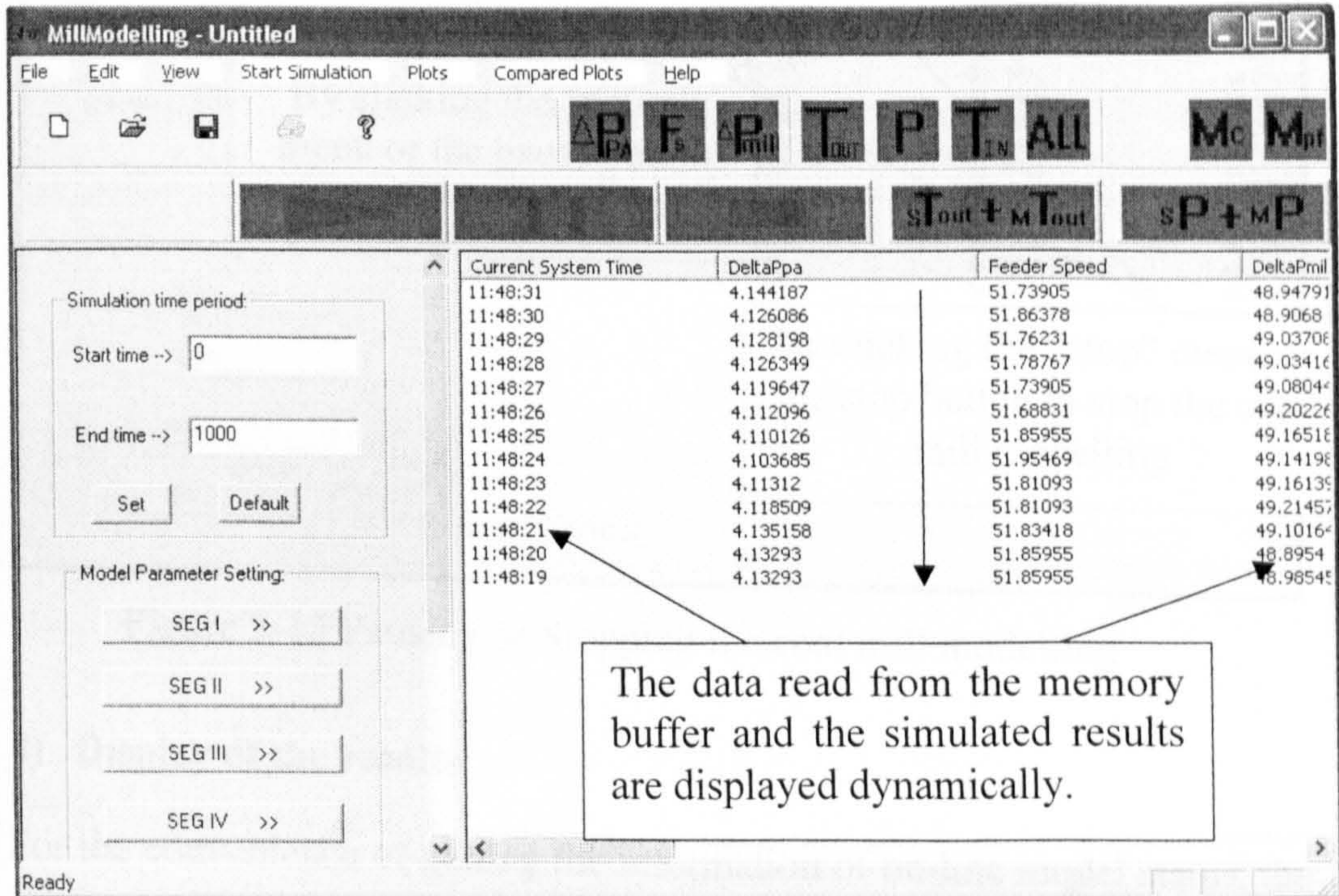


Figure 5-14 Starting the coal mill modelling 2

### 3) Pausing and Stopping the execution of the on-line model

By clicking the “pause” button, the coal mill model execution will be pending until the next “start” command is activated. By clicking the “Stop” button, the program will stop the coal mill model execution and the program will be reset back to the initial condition. Figure 5-15 illustrates a demonstration example.



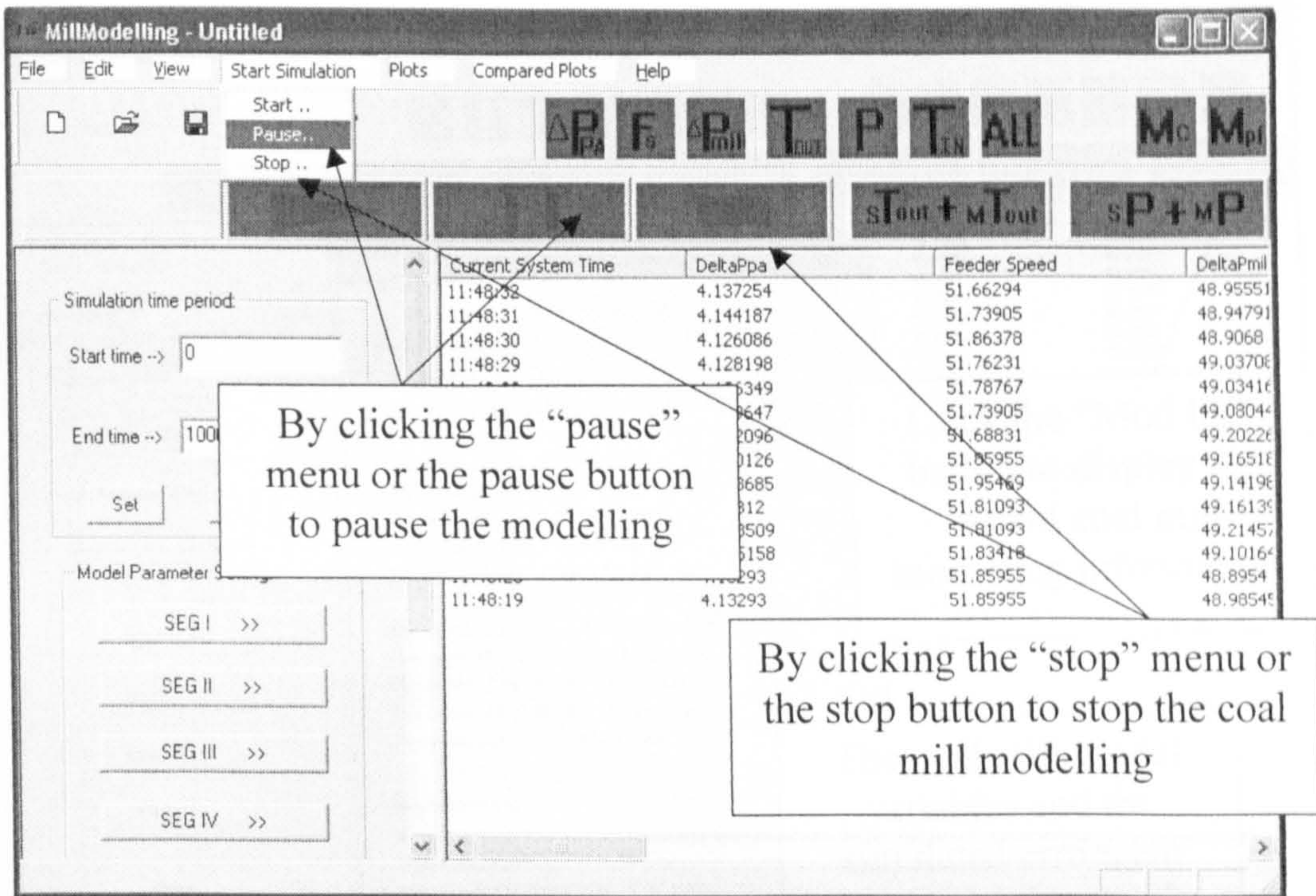


Figure 5-15 Pausing or Stopping the coal mill modelling

#### 4) Display of the results

For the convenience of getting the information of on-line model status, the coal mill modelling information can be summarized and displayed instantly to users. By clicking the submenu 'Modelling Information' under menu 'Plots' or click the "Mod Inf" button at the top toolbar, a dialog box will be generated to display the instant coal mill model information. In the dialog box, the current system time, the number of points that model has run, the instant value of the model variables, and the instant output errors are summarized and displayed. Figure 5-16 gives an example to illustrate the display feature of the program.



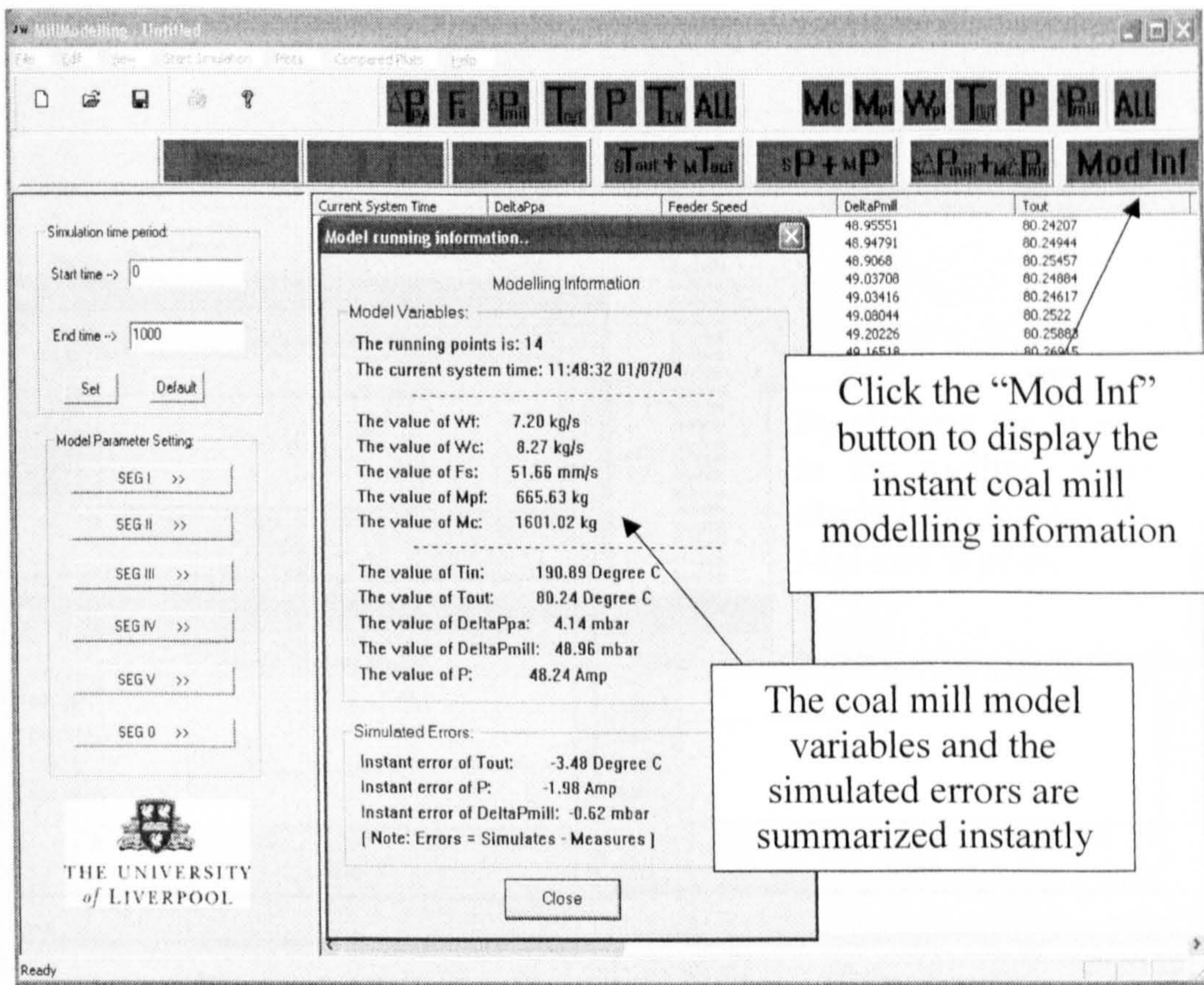


Figure 5-16 Coal mill modelling information display

Other than summarizing the instant coal mill modelling information, the coal mill variables can also be plotted so that the users can read the history of the model performance and also to find the trend of the current model performance. In Figure 5-17, the intermediate variables of the coal mill model are plotted and displayed to users.



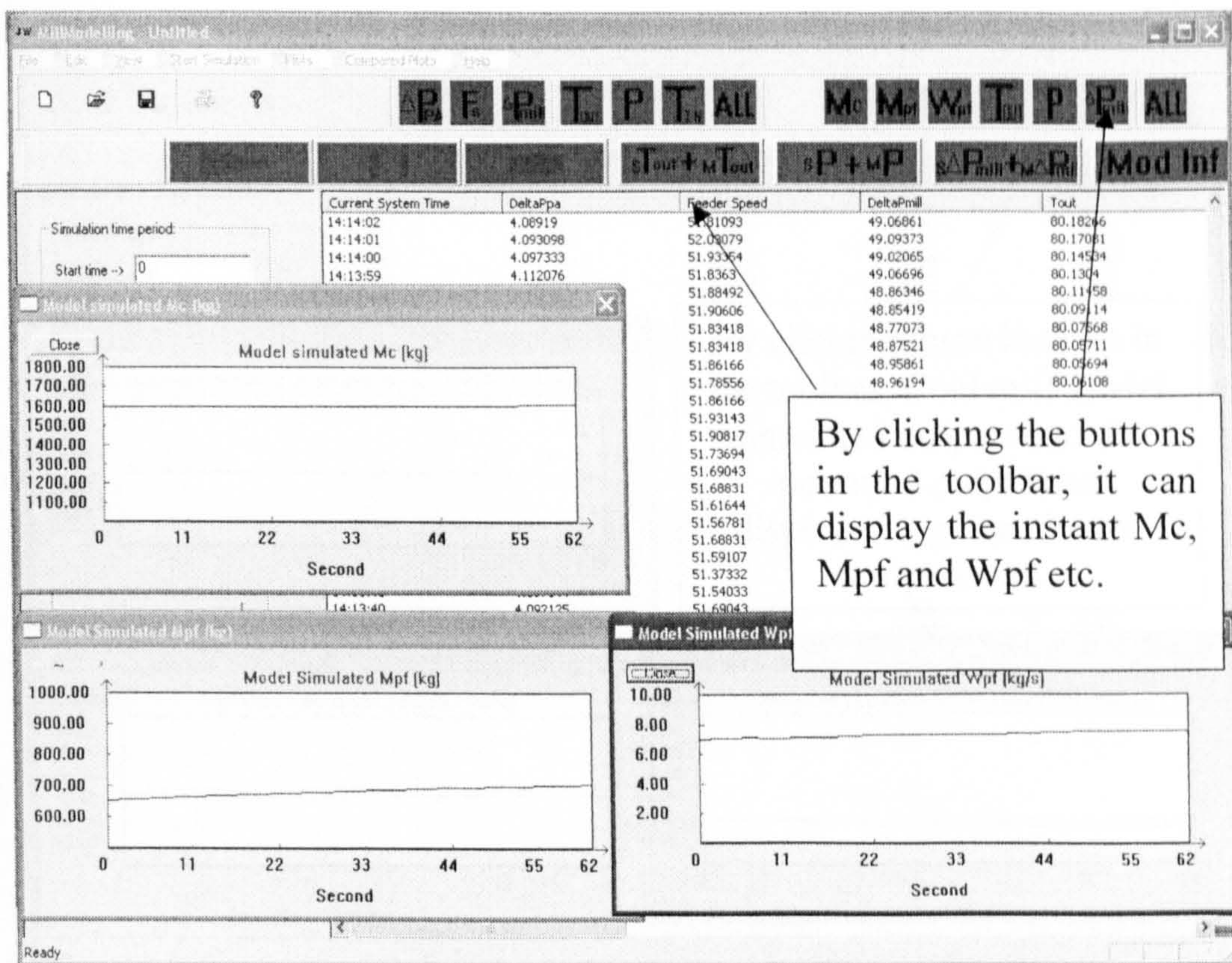


Figure 5-17 Coal mill model variables display

Further more, the software plots the model simulated outputs and the measured outputs in different colours in the same diagram so the users can easily distinguish the measured and estimated outputs and also see the trend of output variations. In Figure 5-18, the red line represents the coal mill measured output and the blue line represents the coal mill model simulated output.



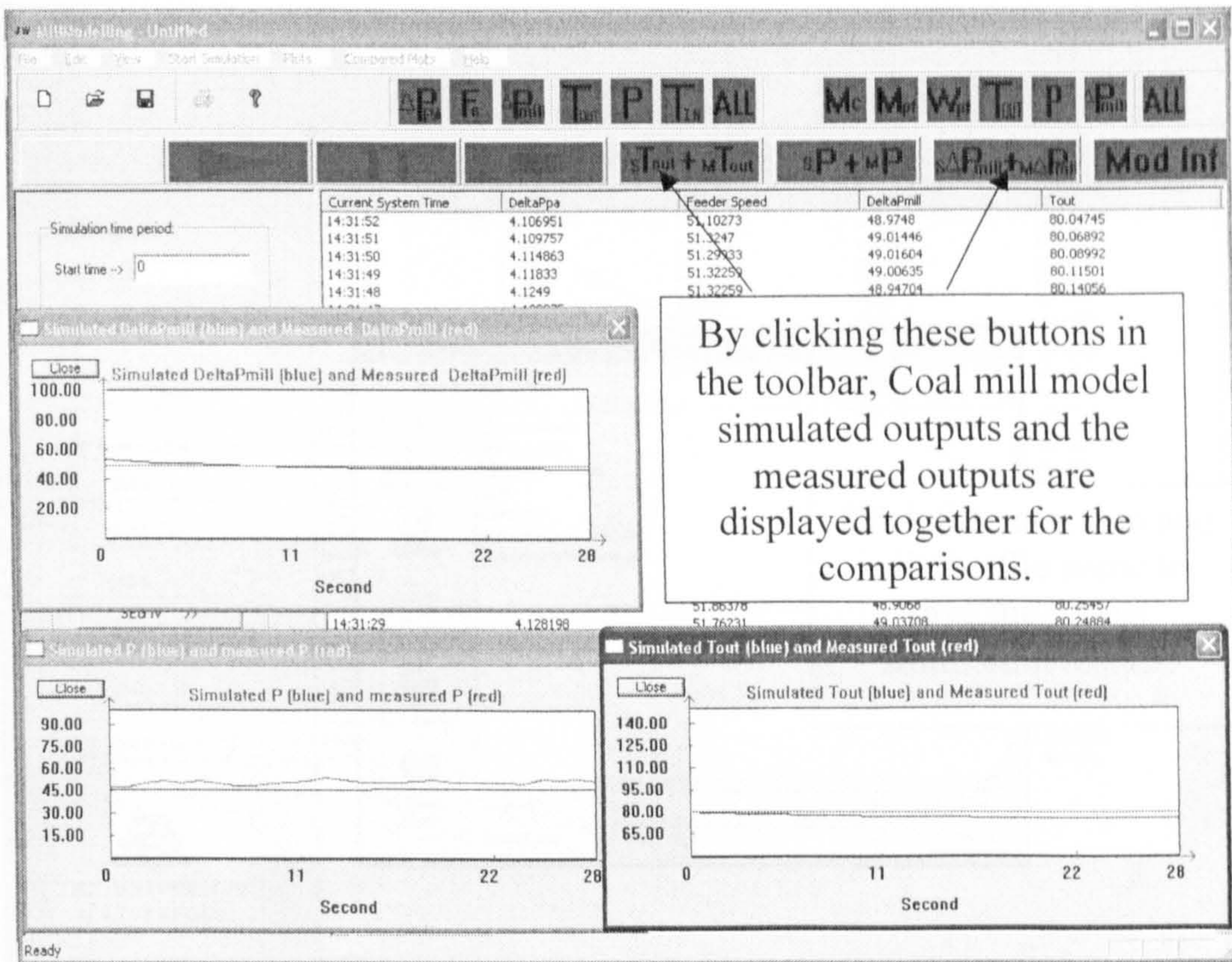


Figure 5-18 Coal mill model simulated outputs and measured outputs.

### 5) Storing the results

In order to keep archiving the simulated, the software provides a function of saving the results to files for future analysis if required. By clicking the submenu 'Save As ..' under menu 'File' or clicking the "Save" icon in the toolbar, it will appear a dialog box for users to put a file name and save the results. Figure 5-19 demonstrates this function.



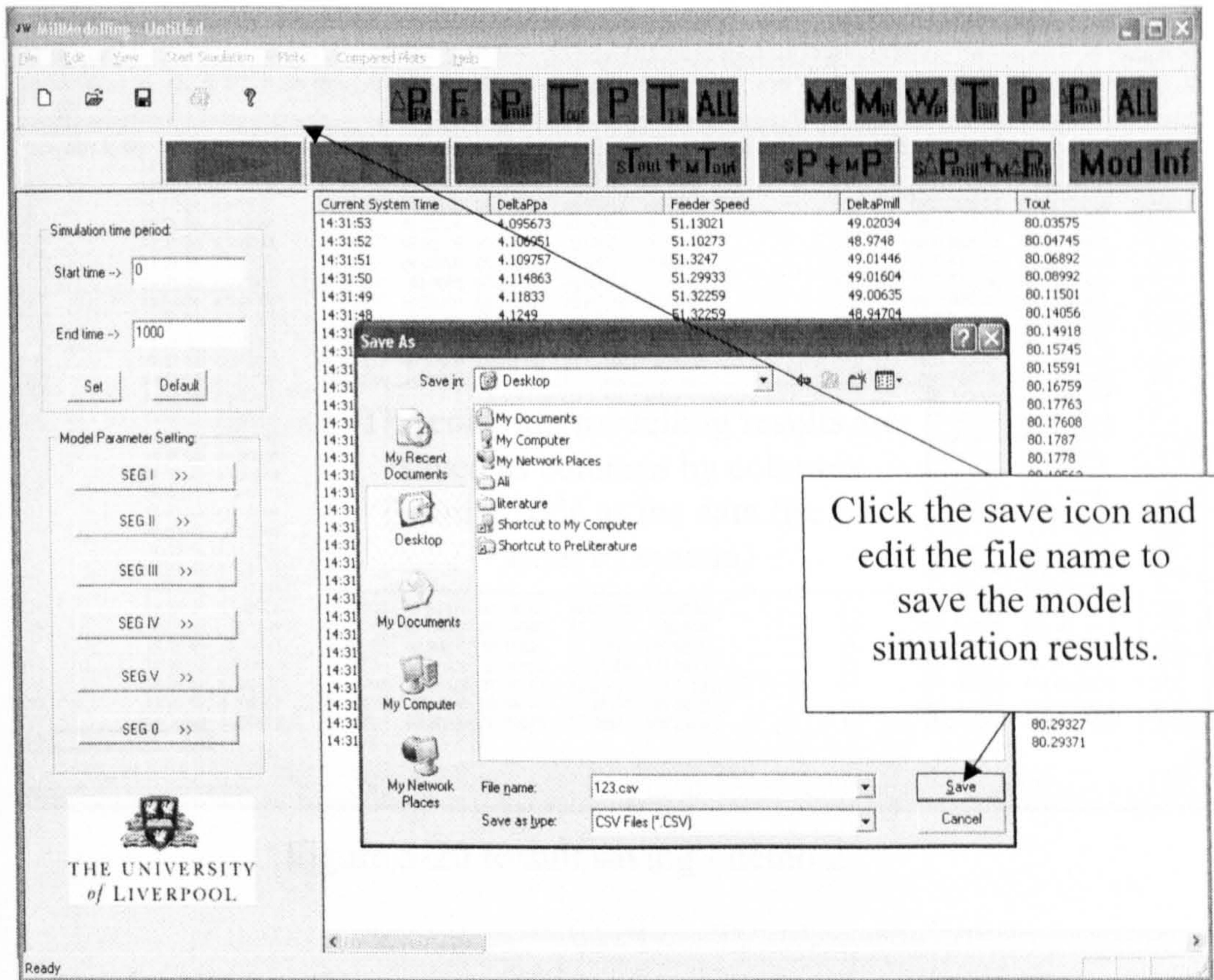


Figure 5-19 Result saving - demo 1

The coal mill model simulated results will be saved as a \*.csv file, which has the same format to the data collected from the PI system in power plants. And the data file can be opened and processed in Microsoft Excel. All the model simulated results ( $M_c$ ,  $M_{pf}$ ,  $W_{pf}$ ,  $\Delta P_{mpd}$ ,  $\hat{T}_{out}(t)$ ,  $\hat{P}(t)$ ,  $\Delta \hat{P}_{mill}(t)$ ) and the on-line measured data ( $F_s$ ,  $\Delta P_{pa}$ ,  $T_{in}$ ,  $\Delta P_{mill}$ ,  $T_{out}$ ,  $P$ ) are saved into files and the data of variables are organised in the format of column by column as shown in Figure 5-20.



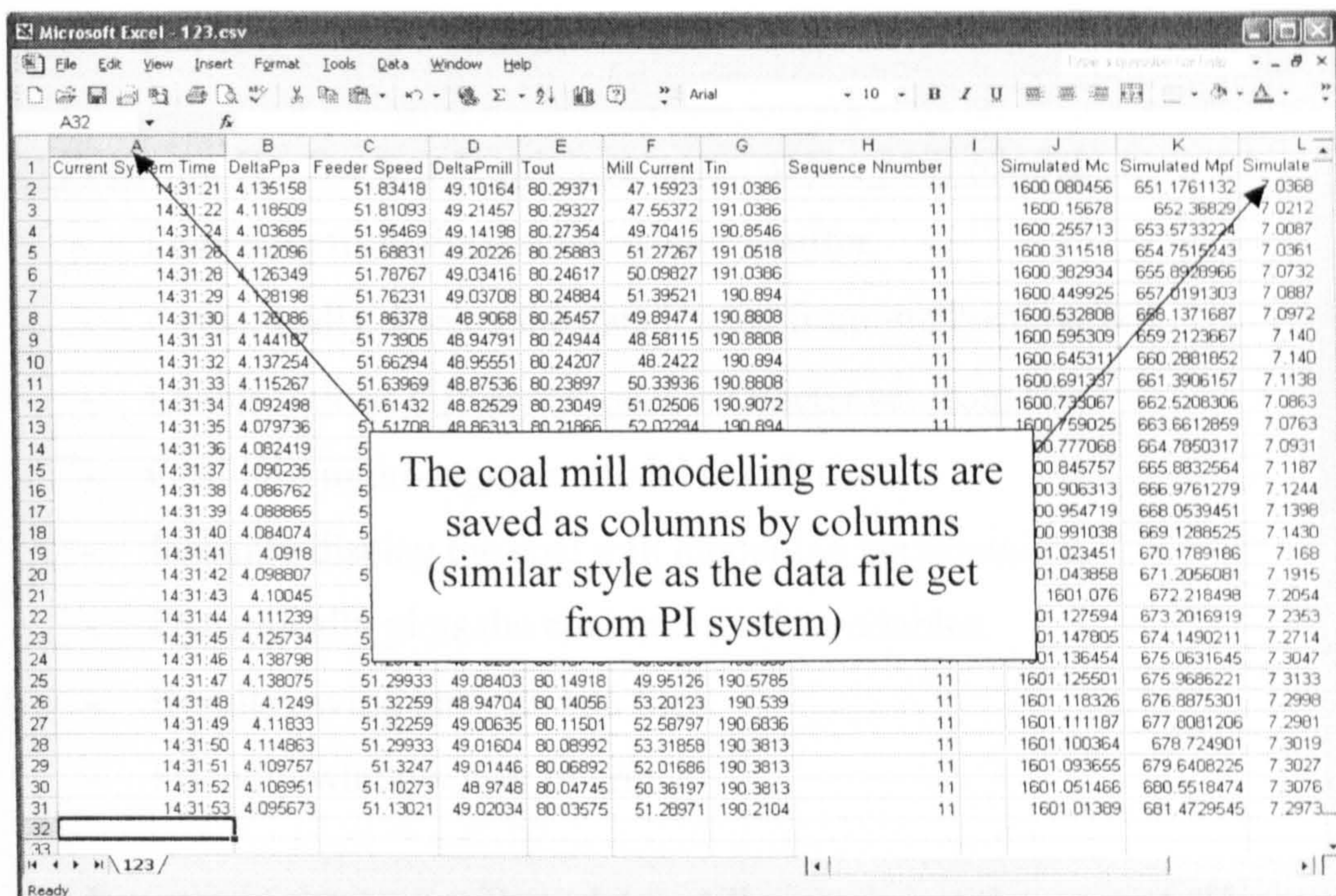


Figure 5-20 Result saving - demo 2

## 5.4 Summary and Discussion

In the chapter, a set of software programs has been developed for on-line implement of the coal mill model. Based on the shared memory scheme, the software is designed to have two parts: Program I - Data Supplying and Program II - On-line Implementation of the Mill Model. Program I is particularly designed for simulating the data supplying environment in a power plant. Program II is particularly designed for on-line implementation of the six segment coal mill model. The summary of features or functions of the software is as follows:

### 1) Program I - Data Supplying:

- Read the data from data files.
- Display the loaded data file in the main window plane.
- Load the data into the shared memory buffer in every 1 second.
- Dynamically display the data loaded into memory.



- Friendly window user interface

## **2) Program II - On-line Implementation of the Mill Model**

- Load data from the shared memory buffer.
- Dynamically display the data loaded from memory buffer.
- Enable to load different model parameter set from files.
- Coal mill multi-segment model simulations.
- Instantly display the coal mill modelling performance.
- Dynamically plots the coal mill model variables.
- Results saving back to data files.
- Friendly window user interface

On-line test of the coal mill model is still on-going at the present. The on-line model will achieve the requirements from the power system engineers and they will gain the insight knowledge of the mill plant from the predicted variable values, especially, the internal immeasurable variables like  $M_c$ ,  $M_{pf}$ ,  $W_{pf}$  etc. (see Figure 5-17) simultaneously. All these knowledge will no doubt contribute for improvement of the efficiency of mill operation and the boiler combustion.



## **PART II: AGGREGATE LOAD**

### **AREA MODELLING**

#### **Chapter 6**

### **Introduction to Power System Load Modelling**

#### **6.1 Introduction**

Unlike gas and water, electricity cannot be easily stored and the supplier has small control over the load at any time (Machowski *et al.* 1998). Stable operation of a power system depends on the ability to continuously match the electrical output of generation units to the electrical load on the system. With the increases of power flow complexity in a deregulated environment, system dynamic performance assessment becomes a critical issue for reliable operations of a power transmission and distribution grid. Load modelling is one of key steps in accurate assessment of power system grid performance, especially, in power system stability analysis (Wei *et al.* 2005c). However, it is a difficult task to accurately model power system loads due to a number of factors which include:

- a). a large number of diverse load components;
- b). ownership and location of load devices in customer facilities are not directly accessible to the electric utility;
- c). changing load composition with time of days and weeks, seasons, weather and through time;
- d). lack of precise information on the composition of the load;



- e). uncertainties regarding to the characteristics of many different load components, particularly for large variations in power voltage and frequency.

Some progress in load modelling has been made in recent years. Various static and dynamic models, such as constant impedance load model, constant current load model, constant power load model, polynomial load model, exponential load model, frequency-dependent load model, EPRI loadsyn static load model, *etc.* have been developed, where the load modelling methods deal with “bus load” only, and the “load” refers to the representation of the aggregate effect of many individual end-user devices connected to the bus (IEEE Task Force 1993; Price *et al.* 1995). However, almost all distribution systems and load areas (load centres) are supplied by more than one power source to improve the security and reliability of the whole system. As a number of source buses are distributed and connected to the load area rather than one single unified bus, the bus load model is reluctant to represent the load area.

In nowadays power system research, the power flow calculation is very important. By constructing the admittance matrix according to the network structure and the branch details, the power flow calculation derives the power flow in each branch and also the voltage in each node in a power distribution network. There are two methods that are commonly used in power system simulation software, namely, the Gauss-Seidel method and Newton-Raphson method. Inspired by the iterative idea, these two methods work very well for the power flow calculation, where Gauss-Seidel method works on a simple iterative calculation and Newton-Raphson method works in a more complicated but fast way of calculation.

This chapter will start from the reviews of the standard load models recommended by the IEEE task force, where the aggregated bus load



model are constructed to represent the relationship between a bus voltage (magnitude and frequency) and the power (active and reactive) in the load bus. Afterward, the Aggregated Load Area Model (ALAM) is introduced to model the aggregated load area instead of a load bus, where the scheme of how to model an aggregated load area is explained and illustrated. At the end of the chapter, the power flow calculations using the Newton-Raphson method are illustrated. Comparing with the Gauss-Seidel method as illustrated in Appendix IV, the one with best performance is adopted for power system analysis throughout the project.

## **6.2 The Standard Load Models**

In power system engineering, the term 'load' may be defined differently to represent or reflect different situation (IEEE Task Force 1993), for example,

- a). a device, connected to a power system, which consumes power;
- b). the total power (active and/or reactive) consumed by all devices connected to a power system;
- c). the power output of a generator or generating plant;
- d). a portion of the system that is not explicitly represented in a system model, but rather is treated as if it were a single power-consuming device connected to a bus in the system model.

Definition 'd)' refers to the load considered in the project. As illustrated in Figure 6-1, the bus load in this context includes not only the connected load devices, but also some of the following: i). the transformers; ii). feeders; iii) shunt-capacitors; iv). voltage regulators; v). customer wiring, transformers and capacitors. Load represents the aggregation of hundreds or thousands of individual component devices such as motors, lighting, and electrical appliances (Price *et al.* 1995).



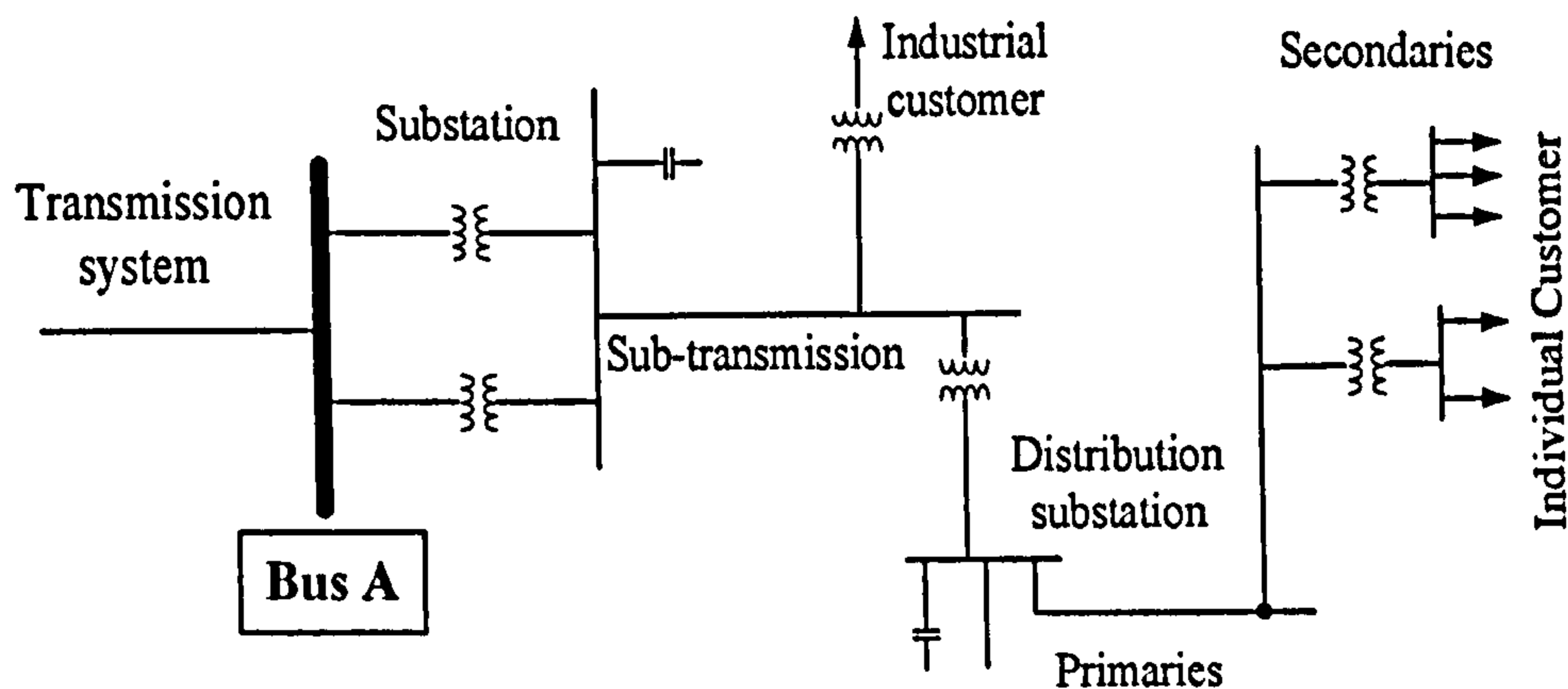


Figure 6-1 “Bus Load”, including feeders, transformers, and shunt capacitors, as well as load devices

A load model is a mathematical representation of the relationship between a bus voltage (magnitude and frequency) and the power (active and reactive) or current flowing into the bus load (IEEE Task Force 1993). There are many standard models recommended by the IEEE for power flow and dynamic simulation programs (IEEE Task Force 1993; Price *et al.* 1995). Load models can be classified into static and dynamic models (Kundur *et al.* 1994). A static load model is not dependent on time, therefore it describes the relationship of the active and reactive power at steady state time while considering the voltage and/or frequency at the same instant of time. On the other hand, a dynamic load model expresses this relationship at any instant time, as a function of the voltage and/or frequency at past instant of time, including normally the present moment (Grainger *et al.* 1994). A brief description of some of these models is given below.

### 1) Constant Impedance Load Model (CILM)

The CILM is a constant static load model where the power varies directly with the values of the voltage magnitude. It may also be called a constant admittance load model. The application for this load model could be the pure resistance circuits, e.g. Resistance Space Heater, which can be



represented by the equations as follows:

$$P \propto V^2 \Rightarrow \frac{P}{P_0} \propto \frac{V^2}{V_0^2} \quad (6-1)$$

$$Q \propto V^2 \Rightarrow \frac{Q}{Q_0} \propto \frac{V^2}{V_0^2} \quad (6-2)$$

where  $V$ ,  $P$  and  $Q$  are the voltage, active and reactive power respectively.  $V_0$ ,  $P_0$  and  $Q_0$  normally take the values of the initial system operating condition for the study.

### 2) Constant Current Load Model (CCLM)

The CCLM is a static load model where power varies directly with the voltage magnitude. The application for this load model could be the Mix Resistive and Motor Devices, which can be described by Equations (6-3) and (6-4):

$$P \propto V \Rightarrow \frac{P}{P_0} \propto \frac{V}{V_0} \quad (6-3)$$

$$Q \propto V \Rightarrow \frac{Q}{Q_0} \propto \frac{V}{V_0} \quad (6-4)$$

where  $V$ ,  $V_0$ ,  $P$ ,  $P_0$ ,  $Q$ , and  $Q_0$  have the same meaning as explained in 1).

### 3) Constant Power Load Model (CPLM)

The CPLM is a static load model where the power does not vary with changes in voltage magnitude. It may also be called constant MVA load model. The application for this load model could be the Heater Equipment with Thermostat, which can be represented by the equations below:

$$P \sim \text{Contant} \Rightarrow \frac{P}{P_0} \sim \text{Contant} \quad (6-5)$$

$$Q \sim \text{Contant} \Rightarrow \frac{Q}{Q_0} \sim \text{Contant} \quad (6-6)$$



where  $V$ ,  $V_0$ ,  $P$ ,  $P_0$ ,  $Q$  and  $Q_0$  have the same meaning as explained above.

#### 4) Exponential Load Model (ELM)

The ELM is a static load model that represents the power relationship to voltage as an exponential equation, usually in the following form:

$$P = P_0 \left( \frac{V}{V_0} \right)^{np} \quad (6-7)$$

$$Q = Q_0 \left( \frac{V}{V_0} \right)^{nq} \quad (6-8)$$

where  $V$ ,  $V_0$ ,  $P$ ,  $P_0$ ,  $Q$  and  $Q_0$  have the same defined meanings as explained above.

The  $np$  and  $nq$  are the exponential indices in the model. Common values for the exponential indices for different load components are shown in Table 6-1.

Table 6-1 Common values for exponential indices  $np$  and  $nq$

Load Component	$np$	$nq$
Air Conditioner	0.50	2.50
Resistance Space Heater	2.00	0.00
Fluorescent Lighting	1.00	3.00
Pumps, Fans Other Motors	0.08	1.60
Large Industrial Motors	0.05	0.05
Small Industrial Motors	0.10	0.60

For special cases, where  $np$  or  $nq$  are equal to 0, 1, and 2, the load model represents the CPLM, the CCLM and CILM, respectively.

#### 5) Polynomial Load Model (PLM)

The PLM is a static load model that represents the power relationship to the voltage magnitude as a polynomial equation, usually in the following form:



$$P = P_0 \left[ a_1 \left( \frac{V}{V_0} \right)^2 + a_2 \left( \frac{V}{V_0} \right) + a_3 \right] \quad (6-9)$$

$$Q = Q_0 \left[ a_4 \left( \frac{V}{V_0} \right)^2 + a_5 \left( \frac{V}{V_0} \right) + a_6 \right] \quad (6-10)$$

where  $V$ ,  $V_0$ ,  $P$ ,  $P_0$ ,  $Q$  and  $Q_0$  have the same meanings as defined above.  $a_1$  to  $a_6$  are the coefficient parameters of this polynomial model. This model is sometimes referred to as a “ZIP” model since it consists of the sum of constant impedance (Z), constant current (I), and constant power (P).

#### 6) Exponential Dynamic Load Model (EDLM)

The EDLM is a dynamic load model, which was proposed by Karlsson and Hill in 1994 (Karlsson *et al.* 1994). The model is presented in equations (6-11) and (6-12) as a set of non-linear equations, where active and reactive power have a non-linear dependency on the voltage.

$$T_p \frac{dP_r}{dt} + P_r = P_0 \left( \frac{V}{V_0} \right)^{a_t} - P_0 \left( \frac{V}{V_0} \right)^{a_s} \quad (6-11)$$

$$P_l = P_r + P_0 \left( \frac{V}{V_0} \right)^{a_s} \quad (6-12)$$

where  $V_0$  and  $P_0$  are the voltage and power consumption before the voltage changed,  $P_r$  is the active power recovery,  $P_l$  is the total active power response,  $T_p$  is the active load recovery time constant,  $a_t$  is the transient active load-voltage dependence, and  $a_s$  is the steady state active load which is voltage dependent. Similar equations are also valid for reactive power.



### 6.3 Aggregate Load Area Modelling (ALAM)

As introduced in Section 6.2, most of the existing load modelling methods only deal with “bus load”, where “load” refers to the representation of the aggregate effect of many individual end-user devices connected to the bus. To model the load for a specified area, Wen *et al* proposed an aggregate load area model (ALAM) in 2003 (Wen *et al.* 2003a; Wen *et al.* 2003b). It represents the load subject to the “area” rather than the “bus” and gives a degree of network reduction, wherein the equivalent load model area is chosen from the standard bus load model.

Similar to the load model for the individual bus, an ALAM is a mathematical representation of the relationship between the total power injected into (active and reactive) and the voltage (magnitude and frequency) at the load area. As a result, for load modelling of the area load, not only the overall characteristics of the loads in the area but also the transmission and distribution network should be modelled. For example, the load area that composes of seven load buses (see Figure 6-2) can be aggregately modelled as a fictitious load bus with an equivalent load connected, where the fictitious load bus is connected with the original power system by fictitious transmission lines (see Figure 6-3). Since the active power  $P$  and reactive power  $Q$  consumed in each load buses of the power system can be represented by Equations (6-9) and (6-10), the fictitious load bus therefore can be modelled as follows (Wen *et al.* 2003a; Wen *et al.* 2003b):

$$P_f = [a_{f1}V_f^2 + a_{f2}V_f + a_{f3}] \quad (6-13)$$

$$Q_f = [a_{f4}V_f^2 + a_{f5}V_f + a_{f6}] \quad (6-14)$$

where  $P_f$  is the per unit value of active power consumed in the fictitious load bus;  $Q_f$  is the per unit value of reactive power consumed in the



fictitious load bus;  $V_f$  is the per unit value of fictitious load bus voltage magnitude; and  $a_{f1} \sim a_{f6}$  are the parameters of the model for the fictitious load bus.

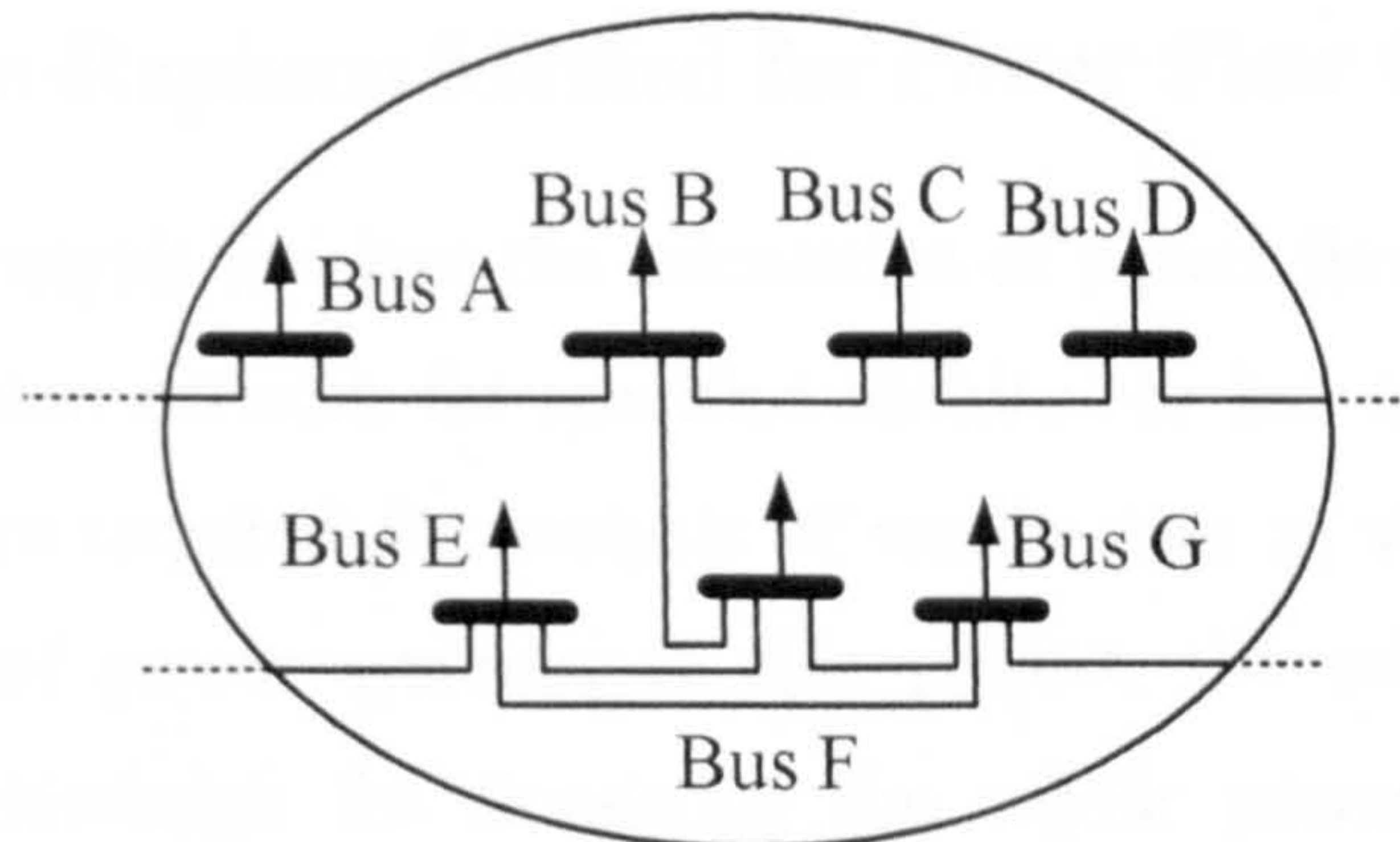


Figure 6-2 A load area composed of seven load buses

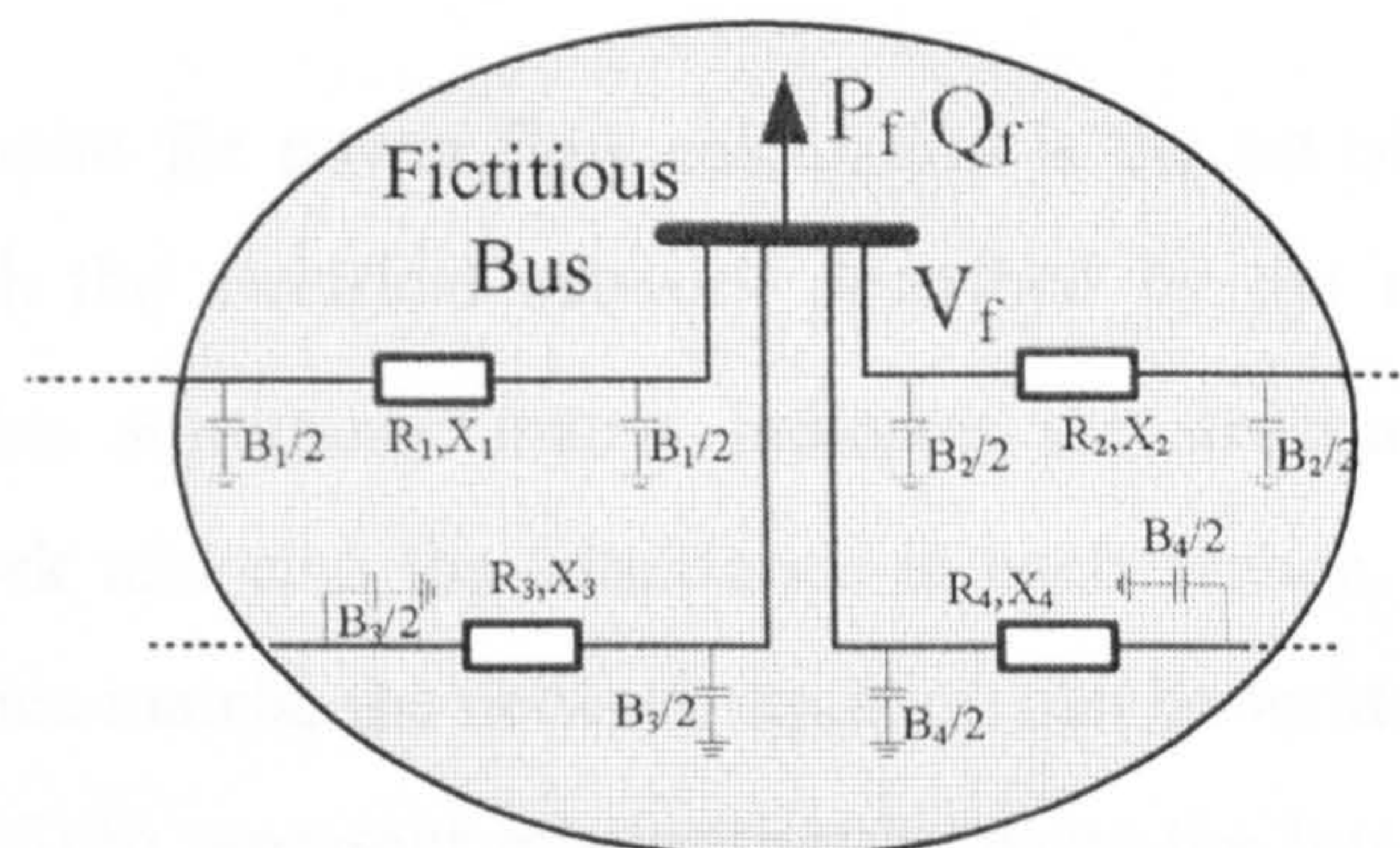


Figure 6-3 The fictitious load bus and its connected transmission lines

As the fictitious load bus does not really exist, there are a number of unknown parameters in the ALAM, which are listed as follows:

- the values of the model parameters  $a_{f1} \sim a_{f6}$ ;
- the parameters of the fictitious transmission lines: the line resistance  $R$ , the line reactance  $X$ , and the shunt susceptance  $B$ .

In this thesis, all these unknown parameters can be identified using the Genetic Algorithm (GA). An alternative method for identifying these unknown parameters using the Particle Swarm Optimization (PSO) is reported in 2005 (Wei *et al.* 2005d; Wei *et al.* 2005e). The details of the



identification process of the ALAM will be described in the following chapter.

## 6.4 Newton-Raphson Method for Power Flow Calculation

Power flow analysis involves the calculation of power flows and voltages of a transmission network for specified terminal or bus conditions. Such calculations are required for analysis of steady-state as well as dynamic performance of power systems. In this project, the calculation is the foundation knowledge for simulating the whole power system while operation conditions change in the buses or branches.

The starting point for power flow calculation is the set of generation and load data with the electrical network described by the node admittance matrix  $\bar{Y}$ . This admittance matrix indicates the structure of the power system network and also the admittance in each branch. In terms of the node admittance matrix, the network equation can be written in the form of Equation (6-15) to represent relationship between the bus current and bus voltage (Kundur *et al.* 1994):

$$\begin{bmatrix} \tilde{I}_1 \\ \tilde{I}_2 \\ \dots \\ \tilde{I}_n \end{bmatrix} = \begin{bmatrix} Y_{11} & Y_{12} & \dots & Y_{1n} \\ Y_{21} & Y_{22} & \dots & Y_{2n} \\ \dots & \dots & \dots & \dots \\ Y_{n1} & Y_{n2} & \dots & Y_{nn} \end{bmatrix} \begin{bmatrix} \tilde{V}_1 \\ \tilde{V}_2 \\ \dots \\ \tilde{V}_n \end{bmatrix} \quad (6-15)$$

where

$n$  is the total number of nodes.

$Y_{ii}$  is the self admittance of node  $i$ .

$Y_{ij}$  is mutual admittance between nodes  $i$  and  $j$ .

$\tilde{V}_i$  is the phasor voltage to ground at node  $i$ .

$\tilde{I}_i$  is the phasor current flowing into the network at node  $i$ .



Taking 14-bus power system as shown in Figure 6-4 as an example published by IEEE (Zimmerman *et al.* 2004), the admittance matrix  $\bar{Y}$  is:

$$\bar{Y} = \begin{bmatrix} Y_{11} & Y_{12} & 0 & 0 & Y_{15} & 0 & 0 & 0 & 0 & 0 & 0 & 0 & 0 & 0 \\ Y_{21} & Y_{22} & Y_{23} & Y_{24} & Y_{25} & 0 & 0 & 0 & 0 & 0 & 0 & 0 & 0 & 0 \\ 0 & Y_{32} & Y_{33} & Y_{34} & 0 & 0 & 0 & 0 & 0 & 0 & 0 & 0 & 0 & 0 \\ 0 & Y_{42} & Y_{43} & Y_{44} & Y_{45} & 0 & Y_{47} & 0 & 0 & 0 & 0 & 0 & 0 & 0 \\ Y_{51} & Y_{52} & 0 & Y_{54} & Y_{55} & Y_{56} & 0 & 0 & 0 & 0 & 0 & 0 & 0 & 0 \\ 0 & 0 & 0 & 0 & Y_{65} & Y_{66} & 0 & 0 & 0 & 0 & Y_{6,11} & Y_{6,12} & Y_{6,13} & 0 \\ 0 & 0 & 0 & Y_{7,4} & 0 & 0 & Y_{7,7} & Y_{7,8} & Y_{7,9} & 0 & 0 & 0 & 0 & 0 \\ 0 & 0 & 0 & 0 & 0 & 0 & Y_{8,7} & Y_{8,8} & 0 & 0 & 0 & 0 & 0 & 0 \\ 0 & 0 & 0 & Y_{9,4} & 0 & 0 & Y_{9,7} & 0 & Y_{9,9} & Y_{9,10} & 0 & 0 & 0 & Y_{9,14} \\ 0 & 0 & 0 & 0 & 0 & 0 & 0 & 0 & Y_{10,9} & Y_{10,10} & Y_{10,11} & 0 & 0 & 0 \\ 0 & 0 & 0 & 0 & 0 & Y_{11,6} & 0 & 0 & 0 & Y_{11,10} & Y_{11,11} & 0 & 0 & 0 \\ 0 & 0 & 0 & 0 & 0 & Y_{12,6} & 0 & 0 & 0 & 0 & 0 & Y_{12,12} & Y_{12,13} & 0 \\ 0 & 0 & 0 & 0 & 0 & Y_{13,6} & 0 & 0 & 0 & 0 & 0 & Y_{13,12} & Y_{13,13} & Y_{13,14} \\ 0 & 0 & 0 & 0 & 0 & 0 & 0 & 0 & Y_{14,9} & 0 & 0 & 0 & Y_{14,13} & Y_{14,14} \end{bmatrix} \quad (6-16)$$

where the values for the non-zero items of the admittance matrix are listed in Table 6-2.

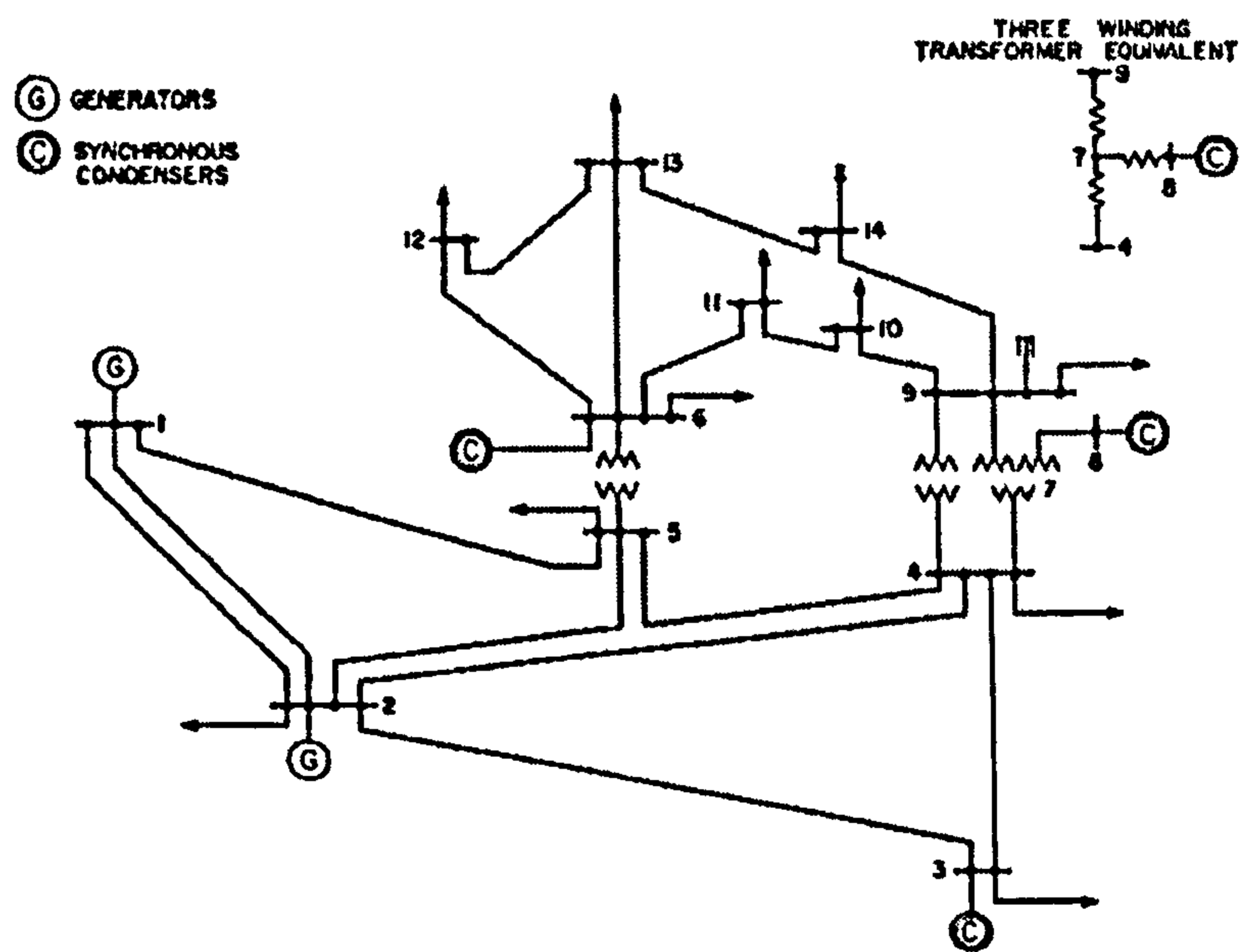


Figure 6-4 IEEE 14-bus power system (Zimmerman *et al.* 2004)

Equation (6-15) could be linearised if the current injection  $\bar{I}_i$  were known. However, in practice, the current injections cannot be obtained for most



nodes. The current at any node  $k$  is related to  $P$ ,  $Q$  and  $\tilde{V}$  as described in (6-17):

$$\tilde{I}_k = \frac{P_k - jQ_k}{\tilde{V}_k^*} \quad (6-17)$$

where  $P_k$  and  $Q_k$  are the real power and reactive power in the bus  $k$ . For the  $PQ$  buses, the  $P$  and  $Q$  are specified; and for the  $PV$  buses, the  $P$  and the magnitude of  $\tilde{V}$  are specified. For other types of buses, the relationships between  $P$ ,  $Q$ ,  $\tilde{V}$  and  $\tilde{I}$ , are defined by the characteristics of the devices connected to the buses.

Table 6-2 The admittance values in Y

$Y_{1,1} = 6.0250 - j19.4471i;$	$Y_{1,2} = -4.9991 + j15.2631i;$	$Y_{1,5} = -1.0259 + 4.2350i;$
$Y_{2,1} = -4.9991 + 15.2631i;$	$Y_{2,2} = 9.5213 - 30.2721i;$	$Y_{2,3} = -1.1350 + 4.7819i;$
$Y_{2,4} = -1.6860 + 5.1158i;$	$Y_{2,5} = -1.7011 + 5.1939i;$	$Y_{3,2} = -1.1350 + 4.7819i;$
$Y_{3,3} = 3.1210 - 9.8224i;$	$Y_{3,4} = -1.9860 + 5.0688i;$	$Y_{4,2} = -1.6860 + 5.1158i;$
$Y_{4,3} = -1.9860 + 5.0688i;$	$Y_{4,4} = 10.5130 - 38.6542i;$	$Y_{4,5} = -6.8410 + 21.5786i;$
$Y_{4,7} = 0 + 4.8895i;$	$Y_{4,9} = 0 + 1.8555i;$	$Y_{5,1} = -1.0259 + 4.2350i;$
$Y_{5,2} = -1.7011 + 5.1939i;$	$Y_{5,4} = -6.8410 + 21.5786i;$	$Y_{5,5} = 9.5680 - 35.5336i;$
$Y_{5,6} = 0 + 4.2574i;$	$Y_{6,5} = 0 + 4.2574i;$	$Y_{6,6} = 6.5799 - 17.3407i;$
$Y_{6,11} = -1.9550 + 4.0941i;$	$Y_{6,12} = -1.5260 + 3.1760i;$	$Y_{6,13} = -3.0989 + 6.1028i;$
$Y_{7,4} = 0 + 4.8895i;$	$Y_{7,7} = 0 - 19.5490i;$	$Y_{7,8} = 0 + 5.6770i;$
$Y_{7,9} = 0 + 9.0901i;$	$Y_{8,7} = 0 + 5.6770i;$	$Y_{8,8} = 0 - 5.6770i;$
$Y_{9,4} = 0 + 1.8555i;$	$Y_{9,7} = 0 + 9.0901i;$	$Y_{9,9} = 5.3261 - 24.0925i;$
$Y_{9,10} = -3.9020 + 10.3654i;$	$Y_{9,14} = -1.4240 + 3.0291i;$	$Y_{10,9} = -3.9020 + 10.3654i;$
$Y_{10,10} = 5.7829 - 14.7683i;$	$Y_{10,11} = -1.8809 + 4.4029i;$	$Y_{11,6} = -1.9550 + 4.0941i;$
$Y_{11,10} = -1.8809 + 4.4029i;$	$Y_{11,11} = 3.8359 - 8.4970i;$	$Y_{12,6} = -1.5260 + 3.1760i;$
$Y_{12,12} = 4.0150 - 5.4279i;$	$Y_{12,13} = -2.4890 + 2.2520i;$	$Y_{13,6} = -3.0989 + 6.1028i;$
$Y_{13,12} = -2.4890 + 2.2520i;$	$Y_{13,13} = 6.7249 - 10.6697i;$	$Y_{13,14} = -1.1370 + 2.3150i;$
$Y_{14,9} = -1.4240 + 3.0291i;$	$Y_{14,13} = -1.1370 + 2.3150i;$	$Y_{14,14} = 2.5610 - 5.3440i;$

By adopting the node admittance matrix shown above together with the information specified in the PV, PQ or other types of buses from a power system, the formulated power flow problem can be solved using many iterative methods, e.g. Newton-Raphson method and Gauss-Seidel method.



The Newton-Raphson method is the most popular method for solving the power flow problem due to its fast convergence rate and short computational time consumed. Introductions to the Newton-Raphson method are given in the following part of this chapter. And the introduction to the Gauss-Seidel method is given in Appendix V.

Newton-Raphson method, also called the Newton's method, is a root-finding algorithm that uses the first term of the Taylor series of a function in the vicinity of a suspected root. By applying the Newton-Raphson method, the complex equation (6-18) can be rewritten as two equations in terms of two real variables instead of one complex variable (Kundur *et al.* 1994).  $P$  and  $Q$  for each bus are functions of voltage magnitude  $V$  and angle  $\theta$  of all buses.

$$P_k = V_k \sum_{m=1}^n (G_{km} V_m \cos \theta_{km} + B_{km} V_m \sin \theta_{km}) \quad (6-18)$$

$$Q_k = V_k \sum_{m=1}^n (G_{km} V_m \sin \theta_{km} - B_{km} V_m \cos \theta_{km}) \quad (6-19)$$

where  $G_{km}$  and  $B_{km}$  are the conductance and susceptance of the admittance  $Y_{km}$ ;  $\theta_{km}$  is the angle between  $V_k$  and  $V_m$ .

For the  $PQ$  buses, the active power and reactive power at each bus are specified. Using superscript  $sp$  to denote the specified values, we can derive:

$$\begin{aligned} P_1(\theta_1, \dots, \theta_n, V_1, \dots, V_n) &= P_1^{sp} \\ \dots \quad \dots \quad \dots \quad \dots \quad \dots \quad \dots & \\ P_n(\theta_1, \dots, \theta_n, V_1, \dots, V_n) &= P_n^{sp} \\ Q_1(\theta_1, \dots, \theta_n, V_1, \dots, V_n) &= Q_1^{sp} \\ \dots \quad \dots \quad \dots \quad \dots \quad \dots \quad \dots & \\ Q_n(\theta_1, \dots, \theta_n, V_1, \dots, V_n) &= Q_n^{sp} \end{aligned} \quad (6-20)$$

Using the Taylor's theorem, Equation (6-20) can be expanded to be



Equation (6-21), where the partial derivatives of the order greater than 1 in the series of terms of the Taylor's expansion have been neglected.

$$\begin{bmatrix} P_1^p - P_1(\theta_1^{(0)}, \dots, \theta_n^{(0)}, V_1^{(0)}, \dots, V_n^{(0)}) \\ \dots \dots \dots \dots \dots \dots \dots \dots \\ P_n^p - P_n(\theta_1^{(0)}, \dots, \theta_n^{(0)}, V_1^{(0)}, \dots, V_n^{(0)}) \\ Q_1^p - Q_1(\theta_1^{(0)}, \dots, \theta_n^{(0)}, V_1^{(0)}, \dots, V_n^{(0)}) \\ \dots \dots \dots \dots \dots \dots \dots \dots \\ Q_n^p - Q_n(\theta_1^{(0)}, \dots, \theta_n^{(0)}, V_1^{(0)}, \dots, V_n^{(0)}) \end{bmatrix} = \underbrace{\begin{bmatrix} \left(\frac{\partial P_1}{\partial \theta_1}\right)_0 \dots \left(\frac{\partial P_1}{\partial \theta_n}\right)_0 \left(\frac{\partial P_1}{\partial V_1}\right)_0 \dots \left(\frac{\partial P_1}{\partial V_n}\right)_0 \\ \dots \dots \dots \dots \dots \dots \dots \dots \\ \left(\frac{\partial P_n}{\partial \theta_1}\right)_0 \dots \left(\frac{\partial P_n}{\partial \theta_n}\right)_0 \left(\frac{\partial P_n}{\partial V_1}\right)_0 \dots \left(\frac{\partial P_n}{\partial V_n}\right)_0 \\ \left(\frac{\partial Q_1}{\partial \theta_1}\right)_0 \dots \left(\frac{\partial Q_1}{\partial \theta_n}\right)_0 \left(\frac{\partial Q_1}{\partial V_1}\right)_0 \dots \left(\frac{\partial Q_1}{\partial V_n}\right)_0 \\ \dots \dots \dots \dots \dots \dots \dots \dots \\ \left(\frac{\partial Q_n}{\partial \theta_1}\right)_0 \dots \left(\frac{\partial Q_n}{\partial \theta_n}\right)_0 \left(\frac{\partial Q_n}{\partial V_1}\right)_0 \dots \left(\frac{\partial Q_n}{\partial V_n}\right)_0 \end{bmatrix}}_{\text{Jacobian}} \begin{bmatrix} \Delta \theta_1^{(0)} \\ \dots \\ \Delta \theta_n^{(0)} \\ \Delta V_1^{(0)} \\ \dots \\ \Delta V_n^{(0)} \end{bmatrix} \quad (6-21)$$

where  $\theta_1^{(0)}, \dots, \theta_n^{(0)}, V_1^{(0)}, \dots, V_n^{(0)}$  are the initial estimates of the solution of  $\theta_1, \dots, \theta_n, V_1, \dots, V_n$ ;  $\Delta \theta_1^{(0)}, \dots, \Delta \theta_n^{(0)}, \Delta V_1^{(0)}, \dots, \Delta V_n^{(0)}$  are the corrections necessary to the estimated values. Updated values to the solutions in the  $i^{\text{th}}$  iteration are given in the following form:

$$\begin{aligned} \theta_1^{(i)} &= \theta_1^{(i-1)} + \Delta \theta_1^{(i-1)} \\ &\dots \dots \dots \\ \theta_n^{(i)} &= \theta_n^{(i-1)} + \Delta \theta_n^{(i-1)} \\ V_1^{(i)} &= V_1^{(i-1)} + \Delta V_1^{(i-1)} \\ &\dots \dots \dots \\ V_n^{(i)} &= V_n^{(i-1)} + \Delta V_n^{(i-1)} \end{aligned} \quad (6-22)$$

The updated values are inserted into Equation (6-21) and the process is repeated until the errors shown on the left hand side of the Equation (6-22) are within the range of a specified tolerance.

In formulating Equation (6-22), we have assumed that all buses are  $PQ$  buses. For a  $PV$  bus, only  $P$  is specified and the magnitude of  $V$  is fixed. Therefore, terms corresponding to  $\Delta \theta$  and  $\Delta V$  would be absent for each



of the  $PV$  buses. And the Jacobian would have only one row and one column for each  $PV$  bus.

Taking the IEEE 14-bus power system shown in Figure 6-4 as an example to demonstrate the Newton-Raphson method discussed above for solving the power flow problem. The convergence trend for a randomly picked-up  $PQ$  bus (bus 4) is shown in Figure 6-5. The calculation converged at the 4<sup>th</sup> iteration, and took 0.120 seconds.

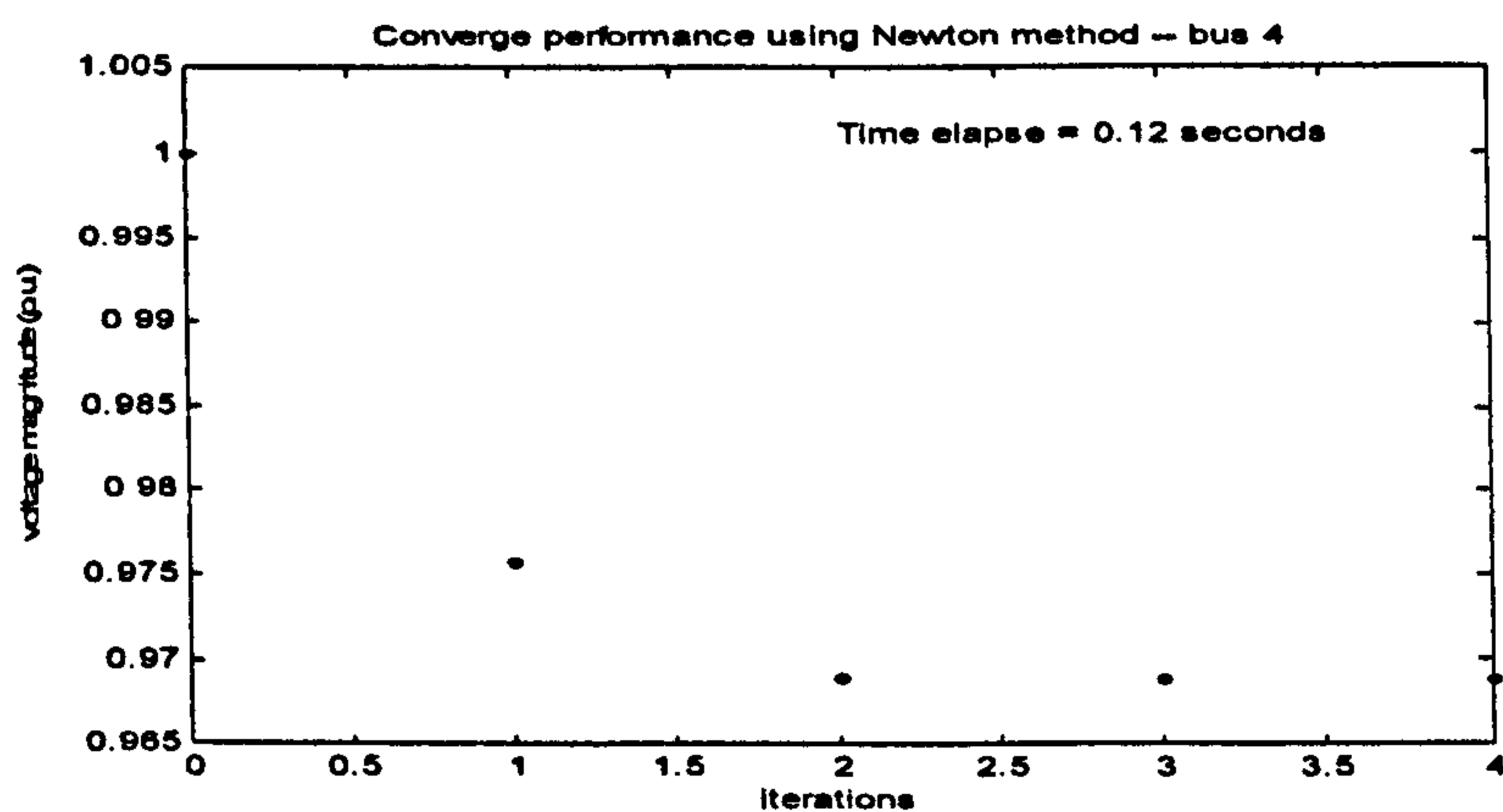


Figure 6-5 The Newton-Raphson method's convergence performance for the bus 4 in the IEEE 14-bus power system

Again, adopting the IEEE 57-bus power system (see Figure 6-7) for the power flow calculation using Newton-Raphson, the convergence performance of a random picking-up  $PQ$  bus (bus 40) is shown in Figure 6-6. And the calculation converged at the 4<sup>th</sup> iteration, and took 0.140 seconds to complete.



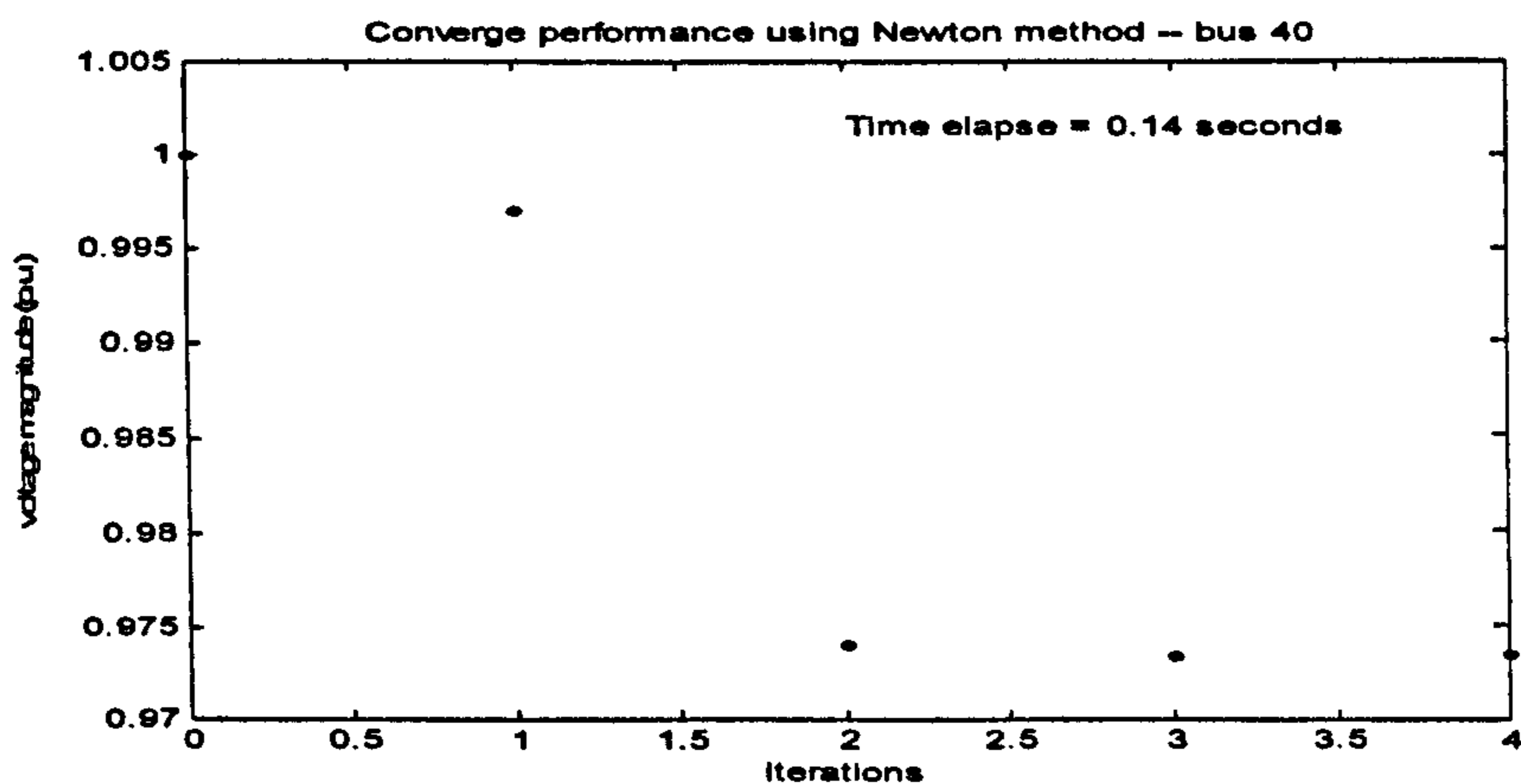


Figure 6-6 The Newton-Raphson method's convergence performance for the bus 40 in the IEEE 57-bus power system

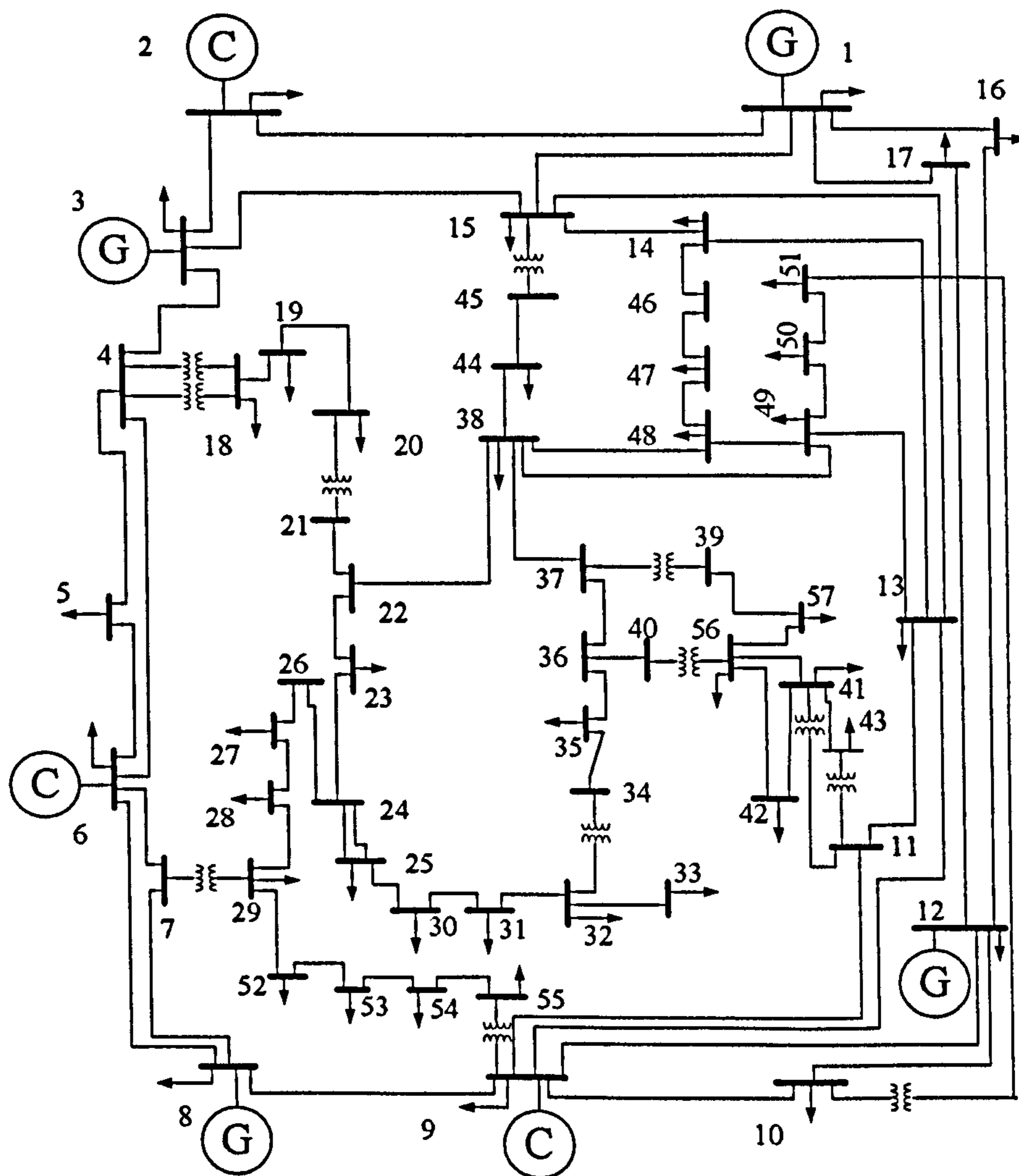


Figure 6-7 IEEE 57-bus power system



## **6.5 Summary and Discussion**

By considering the 'load' as an 'area load' rather than a 'bus load', the ALAM is developed in this chapter particularly for the modelling of the aggregate load area. The chapter starts with the reviews of the standard load models that currently being utilized in the power system research field, where the load models CILM, CCLM, CPLM (ZIP), ELM and PLM are briefly reviewed.

Base on the previous research carried out at the University of Liverpool, introduction of the ALAM is given in the second part of this chapter, which is a novel method for modelling the area load in power system. It is a mathematical representation of the relationship between the total power injected (active and reactive) and the voltage (magnitude and frequency) at the load area. The overall characteristic of the loads in the area and also the transmission and distribution network in the area are modelled.

The power flow calculation is foundation knowledge for simulating the whole power system, and it is the essential tool to simulate the ALAM. Therefore, in the final part of this chapter, the Newton-Raphson method for solving the power flow calculation is illustrated based on the IEEE 14-Bus power system and IEEE 57-Bus power system. Simulation studies show that the Newton-Raphson method offers fast and good convergence rate. Accordingly the Newton-Raphson method is adopted for the power flow calculations while modelling the ALAM in the project.



# Chapter 7

## ALAM Parameter Identification - Three Approaches

### 7.1 Introduction

ALAM was introduced in the previous chapter, which indicated that there are numbers of unknown equivalent parameters needed to be identified for deriving an ALAM. The parameters include resistance, reactance and susceptance for the fictitious branches in the load area, and also the six ZIP load model coefficients to the fictitious load in the load area. To identify all the parameters, different approaches could be used and three of them are introduced in this chapter, namely, Voltage-Two-Step (VTS) approach, Current-Two-Step (CTS) approach, and Directly-One-Step (DOS) approach.

VTS is originally developed by Wen in 2003 (Wen *et al.* 2003a; Wen *et al.* 2003b). The approach is implemented into two steps. In the first step, the branches parameters (resistance, reactance and susceptance) are identified based on a Voltage-Match scheme using Genetic Algorithms. In the second step, the GA is applied again to find the optimal values for the six ZIP load model coefficients. In this approach, short transmission lines are employed to represent the branches in the power system and shunt capacitance were neglected. However, in power system studies, medium length transmission lines are normally used to represent branches, where the shunt capacitance can not be neglected and the nominal- $\pi$  circuit is adopted as the equivalent circuit for the transmission line (Grainger *et al.* 1994; Kundur *et al.* 1994).



By employing the nominal- $\pi$  circuit to represent the branches of power systems, the VTS approach is modified and improved which is published in 2005 (Wei *et al.* 2005c). Detailed descriptions of the modified VTS approach will be given in the chapter.

The CTS approach is relatively new approach for the ALAM. Similar to the VTS approach, it also implements the identification procedure in two steps, in which the parameters of the branches are identified in the first step and the ZIP load coefficients are optimized in the second step. But different from the VTS approach, it uses the Current-Match scheme in identification of the parameters of the branches in the first step rather than using the Voltage-Match scheme. The Voltage-Match scheme is based on the idea that each fictitious voltage calculated by every fictitious branch should be equal to each other. The Current-Match scheme is newly proposed and the principle of the scheme is to minimise the errors between the measured current flow into the load area from the power system considered and the simulated current flow into the fictitious load bus in ALAM, which is used as a criterion in identification of the branches' parameters.

The DOS approach extended the second step calculation of VTS and CTS. The whole procedure is completed in one step, where all the branches' parameters and the ZIP load coefficients are identified together using a new identification scheme entitled "Bus-Match scheme". By minimizing the errors between the measured and simulated bus variables (active power, reactive power, voltage magnitudes, and voltage angles) for the buses outside of load area, all the branches' parameters and the ZIP load coefficients are identified in one step.

In order to illustrate the performances of the three different approaches, the IEEE-14-Bus power system is employed for simulation study. The power



system consists of two generators, twenty branches and fourteen buses. The load area shown in the dotted oval area consists of four branches and two load buses (see Figure 7-1). Applying the ALAM method introduced in the previous chapter, the equivalent power system can be obtained as shown in Figure 7-2, in which the whole load area is treated and modelled as the fictitious load bus 15. There are totally twelve parameters to be identified, which include the series resistance  $R_{6-15}$  of the transmission line I, the series reactance  $X_{6-15}$  of the transmission line I, the line susceptance  $B_{6-15}$  of the transmission line I, the series resistance  $R_{14-15}$  of the transmission line II, the series reactance  $X_{14-15}$  of the transmission line II, the line susceptance  $B_{14-15}$  of the transmission line II, and the six unknown ALAM parameters  $a_{f1} \sim a_{f6}$  as described in Equations (6-13) ~ (6-14).

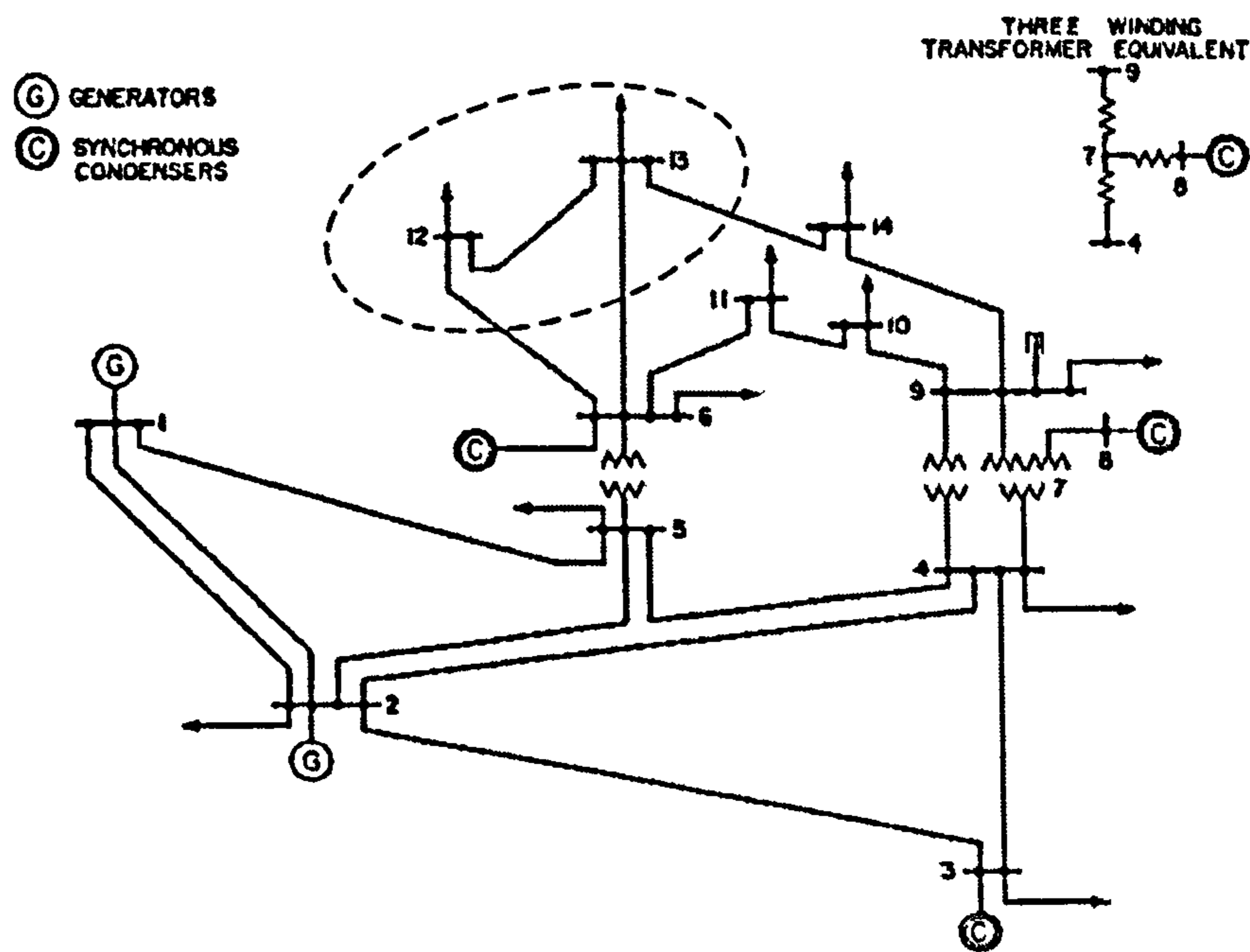


Figure 7-1 The IEEE-14-Bus power system

For the purpose of parameter identification, in order to obtain robust results, three typical operation modes in the power system are set up for illustration of the identification process, which are described as follows:

OS1: Normal operation state, wherein all the values of the bus and branch



are kept as same as the original IEEE 14-bus power system.

OS2: Normal operation conditions but the active power generated in bus 1 decreases by 5% and the active power generated in bus 2 increases by 10%.

OS3: Normal operation conditions but the terminal voltage of generator 1 (bus 1) increases by 10%, the tap ratio of the transformer between bus 5 and bus 6 decreases by 5%.

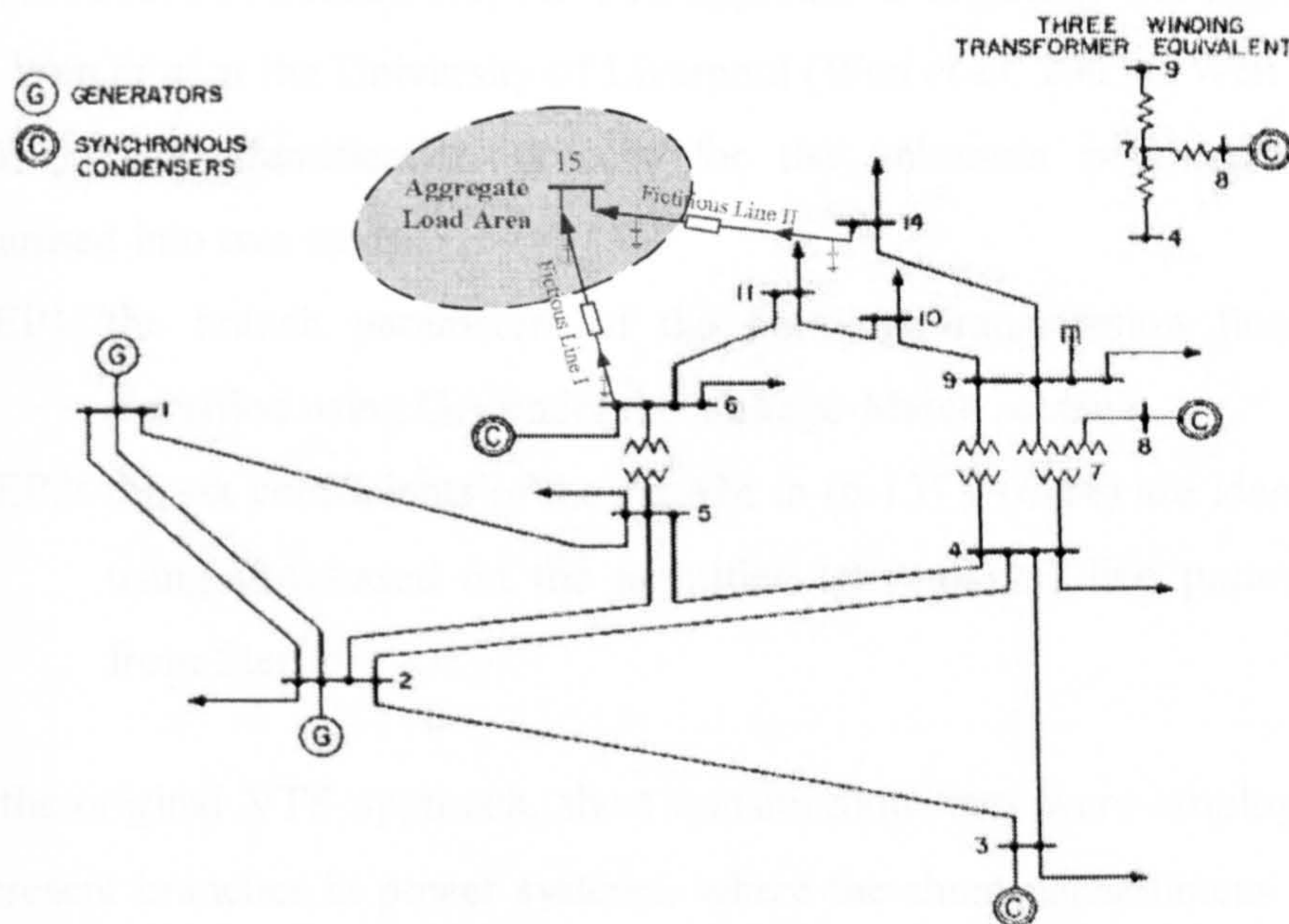


Figure 7-2 The equivalent power system from IEEE 14-bus power system

Similarly, for the purpose of verification, three series studies are carried out to test the identification results under different operation states below:

Test1: Assume the system operates at the normal operation condition, but the active power outputs from generator 2 (bus 2) changes from 10% below its normal load output to 10% higher in 1% increment.

Test2: Assume the system operates at the normal operation condition, but the tap ratio of the transformer between bus 5 and bus 6 changes from 10% below its normal value to 10% higher in 1% increment.

Test3: Assume that the system operates at the normal operation condition,



but the values of voltage outputs from Generator 2 (Bus 2) changes from 10% below its normal output to 10% higher in 1% increment.

## **7.2 ALAM Approach One: Voltage-Two-Step (VTS)**

### **Approach**

As introduced in Section 7.1, the VTS approach is originally developed by Dr. Wen *et al* at the University of Liverpool (Wen *et al.* 2003a; Wen *et al.* 2003b). The identification process for the unknown parameters are organised into two steps:

STEP1: the branch parameters of the fictitious transmission lines are identified using GA under the Voltage-Match scheme;

STEP2: the six coefficients of the ALAM in (6-13) ~ (6-14) are identified using GA based on the identified transmission line parameters from Step 1.

In the original VTS approach, short transmission lines were employed to represent branches in power systems, where the shunt capacitances in the branch were neglected. However, in power system network studies, people normally do not have enough information to tell whether a transmission line is short or medium long. Usually, people would like to use medium length transmission lines to represent all the transmission branches (Kundur *et al.* 1994), which is a very reasonable approximation to a short transmission line as well if the shunt capacitance is set to be zero. And the nominal  $\pi$  circuit is widely used to represent this type of transmission line structure (Grainger *et al.* 1994; Kundur *et al.* 1994). In this project, the nominal  $\pi$  circuit is adopted to represent the transmission line structure in power systems. Schematic of the nominal  $\pi$  circuit is shown in Figure 7-3. The relationship between the voltage at the sending end of the transmission line and the voltage at the receiving end of the transmission line can be



described by the following equation (Grainger *et al.* 1994).

$$\vec{V}_R = \left( 1 + Z \frac{Y}{2} \right) \vec{V}_S - Z \vec{I}_S \quad (7-1)$$

where  $\vec{V}_R$  is the voltage in per unit at the receiving end of the transmission line;  $\vec{V}_S$  is the voltage in per unit at the sending end of the transmission line;  $\vec{I}_S$  is the current of the transmission line in per unit at the sending end;  $Z$  is the impedance of the transmission line in per unit; and  $Y$  is the admittance of the transmission line in per unit.  $\vec{V}_R$ ,  $\vec{V}_S$ ,  $\vec{I}_S$  are all complex variables.

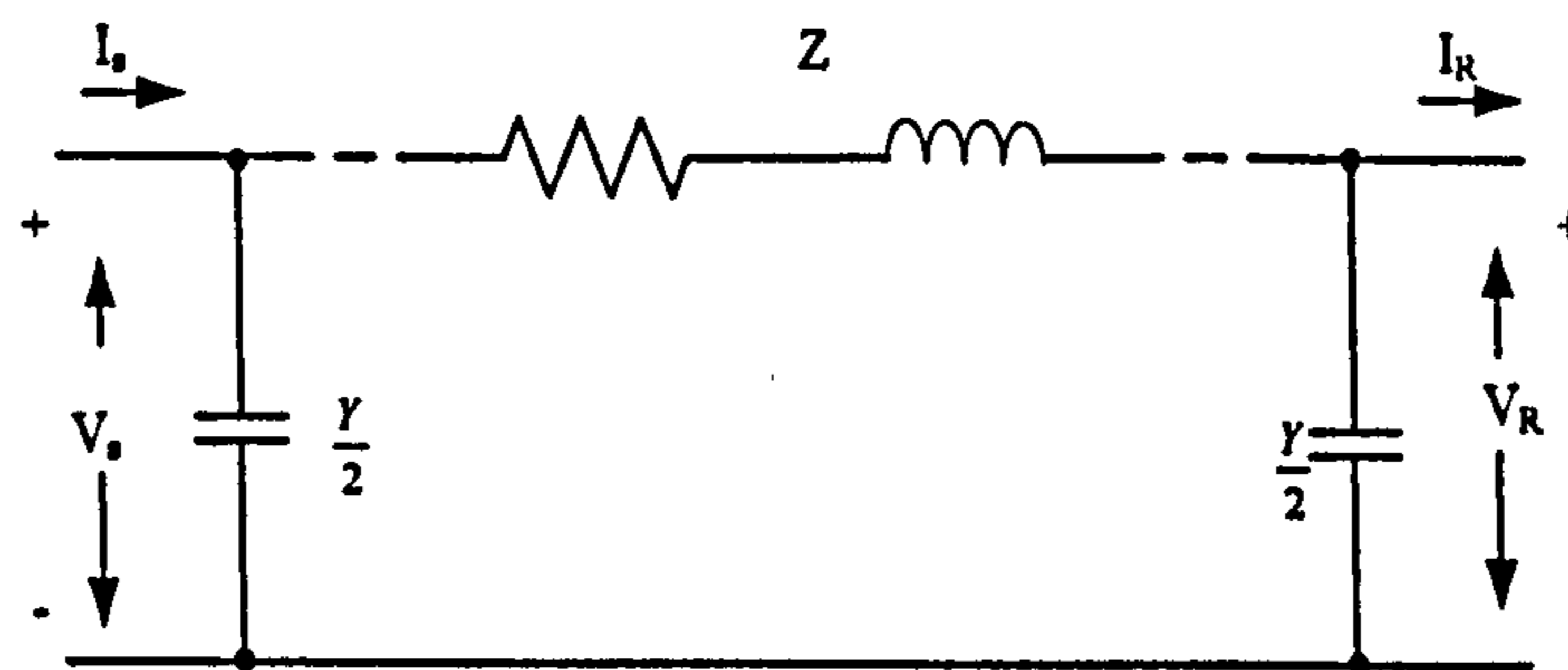


Figure 7-3 Nominal  $\pi$  circuit for the fictitious transmission line

The definition of the line impedance  $Z$  and the line admittance  $Y$  are given in the following equations, in which the line conductance is neglected.

$$Z = R + jX \quad (7-2)$$

$$Y = jB \quad (7-3)$$

where  $R$  is the series resistance of the transmission line in per unit;  $X$  is the series reactance of the transmission line in per unit; and  $B$  is the line susceptance in per unit.

Representing the fictitious transmission lines of the load area shown in Figure 6-3, the branch parameters include the resistance  $R$ , reactance  $X$  and susceptance  $B$  of each transmission line. All the values of these parameters



for the fictitious lines are unknown, and they will be identified in the first step in the Voltage-Two-Step approach under the Voltage-Match scheme. The Voltage-Match scheme is proposed based on the idea that each receiving end voltage of the fictitious load bus calculated by each fictitious transmission line should be equal to each other. According to the nominal circuit described in Equations (7-1) ~ (7-3), the receiving end voltages of the fictitious load bus that connected with  $m$  and  $n$  buses in Figure 6-3 can be derived as follows:

$$\vec{V}_f^n = \left( 1 + (R_n + jX_n) \frac{jB_n}{2} \right) \vec{V}_n - (R_n + jX_n) \vec{I}_n \quad (7-4)$$

$$\vec{V}_f^m = \left( 1 + (R_m + jX_m) \frac{jB_m}{2} \right) \vec{V}_m - (R_m + jX_m) \vec{I}_m \quad (7-5)$$

where  $I_n, I_m$  are the current in per unit flow into the fictitious load bus from the bus  $n, m$  via the fictitious transmission line, which can be measured in the power system;  $V_n, V_m$  is the voltage of the buses  $n, m$ .

Following the Voltage-Match scheme, the receiving end voltages  $\vec{V}_f^n$  and  $\vec{V}_f^m$  should be same in values. Therefore, the fitness function for the STEP1 to identify  $R, X$  and  $B$  of the fictitious transmission lines can be defined as follows:

$$e^{os\_i}_{STEP1}(R, X, B) = \sum_{\substack{m,n(m \neq n) \\ m,n=1,2,\dots}} |\vec{V}_f^m - \vec{V}_f^n| \quad (7-6)$$

$$Fitness = \sum_{os\_i=OS1,OS2,\dots} e^{os\_i}_{STEP1}(R, X, B) \quad (7-7)$$

where  $m, n$  are the buses that connected with the fictitious load bus outside of the load area;  $os\_i$  represents one of the varied operation states of the power system adopted for the identification, which are introduced at the beginning of this chapter.

In the identification STEP2 of the Voltage-Two-Step approach, the GA is

applied again to identify the six parameters of the ALAM ( $a_{f1} \sim a_{f6}$ ). The fitness function is given as follows.

$$P_M = \sum_{n=1,2,\dots} (\bar{V}_f \bar{I}_f^n \cos \theta_n) \quad (7-8)$$

$$Q_M = \sum_{n=1,2,\dots} (\bar{V}_f \bar{I}_f^n \sin \theta_n) \quad (7-9)$$

$$P_f = [a_{f1} V_f^2 + a_{f2} V_f + a_{f3}] \quad (7-10)$$

$$Q_f = [a_{f4} V_f^2 + a_{f5} V_f + a_{f6}] \quad (7-11)$$

$$e^{\text{os}}_{\text{STEP2}}(a_{f1}, \dots, a_{f6}) = w_1 |P_M - P_f| + w_2 |Q_M - Q_f| \quad (7-12)$$

$$\text{Fitness} = \sum_{\text{os}_i = \text{OS1}, \text{OS2}, \dots} e^{\text{os}_i} e^{\text{os}_i - 1}_{\text{STEP2}}(a_{f1}, \dots, a_{f6}) \quad (7-13)$$

where  $n$  is the bus that connected with the aggregate load area via the fictitious transmission line;  $\bar{V}_f$  is the voltage of the fictitious load bus in per unit, which is identified in STEP1;  $\bar{I}_f^n$  is the current in per unit flow into the fictitious load bus via the  $n$  fictitious transmission line, which can be measured in the power system;  $\theta_n$  is the phase angle between  $\bar{V}_f$  and  $\bar{I}_f^n$ ;  $P_f$ ,  $Q_f$  are the per unit value of the active and reactive power consumed in the fictitious load bus, which can be calculated by Equations (6-13) and (6-14); and  $w_1 \sim w_2$  are the weights for the individual errors, which are set to be 1 in this study.

Again employing the real-value SPGA which is introduced in Chapter 3 for the parameter identification in STEP1 and STEP2 using the Voltage-Two-Step approach, the twelve unknown parameters of the equivalent IEEE-14-Bus power system (see Figure 7-2) are identified and are given in Table 7-1.



Table 7-1 The twelve identified parameters of the equivalent IEEE-14-Bus power system

$R_{6-15} = 0.1656 \text{ p.u.}$	$X_{6-15} = 0.3936 \text{ p.u.}$	$B_{6-15} = 0.0127 \text{ p.u.}$
$R_{14-15} = 0.1082 \text{ p.u.}$	$X_{14-15} = 0.7550 \text{ p.u.}$	$B_{14-15} = 0.0033 \text{ p.u.}$
$a_{f1} = 0.1270$	$a_{f2} = -0.1702$	$a_{f3} = 0.0010$
$a_{f4} = 0.2179$	$a_{f5} = -0.3514$	$a_{f6} = 0.0762$

While verifying the identified parameters of the ALAM, the bus variables should be compared with its original ones to see whether the ALAM power system is equivalent to the original system. The bus variables include: active power, reactive power, magnitude of the bus voltage, angle of the bus voltage. In power system studies, the magnitude of the bus voltage gives the most significant information of the power system, so the magnitude of the bus voltage is chosen as a variable to be concerned in the verifications (Wen *et al.* 2003a; Wen *et al.* 2003b). Conducting the three series simulation studies introduced at the beginning of the chapter to vary the ALAM with the identified parameters, the results of the maximum errors of the bus voltages of the equivalent power system are shown in Figures 7-4 ~ 7-6. From the results, it can be seen that the equivalent power system embodied ALAM can give a good degree of equivalent approximation to the original power system even under the conditions of the series changes in the generators outputs and transformer tap ratios.

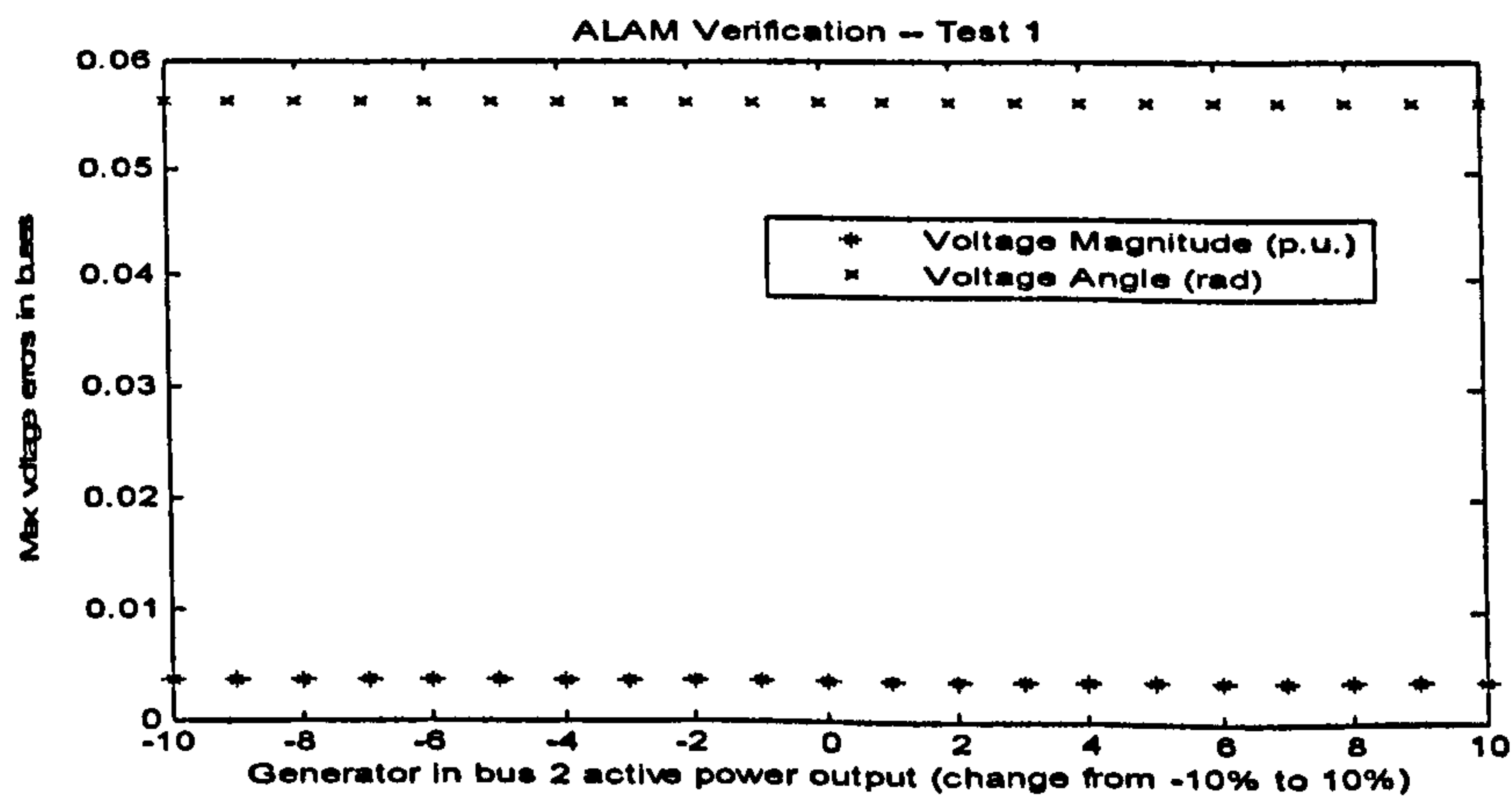


Figure 7-4 Maximum errors of the bus voltages of the equivalent power system approached by CTS in verification Test1.

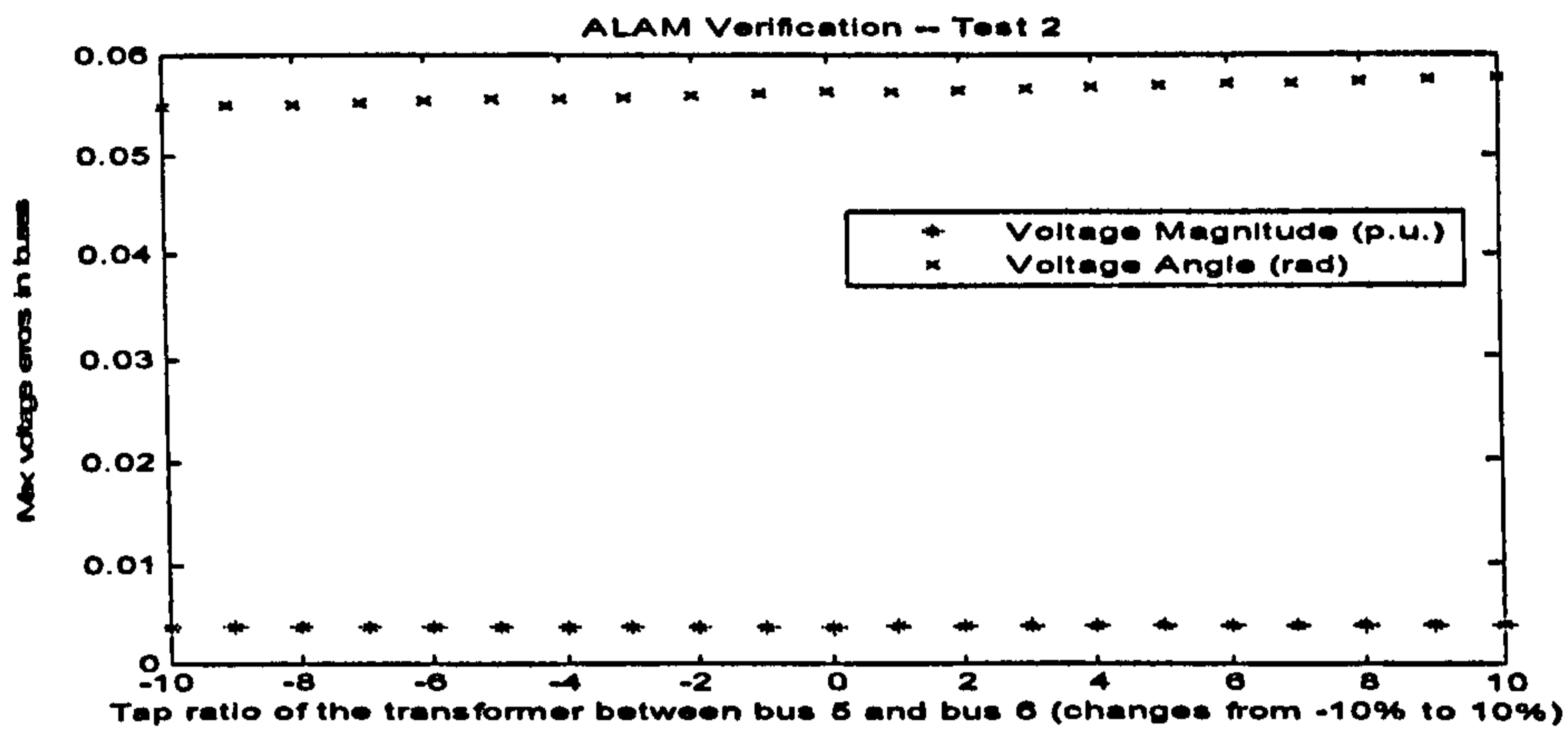


Figure 7-5 Maximum errors of the bus voltages of the equivalent power system approached by CTS in verification Test2.

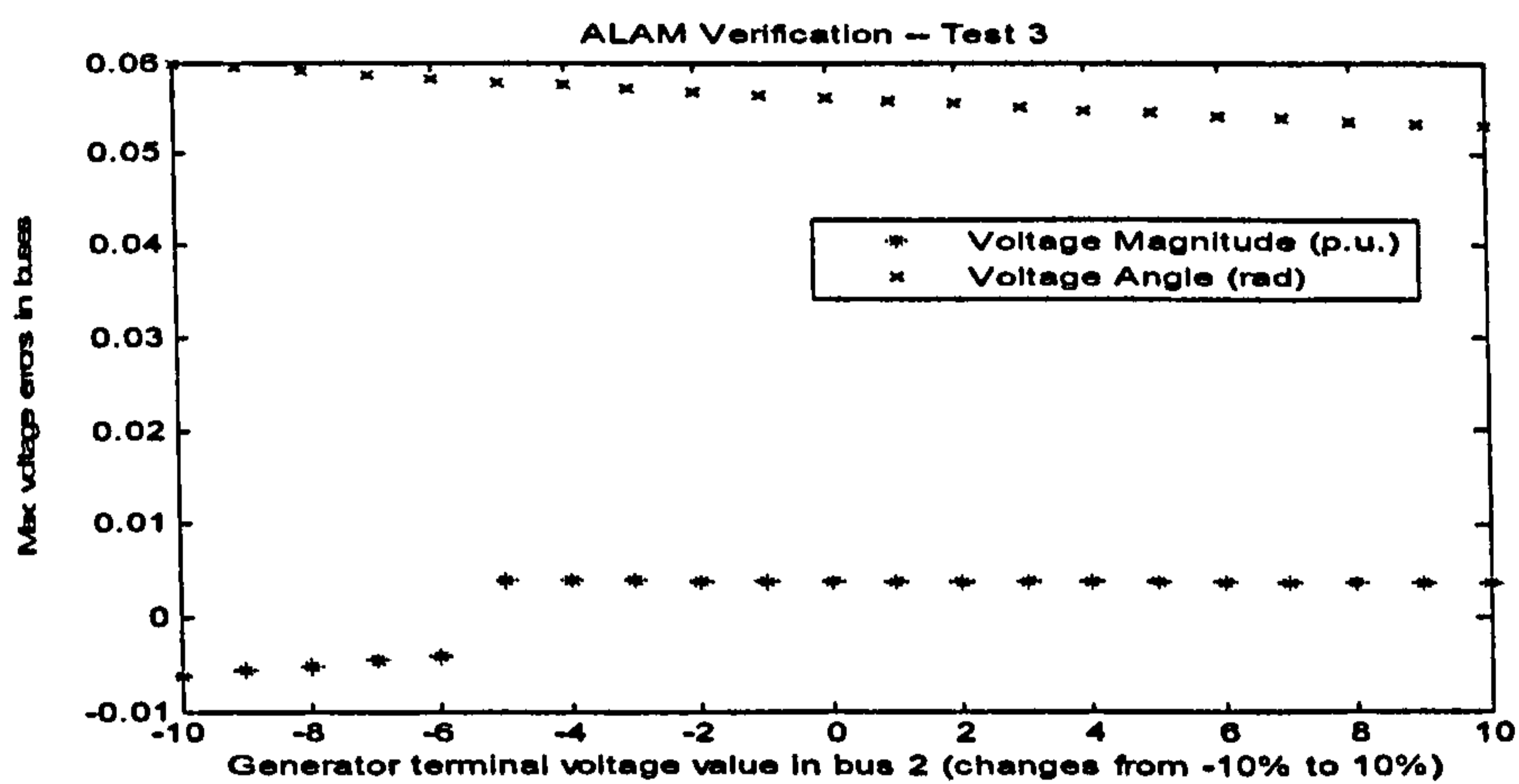


Figure 7-6 Maximum errors of the bus voltages of the equivalent power system approached by CTS in verification Test3.

### 7.3 ALAM Approach Two: Current-Two-Step (CTS) Approach

The CTS is a newly developed approach for the ALAM through my PhD project. Similar to the CTS, the identification process of the unknown parameters in the ALAM has also been organised into two steps, which are shown as follows:

STEP1: the branch parameters of the fictitious transmission lines are identified firstly using GA under the Current-Match scheme.

STEP2: the six unknown parameters of the ALAM in Equations (6-13)



and (6-14) are identified using GA based on the identified transmission line parameters from the first step.

Different from VTS, the CTS employs the Current-Match scheme for identifying the branch parameters in the first step. The Current-Match scheme is based on the idea that total current flow into the fictitious load bus should be equal to the total current flow into the load area, which can be measured in power systems. As introduced in Section 7.2, the fictitious transmission lines can be represented by the nominal  $\pi$  circuits (see Figure 7-3). The current flow into the receiving end of the transmission line is given as follows (Grainger *et al.* 1994):

$$\bar{I}_R = \left[ 1 + \frac{Y}{2} Z \right] \bar{I}_S - \left[ Y + \left( \frac{Y}{2} \right)^2 Z \right] \bar{V}_S \quad (7-14)$$

where  $\bar{I}_R$  is the current in per unit at the receiving end of the transmission line;  $\bar{V}_S$  is the voltage in per unit at the sending end of the transmission line;  $\bar{I}_S$  is the current of the transmission line in per unit at the sending end;  $Z$  is the impedance of the transmission line in per unit;  $Y$  is the admittance of the transmission line in per unit;  $\bar{I}_R$ ,  $\bar{V}_S$ ,  $\bar{I}_S$  are all complex variables.

Following the Current-Match scheme, the fitness function for STEP1 for identification of  $R_i$ ,  $X_i$  and  $B_i$  of the fictitious transmission line is given as follows:

$$\bar{I}_f^n = \left[ 1 + \frac{jB_n}{2} (R_n + jX_n) \right] I_n - \left[ jB_n - \frac{B_n^2}{4} (R_n + jX_n) \right] V_n \quad (7-15)$$

$$I_{f\_Simulated} = \sum_{n=1,2,\dots} \bar{I}_f^n \quad (7-16)$$

$$e^{os}_{STEP1}(R, X, B) = \left| I_{f\_Measured} - I_{f\_Simulated} \right| \quad (7-17)$$

$$Fitness = \sum_{os\_i=OS1,OS2,\dots} e^{os\_i} \text{STEP1}(R, X, B) \quad (7-18)$$

where  $n$  is the bus that is connected with the aggregate load area via the fictitious transmission line;  $\bar{I}_f^n$  is the current flow into the fictitious load bus in per unit, which is derived based on the connecting bus  $n$ ;  $I_n$  is the current in per unit flow into the fictitious load bus via the  $n$  fictitious transmission line, which can be measured in the power system;  $V_n$  is the voltage of bus  $n$ , which can be measured as well.  $I_{f\_Simulated}$  is the simulated current flow into the fictitious load bus, which is the total effect of current flowed into the fictitious load bus via all the fictitious transmission lines;  $I_{f\_Measured}$  is the total effect of current flow into the load area, which is measured in the power system.

Similar to VTS, in STEP2 of the Current-Two-Step approach, the GA is adopted as well to identify the six parameters of the ALAM ( $a_{f1} \sim a_{f6}$ ).

The fitness function is defined as follows:

$$\bar{V}_f = \frac{1}{n} \sum_n \left[ \left( 1 + (R_n + jX_n) \frac{jB_n}{2} \right) \bar{V}_n - (R_n + jX_n) \bar{I}_n \right] \quad (7-19)$$

$$P_M = \bar{V}_f \bar{I}_{f\_Measured} \cos \theta \quad (7-20)$$

$$Q_M = \bar{V}_f \bar{I}_{f\_Measured} \sin \theta \quad (7-21)$$

$$P_f = [a_{f1} V_f^2 + a_{f2} V_f + a_{f3}] \quad (7-22)$$

$$Q_f = [a_{f4} V_f^2 + a_{f5} V_f + a_{f6}] \quad (7-23)$$

$$e^{os\_STEP2}(a_{f1}, \dots, a_{f6}) = w_1 |P_M - P_f| + w_2 |Q_M - Q_f| \quad (7-24)$$

$$Fitness = \sum_{os\_i=OS1,OS2,\dots} e^{os\_i} \text{STEP2}(a_{f1}, \dots, a_{f6}) \quad (7-25)$$

where  $n$  is the bus that connected with the aggregate load area via the fictitious transmission line;  $\bar{V}_f$  is the voltage of the fictitious load bus in



per unit, which is derived based on the identified  $R, X, B$  from the first step using the Current-Two-Step approach;  $I_{f\_Measured}$  is the total effect of the current flow into the load area, which is measured in the power system;  $\theta$  is the phase angle between  $\bar{V}_f$  and  $\bar{I}_{f\_Measured}$ ;  $P_f, Q_f$  are the per unit value of active and reactive power consumed in the fictitious load bus; and  $w_1 \sim w_2$  are the weighting coefficients for the individual errors, which are set to be 1 in this study.

The real-value SPGA is employed which has been introduced in Chapter 3 for parameter identification in STEP1 and STEP2 of the Current-Two-Step approach. The twelve unknown parameters of the equivalent IEEE-14-Bus power system (see Figure 7-2) are identified and given in Table 7-2.

Table 7-2 The twelve identified parameters of the equivalent IEEE-14-Bus power system

$R_{6-15} = 0.6303 \text{ p.u.}$	$X_{6-15} = 0.7888 \text{ p.u.}$	$B_{6-15} = 0.0016 \text{ p.u.}$
$R_{14-15} = 0.2944 \text{ p.u.}$	$X_{14-15} = 0.7645 \text{ p.u.}$	$B_{14-15} = 0.0002 \text{ p.u.}$
$a_{f1} = 0.0689$	$a_{f2} = -0.3552$	$a_{f3} = 0.3498$
$a_{f4} = 0.1415$	$a_{f5} = -0.3376$	$a_{f6} = 0.2005$

Conducting three series tests introduced at the beginning of this chapter to verify the ALAM for the identified parameters, the results are shown in Figures 7-7 ~ 7-9. From the results, it can be seen that the equivalent power system embodied ALAM can give a good degree of agreement to be equivalent to the original power system with the identified parameters using the CTS approach under a series changes in the generators outputs and transformer tap ratios. Comparing with the verification results obtained from the VTS approach, the CTS provide a set of results which are slightly better than those obtained by the VTS, where the maximum errors of the bus voltages in each operation state are getting smaller.

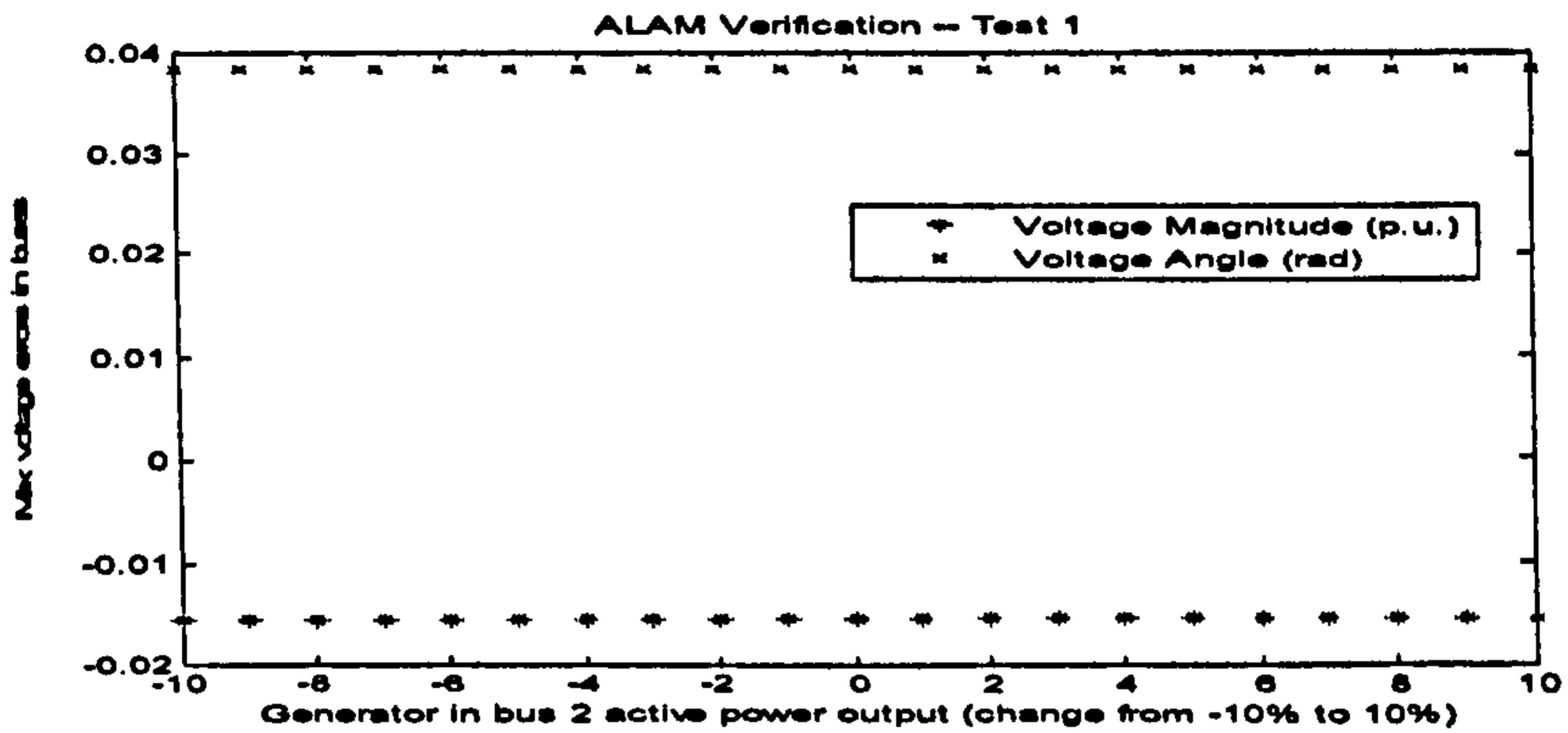


Figure 7-7 Maximum errors of the bus voltages of the equivalent power system approached by CTS in verification Test1.

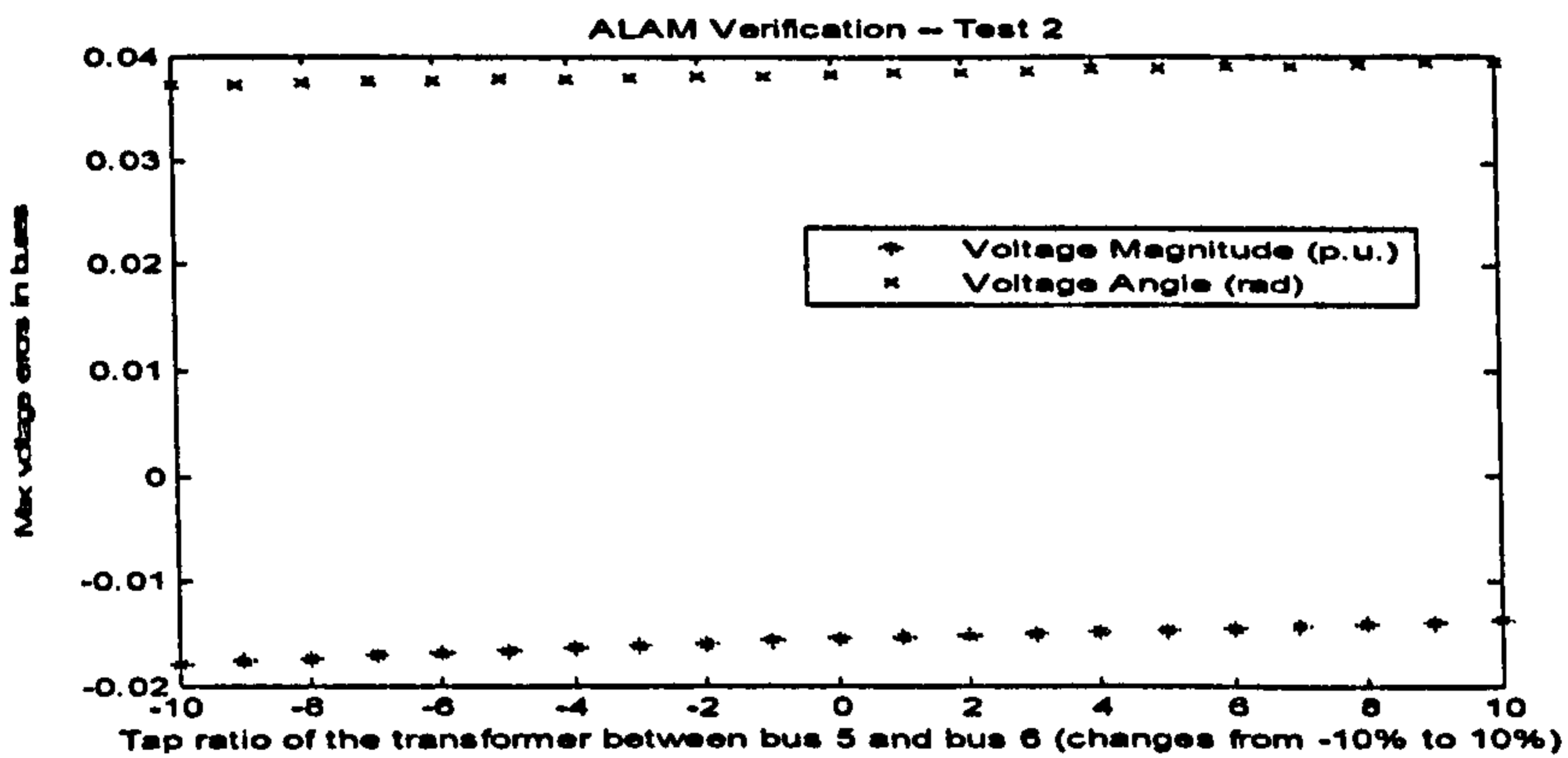


Figure 7-8 Maximum errors of the bus voltages of the equivalent power system approached by CTS in verification Test2.

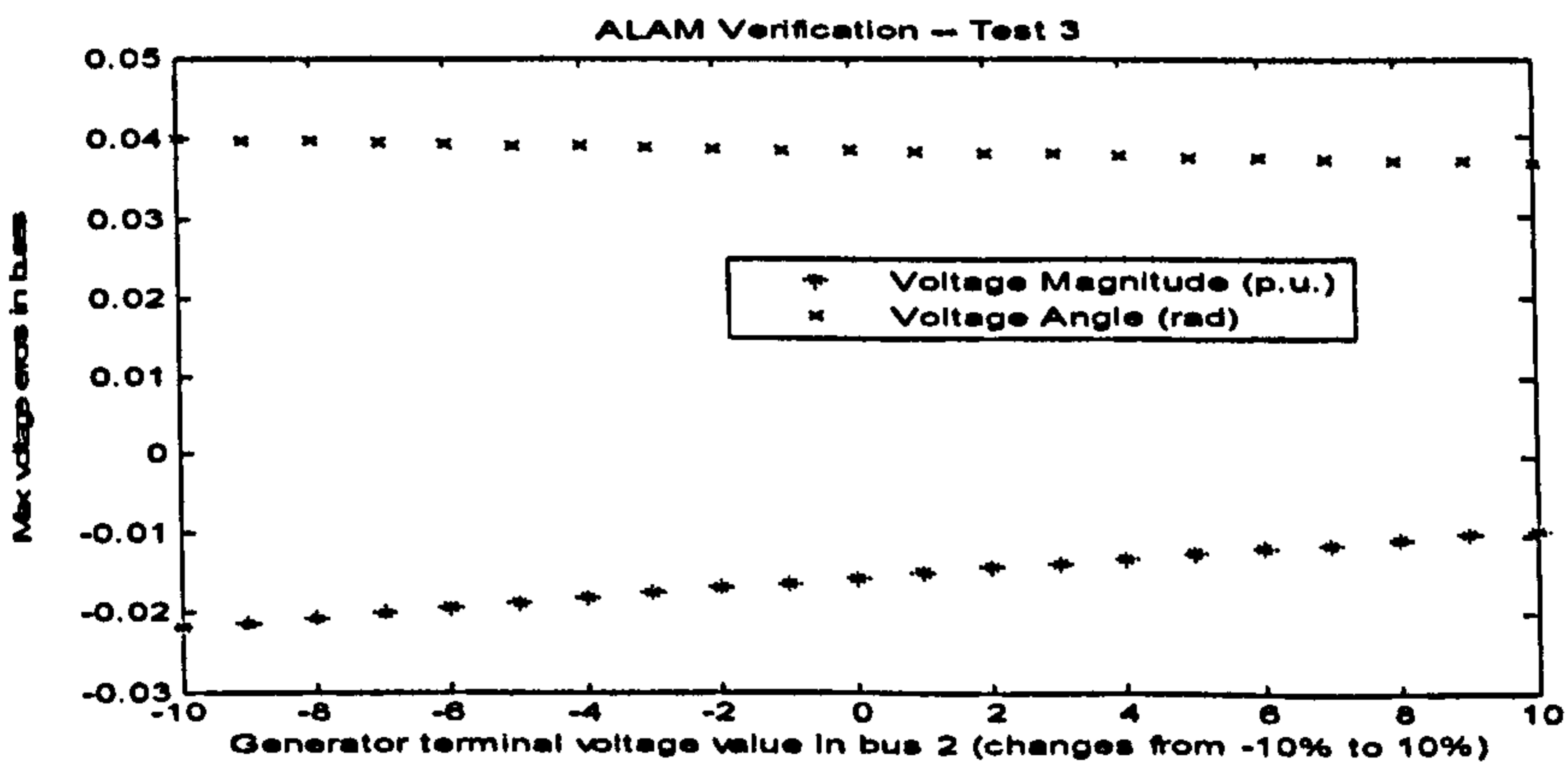


Figure 7-9 Maximum errors of the bus voltages of the equivalent power system approached by CTS in verification Test3.



## 7.4 ALAM Approach Three: Direct-One-Step (DOS)

### Approach

The DOS approach is a simplified approach that combines both the STEPs 1 and 2 in the VTS and CTS into one. All the unknown parameters include the parameters of the fictitious transmission lines and the coefficients of the ZIP load model are identified in one step under the scheme namely Bus-Match, which is shown in Figure 7-10. The Bus-Match scheme can be explained as that the bus variables in the equivalent power system should match the bus variables in the original power system. The whole procedure is based on the network calculation in power systems, which has been introduced in Chapter 6. The parameters ( $R, X, B, a_{f1} \sim a_{f6}$ ) identified using the GA are substituted into the equivalent power system for the power flow calculations and then derives the simulated bus variables. By matching the simulated bus variables to the measured bus variables, the GA evolves, and the parameters will be identified at the end of the process.

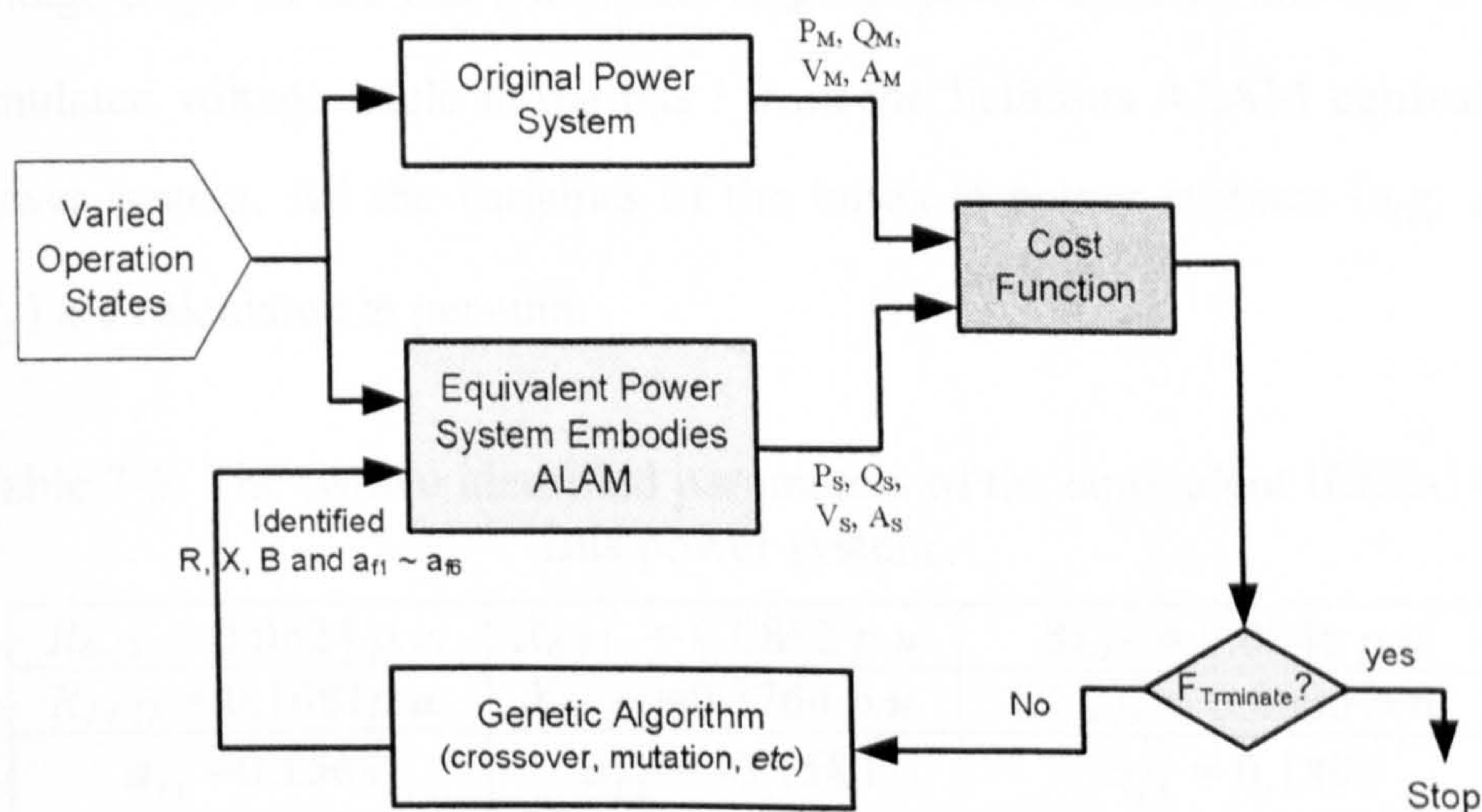


Figure 7-10 The identification process of the DOS approach

The variables (active power, reactive power, voltage magnitude, voltage angle) of the buses outside of the load area between the original power system and the equivalent power system are compared to construct the fitness function for GA, which is given as follows:



$$\text{Fitness}(R, X, B, a_{f1} \sim a_{f6}) = \sum_i (w_1 |P_{Mi} - P_{Si}| + w_2 |Q_{Mi} - Q_{Si}| + w_3 |V_{Mi} - V_{Si}| + w_4 |A_{Mi} - A_{Si}|) \quad (7-26)$$

where,  $i$  is the notation of the buses outside of the fictitious load area in the power system;  $w_1 \sim w_4$  are the weighting coefficients for the individual errors;  $P_{Mi}$  is the measured active power consumed/generated in Bus  $i$  from the original power system;  $P_{Si}$  is the simulated active power consumed/generated in Bus  $i$  from the fictitious ALAM equivalent power system;  $Q_{Mi}$  is the measured reactive power consumed/generated in the bus  $i$  from the original power system;  $Q_{Si}$  is the simulated reactive power consumed/generated in the bus  $i$  from the fictitious ALAM equivalent power system;  $V_{Mi}$  is the measured voltage magnitude in the bus  $i$  from the original power system;  $V_{Si}$  is the simulated voltage magnitude in the bus  $i$  from the fictitious ALAM equivalent power system;  $A_{Mi}$  is the measured voltage angle in the bus  $i$  from the original power system; and  $A_{Si}$  is the simulated voltage angle in the bus  $i$  from the fictitious ALAM equivalent power system. All the variables of the buses in power systems (e.g.  $P_{Mi}$ ,  $P_{Si}$ ) are calculated in per-unit.

Table 7-3 The twelve identified parameters of the equivalent IEEE-14-Bus power system

$R_{6-15} = 0.0624 \text{ p.u.}$	$X_{6-15} = 0.0852 \text{ p.u.}$	$B_{6-15} = 0.0046 \text{ p.u.}$
$R_{14-15} = 0.1081 \text{ p.u.}$	$X_{14-15} = 0.3764 \text{ p.u.}$	$B_{14-15} = 0.0005 \text{ p.u.}$
$a_{f1} = 0.1563$	$a_{f2} = -0.1583$	$a_{f3} = 0.1893$
$a_{f4} = 0.0414$	$a_{f5} = -0.2467$	$a_{f6} = 0.2929$

In this study, the IEEE-14-Bus power system (see Figure 7-1) has been employed for the simulation study of this ALAM approach. Using the DOS approach, the twelve unknown parameters of the IEEE-14-Bus power system are identified which are shown in Table 7-3.



Similarly, the three series tests that carried out to test the equivalent IEEE-14-Bus power system in Section 2.7.2 and 2.7.3 are repeated to verify the twelve identified parameters. The verification results are shown in Figures 7-11 ~ 7-13. Comparing with the results obtained using VTS and CTS approaches, it can be seen that the DOS approach offers a more accurate identifications to the ALAM parameters, where much less errors between the equivalent power system and the original power system exist.

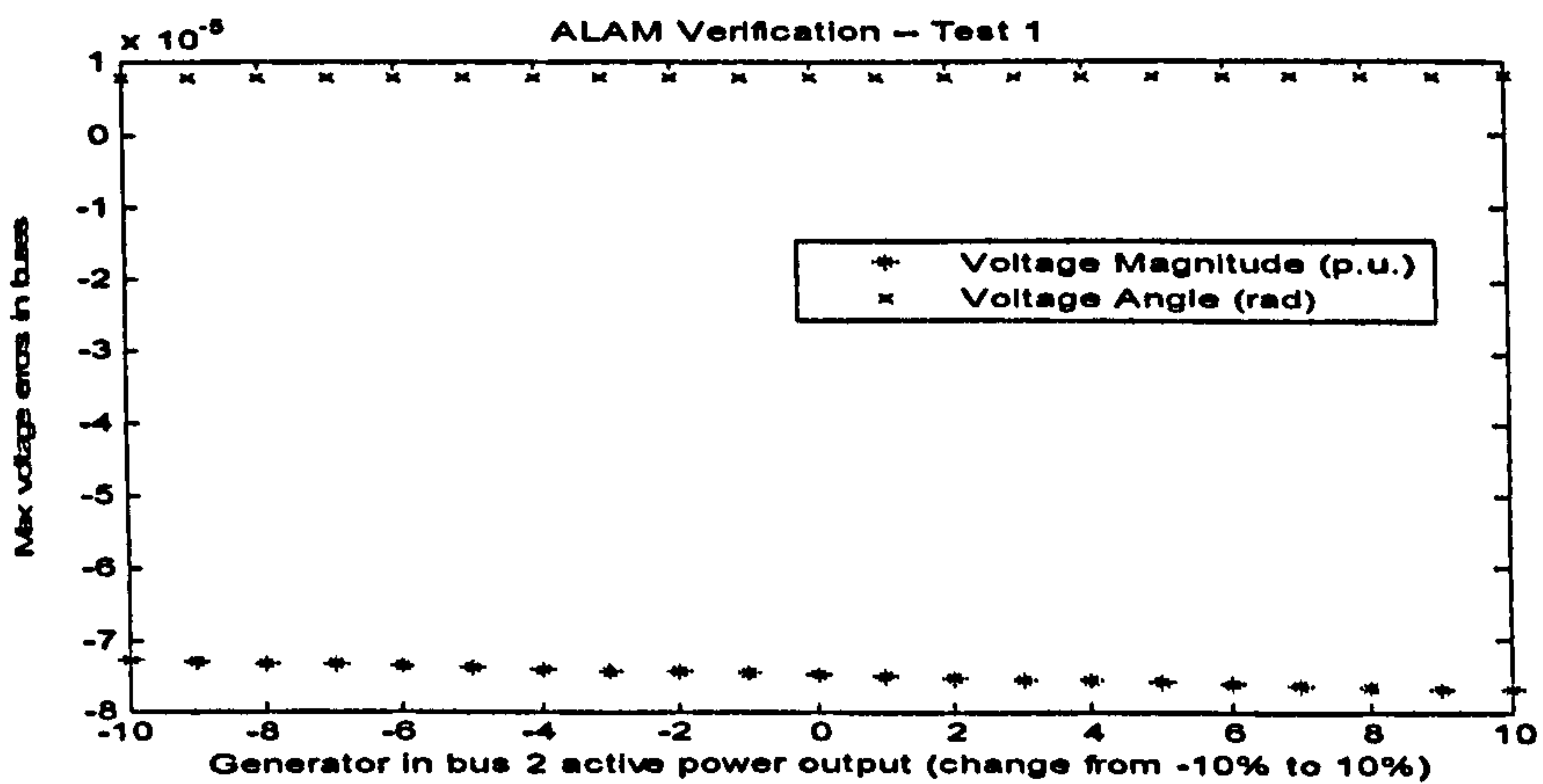


Figure 7-11 Max errors of the bus voltages of the equivalent power system approached by DOS in verification Test 1

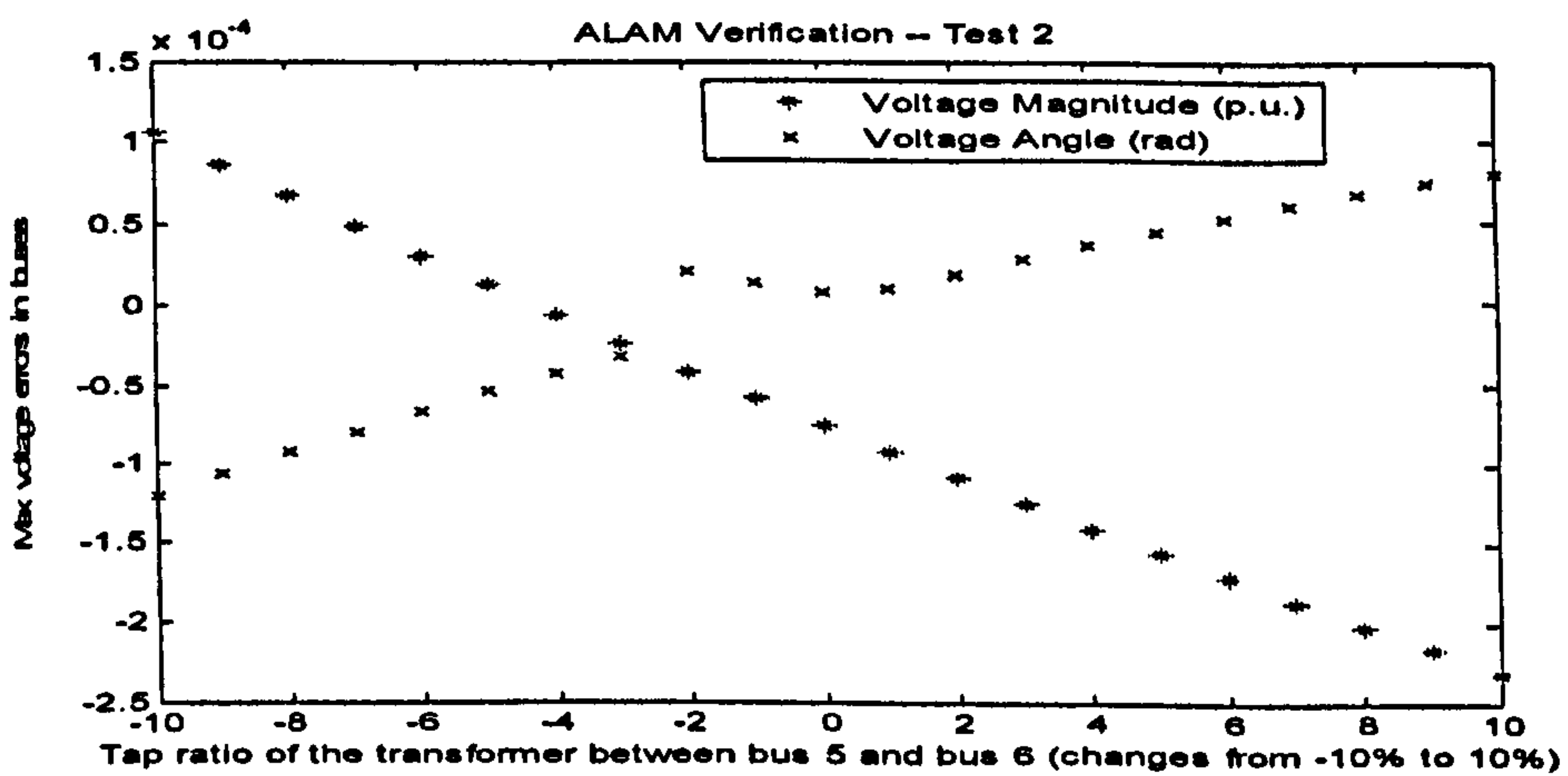


Figure 7-12 Maximum errors of the bus voltages of the equivalent power system approached by DOS in verification Test 2

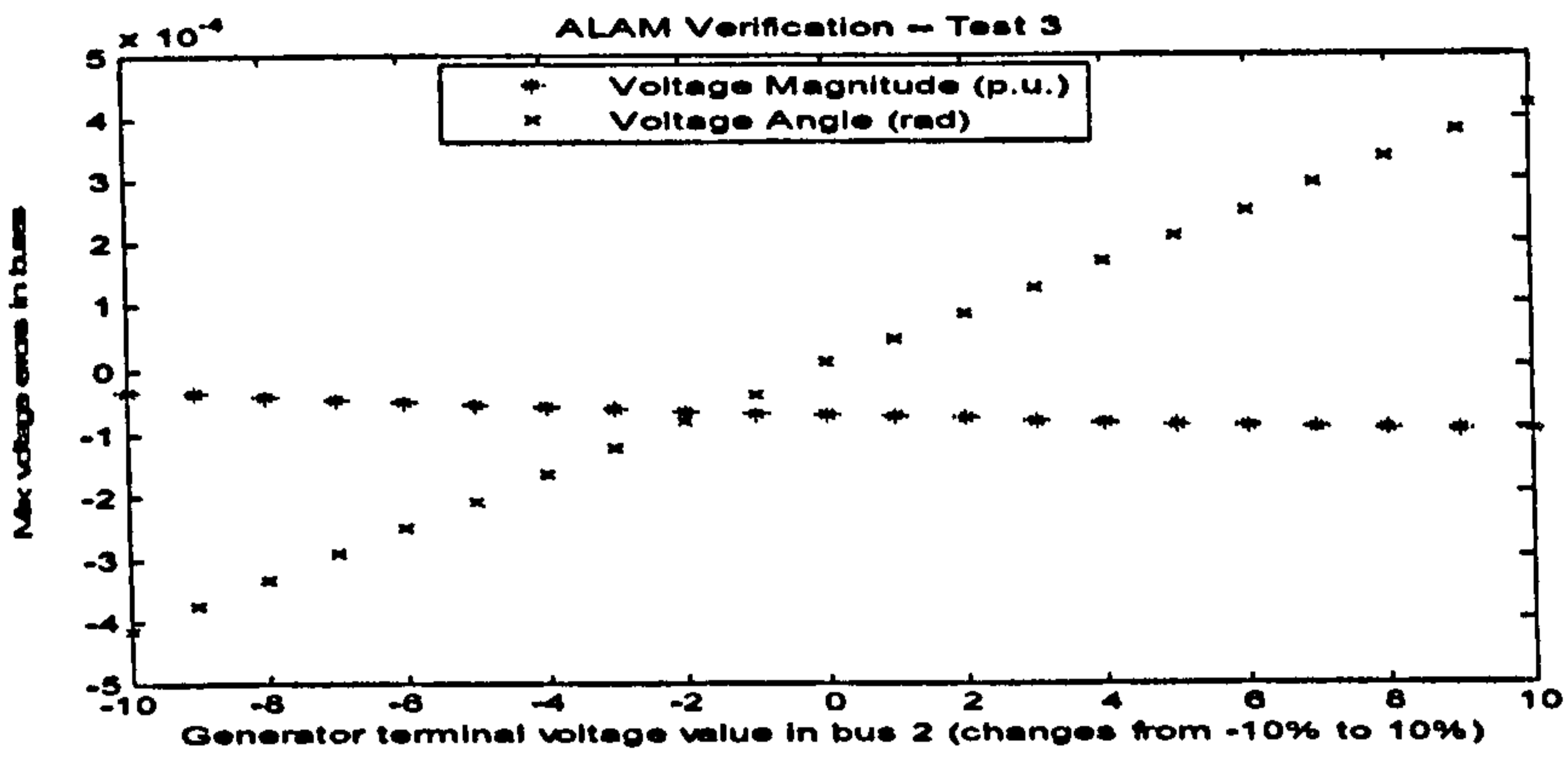


Figure 7-13 Maximum errors of the bus voltages of the equivalent power system approached by DOS in verification Test3

## 7.5 Summary and Discussion

In order to identify the parameters in the ALAM, three different approaches were introduced in this chapter, which are VTS, CTS and DOS. Different identification schemes and processes are employed together with these approaches.

The VTS approach employs the Voltage-Match scheme, which matches the fictitious voltage calculated by each transmission line to identify the branch parameters of the fictitious transmission lines in the first step of the approach. In the second step, the six parameters of the ZIP load model coefficients are identified by matching the simulated power consumes in the fictitious load bus calculated by the ZIP load model with the measured power consumes in the load area derived from the first step of the identification process.

The CTS approach is quite similar to the VTS approach. The whole process has also been organised into two steps. In the first step, the branch parameters of the fictitious transmission lines are identified initially based on the Current-Match scheme. By matching the simulated total current



flow into the load area with the measured current flow into the load area, the scheme identifies the branch parameters in the first step of the approach. In the second step, it applies the same rule as used in the VTS, where the ZIP load model coefficients are identified by matching the simulated power consumes in the fictitious load bus calculated by the ZIP load model with the measured power consumes in the load area derived from the first step of the identification process.

The DOS approach is an extension of the identification STEP2 of the VTS and CTS. The DOS approach uses the Bus-Match scheme to identify all the parameters of the ALAM (branch parameters and ZIP load model coefficients). By matching the simulated values of the bus variables with the measured values of the bus variables from the original power system, all the parameters of the ALAM are identified in one step.

The IEEE-14-Bus power system is employed to illustrate the performances of these three different approaches. Three different operation states of the power system were adopted in the parameter identification process, which is used to enhance the robustness of the identification procedure. A series of verification studies are carried out to test the accuracy of the ALAM identified when varied disturbances are applied to the power system. From the simulation results, it can be seen that DOS gives the most accurate results comparing with the other two approaches. Therefore, in the project, the DOS will be chosen for the ALAM identification in the following studies.

# Chapter 8

## Verification Studies on the ALAM

### 8.1 Introduction

While applying the ALAM method for load modelling in the previous chapters, it is found that ALAM model for different load areas in a power system leads to, sometimes, the results with variations in accuracy. This motivates the verification study on the ALAM method to investigate if the ALAM applying to different load areas in a power system will give the same degree of satisfaction. A large amount of simulation studies to the ALAM have been carried out to achieve the goal of the study which are presented in this chapter. Three different power systems are chosen for this study. They are the IEEE-39-Bus (New England Power System), the IEEE-57-Bus, and the IEEE-118-Bus power system. In each power system, two different load areas have been modelled using the ALAM, and the simulation results are compared to each other. The Direct-One-Step method introduced in Chapter 7 is employed for all the studies in this chapter.

### 8.2 Verification Study of ALAM Based on the IEEE-39-Bus Power System

As shown in Figure 8-1, the IEEE-39-Bus power system consists of ten generators, thirty nine buses, and forty six branches. This power system is also known as the New England power system. Two different load areas, namely Load Area 1 and Load Area 2, are selected to be modelled using the ALAM for this study.



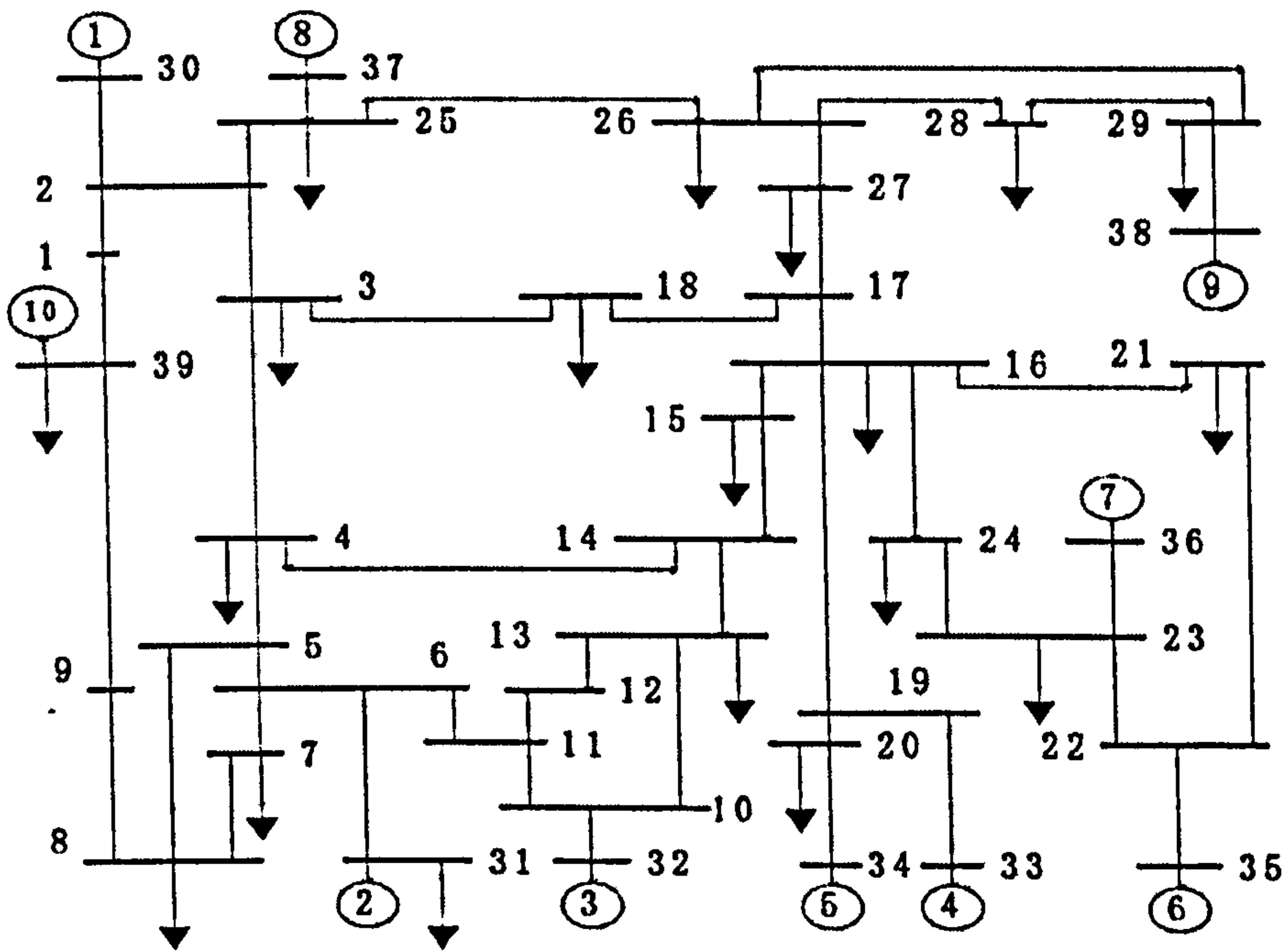


Figure 8-1 IEEE-39 bus power system

The Load Area 1 is composed of load Buses: 14, 15, 16, 17, 18 and 24. The equivalent power system with the aggregated fictitious load bus for the load area is shown in Figure 8-2. In the equivalent power system, the fictitious load bus (bus notation: 40A) is connected with the original power system by seven fictitious transmission lines, which are: Line\_3\_40A, Line\_27\_40A, Line\_21\_40A, Line\_23\_40A, Line\_19\_40A, Line\_13\_40A and Line\_4\_40A. Together with the coefficients of the ZIP load model, there are totally twenty-seven unknown parameters to be identified. The operation states of the power system to identify all these parameters are shown as follows:

- OS1: Normal operation, where all the operating conditions are kept same as the original New-England power system;
- OS2: Normal operation with active power variation, where the active power generated in bus 37 increases by 10% and the active power generated in bus 38 decreases by 5%;
- OS3: Normal operation with variations in voltage, where the terminal



voltage of generator in bus 32 increases by 10% and the tap ratio of the transformer between bus 12 and bus 13 decrease by 5%.

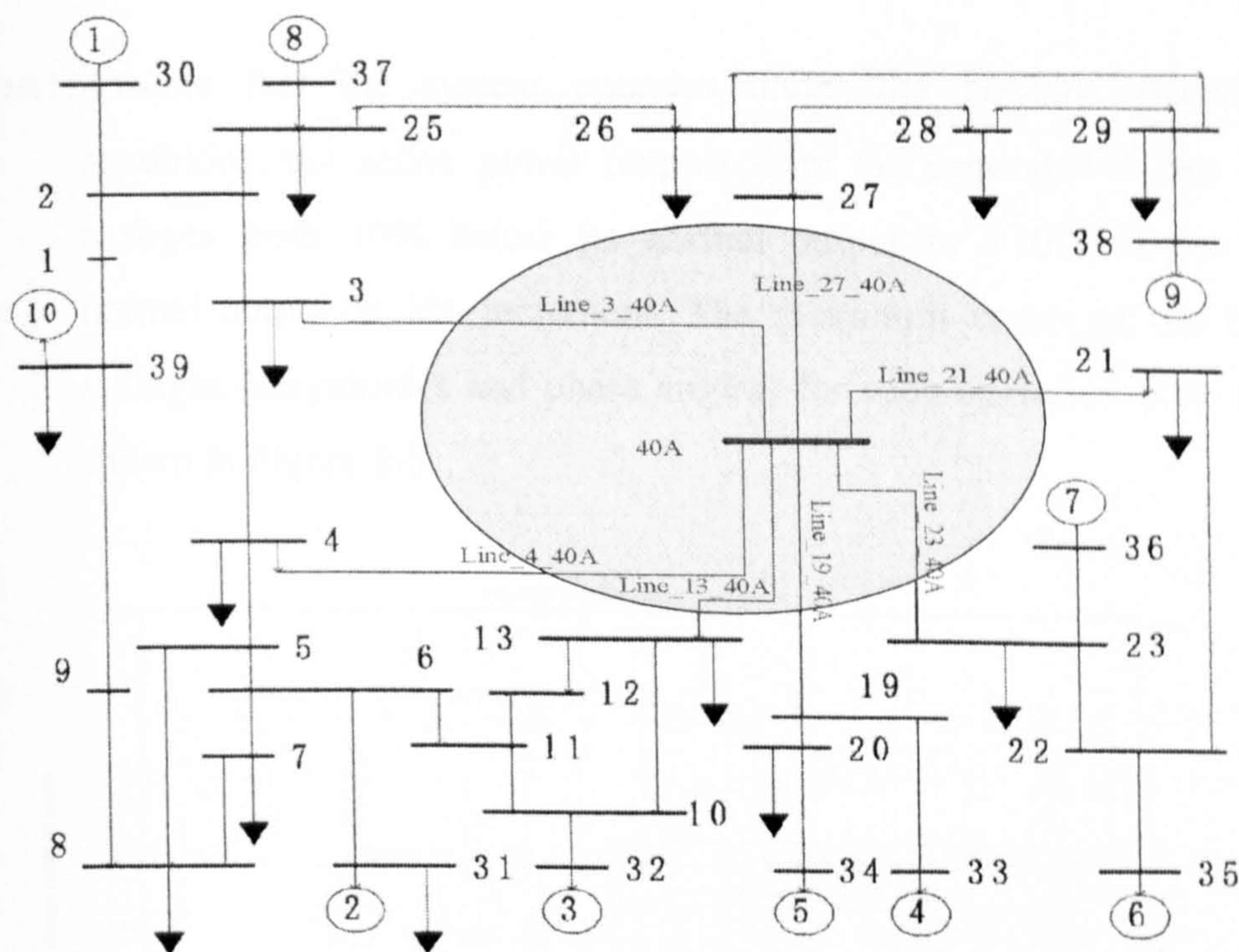


Figure 8-2 Equivalent IEEE-39 bus power system for ALAM of Load Area 1

Following the Direct-One-Step method introduced in Chapter 7, the twenty-seven unknown parameters are identified in Table 8-1.

Table 8-1 The identified parameters for modelling load area 1 in the IEEE-39-Bus power system

$R_{3-40A} = 0.0449 \text{ p.u.}$	$X_{3-40A} = 0.0012 \text{ p.u.}$	$B_{3-40A} = 0 \text{ p.u.}$
$R_{4-40A} = 0.0001 \text{ p.u.}$	$X_{4-40A} = 0.0009 \text{ p.u.}$	$B_{4-40A} = 0 \text{ p.u.}$
$R_{13-40A} = 0.0802 \text{ p.u.}$	$X_{13-40A} = 0.0011 \text{ p.u.}$	$B_{13-40A} = 0 \text{ p.u.}$
$R_{19-40A} = 0.0603 \text{ p.u.}$	$X_{19-40A} = 0.0010 \text{ p.u.}$	$B_{19-40A} = 0 \text{ p.u.}$
$R_{21-40A} = 0.6178 \text{ p.u.}$	$X_{21-40A} = 0.0017 \text{ p.u.}$	$B_{21-40A} = 0 \text{ p.u.}$
$R_{23-40A} = 0.0445 \text{ p.u.}$	$X_{23-40A} = 0.0008 \text{ p.u.}$	$B_{23-40A} = 0.0001 \text{ p.u.}$
$R_{27-40A} = 0.0001 \text{ p.u.}$	$X_{27-40A} = 0.5141 \text{ p.u.}$	$B_{27-40A} = 0 \text{ p.u.}$
$a_{f1} = 0.9274$	$a_{f2} = 0.9970$	$a_{f3} = 3.9871$
$a_{f4} = 0.9431$	$a_{f5} = 0.9786$	$a_{f6} = 3.9901$



Three tests are carried out to test the equivalent IEEE-39-Bus power system to study whether the ALAM can represent the area load under the varied operation states.

Test1: Assume that the system operates under the normal operating conditions, but active power outputs from the generator in bus 37 changes from 10% below its normal output to +10% above its normal output in 1% increment. The maximum errors of the bus voltages (magnitudes and phase angles) for each operation state are shown in Figure 8-3.

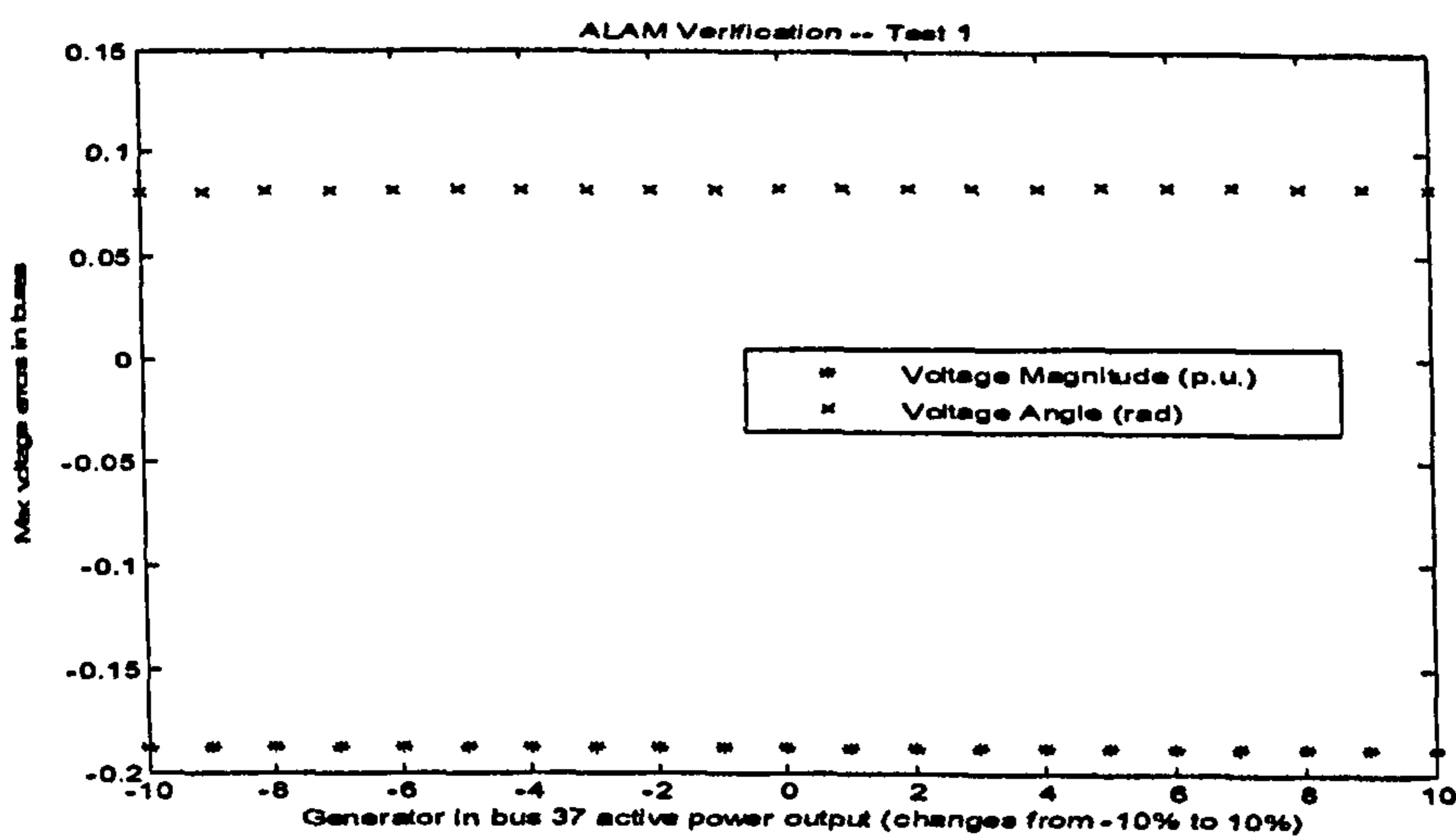


Figure 8-3 Maximum errors of the bus voltages in each operation state while changing the active power output of bus 37 from -10% to 10%

Test2: Assume that the system operates in normal conditions, but the tap ratio of the transformer between bus 12 and bus 13 changes from 10% below its normal output and 10% above its normal value in 1% increment. The maximum errors of the bus voltages (magnitudes and phase angles) for each operation state are shown in Figure 8-4.

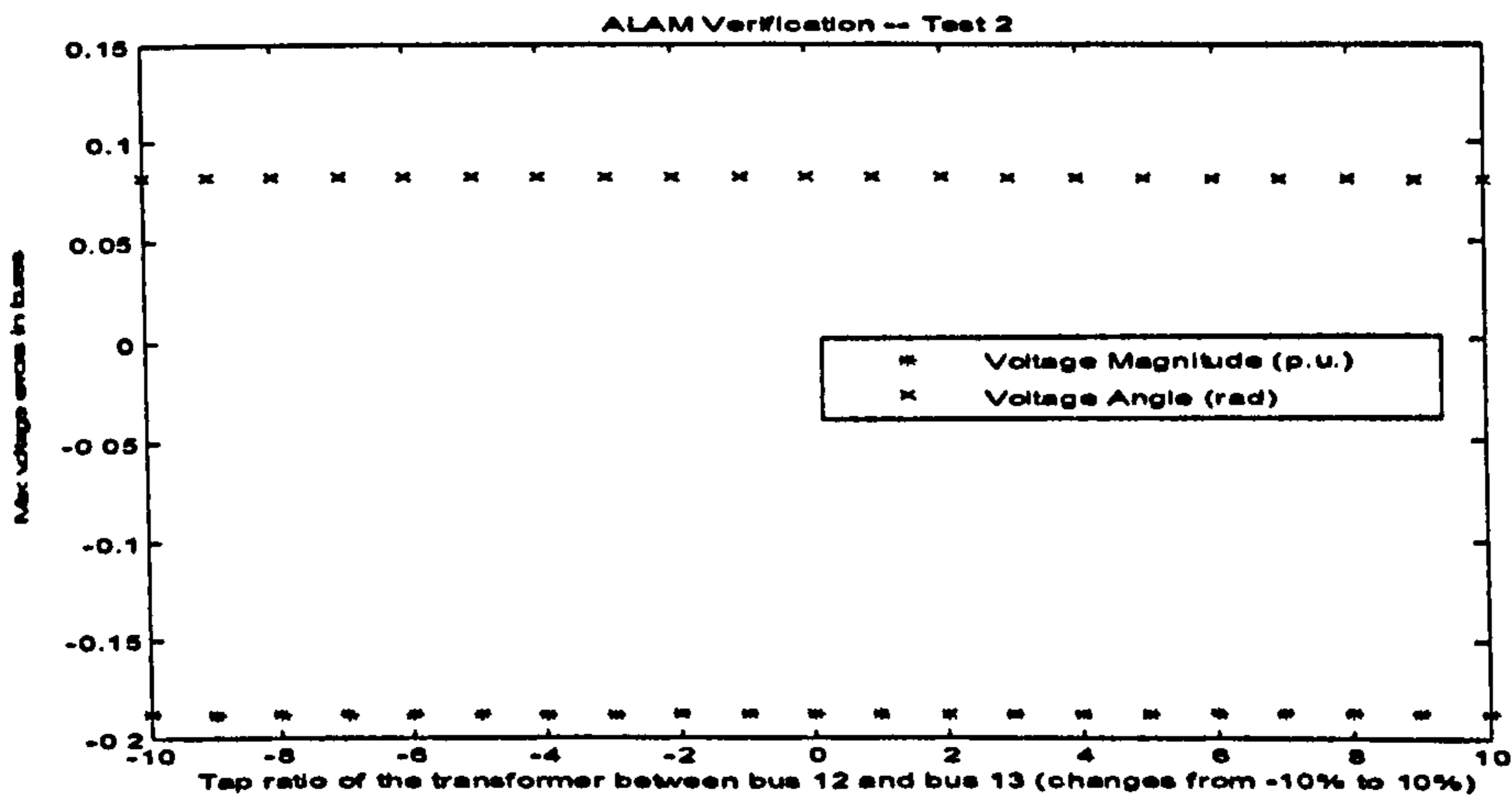


Figure 8-4 Maximum errors of the bus voltages in each operation state while changing tap ratio between bus 12 and bus 13 from 10% below to 10% above its normal operation value

Test 3: Assume that the system operates with the normal operating conditions, but the value of voltage outputs from generator in bus 32 changes from 10% below to 10% above its normal output in 1% increment. The maximum errors of the bus voltages (magnitudes and phase angles) for each operation state are shown in Figure 8-5.

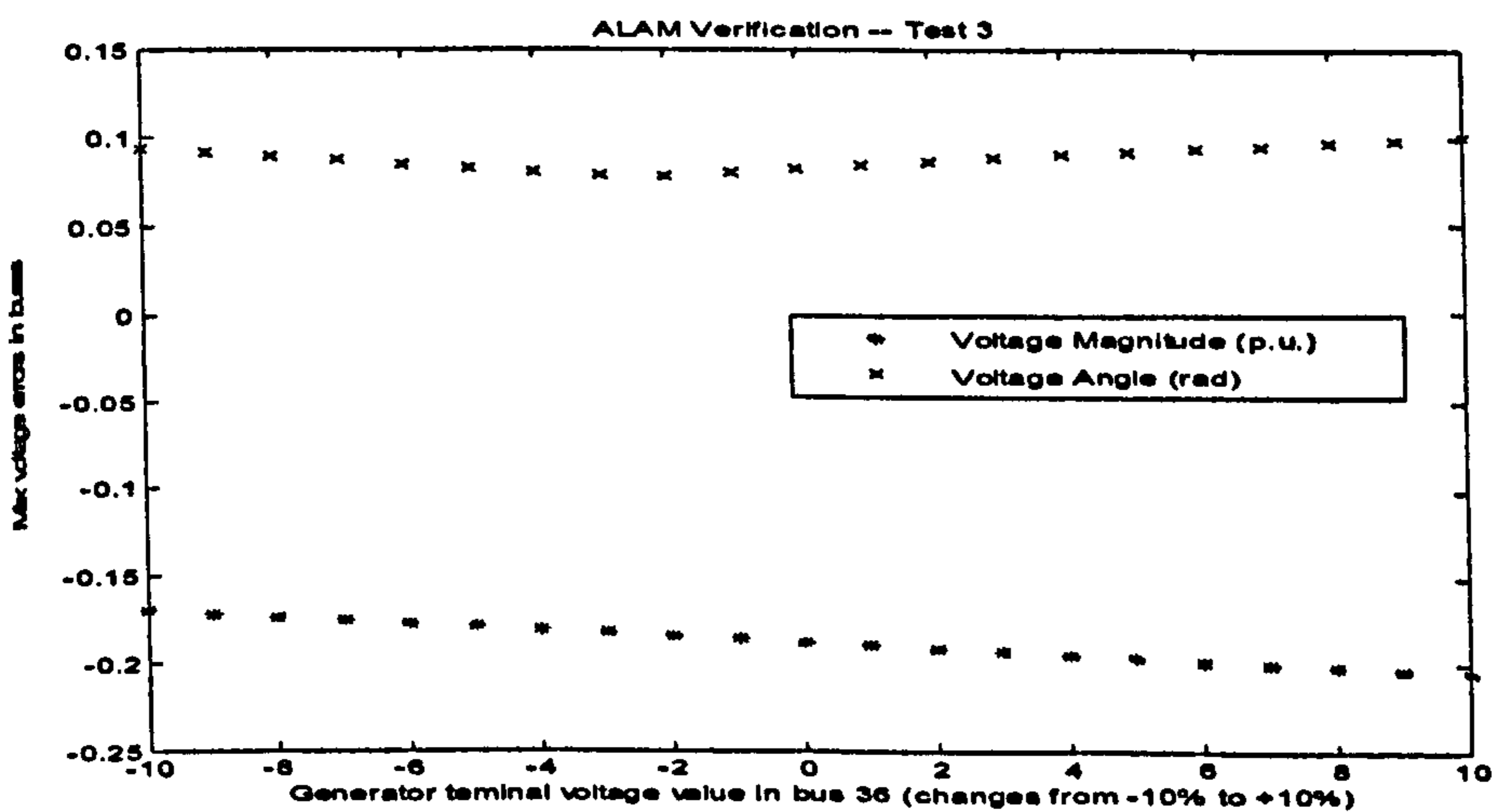


Figure 8-5 Maximum errors of the bus voltages in each operation state while changing the voltage outputs in bus 32 from 10% below to 10% above its normal output



The Load Area 2 is composed of the load Buses: 26, 27, 28 and 29. The equivalent power system embedded aggregated fictitious load bus for the Load Area 2 is shown in Figure 8-6.

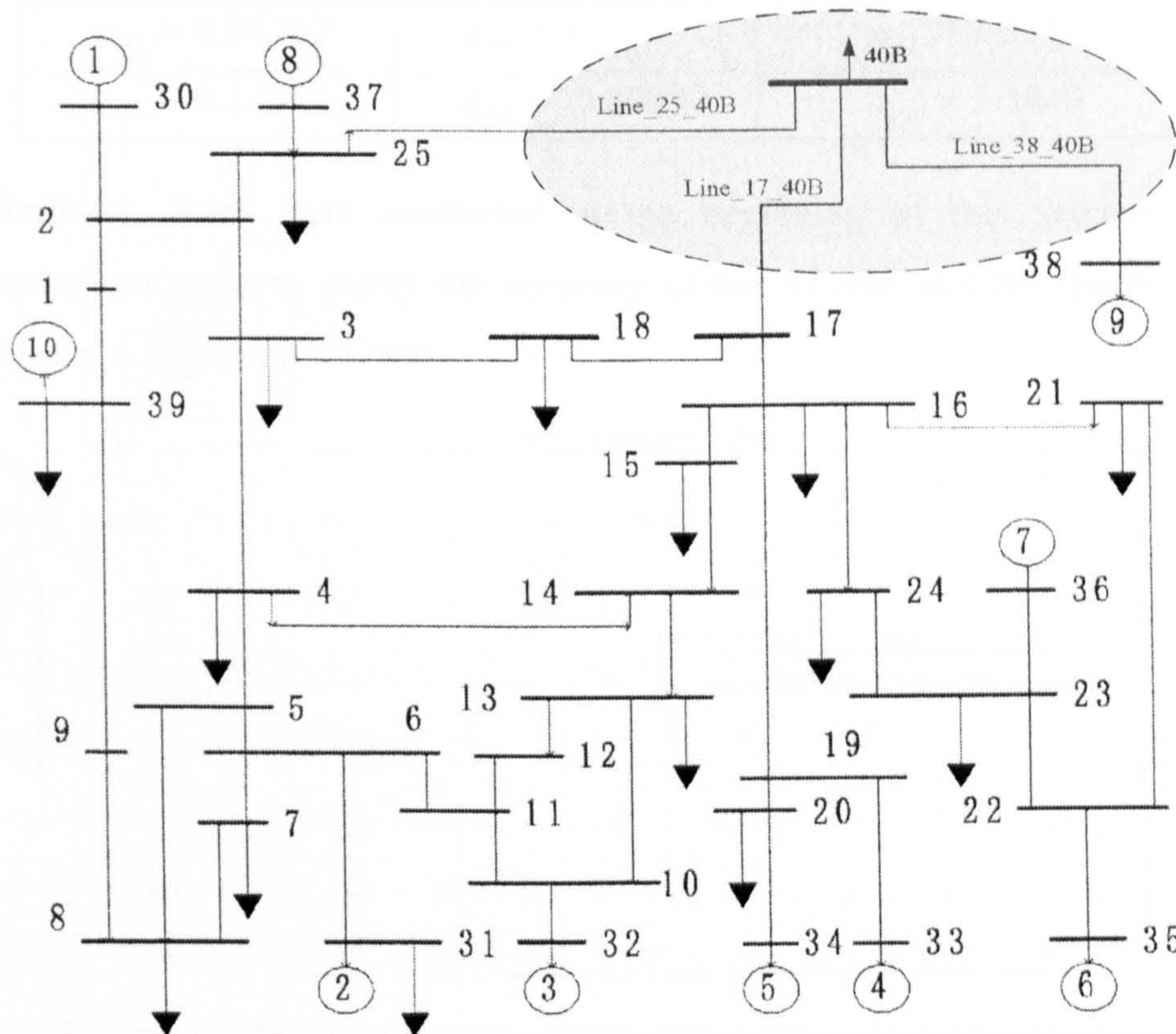


Figure 8-6 Equivalent IEEE-39-Bus power system for ALAM of Load Area 2

In the equivalent power system, the fictitious load bus (bus notation: 40B) is connected with the original power system by three fictitious transmission lines, which are: Line\_17\_40B, Line\_25\_40B, Line\_38\_40B. Together with the parameters of the ZIP load model coefficients, there are totally fifteen unknown parameters to be identified. The operation states introduced above are repeated to identify all these unknown parameters using the Direct-One-Step method. The identified results are given in Table 8-2.

Table 8-2 The identified parameters for modelling load area 2 in the IEEE-39 bus power system

$R_{17-40} = 0.3953 \text{ p.u.}$	$X_{17-40} = 0.6687 \text{ p.u.}$	$B_{17-40} = 0.0147 \text{ p.u.}$
$R_{25-40} = 0.4516 \text{ p.u.}$	$X_{25-40} = 0.3364 \text{ p.u.}$	$B_{25-40} = 0.0148 \text{ p.u.}$
$R_{38-40} = 0.0603 \text{ p.u.}$	$X_{38-40} = 0.0010 \text{ p.u.}$	$B_{38-40} = 0.0145 \text{ p.u.}$
$a_{f1} = 0.91767$	$a_{f2} = 1$	$a_{f3} = 3.6371$
$a_{f4} = 0.2125$	$a_{f5} = -0.49999$	$a_{f6} = 1.3449$

Similarly, three tests conducted at the beginning of this section are performed again to verify the accuracy of the ALAM and the results are shown in Figures 8-7 ~ 8-9.

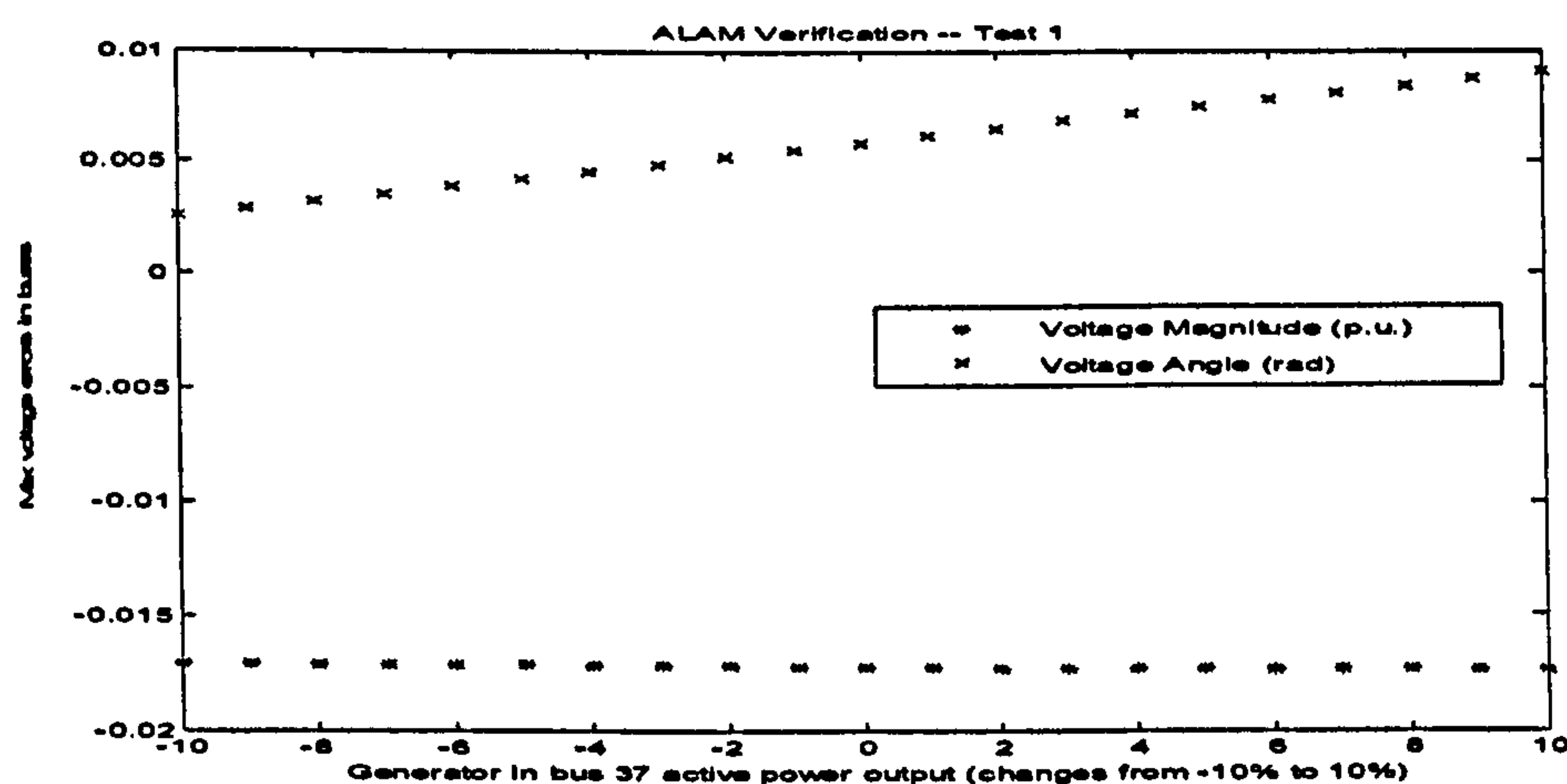


Figure 8-7 Maximum errors of the bus voltages in each operation state while changing the active power output of bus 37 from 10% below to 10% above its normal operation value

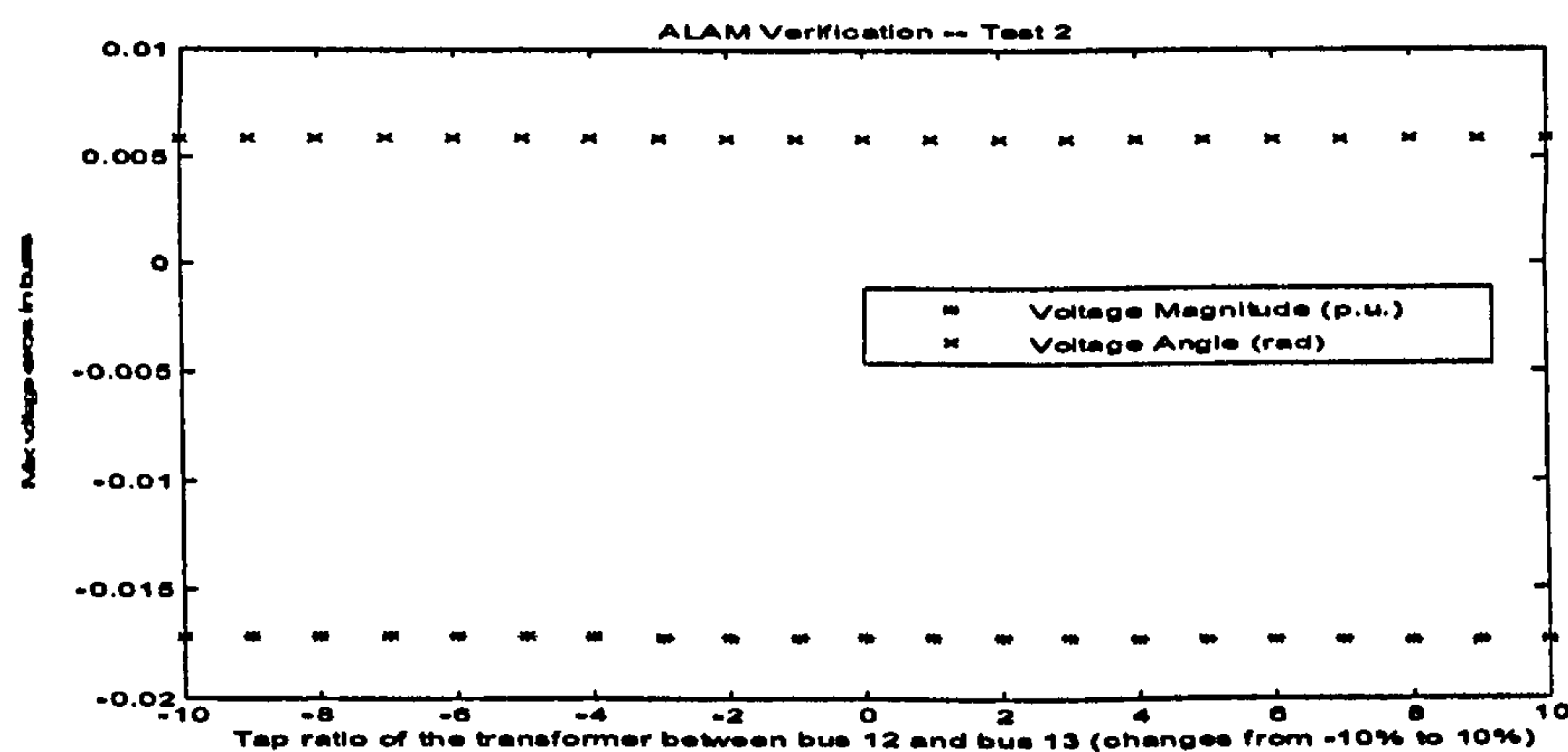


Figure 8-8 Maximum errors of the bus voltages in each operation state while changing tap ratio between bus 12 and bus 13 from 10% below to 10% above its normal operation value



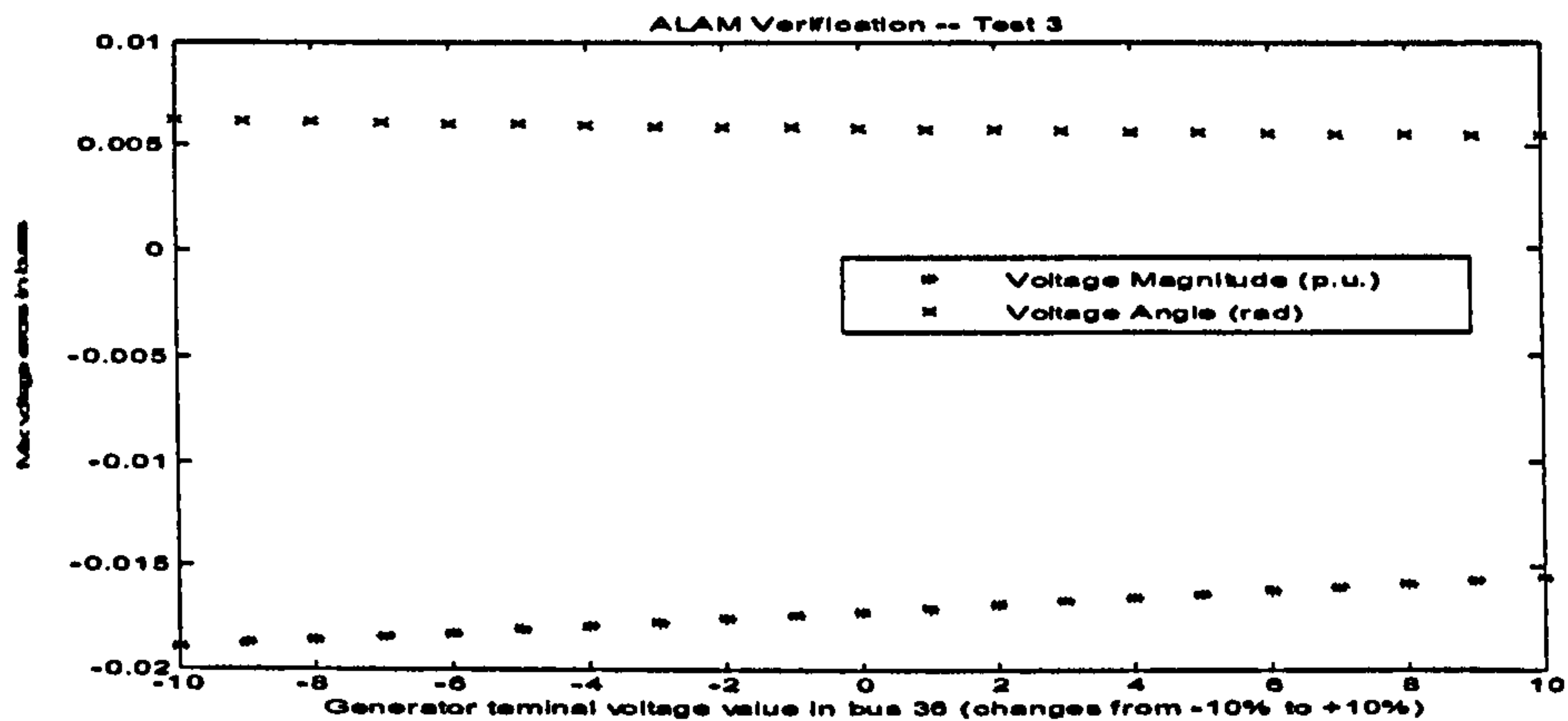


Figure 8-9 Maximum errors of the bus voltages in each operation state while changing the voltage outputs in bus 32 from 10% below to 10% above its normal operation value

Comparing the results of the ALAM obtained from the two different load areas, it can be seen that the results are not very consistent, that is, not all the load areas can give the same degree of satisfactions while the ALAM method is applied. The Load Area 1 composes of six load buses and contains twenty seven parameters to be identified. The Load Area 2 composes of four load buses, and contains fifteen parameters to be identified. From the results, the ALAM for Load Area 2 gives more accurate results than those given by the ALAM for Load Area 1.

### 8.3 Verification Study of ALAM Based on the IEEE-57-Bus Power System

As shown in Figure 8-10, the IEEE-57-Bus power system consists of four generators, fifty seven buses, and eighty branches. Similar to Section 8.2, two different load areas, namely Load Area I and Load Area II, are selected to be modelled using the ALAM for this study.

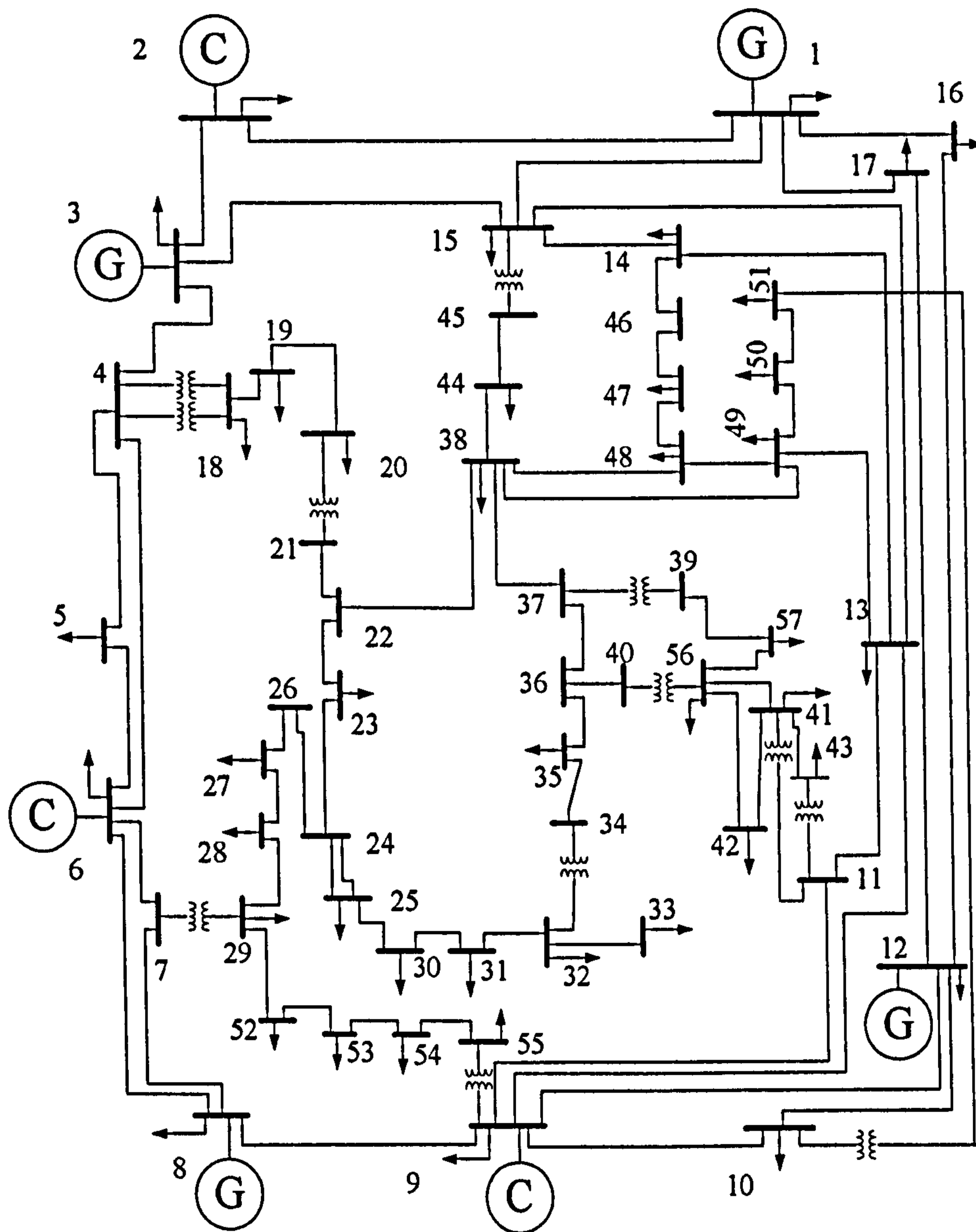


Figure 8-10 The original IEEE 57-bus power system

The Load Area I composes of the load Buses: 14, 46, 47, 48, 49, 50 and 51. The equivalent power system with the aggregated fictitious load bus for the load area is shown in Figure 8-11. In the equivalent power system, the fictitious load bus (bus notation: 58A) is connected with the original power system by four fictitious transmission lines, which are: Line\_10\_58A, Line\_13\_58A, Line\_15\_58A and Line\_38\_58A. Together with the coefficients of the ZIP load model,



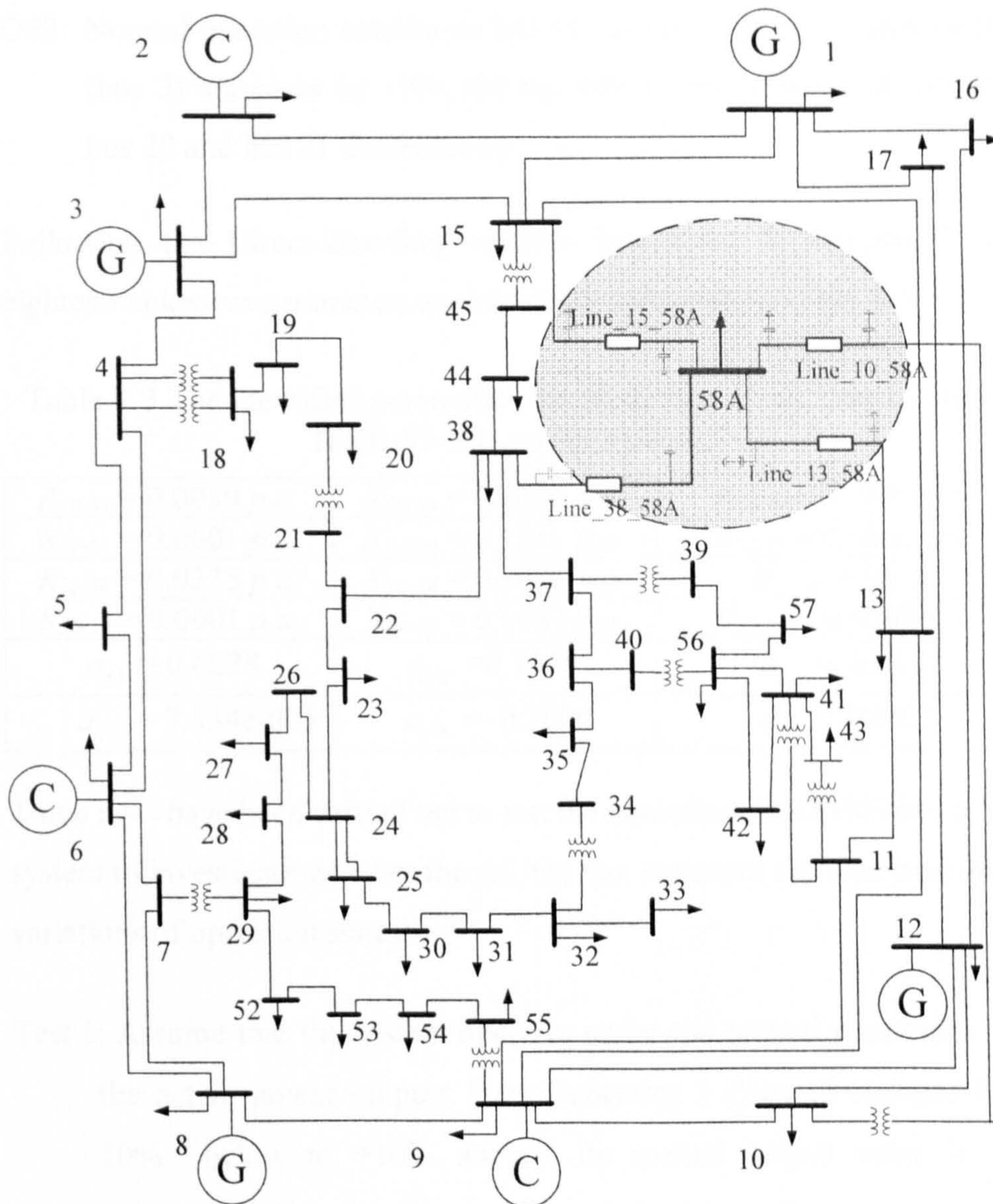


Figure 8-11 Equivalent IEEE-57-Bus power system for aggregating load area 1

there are totally eighteen unknown parameters to be identified. The operation states of the power system discussed in identifying all these parameters are listed as follows:

- OS1: Normal operation conditions, where all the bus variables are kept in the same as the original IEEE-57-Bus power system;
- OS2: Normal operation conditions, but the active power generated in bus 1 increases by 10%, the active power generated in bus 8 decreases by 5%.



OS3: Normal operation conditions but the terminal voltage of generator 3 (bus 3) increases by 10%, the tap ratio of the transformer between bus 20 and bus 21 decreases by 5%.

Following the Direct-One-Step method introduced in Chapter 7, the eighteen unknown parameters are identified and listed in Table 8-3.

Table 8-3 The identified parameters for modelling Load Area I in the IEEE-57-Bus power system

$R_{10-58} = 0.0089 \text{ p.u.}$	$X_{10-58} = 0.0060 \text{ p.u.}$	$B_{10-58} = 0.0099 \text{ p.u.}$
$R_{13-58} = 0.0001 \text{ p.u.}$	$X_{13-58} = 0.1641 \text{ p.u.}$	$B_{13-58} = 0.0001 \text{ p.u.}$
$R_{15-58} = 0.0335 \text{ p.u.}$	$X_{15-58} = 0.1078 \text{ p.u.}$	$B_{15-58} = 0 \text{ p.u.}$
$R_{38-58} = 0.0001 \text{ p.u.}$	$X_{38-58} = 0.1083 \text{ p.u.}$	$B_{38-58} = 0.0149 \text{ p.u.}$
$a_{f1} = 0.6228$	$a_{f2} = 0.1368$	$a_{f3} = 0.1432$
$a_{f4} = 7.534\text{e-}005$	$a_{f5} = -0.5000$	$a_{f6} = 0.0622$

Three tests have been carried out to test the equivalent IEEE-57-Bus power system to investigate whether the ALAM can represent the area load under variations of operation states:

Test 1: Assume that the system operates under the normal conditions, but the active power outputs from Generator 1 (Bus 1) changes from 10% below to +10% above its normal output value in 1% increment.. The maximum errors of the bus voltages (magnitudes and phase angles) in each operation state are shown in Figure 8-12.



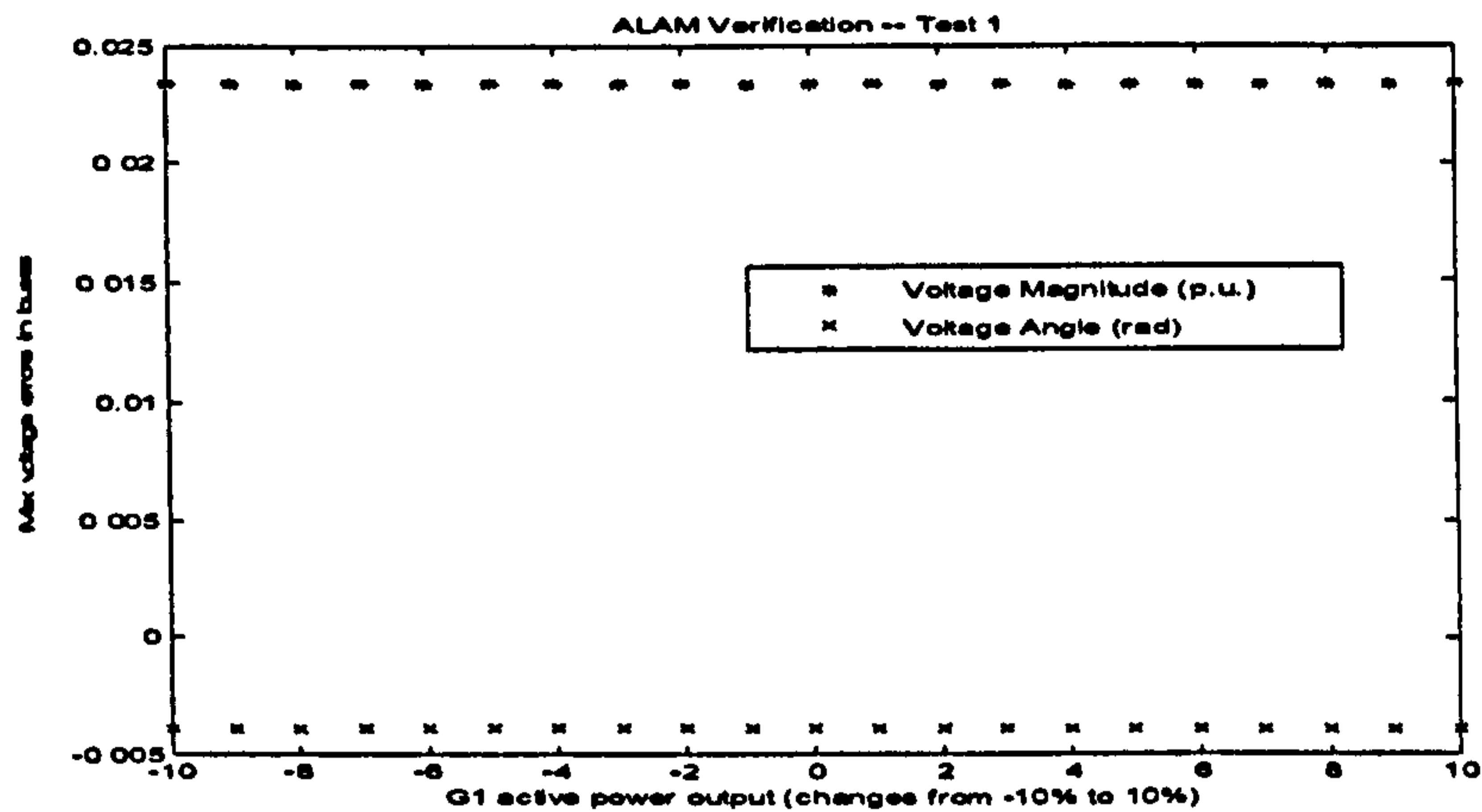


Figure 8-12 Maximum errors of the bus voltages in each operation state while changing the active power output of bus 1 from -10% to 10%

Test 2: Assume that the system operates under the normal conditions, but the tap ratio of the transformer between Bus 20 and Bus 21 change from 10% below to +10% above its normal operation value in 1% increment. The maximum errors of the bus voltages (magnitudes and phase angles) for each operation state are shown in Figure 8-13.

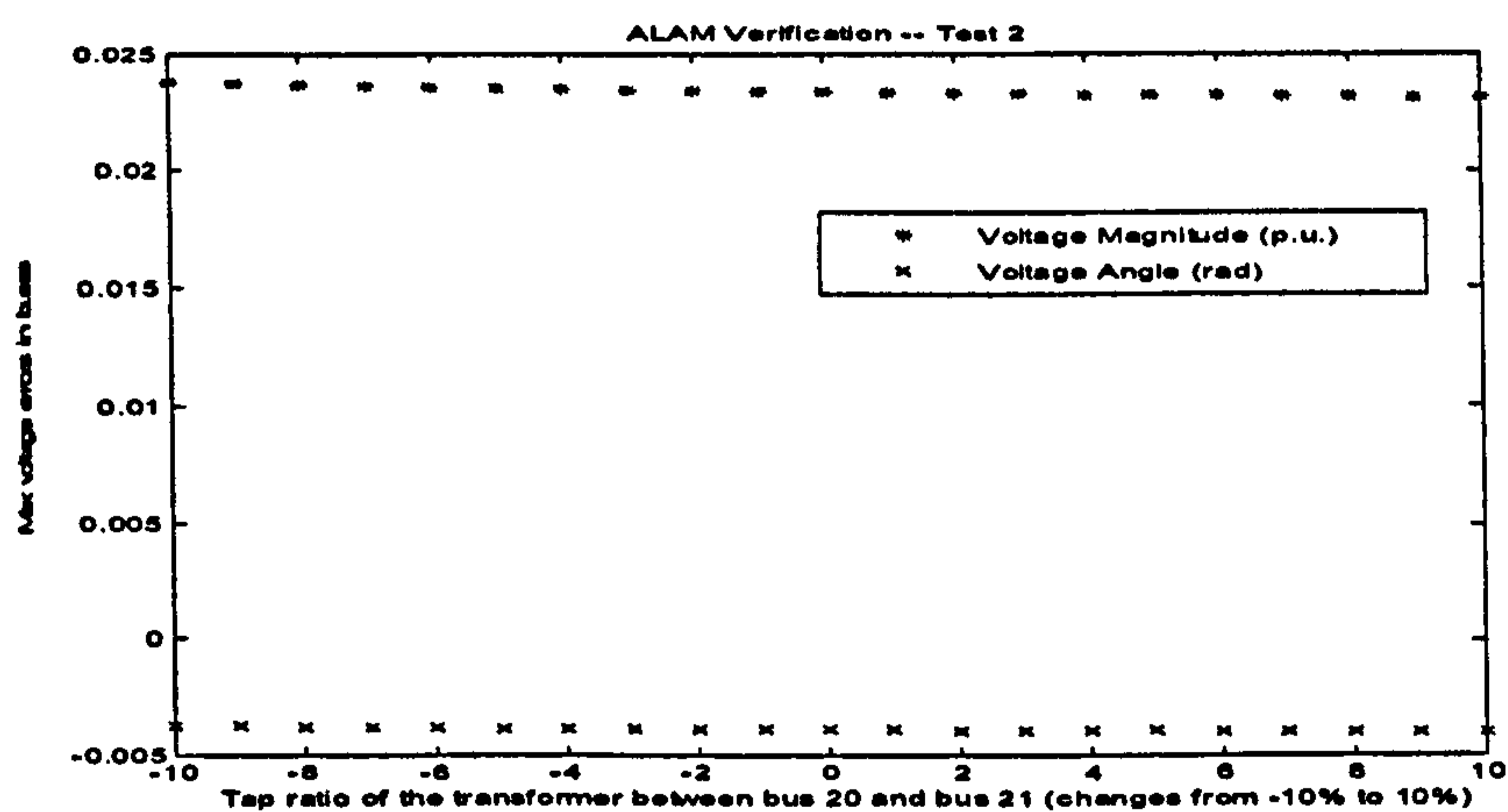


Figure 8-13 Maximum errors of the bus voltages in each operation state while changing tap ratio between bus 20 and bus 21 from 10% below to 10% above its normal operation value

Test 3: Assume that the system operates under the normal operating conditions, but The values of the voltage outputs from Generator 3 (Bus 3) changes from 10% below to +10% above its normal output

in 1% increment. The maximum errors of the bus voltages (magnitudes and phase angles) for each operation state are shown in Figure 8-14.

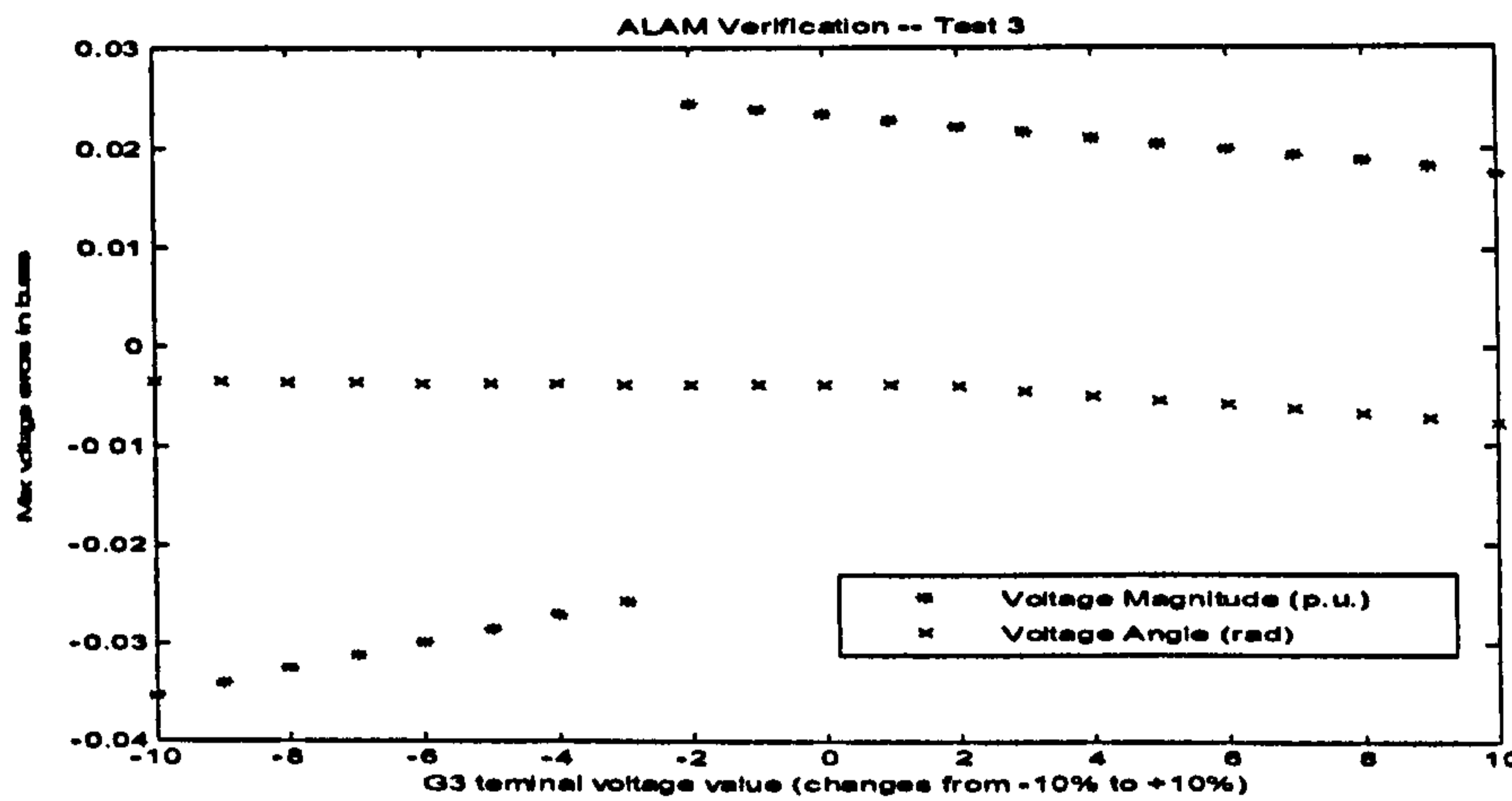


Figure 8-14 Maximum errors of the bus voltages in each operation state while changing the voltage outputs in bus 3 from 10% below to 10% above its normal output

The Load Area II is composed of load Buses: 23, 24, 25, 26, 27, 28, 30 and 31. The equivalent power system with the fictitious load bus for the aggregated load area is shown in Figure 8-15. For the equivalent power system, the fictitious load bus (bus notation: 58B) is connected to the original power system by three fictitious transmission lines, which are: Line\_22\_58B, Line\_29\_58B, Line\_32\_58B. Including the parameters of the ALAM, there are total fifteen unknown parameters to be identified. The operation states studied in the previous section are repeated here and all these unknown parameters are identified using the Direct-One-Step method. The identified results are given in Table 8-4.



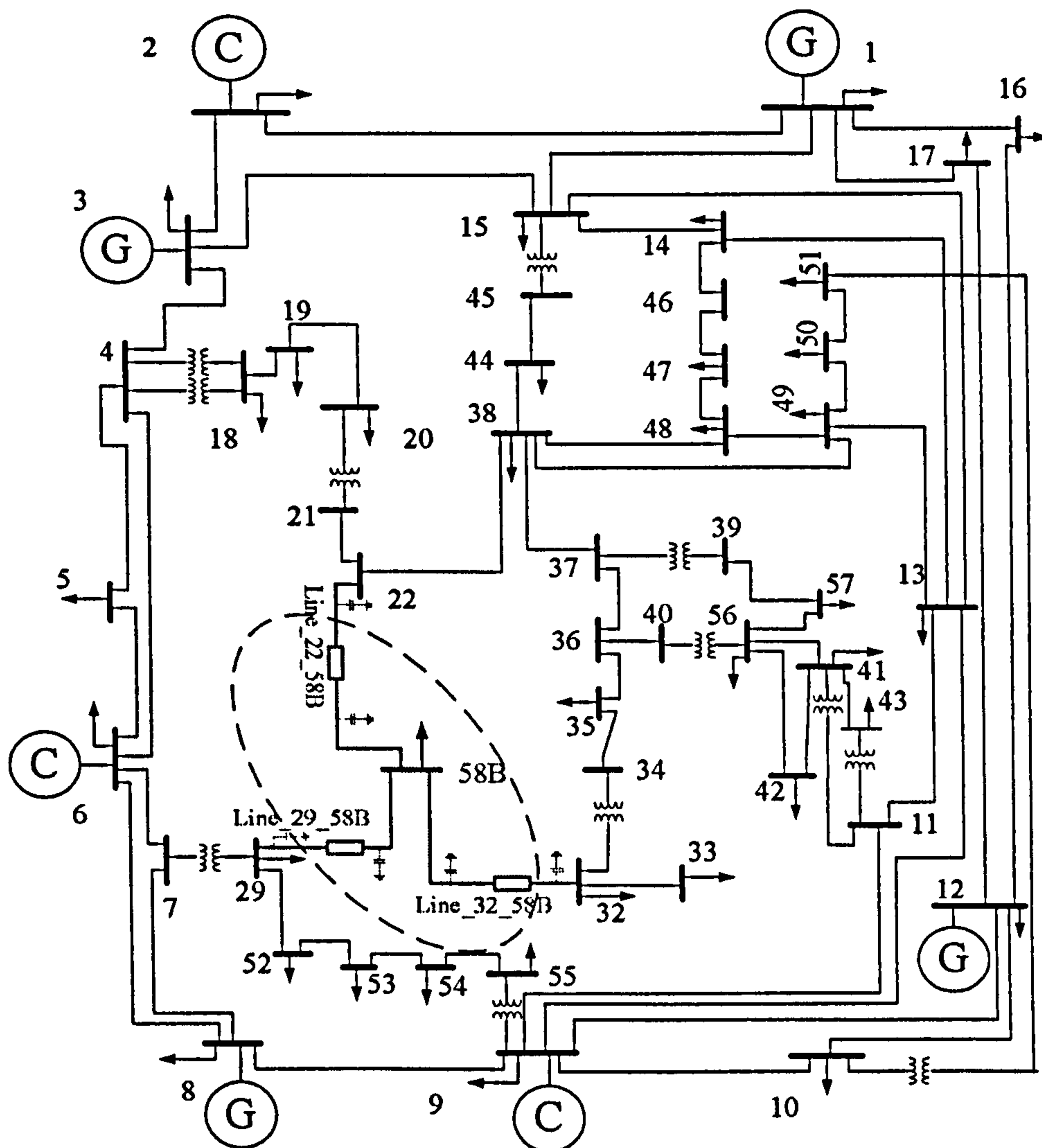


Figure 8-15 Equivalent IEEE-57-Bus power system for aggregating load area 2

Table 8-4 The identified parameters for modelling load area 2 in the IEEE-57-Bus power system

$R_{22-58} = 0.7000 \text{ p.u.}$	$X_{22-58} = 0.9000 \text{ p.u.}$	$B_{22-58} = 0 \text{ p.u.}$
$R_{29-58} = 0.2747 \text{ p.u.}$	$X_{29-58} = 0.5715 \text{ p.u.}$	$B_{29-58} = 0 \text{ p.u.}$
$R_{32-58} = 0.6008 \text{ p.u.}$	$X_{32-58} = 0.0011 \text{ p.u.}$	$B_{32-58} = 0.0092 \text{ p.u.}$
$a_{f1} = 0.22613$	$a_{f2} = -0.38416$	$a_{f3} = 0.50651$
$a_{f4} = 0.32882$	$a_{f5} = -0.32539$	$a_{f6} = 0.029648$

Similarly, the three test studies performed in the previous section are conducted again to investigate the accuracy of the ALAM and the results are shown in Figures 8-16 ~ 8-18.

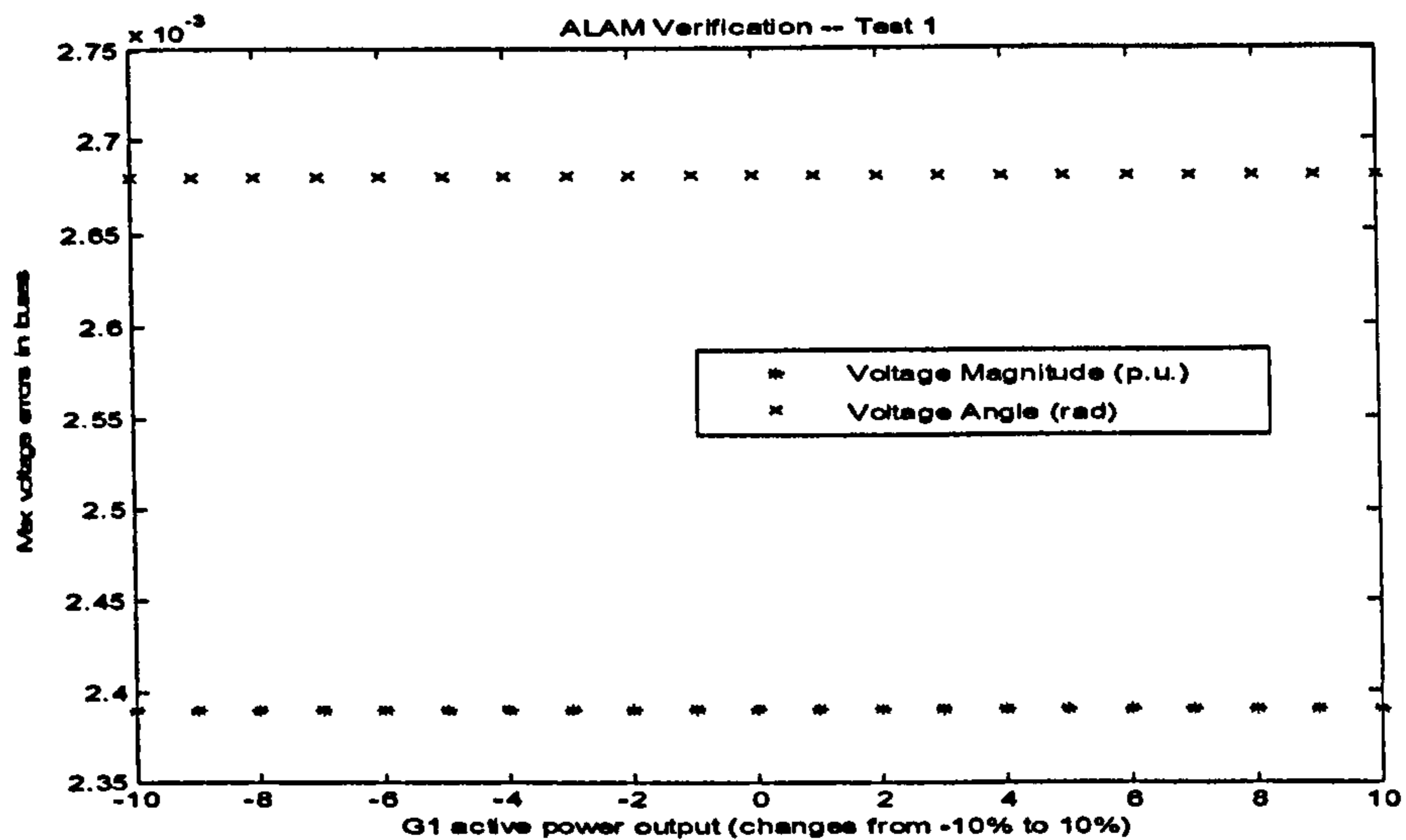


Figure 8-16 Maximum errors of the bus voltages in each operation state while changing the active power output of bus 1 from 10% below to 10% above its normal operation value

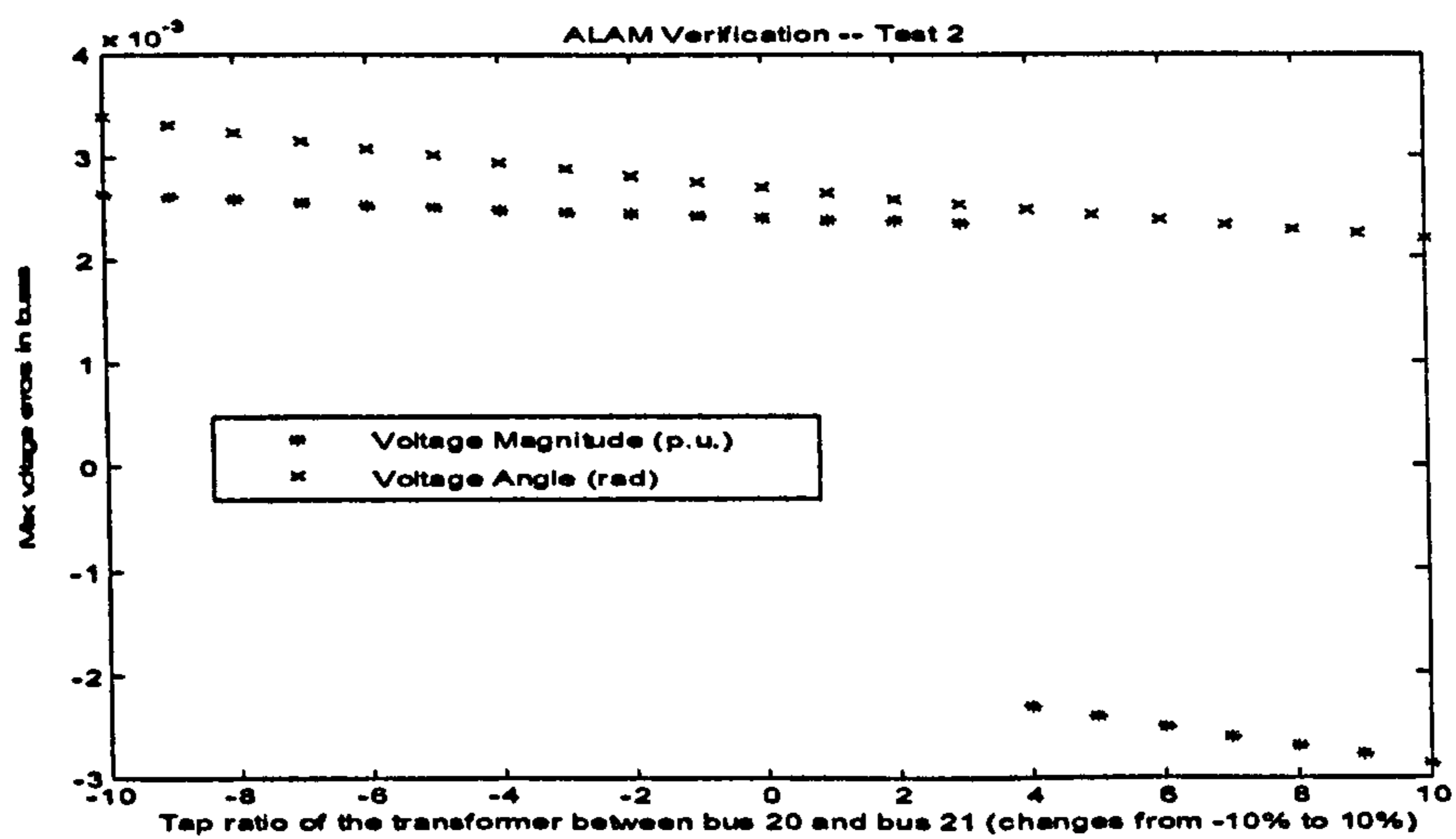


Figure 8-17 Maximum errors of the bus voltages in each operation state while changing tap ratio between bus 20 and bus 21 from 10% below to 10% above its normal operation value



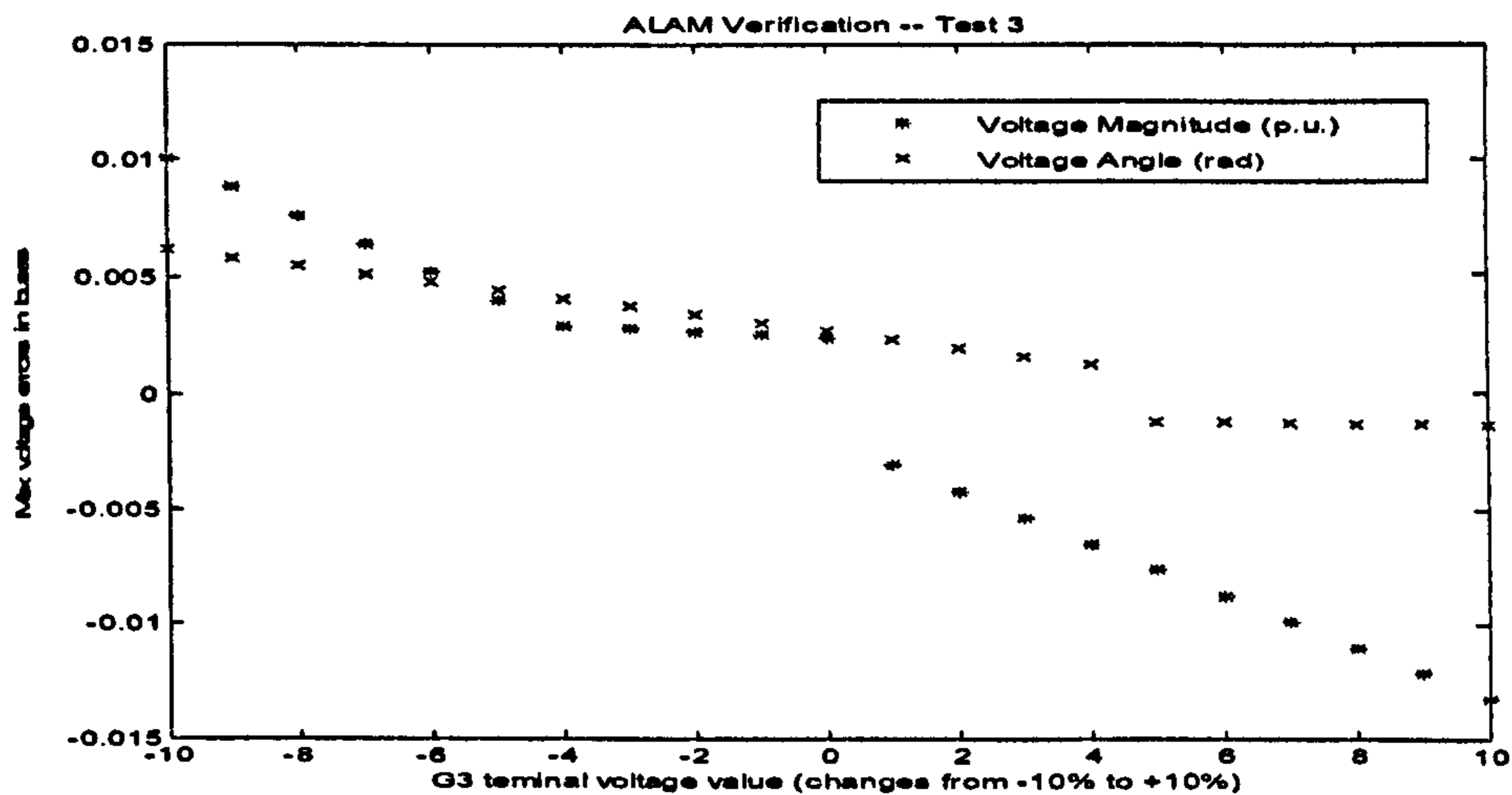


Figure 8-18 Maximum errors of the bus voltages in each operation state while changing the voltage outputs in bus 3 from 10% below to 10% above its normal operation value

Comparing the results of the ALAM obtained from the two different load areas, it can be seen that the results are not very consistent, that is, not all the load areas can give the same degree of satisfactions while the ALAM method is applied. The Load Area I composes of six load buses, and contains eighteen parameters to be identified. The Load Area II consists of eight load buses and contains fifteen parameters to be identified. From the results, the ALAM of Load Area II gives more accurate results than those given by the ALAM of Load Area I.

#### 8.4 Verification Study of ALAM Based on the IEEE-118-Bus Power System

As shown in Figure 8-19, the IEEE-118-Bus power system consists of fifty four generators, one hundred and eighteen buses, and one hundred and eighty six branches. Similar to the previous section, two different load areas, namely Load Area A and Load Area B, are selected to be modelled by the ALAM method for investigations.

The Load Area A consists of the Buses: 93, 94, 95, 96 and 97. The equivalent power system with fictitious load bus for the aggregated load area is shown in Figure 8-20 with the enlarged area. For the equivalent power system, the fictitious load bus (bus notation: 119A) is connected with the original power system by four fictitious transmission lines, which are: Line\_80\_119A, Line\_82\_119A, Line\_92\_119A and Line\_100\_119A. Together with the coefficients of the ZIP load model, there are eighteen unknown parameters to be identified. The operation states of the power system are shown as follows under which the parameters will be identified.

- OS1: Normal operation, where all the bus variables are kept same as those for the original IEEE-118-Bus power system;
- OS2: Normal operation conditions, but the active power generated in Bus 69 increases 10% and the active power generated in Bus 59 decreases by 5%.
- OS3: Normal operation conditions, but the terminal voltage of Generator 1 (bus 1) increases 10% and the tap ratio of the transformer between Bus 65 and Bus 66 decrease by 5%.



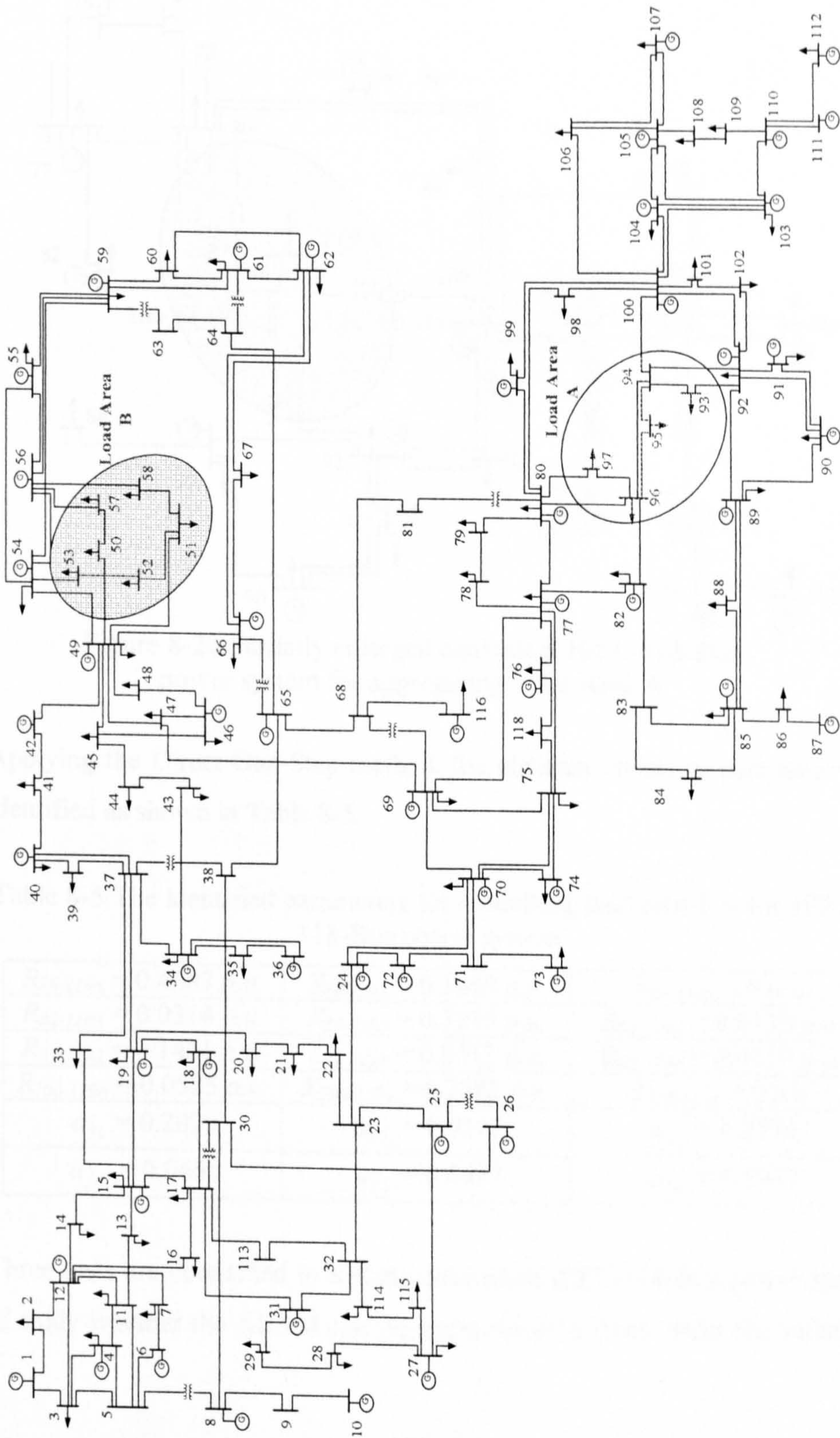


Figure 8-19 The IEEE 118-bus power system with the two load areas, Load Area A and Load Area B



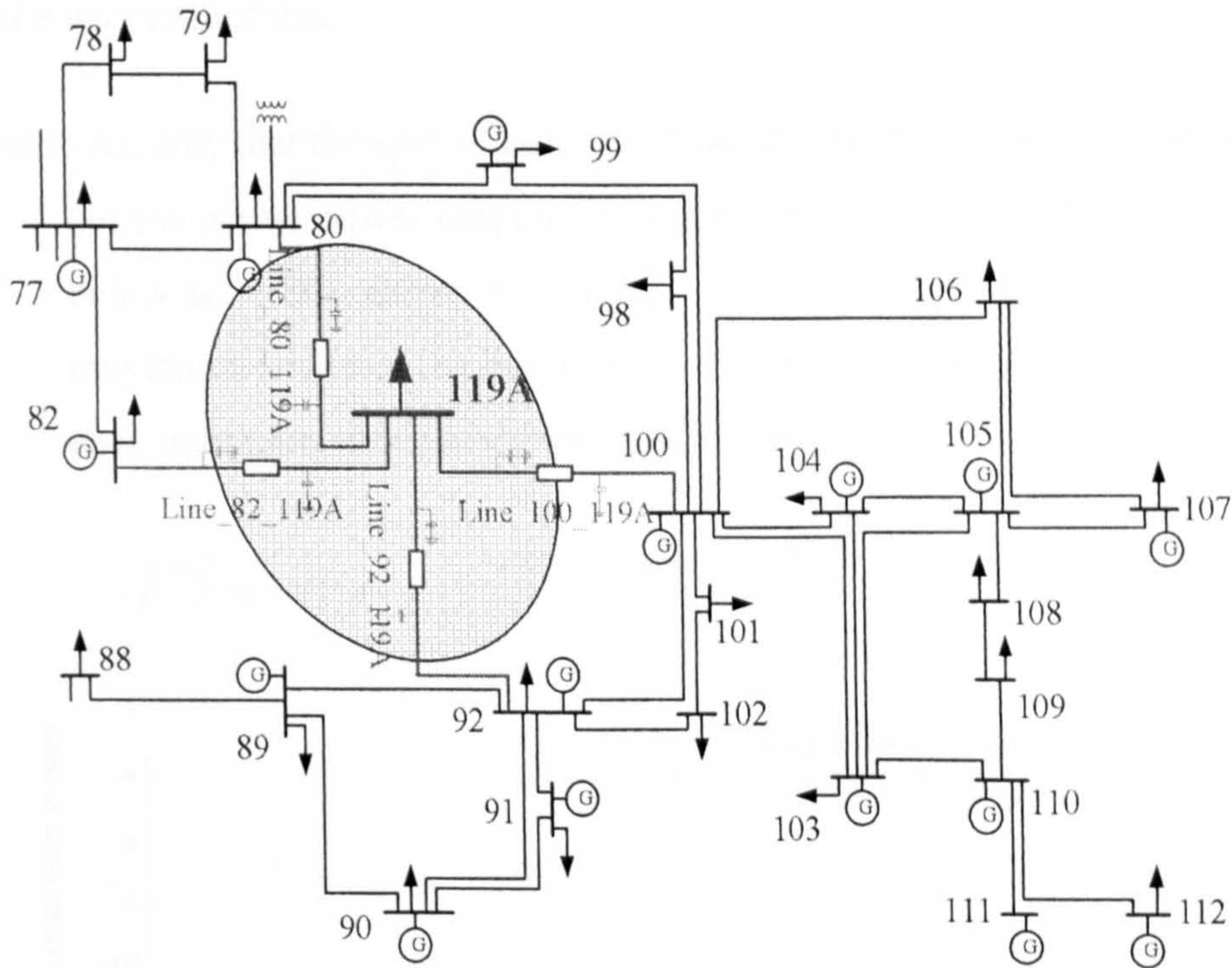


Figure 8-20 Partially enlarged equivalent IEEE-118-Bus power system for aggregating Load Area A

Applying the Direct-One-Step method, the eighteen unknown parameters are identified as shown in Table 8-5.

Table 8-5 The identified parameters for modelling load area 1 in the IEEE-118-Bus power system

$R_{80-119A} = 0.4087 \text{ p.u.}$	$X_{80-119A} = 0.1860 \text{ p.u.}$	$B_{80-119A} = 0 \text{ p.u.}$
$R_{82-119A} = 0.0314 \text{ p.u.}$	$X_{82-119A} = 0.7235 \text{ p.u.}$	$B_{82-119A} = 0.0130 \text{ p.u.}$
$R_{92-119A} = 0.1461 \text{ p.u.}$	$X_{92-119A} = 0.0513 \text{ p.u.}$	$B_{92-119A} = 0.0152 \text{ p.u.}$
$R_{100-119A} = 0.0525 \text{ p.u.}$	$X_{100-119A} = 0.7282 \text{ p.u.}$	$B_{100-119A} = 0 \text{ p.u.}$
$a_{f1} = 0.2023$	$a_{f2} = 0.0317$	$a_{f3} = 0.9774$
$a_{f4} = 0.0666$	$a_{f5} = 0.4697$	$a_{f6} = 0.1937$

Three tests are conducted to test the equivalent IEEE-118-Bus power system to study whether the ALAM can represent the area loads under the variations



of the operation states:

Test 1: Assume that the system operates under its normal operating conditions, but the active power outputs from generator bus 37 changes from 10% below to +10% above its normal output value in 1% increment. The maximum errors of the bus voltages (magnitudes and phase angles) for each operation state are shown in Figure 8-21.

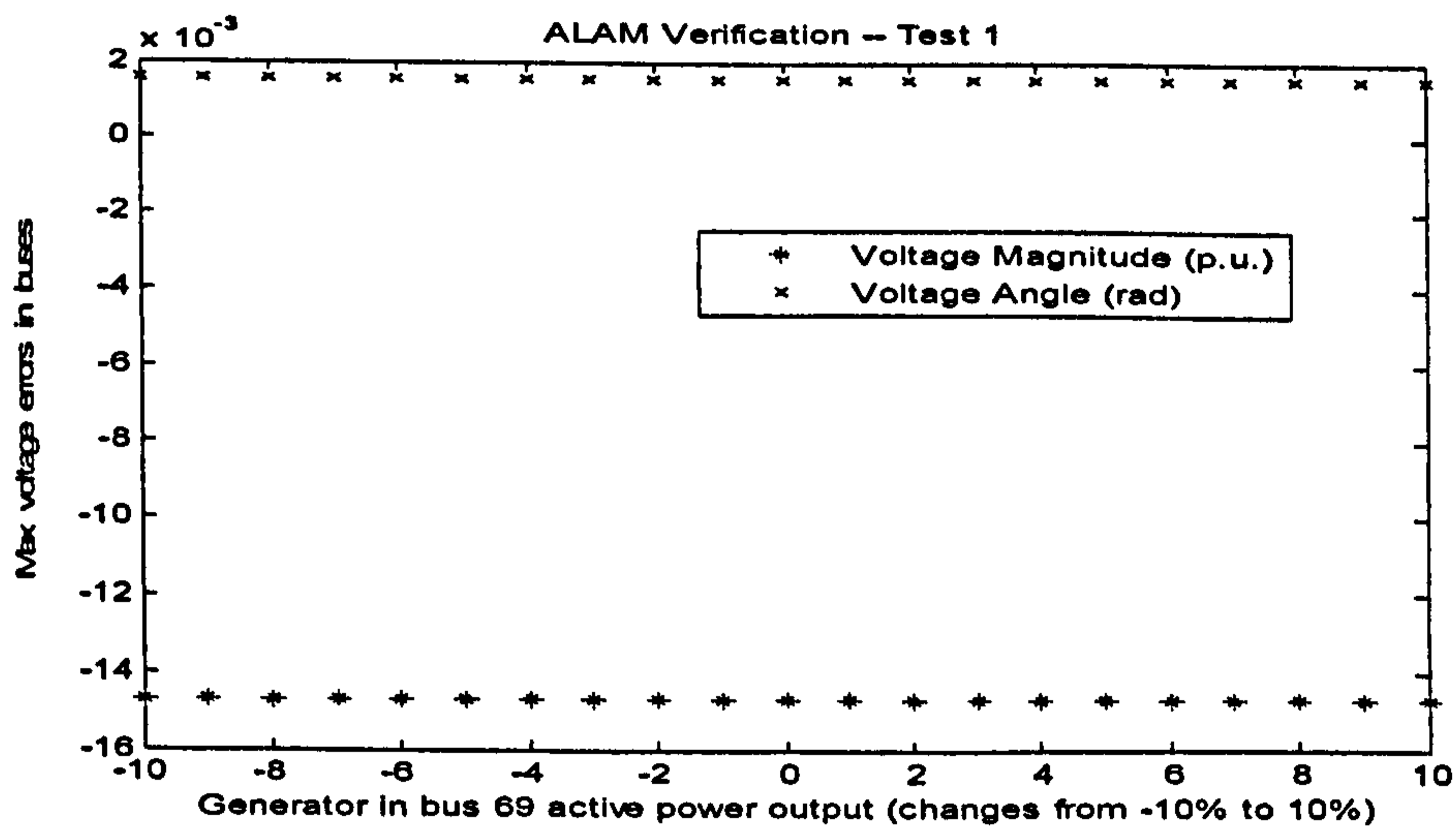


Figure 8-21 Maximum errors of the bus voltages in each operation state while changing the active power output of bus 69 from -10% to 10%

Test 2: Assume that the system operates in normal conditions, but the tap ratio of the transformer between bus 65 and bus 66 change from 10% below to +10% above its normal value in 1% increment. The maximum errors of the bus voltages (magnitudes and phase angles) in each operation state are shown in Figure 8-22.

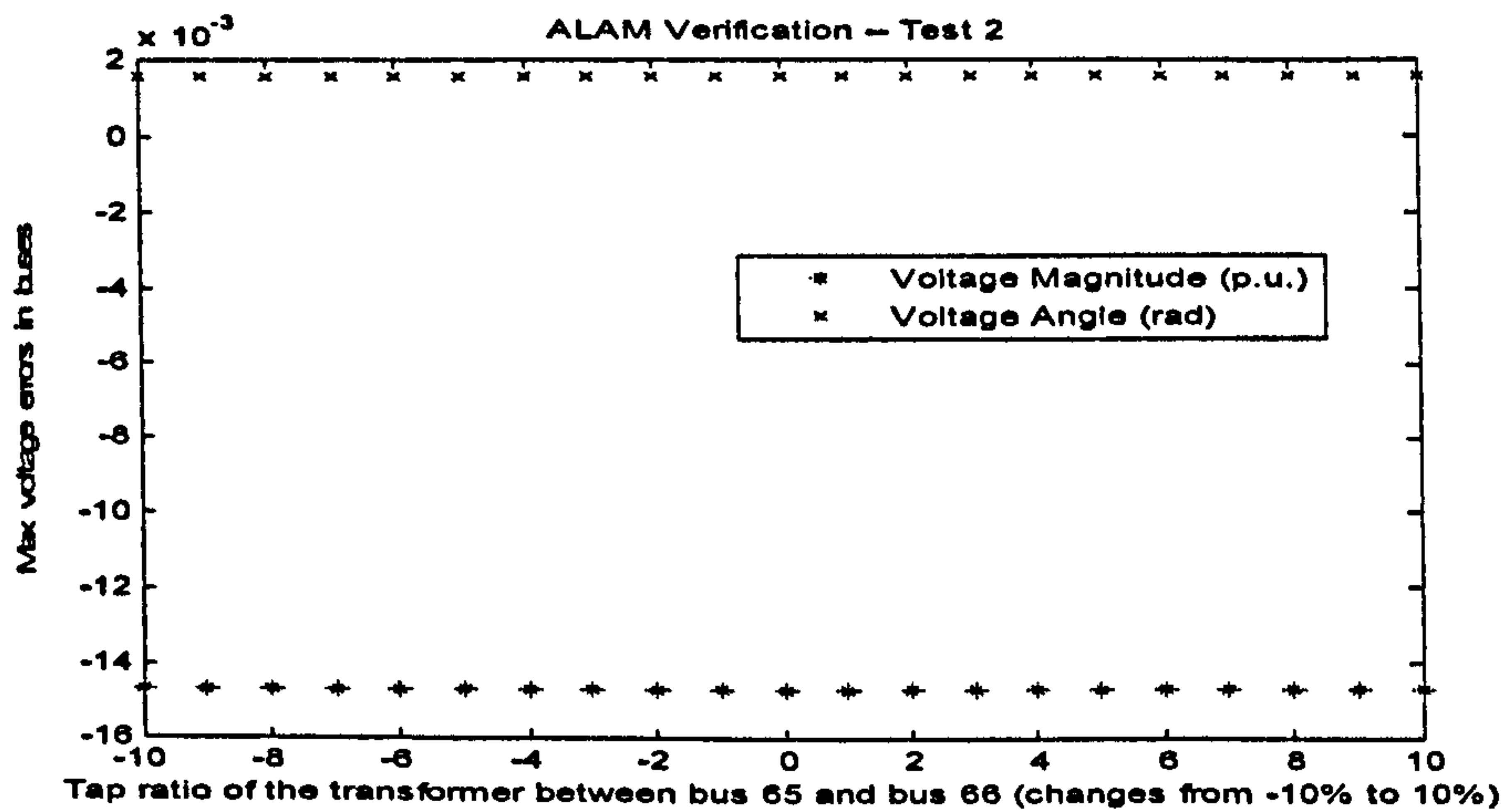


Figure 8-22 Maximum errors of the bus voltages in each operation state while changing tap ratio between bus 65 and bus 66 from 10% below to 10% above its normal output value

Test 3: Assume the system operates in normal conditions, but the value of voltage outputs from generator 1 (Bus 1) changes from 10% below to 10% above its normal output value in 1% increment. The maximum errors of the bus voltages (magnitudes and phase angles) in each operation state are shown in Figure 8-23.

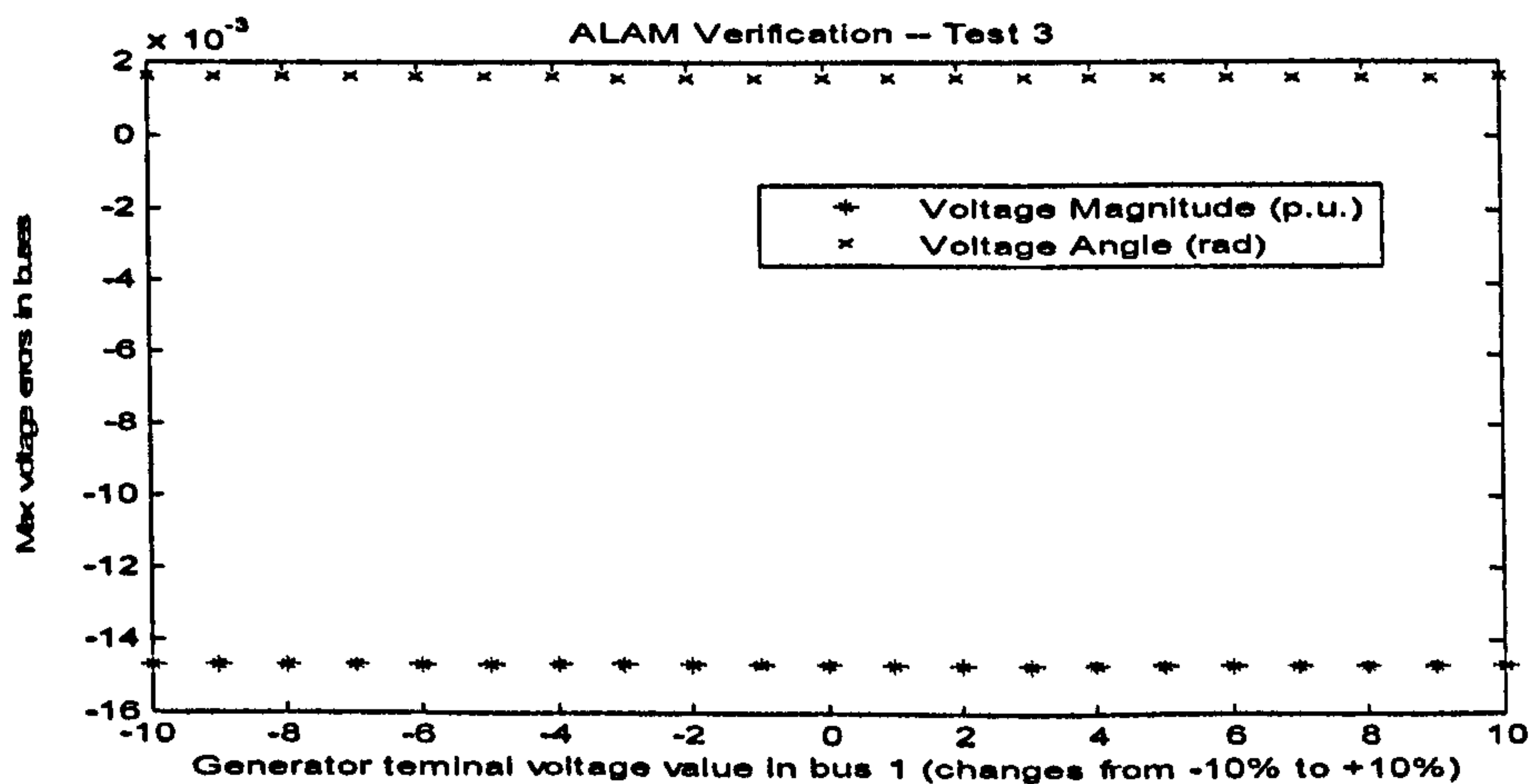


Figure 8-23 Maximum errors of the bus voltages in each operation state while changing the voltage outputs in Bus 1 from 10% below to 10% above its normal output value



The Load Area II consists of the load Buses: 50, 51, 52, 53, 57 and 58. The equivalent power system with the fictitious load bus for the aggregated load area is shown in Figure 8-24. For the equivalent power system, the fictitious load bus (Bus notation: 119B) is connected with the original power system by three fictitious transmission lines, which are: Line\_49\_119B, Line\_54\_119B and Line\_56\_119B. Together with the ZIP load model coefficients, there are total fifteen unknown parameters to be identified. The operation states applied in the previous section are repeated to identify all these unknown parameters using the Direct-One-Step method. The identified results are given in Table 8-6.

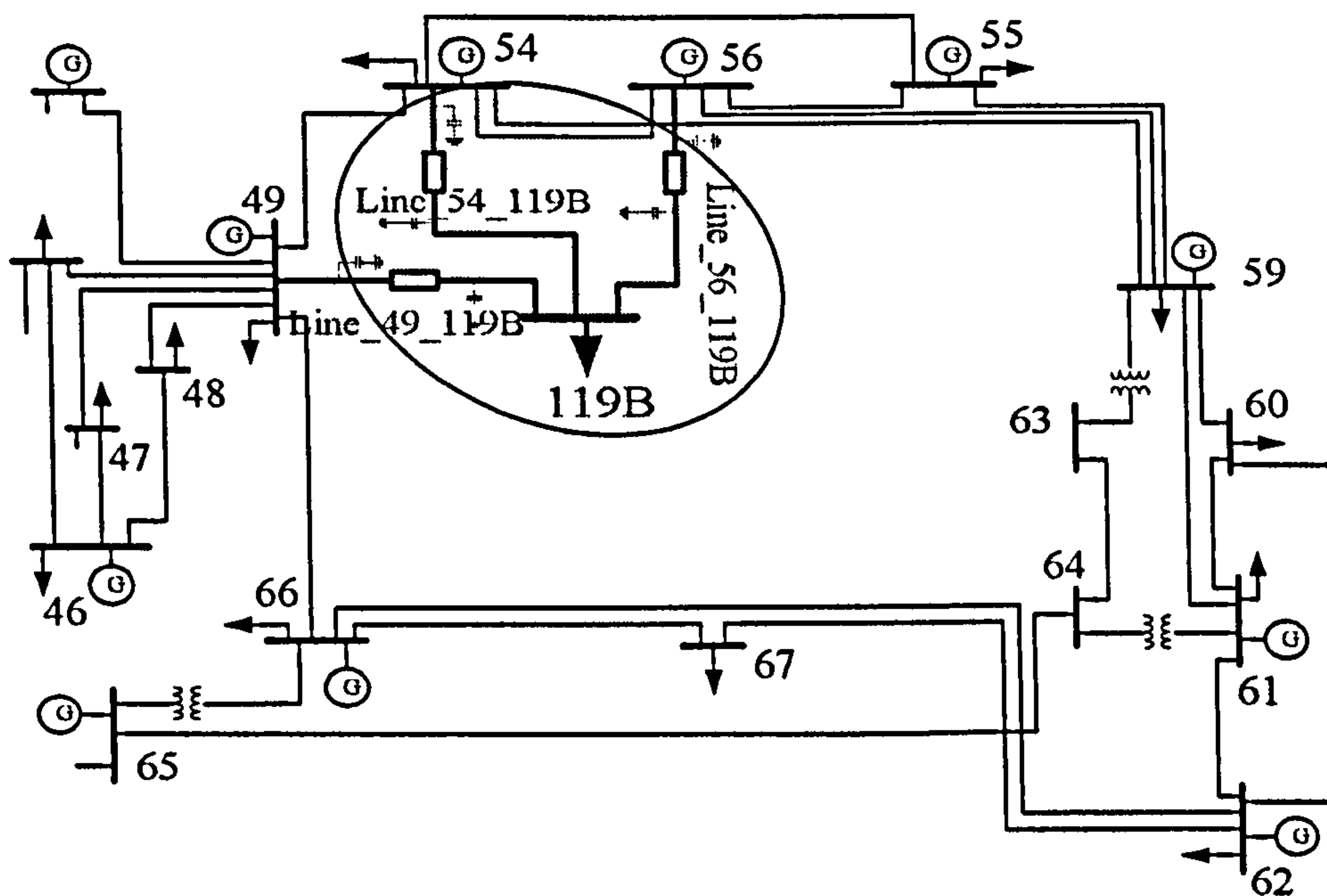


Figure 8-24 Partially enlarged equivalent IEEE-118-Bus power system for aggregating Load Area B

Table 8-6 The identified parameters for modelling load area 2 in the IEEE-118-Bus power system

$R_{49-119} = 0.0485 \text{ p.u.}$	$X_{49-119} = 0.0010 \text{ p.u.}$	$B_{49-119} = 0 \text{ p.u.}$
$R_{54-119} = 0.5152 \text{ p.u.}$	$X_{54-119} = 0.2394 \text{ p.u.}$	$B_{54-119} = 0.0002 \text{ p.u.}$
$R_{56-119} = 0.5635 \text{ p.u.}$	$X_{56-119} = 0.8496 \text{ p.u.}$	$B_{56-119} = 0.0116 \text{ p.u.}$
$a_{f1} = 0.5050$	$a_{f2} = 0.2514$	$a_{f3} = 0.2188$
$a_{f4} = 0.3681$	$a_{f5} = 0.0776$	$a_{f6} = 0.1171$

Similarly, three tests conducted in the previous section are conducted again to investigate the accuracy of the ALAM and the results are shown in Figures 8-25 ~ 8-27.

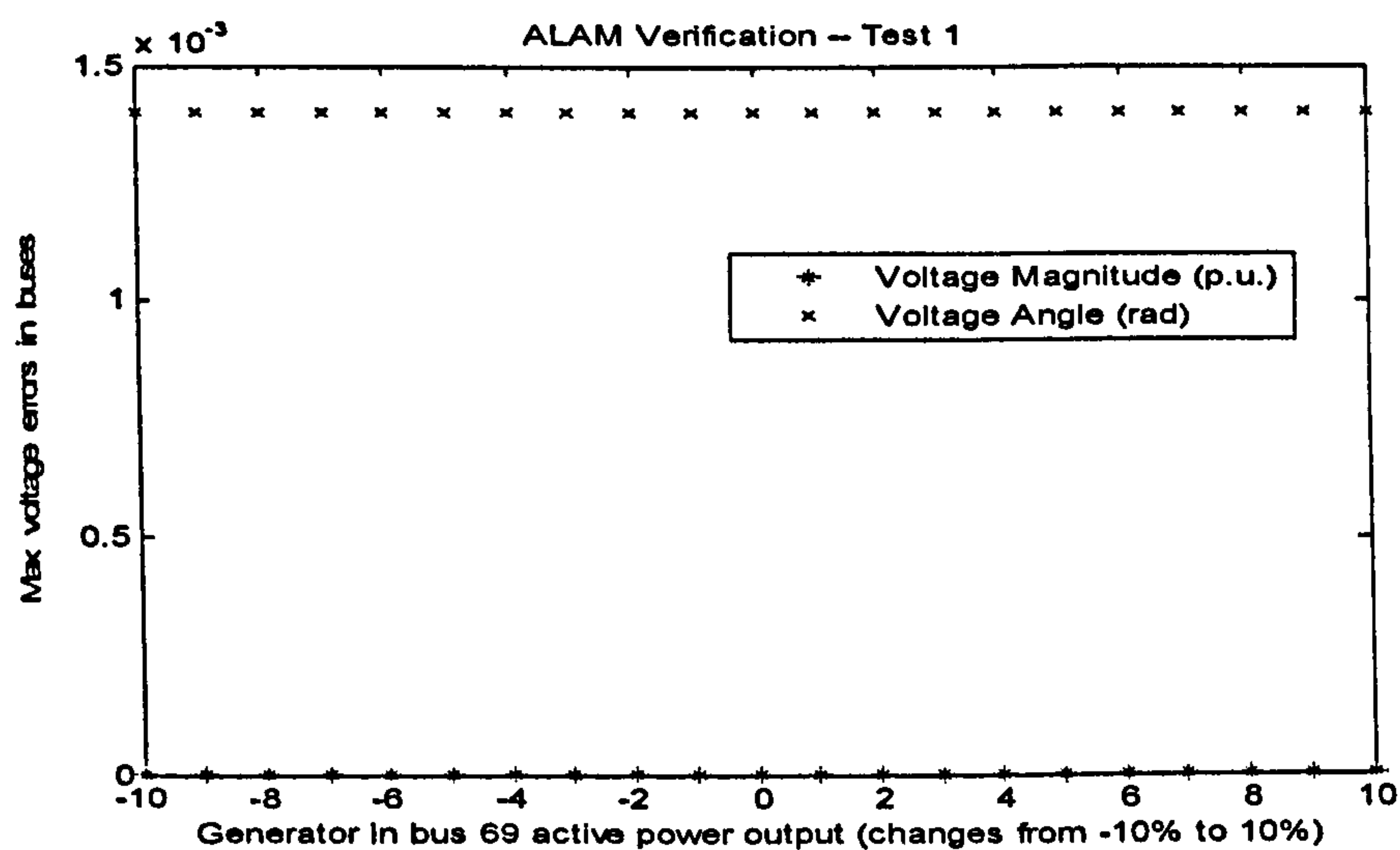


Figure 8-25 Maximum errors of the bus voltages in each operation state while changing the active power output of bus 69 from 10% below to 10% above its normal output value



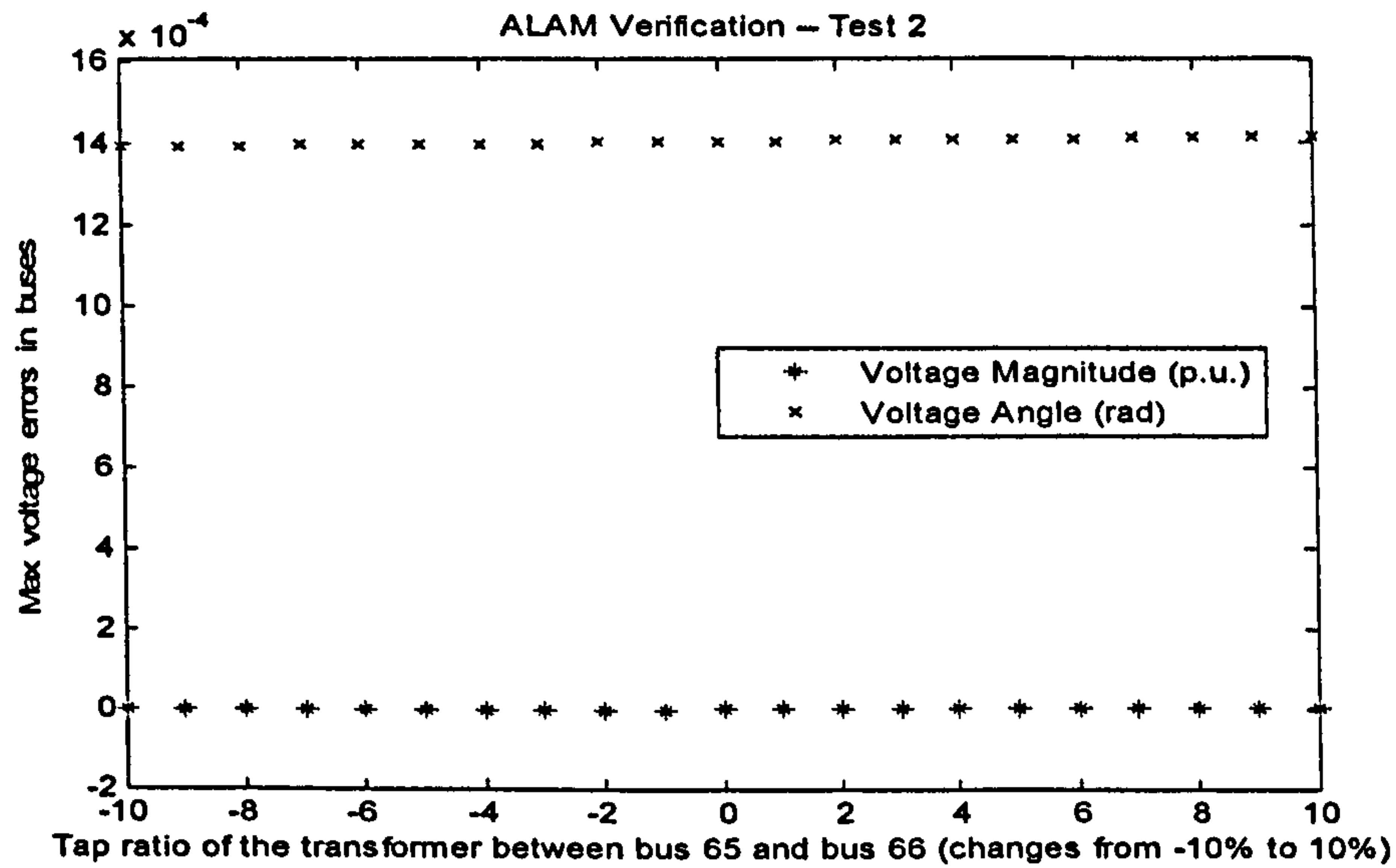


Figure 8-26 Maximum errors of the bus voltages in each operation state while changing tap ratio between Bus 65 and Bus 66 from 10% below to 10% above its normal output value

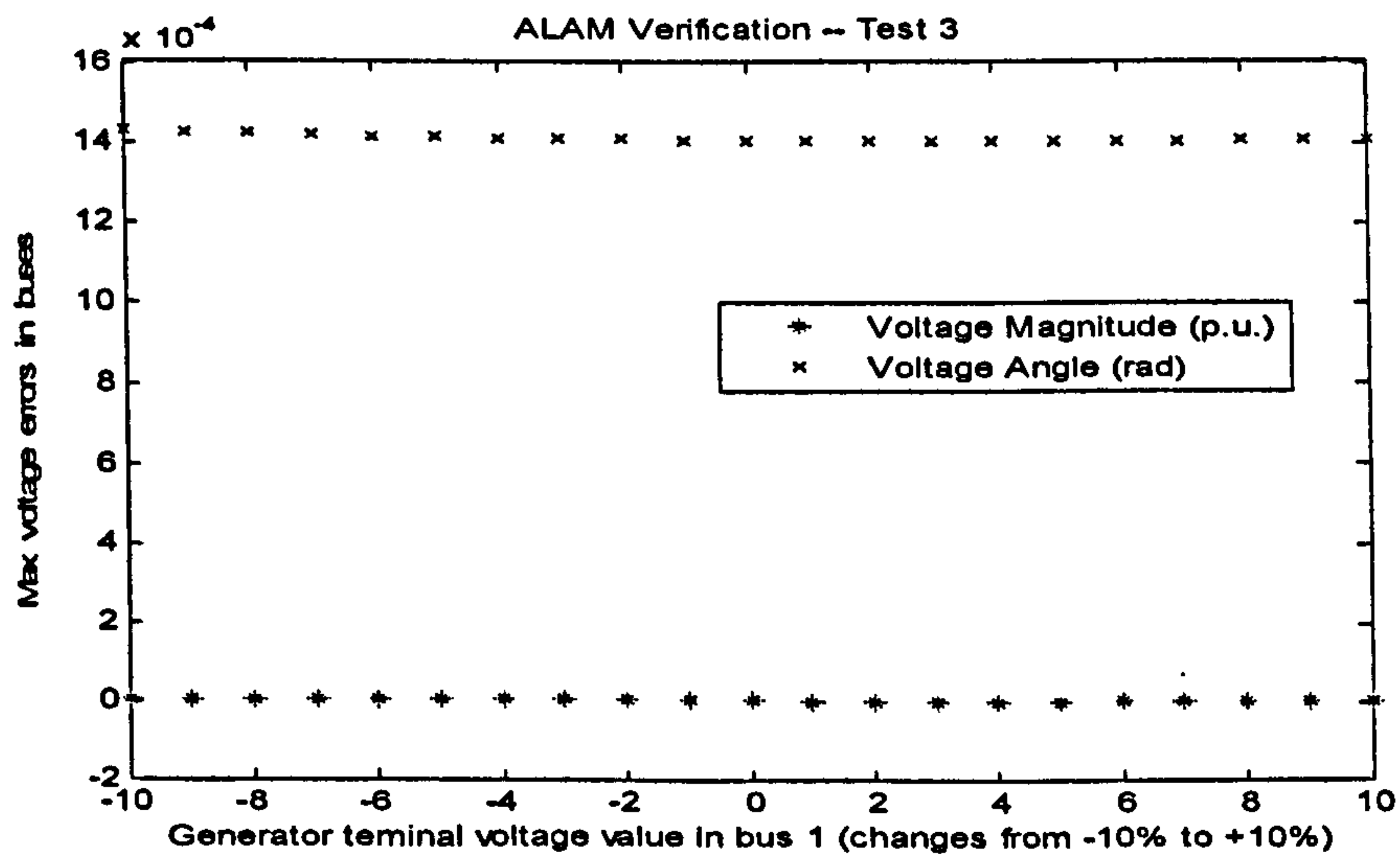


Figure 8-27 Maximum errors of the bus voltages in each operation state while changing the voltage outputs in bus 1 from 10% below to 10% above its normal output value

Comparing the results of the ALAM obtained from the two different load

areas, it can be seen that the results are not very consistent, that is, not all the load areas can give the same degree of satisfactions while the ALAM method is applied.. The Load Area A composes of five load buses and contains eighteen parameters to be identified. The Load Area B consists of six load buses, and contains fifteen parameters to be identified. From the results, the ALAM of Load Area B gives more accurate results than those given by the ALAM of Load Area A.

## **8.5 Summary and Discussion**

In this chapter, simulation studies are carried out to verify the ALAM method. Three different power system prototypes are employed for verification studies, which are shown as follows:

- IEEE-39-Bus power system

Two different load areas are modelled and the results of the ALAM are compared. The Load Area 1 is composed of Buses 14, 15, 16, 17, 18 and 24, where there are twenty seven unknown parameters to be identified; The Load Area 2 is composed of Buses 26, 27, 28 and 29, where there are fifteen unknown parameters to be identified. From the test results, it can be seen that the modelling of Load Area 2 provides much more accurate results than those obtained from the modelling of Load Area 1.

- IEEE-57-Bus power system

Two different load areas are modelled. The Load Area I consists of Buses 14, 46, 47, 48, 49, 50 and 51, where there are eighteen unknown parameters to be identified; The Load Area II is composed of Buses 23, 24, 25, 26, 27, 28, 30 and 31, where there are fifteen unknown parameters to be identified. From the test results, it can be seen that the modelling of Load Area II leads



more accurate results than those obtained through modelling Load Area I.

- IEEE-118-Bus power system

Two different load areas are identified and ALAM models are derived. The Load Area A is composed of Buses 93, 94, 95, 96 and 97, where there are eighteen unknown parameters to be identified. The Load Area B has Buses 50, 51, 52, 53, 57 and 58, where there are fifteen unknown parameters to be identified. From the test results, it can be seen that the modelling of Load Area B gives a slightly more accurate results than those derived through modelling Load Area A.

From the simulation studies, it can be seen that the way of organising the modelling load areas affect the modelling accuracy. It indicated that different choices of load areas for deriving equivalent load model will result in very different levels of accuracy. The rules for forming ALAM are summarised as follows, which are provisional and further studies are required for more concrete conclusions.

1. Comparing the results of ALAM obtained from the IEEE-39-Bus, IEEE-57-Bus and the IEEE-118-Bus power systems, it can be seen that the IEEE-118-Bus power system leads more accurate results, where the load areas in the simulation of the IEEE-118-Bus power system is only formed from a very small portion of the system. It shows that the smaller portion of load buses in a power system to be aggregated can achieve better accuracy results of the ALAM. So, the ALAM method may be more suitable for modelling larger scale of power systems in load analysis.
2. From the simulation of the IEEE-39-Bus, IEEE-57-Bus and the IEEE-118-Bus power systems, the second load area for all examples provide

more accurate ALAM results than the first load area, where less unknown parameters to be identified in the ALAM of the second load area. So, while applying the ALAM method, if the equivalent area covers less fictitious transmission lines and has less parameters to be identified, the ALAM method derives more accurate results, which means less uncertain factors affecting the optimisation results.



## **Chapter 9**

# **Summary and Recommendations for Future Work**

### **9.1 Summary**

With the support from RWEnPower Plc. and National Grid Plc., two particular studies in power system modeling have been carried out in this research: development of coal mill models and development of the simplified area electricity load models. The main contributions are summarised as follows:

- An improved normal grinding process coal mill model is developed by taking consideration of the thermal inertia in the thermodynamic process of the coal mill system. The simulation study using on-site measurement data indicated that the model accuracy has been improved compared with the previously reported model.
- The coal mill operational sequence has been investigated in detail and a new six-segment coal mill model is developed. The whole coal milling process is covered by this model, especially the start-up and shut-down processes. The model has been validated and its performance has convinced the plant engineers to adopt the model for mill condition monitoring.
- A prototype software package for on-line implementation of the coal mill model has been developed. This software has now been passed onto RWEnPower Plc. for condition monitoring and safety improvement. The shared memory technique was employed in the program to offer a more

generic platform in order to accommodate different data acquisition systems used by different power plants.

- Based on the Voltage-Two-Step approach developed by Liverpool, two new approaches for the ALAM are proposed, which are entitled Current-Two-Step approach and Direct-One-Step approach. The Current-Match scheme and the Bus-Match scheme are proposed respectively for these two approaches.
- Verification studies of the ALAM have been investigated. Extensive simulation studies of the ALAM have been performed and the results have been compared to each other. From this study, essential characteristics and rules for forming an ALAM are provided and summarised in Chapter 8.
- The mathematical expressions of fitness function to achieve better convergence rates of GAs have been further studied. Instead of using traditional mean squared errors fitness function structure, the sum of absolute values of errors is used to form the fitness function which has been shown to offer a better GA convergence and lead to more accurate results for those parameters identified for the dynamic system problems.

## **9.2 Recommendations for Future Work**

Following the successful completion of the project, a research funding for a two year research project has been awarded to the university which will move the project further for modelling and safety monitoring of tube ball mills in power plants. Different from the vertical spindle coal mills studied in this thesis, tube ball mills are classified to belong to the low speed coal mill category which works on the tumbling action of the balls to crush coal to powders. The aim of the project is to develop a software package for on-line



mill condition and safety monitoring with particular emphasis on the following objectives:

- extend the current model from E-type vertical spindle mills to the tube ball mills;
- to identify coal quality variations through recognising the variation patterns of mill model parameters and dynamics;
- to detect apparent mill defects or instrumentation problems using on-line mill modelling;
- to estimate the quantity of deposit coal in the mill, which is essential for predicting potential mill fires;
- to predict potential fires through identification of the patterns of mill data and model parameter variations.

All the project tasks can be considered for the immediate future work.

The study of ALAM is still in its early stage and there are a number of issues and topics to be addressed in the future. Here, a few recommendations are made. The ZIP load model has been employed to model the relationship between power consumes in the load area and the fictitious voltage of the load area. Simulation studies show that the ALAM can offer a good degree of satisfaction while modelling small portion of the load area in a giant power system. For future work, different bus load models, e.g. the Exponential Load Model, should be adopted as well to study whether it can offer the same degree of satisfaction. Although three different approaches of the ALAM are discussed in this thesis, it is anticipated that different ways should be explored to improve the accuracy of ALAM in representation of the load area.

## References

- Alonge, F., F. D'Ippolito and F. M. Raimondi (2001). "Least squares and genetic algorithms for parameter identification of induction motors." Control Engineering Practice 9(6): 647-657.
- Anon (1993). "Load representation for dynamic performance analysis." IEEE Transactions on Power Systems 8(2): 472-482.
- Baker, J. E. (1987). "Reducing Bias and Inefficiency in the Selection Algorithm." Proceedings of the Second International Conference on Genetic Algorithms and their Application: pp. 14-21.
- Blach, L., R. Wasniowski and T. Wisniewski (1978). "MATHEMATICAL MODEL AND ALGORITHMS OF OPTIMAL CONTROL OF COAL MILLING PROCESS IN THE BILL MILL." MCIC Report (Metals and Ceramics Information Center): 279-283.
- Bollinger, K. E. and H. R. Snowden (1983). "The Experimental-Determination of Coal Mill Models." Ieee Transactions on Power Apparatus and Systems 102(6): 1473-1477.
- Bollinger, K. E. and H. R. Snowden (1986). "FIELD TEST RESULTS FOR MULTI-VARIABLE CONTROL OF A COAL-MILL." IEEE Transactions on Power Systems PWRS-1(1): 96-100.
- Bramlette, M. F. and R. Cusic (1989). A Comparative-Evaluation of Search Methods Applied to Parametric Design of Aircraft. Proceedings of the Third International Conference on Genetic Algorithms. J. D. Schaffer. San Mateo, Morgan Kaufmann Pub Inc: 213-218.
- CEGB (1963). Modern Power Station Practice, Central Electricity Generating Board, London, Vol 2, pp10-15.
- Chipperfield, A., P. Fleming, H. Pohlherim and C. Fonseca (1994A). Genetic algorithm toolbox for use with Matlab. Department of automatic control and systems engineering, University of Sheffield.
- Chipperfield, A. J., P. J. Fleming and C. M. Fonseca (1994B). Genetic



## References

---

algorithm tools for control systems engineering. Adaptive computing in engineering design and control. Plymouth, UK.

Chumsamutr, R. and T. Fujioka (2003). "Development of car-following model with parameter identification by genetic algorithm." JSME International Journal, Series C: Mechanical Systems, Machine Elements and Manufacturing 46(1): 188-196.

Corti, L., A. de Marco and A. Zizzo (1984). Mathematical model of a coal mill. International Conference on Power Plant Simulation. Cuernavaca; Morelos (Mexico DF). 19-21 Nov.: 206-211.

Davis, L. (1987). Genetic Algorithms and Simulated Annealing, Morgan Kaufmann Publishers Inc.

DTI (2001). Pulverised coal-fired power station boilers, Department of Trade and Industry (DTI). **CB010**.

Eberhart, R. C. and Y. Shi (1998). Comparison between genetic algorithms and particle swarm optimization. **1447**: 611.

EDF Plc (1981). Pulverised Fuel System (operational manual): 10-13.

EI-Wakil, M. M. (1985). Power Plant Technology, McGraw-Hill Book Company.

Fan, G. Q. and N. W. Rees (1994). Modelling of vertical spindle mills in coal fired power plants, Sydney, USA, IE Aust, Crows Nest, NSW, Aust.

Fan, G. Q. and N. W. Rees (1997). "An intelligent expert system (KBOSS) for power plant coal mill supervision and control." Control Engineering Practice 5(1): 101-108.

Fernando, R. (2006). Public attitudes to coal-fired power plant, IEA Clean Coal Centre: CCC/117.

Grainger, J. J. and W. D. Stevenson (1994). Power System Analysis, McGraw-Hill, pp196-205.

Hamiane, M. (2000). "Identification of a pulverized fuel mill from normal operating records using a multivariable polynomial matrix model."

## References

---

- International Journal of Modelling and Simulation 20(3): 227-235.
- Horowitz, S. H. and A. G. Phadke (2003). "Boosting Immunity to Blackouts." IEEE Power and Energy Magazine 1(5): 47-53.
- Houck, C., J. Joines and M. Kay (1995). "A Genetic Algorithm for Function Optimization: A Matlab Implementation." NCSU-IE TR 95-09.
- IEEE Task Force (1993). "Load representation for dynamic performance analysis." IEEE Transactions on Power Systems 8(2): 472-482.
- Karlsson, D. and D. J. Hill (1994). "Modelling and identification of nonlinear dynamic loads in power systems." IEEE Transactions on Power Systems 9(1): 157-166.
- Karr, C. L. (1993). Genetic algorithms for modelling, design, and process control, Washington, DC, USA, Publ by ACM, New York, NY, USA.
- Karr, C. L. and B. Weck (1996). "Computer modelling of mineral processing equipment using fuzzy mathematics." Minerals Engineering 9(2): 183-194.
- Krishnakumar, K. and D. E. Goldberg (1992). "Control-System Optimization Using Genetic Algorithms." Journal of Guidance Control and Dynamics 15(3): 735-740.
- Kundur, P., N. J. Balu and M. G. Lauby (1994). Power system stability and control, McGraw-Hill, USA, pp205-pp313.
- Lee, K. Y., Y. M. Park and J. L. Ortiz (1985). "A UNITED APPROACH TO OPTIMAL REAL AND REACTIVE POWER DISPATCH." IEEE Transactions on Power Apparatus and Systems PAS-104(5): 1147-1153.
- Lu, s., t. ren, x. Jiang and f. Cheng (2002). Da Xing Huo Dian Ji Zhu Xi Tong Fang Zhen Yu Jian Mo, Tshinghua ying shua chuang, pp152-153.
- Machowski, J., F. W. Bialek and J. R. Bumby (1998). Power system dynamics and stability, Wiley.
- MathWorks Inc. (2004). Genetic Algorithm Direct Search Toolbox V1.02,



## References

---

MathWorks, Inc.

Mitchell, M. (1996). An introduction to genetic algorithms, Massachusetts Institute of Technology.

Muehlenbein, H., M. Schomisch and J. Born (1991). "Parallel genetic algorithm as function optimizer." Parallel Computing 17(6-7): 619-632.

Neal, P. W., J. Waddington and R. G. Wilson (1980). "DETERMINATION OF MILL AND BOILER CHARACTERISTICS AND THEIR EFFECT ON STEAM PRESSURE CONTROL." Chemical Engineering Science 35(10): 2107-2114.

Nyarko, E. K. and R. Scitovski (2004). "Solving the parameter identification problem of mathematical models using genetic algorithms." Applied Mathematics and Computation (New York) 153(3): 651-658.

Peet, W. J. and T. K. P. Leung (1994). Dynamic simulation application in modern power plant control and design, Hong Kong, Hong Kong, Publ by IEE, Stevenage, Engl.

Prasher, C. L., Ed. (1981). Crushing and grinding process handbook, John Wiley, New York.

Price, W. W., S. G. Casper, C. O. Nwankpa, R. W. Bradish, H. D. Chiang, C. Concordia, J. V. Staron, C. W. Taylor, E. Vaahedi and G. Wu (1995). "Bibliography on load models for power flow and dynamic performance simulation." IEEE Transactions on Power Systems 10(1): 523-538.

Price, W. W., C. W. Taylor, W. W. Price, G. J. Rogers, K. Srinivasan, C. Concordia, M. K. Pal, K. C. Bess, P. Kundur, B. L. Agrawal, J. F. Luini, E. Vaahedi and B. K. Johnson (1995). "Standard load models for power flow and dynamic performance simulation." IEEE Transactions on Power Systems 10(3): 1302-1313.

QAA. (2006). "Map of Power Stations." from <http://www.ukqaa.org.uk/PowerStation.html#Map>.

Rashtchi, V., E. Rahimpour and E. M. Rezapour (2006). "Using a genetic algorithm for parameter identification of transformer R-L-C-M

## References

---

- model." Electrical Engineering 88(5): 417-422.
- Rees, N. W. (1998). Advanced control of power plant, Swansea, UK, IEE, Stevenage, Engl.
- Rees, N. W. and G. Q. Fan (2003). "Modelling and control of pulverised fuel coal mills." IEE Power & Energy Series 43: Thermal Power Plant Simulation and Control: 63-99.
- Rees, N. W. and C. X. Lu (2002). "Some thoughts on the advanced control of electric power plants." Transactions of the Institute of Measurement and Control 24(2): 87-106.
- RWE Innogy Plc (2000). Pulverised fuel mills. Power Plant Handbook, Innogy Plc Internal Documents. DID-2/2/12 Issue 3-5/86.
- RWE Innogy Plc (2002). Introduction booklet.
- Shi, D., X. Xie and L. Tong (2005). Studies on parameter identification using genetic algorithm in power system, Dalian, China, Institute of Electrical and Electronics Engineers Inc., Piscataway, NJ 08855-1331, United States.
- Srinivasan, K. and C. Lafond (1995). "Statistical analysis of load behavior parameters at four major loads." IEEE Transactions on Power Systems 10(1): 387-392.
- Thomakos, S. (2000). Test Report, Process Control. Internal Report, Innogy Plc.
- Wan, H. (1999). Calculate the parameters of the coal mill model using genetic algorithms. Internal Report, University of Liverpool.
- Wang, J., J. D. Wang, N. Daw and Q. H. Wu (2004). "Identification of pneumatic cylinder friction parameters using genetic algorithms." IEEE/ASME Transactions on Mechatronics 9(1): 100-107.
- Wang, L., M. Klein, S. Yirga and P. Kundur (1997). "Dynamic reduction of large power systems for stability studies." IEEE Transactions on Power Systems 12(2): 889-895.



## References

---

- Wei, J. (2002). Coa mill modelling using Evolutionary Computation Techniques, University of Liverpool. MSc thesis in Intelligence Engineering: pp12-pp31.
- Wei, J., J. Wang, Q. H. Wu and N. Lu (2005d). "Power system aggregate load area modelling by particle swarm optimization." Proc. of the 11th Chinese Automation & Computing Society Conference in the UK, Sheffield, England: 55-60 (Nominate to the best paper award, and invite to publish in the International Journal of Automation and Computing.).
- Wei, J., J. Wang, Q. H. Wu and N. Lu (2005e). "Power System Aggregate Load Area Modelling by Particle Swarm Optimization." International Journal of Automation and Computing Vol. II: 171-178.
- Wei, J. L., J. Wang, L. Yang and Q. H. Wu (2005c). Power system aggregate load area modeling. Proceedings of the IEEE Power Engineering Society Transmission and Distribution Conference. Dalian, China, Institute of Electrical and Electronics Engineers Inc., Piscataway, NJ 08855-1331, United States. 2005: 1-6.
- Wei, J. L., J. H. Wang and Q. H. Wu (2004a). Study of Fitness Function in Identifying Unknown Parameters of Dynamic Processes using Genetic Algorithms. Proc. of Postgraduate Research Conference in Electronics, Photonics, Communications and Networks, and Computing Scienc, Hertfordshire UK, p123 - p124,.
- Wen, J. Y., L. Jiang, Q. H. Wu and S. J. Cheng (2003b). "Power system load modeling by learning based on system measurements." IEEE Transactions on Power Delivery 18(2): 364-371.
- Wen, J. Y., Q. H. Wu, K. I. Nuttall, D. W. Shimmin and S. J. Cheng (2003a). "Construction of power system load models and network equivalence using an evolutionary computation technique." International Journal of Electrical Power and Energy Systems 25(4): 293-299.
- Wu, Q. H., J. Y. Wen, K. I. Nuttall, D. W. Shimmin and S. J. Cheng (2003). "Power system load modeling by evolutionary computation based on system measurements." Electric Power Components and Systems 31(5): 423-439.

## References

---

Zhang, Y. G. (1999a). Coal mill modelling by machine learning based on on-site measurements. Internal Report, University of Liverpool.

Zhang, Y. G. (1999b). Improvement on the coal mill model of didcot A power station. Internal Report, University of Liverpool.

Zhang, Y. G., Q. H. Wu, J. Wang, G. Oluwande, D. Matts and X. X. Zhou (2002). "Coal mill modeling by machine learning based on onsite measurements." IEEE Transactions on Energy Conversion 17(4): 549-555.

Zimmerman, R. D., C. E. Murillo-Sanchez and D. Gan. (2004). "MATPOWER-A Matlab Power System Simulation Package." from <http://www.pserc.cornell.edu/matpower/>.



# Appendix I: Mill Operation Sequence

## Table

Function: Mill Start/Shutdown Sequence		APACS Path: Ref.25.2			
APMSPath:BoilerX firing Group:Mill:dummy:Sequence		APMS ALIAS: Mill X Seq			
STATE TRANSITION TABLE					
Step No	Step Name	ACTION	TRANSITION	Next step	Timeout
0	Idle	Generate FALSE Pre Start Check Messages[A]  Reset PA Fan Actuator SIC Request (MLX_SEQ_ACT_SIC=FALSE) Reset Mill Outlet Temp SIC Request (MLX_SEQ_ACT_SIC=FALSE) Reset Sec Air Damper Actice Flag (MLSQ_X_SA_ACTRQ=FALSE) Reset PA Diff Setpoint SIC Request(start Seq) (MLX_STRT_DPSIC=FALSE) Reset PA Diff Setpnt SIC Request(Shutdown Seq) (MLX_SHDN_DPSIC=FALSE) Reset Tempering Air Damper SIC Request (MLX_TADMP_SIC=FALSE) Reset Mill Feeder Speed SIC Request (MLX_SHDN_FDR_SIC=FALSE) Set Mill Sequence Idle Flag (MLX_SEQ_IDLE)	APMS Mill Start Command (MLX_SEQ_STRT=TRUE)  AND Pre-start Checks OK (MLX_PSC_OK=TRUE)  [A]	1	None
1	CHK_N RVS				
2	Set Mill Temp Setpoint , Open PA Fan Damper and Start Lube Oil	Set Mill Outlet Temp SIC Request (MLX_SEQ_TMPSIC=TRUE) Set Mill Outlet temp Setpoint to coal Type Value (MLX_SEQ_TMPDV= MLTMP_MLSEQ_SP)  Set PA Fan Suction Damper SIC Request (PAX_SCT_DMP_SEQ=TRUE) Set PA Fan Suction Damper DV	Mill Outlet Temp Setpoint under Sequence control (MLX_SEQ_DV_ACT=TRUE)  AND PA Fan Suction Damper Opened (PA_DAMPER_OPD=TRUE)  [C]  AND Sufficient Oil Burners in Service	2	Device

*Appendix I: Mill Operation Sequence Table*

	Pump	(PAX_SCT_DMP_SDV=100.0) Start Mill Lub Oil Pump (MLX_LUB_PP_SCL=TRUE)	(MLX_BRN_FLME_CH=TRUE)		
3	Set IR To Coal Fire Position	Set PA Diff Setpoint SIC Request (MLX_STRT_DPSIC=TRUE) PA Diff Setpoint To 4.4 mbar (MLX_STRT_DPDV=4.4)	PA Diff Greater Than 4.3 mbar (PADIFF_IPSN=TRUE) AND Sufficient Oil Burners in Service (MLX_BRN_FLME_CH=TRUE) AND PA Fan Active(PAX_ACTVE=TRUE)	3	60 Sec
4	PA Diff Delay	Start PA Diff Delay Timer	Timer Complete	4	11 Sec
5	Check Lube Oil pump Pressure and Mill Temper ature		Mill Lube Oil Pressure OK (MLX_LUB-PRS_SW=TRUE) AND Mill Temperature OK (MILL-TEMPI=TRUE) [F] AND Sufficient Oil Burners in Service (MLX_BRN_FLME_CH=TRUE)	5	5 Minutes
6	Set Sec Air Damper Active Criteria	Set Sec Air Damper Active Flag (MLSQ_X_SA_ACTRQ=TRUE)	SA Damper A in Active Auto (WBP_XA_ACTAUT=TRUE) AND SA Damper B in Active Auto (WBP_XB_ACTAUT=TRUE) AND Windbox Pressure at Least 5 mbar AND Pressure Signals Valid (WBOX_PRE_OK=TRUE) [E] AND Sufficient Oil Burners in Service (MLX_BRN_FLME_CH=TRUE)	6	1 Minutes
7	Start Mill	Close Mill ACB (MLX_ACB_SCL=TRUE)	Mill Running (MILL_X_RNG) AND Sufficient Oil Burners in Service (MLX_BRN_FLME_CH=TRUE)	7	Device



*Appendix I: Mill Operation Sequence Table*

			E)		
8	Mill Partial Start-up Complete	Mill Partial Start-up Complete (MLX_PT_STRT_CMPT=TRUE)	Mill Partial Hold Not Set (GPMLX_HOLD2=FALSE)  Mill Shutdown Command from APMS (MLX_SEQ_SHDN=TRUE)	8  11	None
9	Start Feeder	Close Mill feeder ACB (MLX_FDR_SCL=TRUE) Reset Sec Air Damper Active Flag (MLSQ_X_SA_ACTRQ=FALSE)	Mill Feeder Running (MLX_FDR_CDC=TRUE) AND Sufficient Oil Burners in Service (MLX_BRN_FLME_CH=TRUE) AND PA Fan Active (PAX_ACTVE=TRUE)	9	Device
10	Checkin g Feeder Speed		Mill Feeder Speed at Minimum (MLX_FDRSPD_OK=TRUE) [G] AND TFC recognises Mill in service (MLX_IN_SERV=TRUE)	10	1 min
11	Mill Start Complete	Set Mill Start Sequence Complete (MLX_STRT_CMPLT=TRUE) Reset Mill Outlet Temp SIC Request (MLX_SEQ_TMPSIC) Reset PA Diff Setpoint SIC Request (MLX_STRT_DPSIC)	Mill Shutdown Complete Form Apms (MLX_SEQ_SHDN=TRUE)	11	None
12	Set Tempering Air to fully Cold	Set Mill Tempering Air Damper SIC Request (MLX_TADMP_SIC=TRUE) Set Mill Tempering Air To Fully Cold (MLX_TADMP_DV=0.0)	Tempering Air Damper in Auto (MLX_SHDN_DV2_ACT=TRUE) Tempering Air Damper in Position (TA_DMP_X_INPON=TRUE)	12	30 Sec
13	Tempering Air delay	Start Tempering Air delay Timer	Timer Complete	13	61Sec
14	Set feeder Speed To Minimum	Set Feeder Speed SIC Request (MLX_SHDN_FDR_SIC=TRUE) Set Feeder Speed To Minimum (MLX_SHDN_FDR_DV=0.0)	Feeder At Minimum (MLX_FDR_INPOS=TRUE)	14	30 Sec

*Appendix I: Mill Operation Sequence Table*

15	Set PA Diff Setpoint To 4 mbar	Set PA Diff Setpoint SIC Request (MLX_SHDN_DPSIC=TRUE) Set PA Diff Setpoint To 4 mbar (MLX_SHDN_DPDV=40)	Always Continue	15	None
16	Delay	Start Delay Timer	Time Complete	16	181Sec
17	Trip Feeder	Trip Feeder (MLX_FDR_SOP=TRUE)	Mill Feeder Not Running (MLX_FDR_ODC=TRUE)	17	Device
18	Hold Point	Mill Partial Shutdown Complete (MLX_PTSHDN_CMPLT=TRUE)	Mill Partial Hold Not Set (GPMLX_HOLD2=FALSE)	18	None
19	Grnd Delay	Start Grind Delay Timer	Time Complete	19	11Sec
20	Trip Mill	Stop Mill (MLX_ACB_SOP=TRUE)	Mill ACB Opened (MLX_ACB_ODC=TRUE)	20	Device
21	Set Mill Temperature	Set Mill Outlet Temp SIC Request (MLX_SEQ_TMPSIC=TRUE) Set Mill Temperature Setpoint To 10°C (MLX_SEQ_TMPDV=10.0)	SA Damper A Closed (MLX_SAA_DMP_LL=TRUE) AND SA Damper B Closed (MLX_SAB_DMP_LL=TRUE)	21	Device
22	Close PA Fan Induction Regulator To 15%	Set PA Fan Ind Reg SIC Request (MLX_SEQ_ACT_SIC=TRUE) Close Induction Regulator To 15% (MLX_SEQ_ACT_DV=15.0)	Induction Regulator At 15% (PA_ACT_X_IPSN=TRUE) [B]	22	Device
23	Set PA Fan Damper to Mill Warming Position	Set PA Fan Suction Damper To 25% Open (Mill Warming Position) (PAX_SCT_DMP_SDV=25.0)	Damper At 25% (PAX_SCT_DMP_IPS=TRUE) [B]	23	Device
24	Mill Shutdown Sequence Complete	Set Mill Shutdown Sequence Complete (MLX_SHDN_CMPLT=TRUE)	Always Continue	0	None



## Appendix II: Validation results using Data Set C

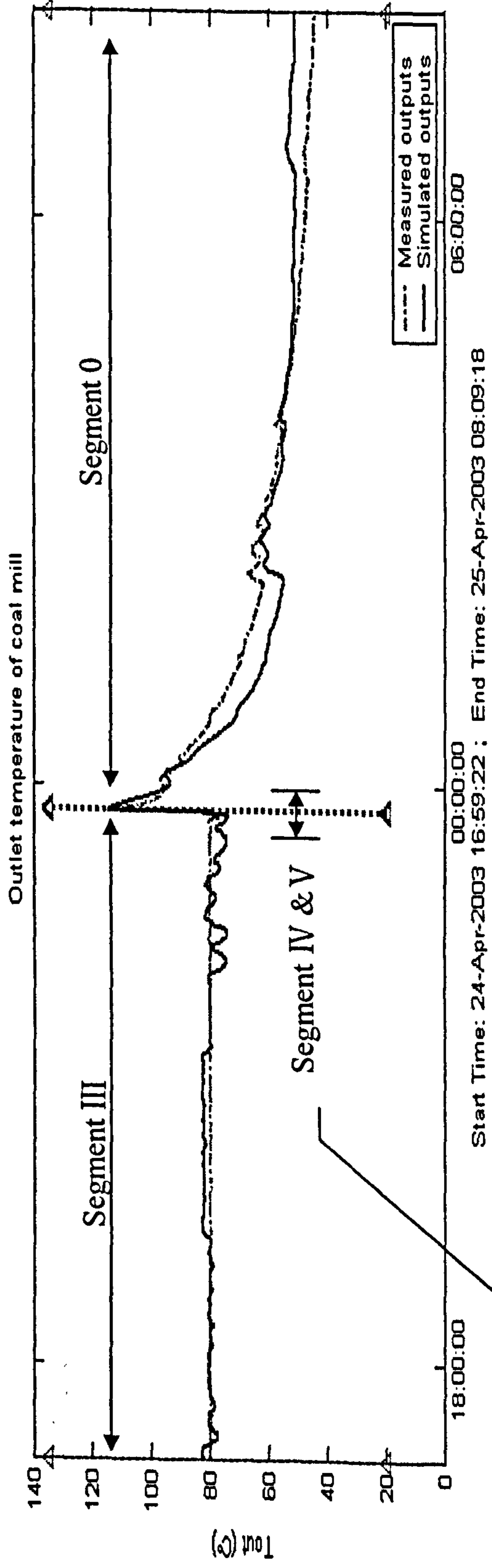


Figure A.1.1 Simulated and measured mill outlet temperature for all segments using Data Set C

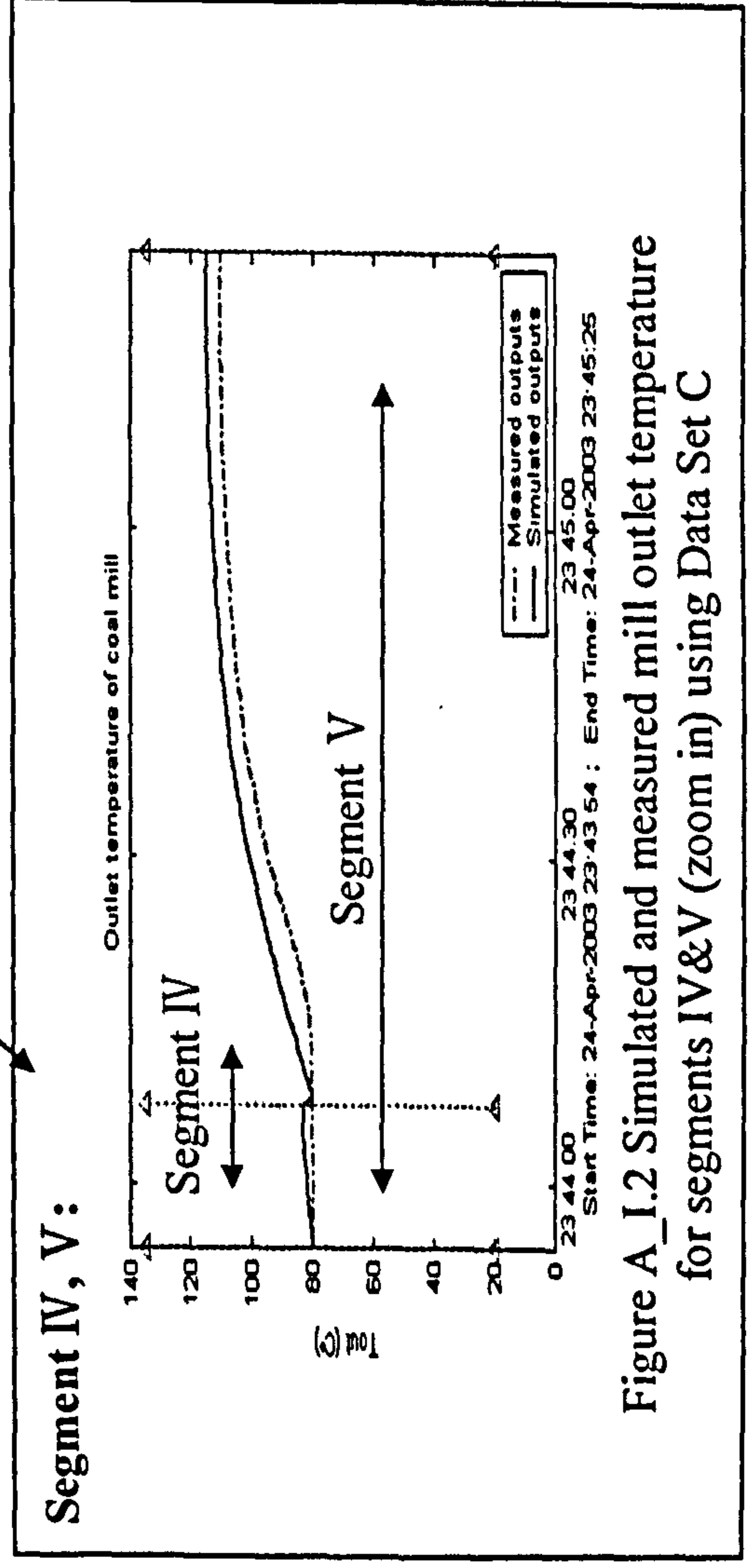


Figure A.1.2 Simulated and measured mill outlet temperature for segments IV&V (zoom in) using Data Set C

Appendix II: Validation Results Using Data Set C

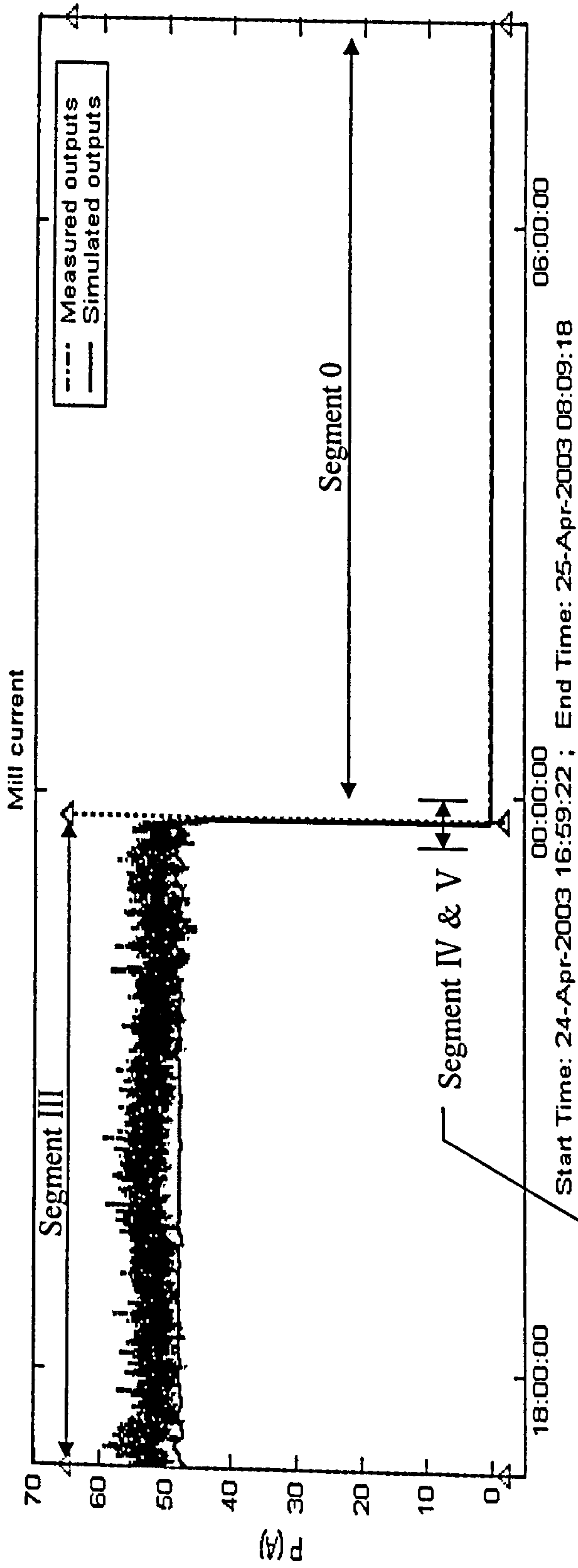


Figure A\_I.3 Simulated and measured mill current for all segments using Data Set C

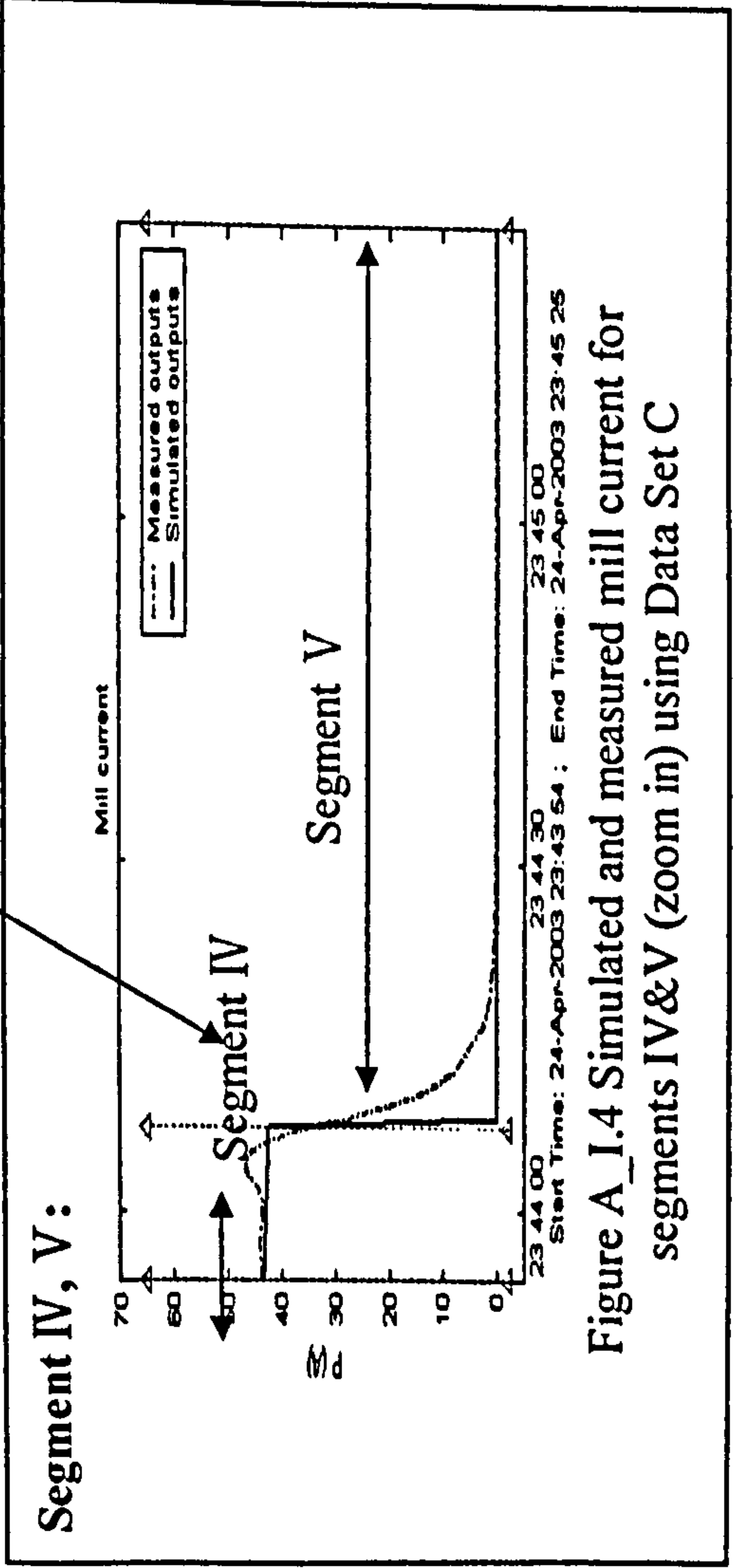
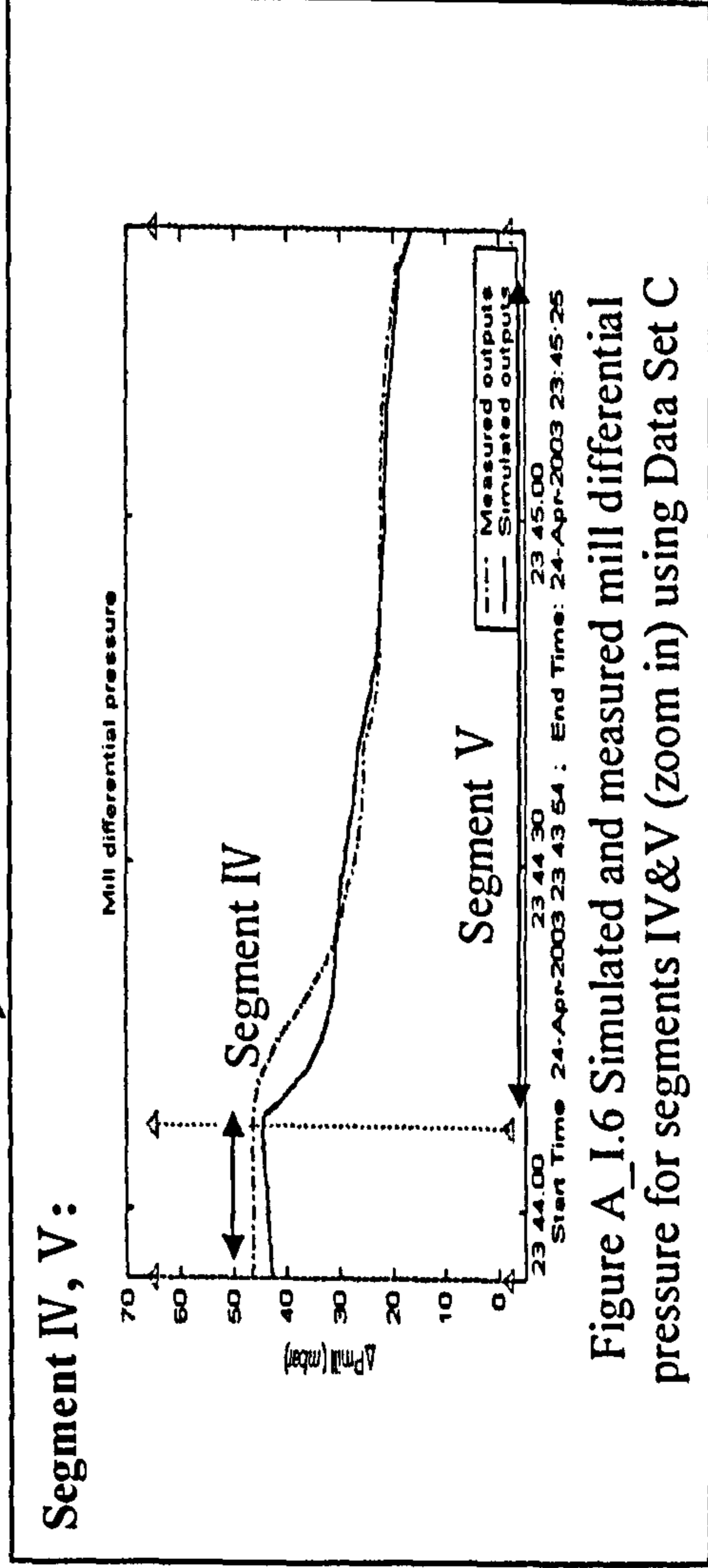
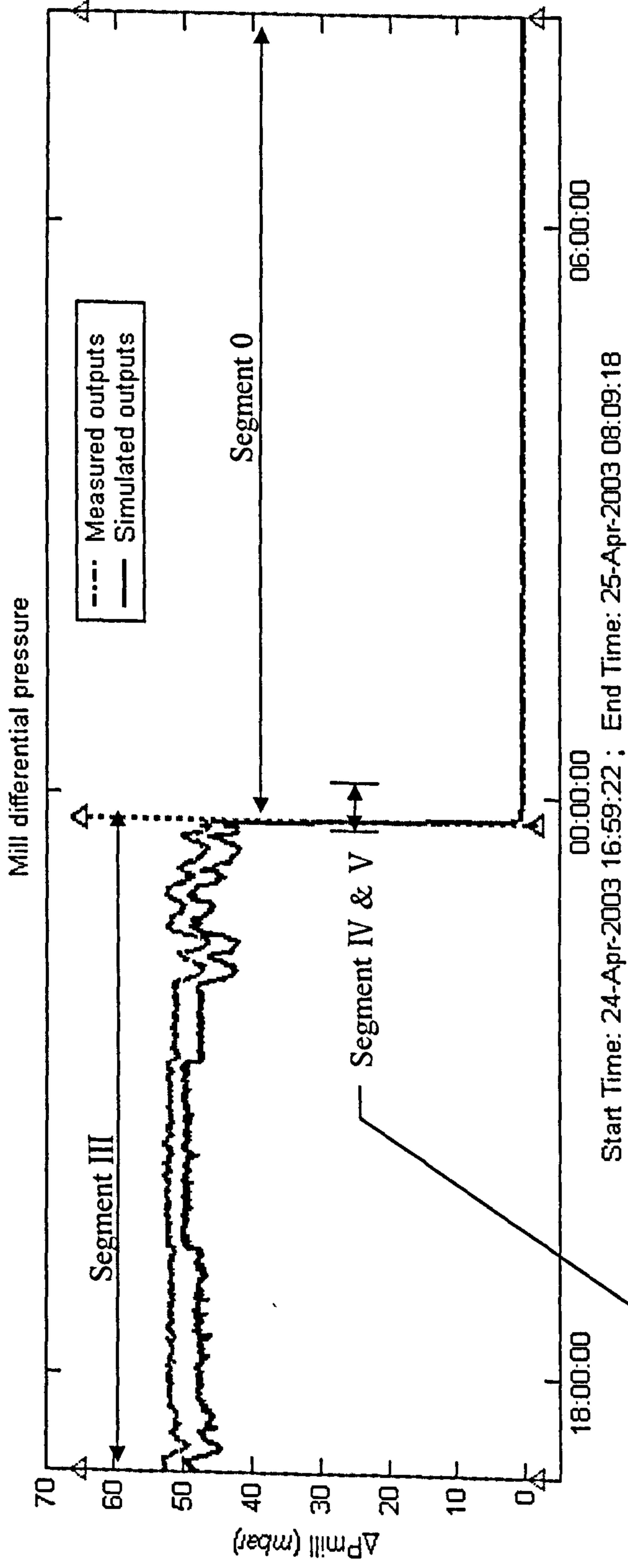


Figure A\_I.4 Simulated and measured mill current for segments IV&V (zoom in) using Data Set C



Appendix II: Validation Results Using Data Set C



Appendix II: Validation Results Using Data Set C

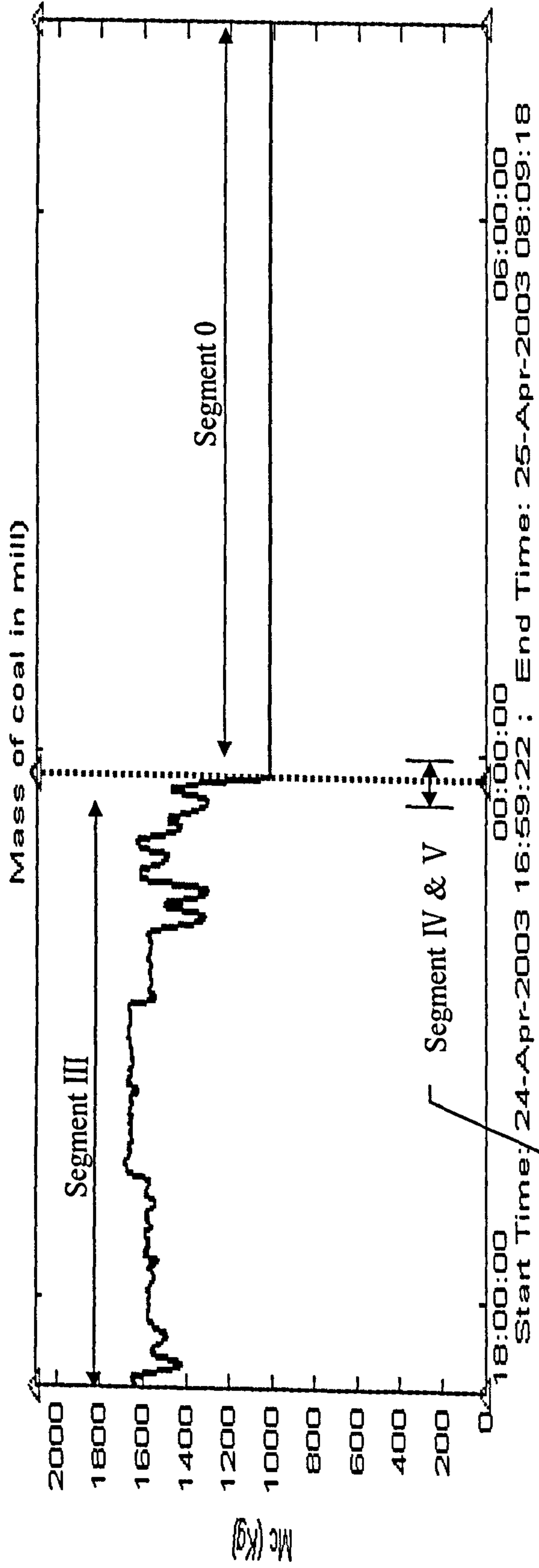


Figure A\_I.7 Simulated coal mass in mill for all segments using Data Set C

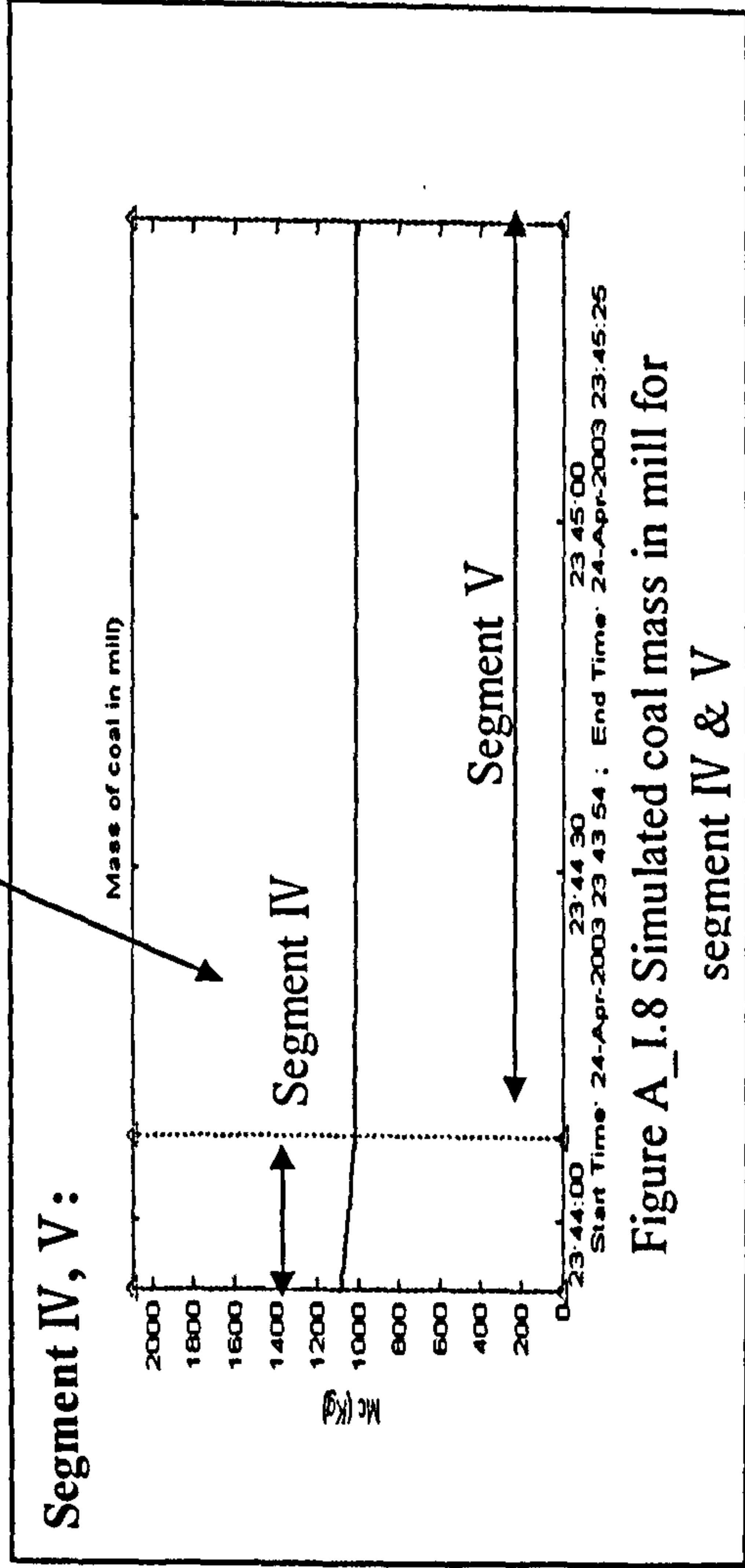


Figure A\_I.8 Simulated coal mass in mill for segment IV & V



Appendix II: Validation Results Using Data Set C

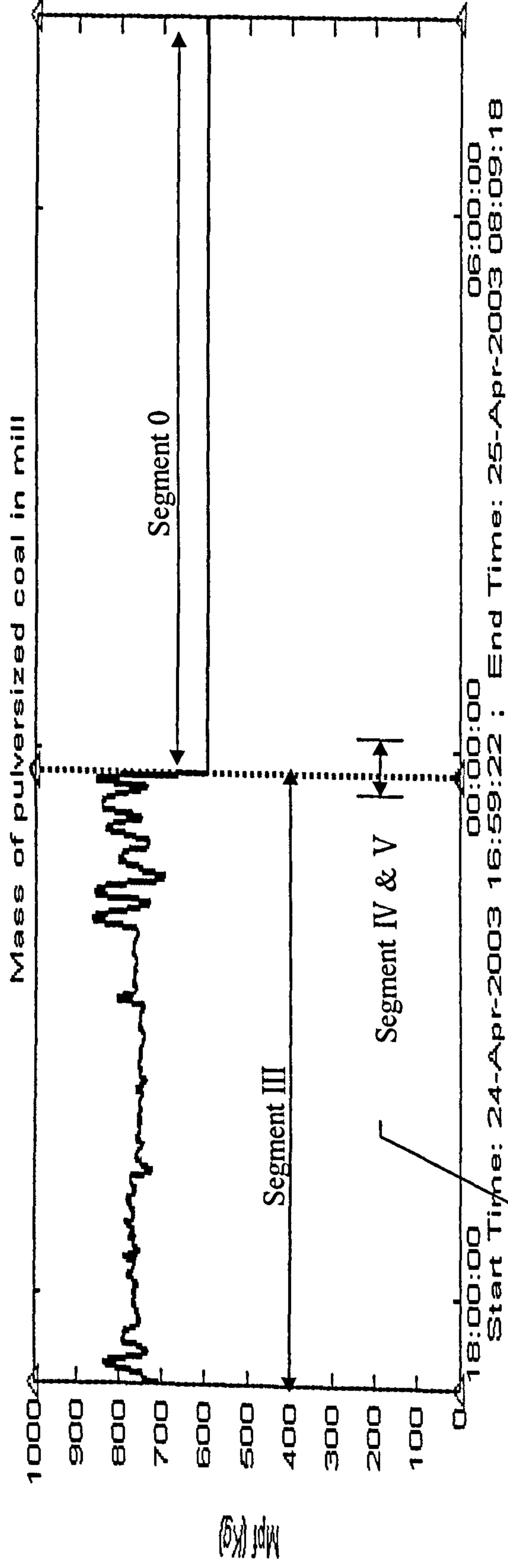


Figure A\_I.9 Simulated pulverized mass of coal in mill for all segments using Data Set C

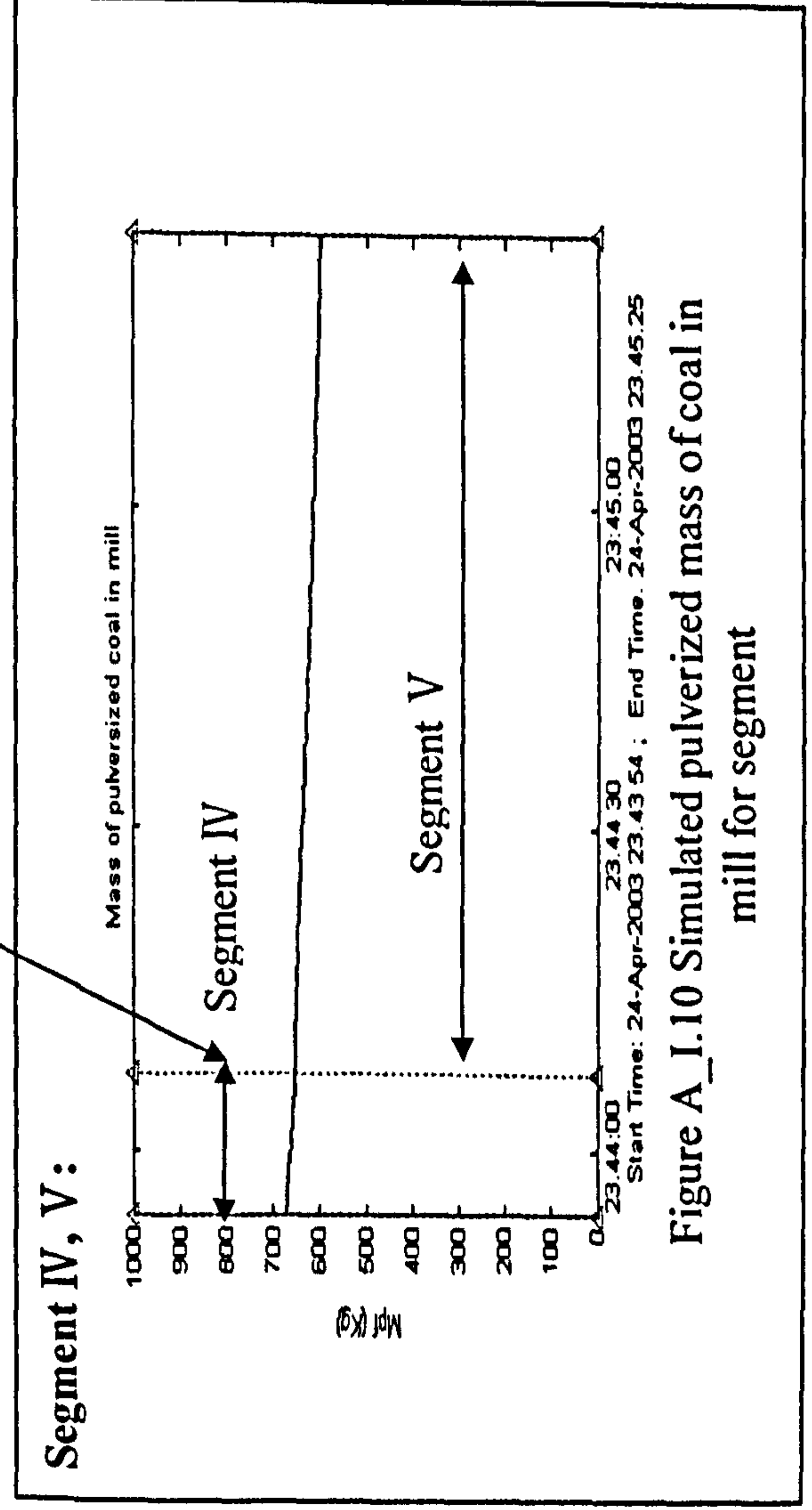


Figure A\_I.10 Simulated pulverized mass of coal in mill for segment

Appendix II: Validation Results Using Data Set C

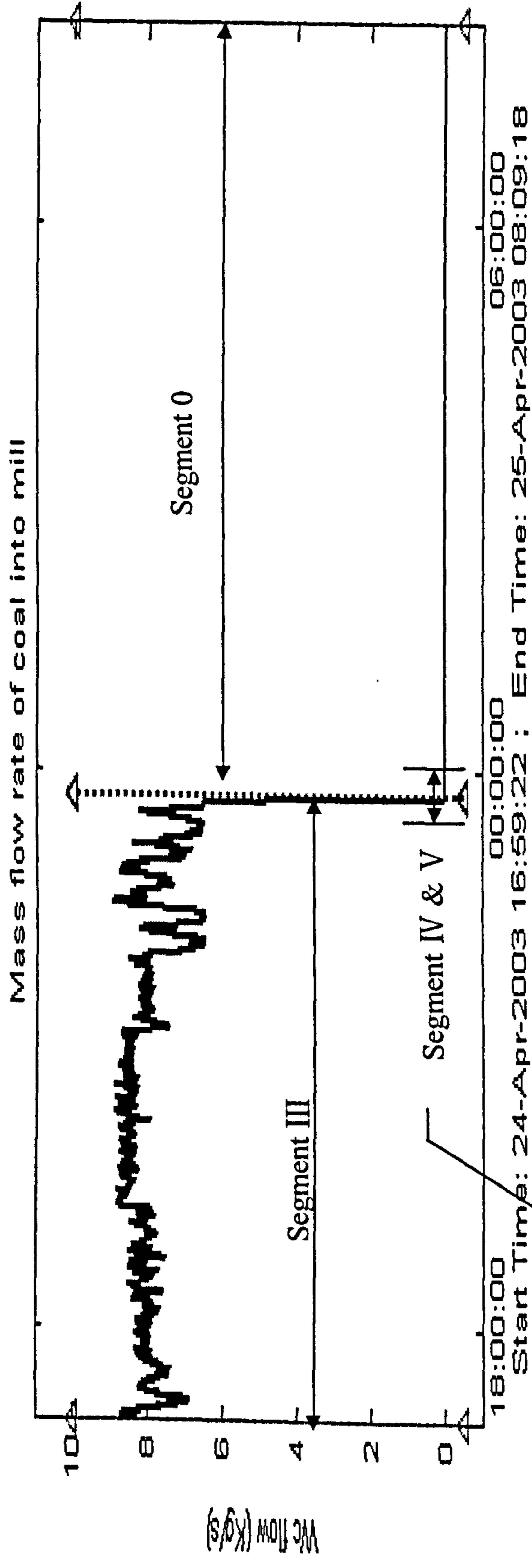


Figure A\_I.11 Coal mass flow rate into mill for all segments using Data Set C

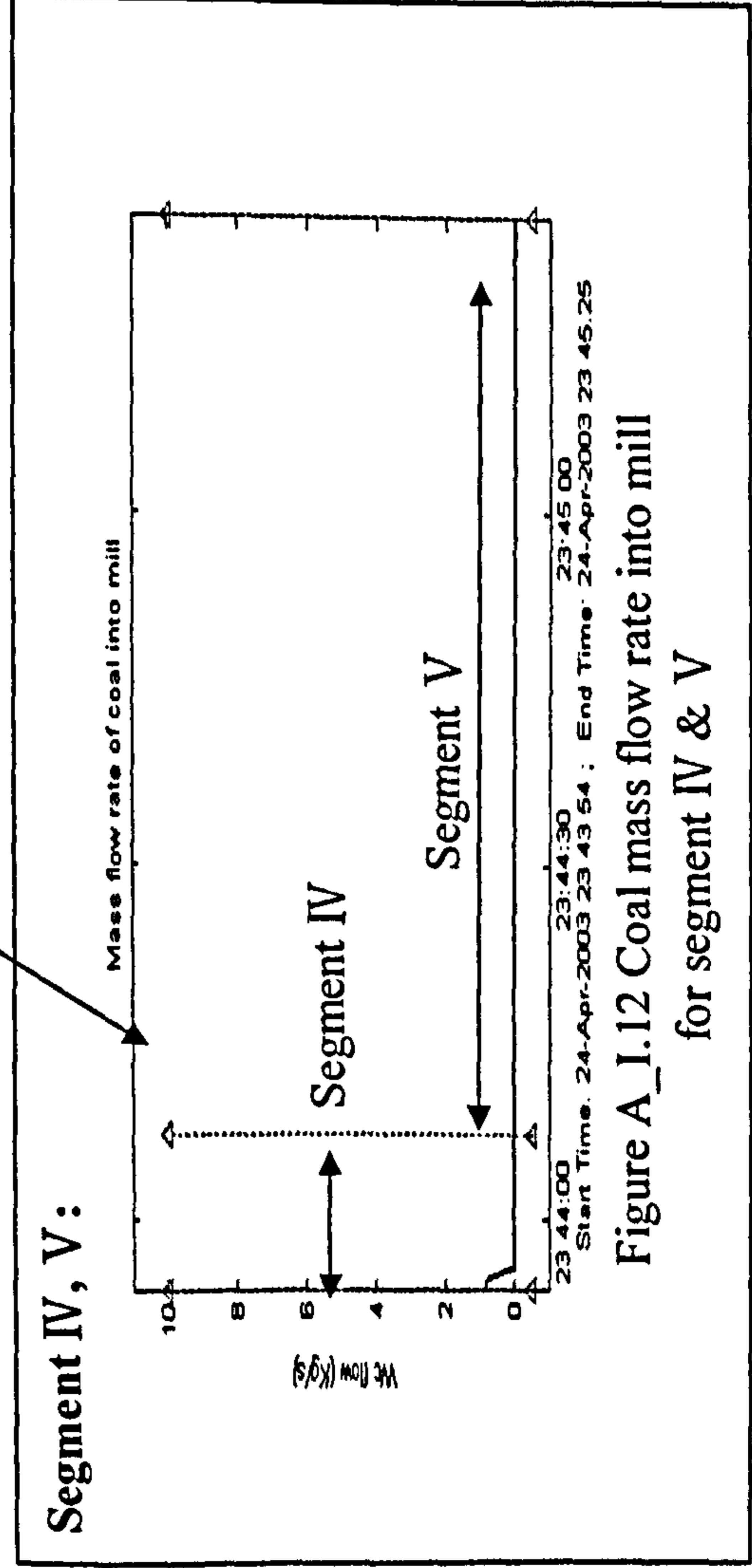


Figure A\_I.12 Coal mass flow rate into mill for segment IV & V



Appendix II: Validation Results Using Data Set C

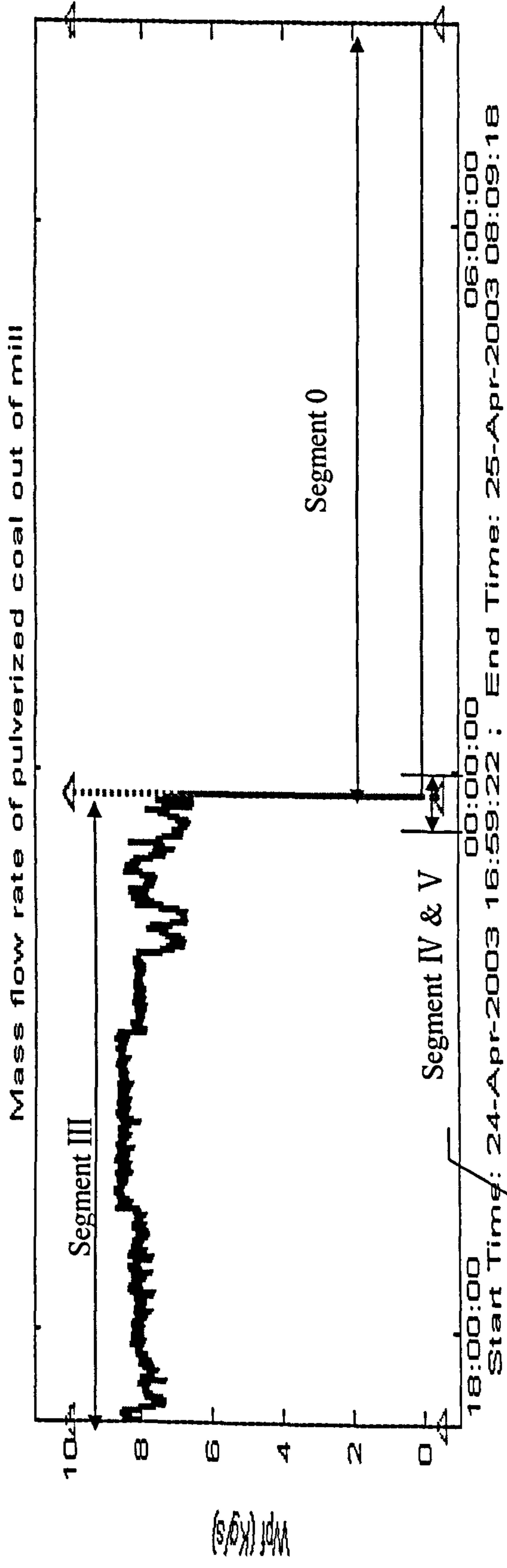


Figure A\_I.13 Simulated pulverized mass flow rate out of mill for all segments using Data Set C

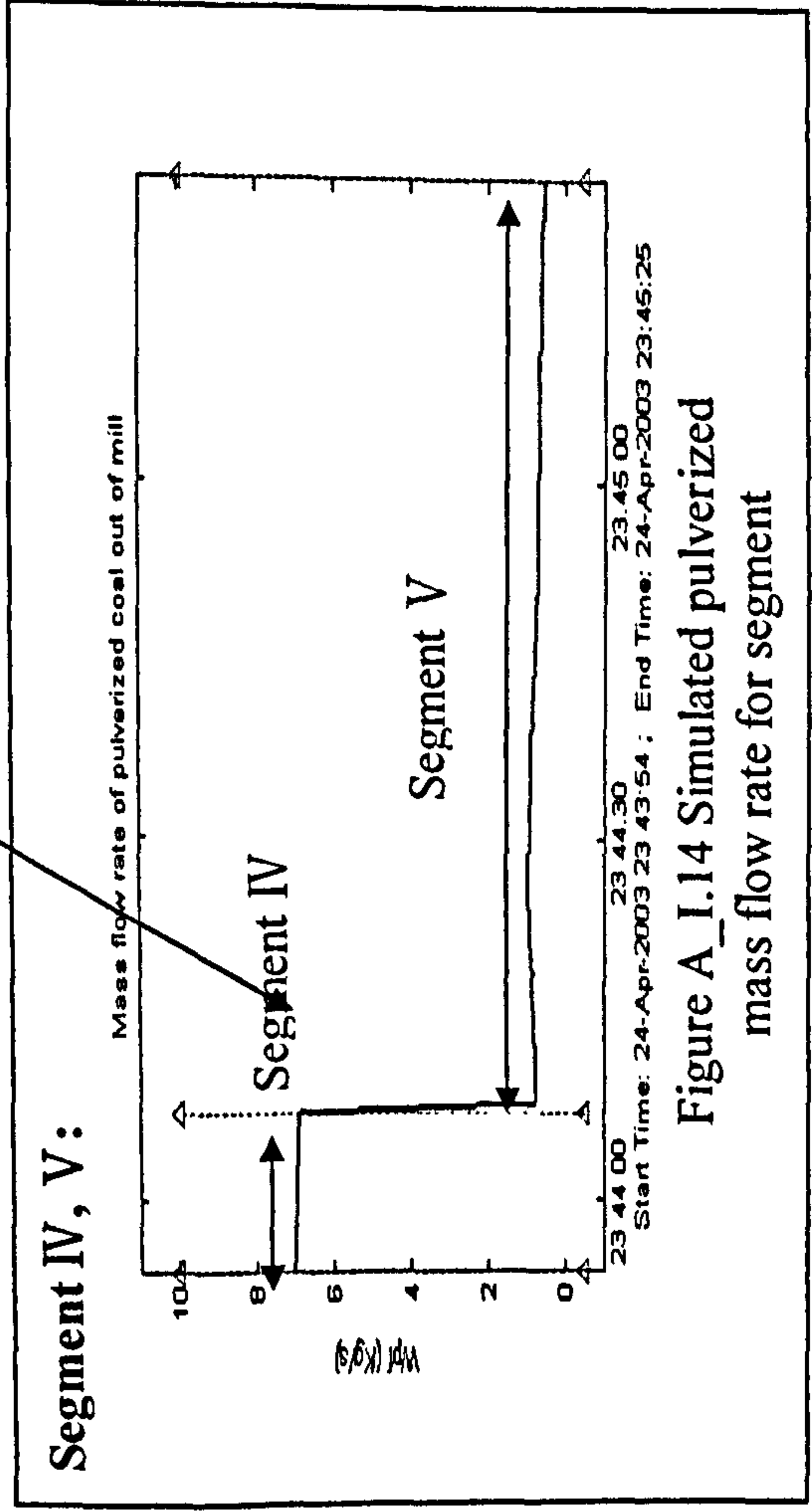


Figure A\_I.14 Simulated pulverized mass flow rate for segment